Pramin Norachan

89/325 Moo 17, Dcondo Campus Dome-Rangsit, Klong Nueng,
Klong Luang, Pathumthani, Thailand, 12120
Mobile: **66-88-548-4991**
Email: lee.min.krub@gmail.com

July 4, 2022

Cover Letter

To Whom It May Concern:

I am extremely interested in applying for a **Structural Engineer** position in your company. I graduated in Bachelor's Degree of Civil Engineering with first class honors from KMITNB, Thailand, on March 2003, Master's Degree of Structural Engineering from AIT, Thailand, on May 2005, and Doctoral Degree of Civil and Environmental System Engineering (Structural Engineering) from Konkuk University, South Korea, on February 2012.

I worked as a structural engineer for Palmer & Turner (Thailand) Co., Ltd., after earning the Master's Degree approximately one and half year. My works were concerned with structural design of RC tall buildings. Then, I continuously studied the Doctoral Degree in the field of Structural Engineering. My doctoral dissertation is related to development of a solid-shell element on a finite element software for structural analysis including geometric and material nonlinearities.

After earning Ph.D. until the present, I have been working for AIT Solutions over 10 years and on more than 25 projects giving me a broad set of experiences when designing buildings and other structures. I am responsible for modeling, analysis, evaluation and design of buildings, performance-based seismic design of buildings, and seismic evaluation and retrofit of existing buildings. Currently, I am working in the position of a coordinator who controls the entire projects by guiding and assigning design works to junior engineers and contacts the clients.

Finally, I am an enthusiastic person and I believe that my academic training and my work experiences as a structural engineer prepare me to be an effective member in your team. Furthermore, I will welcome a personal interview at your convenience to discuss this opportunity with you. I can be reached in confidence at the contacts above and will look forward to hearing from you soon.

Thank you for your time and consideration.

Sincerely,

Pramin Norachan

Enclosure: Resume, Certificates, Paper Publications, Seminar and Training

PRAMIN NORACHAN (Ph.D.)

Address
89/325 Moo 17, Dcondo Campus Dome-Rangsit,
Klong Nueng, Klong Luang,
Pathumthani, Thailand, 12120
Mobile: **66-88-548-4991**
Email: lee.min.krub@gmail.com

PERSONAL DETAILS

Nationality: Thai
Born: December 4, 1979

EDUCATION

Ph. D. in Civil and Environmental System Engineering (Structural Engineering), February 2012
Konkuk University, Seoul, Korea.

M Eng. in Structural Engineering, May 2005
Asian Institute of Technology, Pathumthani, Thailand.

B Eng. in Civil Engineering (First Class Honor), March 2003
King Mongkut's Institute of Technology North Bangkok, Thailand.

ENGINEERING LICENSE

Professional Engineer in Civil Engineering (Thailand)

WORK EXPERIENCES

AIT Solutions (Thailand), February 2012 – Present
(Coordinator, Civil & Structural Engineering Unit)
Responsible for modeling, analysis, evaluation and design of buildings, performance-based seismic design of buildings, nonlinear modeling, analysis and design of structures, seismic evaluation and retrofit of existing buildings, BRB and CFRP design for strengthening and retrofitting RC structures.

Project

- Advisory services on performance-based seismic evaluation of building 1 of Hines Atrium Place, Gurugram, India
- Seismic evaluation and retrofit design of Campus One Bridgetowne East existing building using buckling restrained braces (BRB), Pasig City, Philippines
- Structural design review of diaphragm segments of the bridge No.13, Port Access Elevated Highway (PAEH) Project, Sri Lanka
- Structural design review of foundations for dynamic equipment of degassing pelletizer structure, Vietnam

- Structural system development code-based design review of One Gulshan Building, 15-story building, Bangladesh
- Performance-based seismic design of 8990 Urban Deca Cubao condominium project, 45-story residential building with precast bearing wall system, Philippines
- Performance-based seismic design of 5 buildings, Langsuan Village Project, 40-story building (APS), 33-story building (APL), 20-story building (APW), 17-story building (TPV), and 15-story building (LPV), Bangkok, Thailand
- Performance-based seismic design of 140-Wireless project, 23-story office building, Bangkok, Thailand
- Performance-based seismic design of Plum condo project, 38-story residential building with precast bearing wall system, Nonthaburi, Thailand
- Seismic evaluation and retrofit of UNESCAP Secretariat and Service buildings, Bangkok, Thailand
- Seismic evaluation of Royal Textile Academy building, 3-story RC frame structure including 2-story basement levels, Thimphu, Bhutan
- Seismic Evaluation and Retrofit of Staff and Amenities Building, Hotel Yak and Yeti, 4-story RC frame building, Kathmandu, Nepal
- Experimental Seismic Fragility of Siam Gypsum Partition Walls, Bangkok, Thailand
- Performance-based seismic design of Hotel Nikko, Tumon, Guam
- Structural design review and re-design of the single-layer super reticulated steel domes with a large span of 86 m at wat Buddhasaengdham, Saraburi, Thailand
- Performance-based seismic evaluation and progressive collapse evaluation of Ireo City Office towers, 32-story office and 34-story hotel buildings, India
- Performance-based seismic evaluation of Roxas Triangle Towers (Tower 2), 55-story high-rise building, Makati City, Philippines
- Performance-based seismic evaluation of the tall building for Living Stone Project, 53-story building, Manila, Philippines
- Design review of amount of reinforcement surrounding at openings of precast concrete wall panels, Thailand
- Performance-based seismic evaluation of the Nepal Rastriya secondary school building Project, 5-story building, Kathmandu, Nepal
- Performance-based seismic evaluation of the La Durbar Convention Center Project, 3-story building, Kathmandu, Nepal
- Foundation design review of the tall building for Trump tower, Manila, Philippines
- Foundation design review of the tall building for M-Place Ortigas, Manila, Philippines
- Transfer slab design of the tall building for Studio A residential condominium, Quezon city, Philippines

- FRP design for strengthening and retrofitting of Manila international airport project, Manila, Philippines
- Performance evaluation of Pruksa precast concrete wall between single and double layers of steel reinforcement, Thailand

Palmer & Turner (Thailand) Co., Ltd., January 2007–November 2007, and June 2005–October 2005
Worked as a structural engineer responsible in analyzing and designing tall buildings, such as mat foundations, car parking, flat slab and structural parts of buildings.
Project
- Modeling, analysis, and design of the Siri at Sukhumvit Project, 48-story residential building, Bangkok, Thailand

COMPUTER SKILLS

Programming Language and Software
Visual Basic, Fortran 95, HTML, CSS, JavaScript, VBA,
MATLAB, MathCAD, Maple 9,
SAP2000, ETABS, PERFORM-3D, SAFE, CsiCOL, CsiBridge, AutoCAD,
Microsoft Office

Software Development
PX (Perform-3D eXtension) - Extended Pre and Post Processing Software for PERFORM-3D

HONOR

Royal Thai Government (RTG)
Full scholarship for the master's degree in engineering,
Asian Institute of Technology, Thailand.

TEACHING

AIT Classes, 2015 – Present
- Overview of finite element modeling and analysis of tall buildings, CE 72.32 – Design of Tall Buildings.
- Introduction to ETABS (Basic Concepts and Tools), CE 72.32 – Design of Tall Buildings.
- Seismic design of cast-in-place concrete diaphragms, chords and collectors, CE 72.32 – Design of Tall Buildings.
- Design of reinforced concrete foundations, CE 72.32 – Design of Tall Buildings.
- Prestressed concrete (basic concepts), CE 72.52 – Advanced Concrete Structures.
- Retrofit and design of RC buildings (basic concepts), CE 72.52 – Advanced Concrete Structures.
- Retrofit and design of RC buildings (FRP design for RC members), CE 72.52 – Advanced Concrete Structures.

- Introduction to MATLAB, CE 72.52 – Advanced Concrete Structures.

Seminar on Designing of Special Structural Members for Earthquake Resistance, Thailand Concrete association (TCA), Bangkok, Thailand, 2019

- Seismic design of cast-in-place concrete diaphragms, chords and collectors, general concepts & design examples.

Seminar on New Approaches of Structural Design for Earthquake Resistance, Thailand Concrete association (TCA), Bangkok, Thailand, 2019

- Performance-based seismic design of tall buildings

Seminar on Precast Concrete Structural Systems: The Future and Applications in Building Industry in Myanmar, Yangon, Myanmar, 2018

- Performance-based seismic evaluation of hybrid structural systems.

Seminar on Modelling, Analysis, Evaluation and Construction of High-Rise Buildings, Thailand Concrete association (TCA), Bangkok, Thailand, 2018

- Performance-based seismic design of tall buildings, general concepts & case studies.

Technical Seminar and Workshop on Performance-based Structural Design of Tall Buildings, Bangkok, Thailand, 2018

- Performance-based seismic design of tall buildings, case studies.

Seminar and Workshop on Design of Tall Buildings: Trends and Advancements for Structural Performance, Bangkok, Thailand, 2016

- Seismic design of cast-in-place concrete diaphragms, chords and collectors, and seismic design of reinforced concrete foundations.

Seminar on Technologies of Seismic Strengthening of Buildings, Chiang Mai, Thailand, 2015

- Nonlinear modeling and analysis of buildings using commercial finite element programs, and examples of seismic evaluation and strengthening of reinforced concrete buildings.

Rajamangala University of Technology Tawan-ok: Uthenthawai Campus Classes, 2014 – 2015

- Structural dynamics and building design, Advanced Theory of Structure, 07-12-503.

ACTIVITIES

7th Asia Conference on Earthquake Engineering, Seismic Resilience for Safer Cities and Infrastructures, Bangkok, Thailand, 2018
Session chair of the event**.**

Concrete Training Project, Thailand, 2003
Concrete technology tutor at King Mongkut's Institute of Technology North Bangkok.

Thai-German Engineering Project (TEP), Thailand, 2000
Mathematics and Physics tutor at King Mongkut's Institute of Technology North Bangkok.

THESIS & DISSERTATION

Doctoral Degree
A Co-Rotational 8-node Solid-Shell Element for Three-Dimensional Analysis of Prestressed Concrete Structures.

Master's Degree
Design Improvement of R/C Interior Beam-Column Joint in Low to Moderate Seismic Risk Region.

Bachelor's Degree
Behavior of Concrete Mixed with Shreded Poryethylene Tetraphalate (PET) plastic.

RESEARCH AREAS

Performance-based seismic design of tall buildings
Seismic evaluation and retrofit of buildings
Structural design of precast concrete buildings
Development of a finite element program XFINAS
Geometrical and material nonlinearities base on FEM
Construction stage analysis of prestressed concrete bridges
Time-dependent analysis of prestressed concrete structures
Simulation of wave and current forces on offshore structures

PAPERS & CONFERENCES

Pramin Norachan, Ki-Du Kim, Eugenio Onate, Analysis of Segmentally Constructed Prestressed Concrete Bridges using Hexahedral Element with Realistic Tendon Profiles, **Journal of Structural Engineering (ASCE)**, Vol. 140(6), 2013.

Pramin Norachan, Songsak Suthasupradit, Ki-Du Kim, A co-rotational 8-node degenerated thin-walled element with assumed natural strain and enhanced assumed strain, **Finite elements in analysis and design**, Vol. 50, 70–85, 2012.

Bunlue Kimuam, Pramin Norachan, and Nonthachat Kunprapha, Seismic Evaluation and Retrofit of an Existing Reinforced Concrete School Building in Northern Thailand, **The 22nd National Convention on Civil Engineering, Nakhon Ratchasima, Thailand**, 2017

Phirawat Chantharin, Pramin Norachan, and Nonthachat Kunprapha, A Comparison of Nonlinear Static and Dynamic Analyses of RC Buildings under Seismic Loads, **The 22nd National Convention on Civil Engineering, Nakhon Ratchasima, Thailand**, 2017

Naveed Anwar, Thaung Htut Aung, Pramin Norachan, and Wanassanun Kerlken, Case Study: Performance-base Design of Ductile Core Wall Building, **EASEC-14, Structural Engineering and Construction Conference, Ho Chi Minh City, Vietnam**, 2016

Naveed Anwar, Pramin Norachan, Thaung Htut Aung, Challenges of a Single-Layer Reticulated Inverted Monk Bowl, **IABSE Conference – Structural Engineering: Providing Solutions to Global Challenges, Geneva, Switzerland**, 2015

N. Anwar, P. Norachan, P. Warnitchai, T. Htut Aung, An Overview of Analysis and Design of a Single-Layer Reticulated Inverted Monk Bowl Dome, **The 7th Regional Symposium on Infrastructure Development, Bangkok, Thailand**, 2015

Pramin Norachan, Ki-Du Kim, Kyung-Chul Kim, Time-dependent analysis of PWR prestressed concrete containment considering realistic tendon profile, **The 2011 World Congress on Advances in Structural Engineering and Mechanics**

Pramin Norachan, Ki-Du Kim, Finite Element Analysis of Offshore Wind Turbines under Environmental Loadings, **The 6th International Symposium on Steel structures (ISSS)**, 2011.

Songsak Suthasupradit, Panot Chobsilprakob, Pramin Norachan, Ki-Du Kim, A co-rotational 9-node assumed strain element for large diaplacement elasto-plastic analysis of plates and shells, **Conference of Korean Society of Steel Construction**, 2008.

Panot, Songsak, Pramin, Kim Ki-Du, A Nonlinear Co-Rotational Quasi-Conforming 4-Node Shell Element using Ivanov-Ilyushin Yield Criteria, **Journal of Korean Society of Steel Construction**, 20 (2008) 409-419.

Se-Hun Lee, Songsak Suthasupradit, Panot Chobsilprakob, Ki-Du Kim, Pramin Norachan, Jae-Yoon Cha, Large Displacement Elasto-Plastic Analysis of Shell Structures Using an Eight-Node Solid-Shell Element ,**International Symposium on Steel Structures**, 2009.

Sacharuck Pornpeerakeat, Panot Chobsilprakob, Pramin Norachan, Ki-Du Kim, Kim Do, Nonlinear Formulation of Biot's Consolidation via Enhanced Assumed Strain Method, **Advances in Structural Engineering and Mechanics (ASEM)**, 2008.

REFERENCE

Naveed Anwar, Ph.D., Vice President for Knowledge Transfer, AIT Consulting Director, ACECOMS, Affiliate Faculty, Structural Engineering, AIT, Pathumthani, Thailand.
Email mailto:KIMKD@KONKUK.AC.KRnanwar@ait.asia

Professor Pennung Warnitchai, School of Engineering & Technology, Asian Institute of Technology (AIT), Pathumthani, Thailand.
Email pennung.ait@gmail.com

Professor Kim Ki-Du, Department of Civil and Environmental System Engineering, Konkuk University, Seoul, Korea.
Email kimkd@konkuk.ac.kr

제 12-D-329 호

KONKUK UNIVERSITY

1 HWAYANG-DONG,GWANGJIN-GU
SEOUL,143-701,KOREA

DECEMBER 21, 2011

OFFICE OF ACADEMIC AFFAIRS

CERTIFICATE

TO WHOM IT MAY CONCERN :

NAME IN FULL : NORACHAN PRAMIN

DATE OF BIRTH : DECEMBER 04, 1979

SCHOOL : GRADUATE SCHOOL

DEPARTMENT : CIVIL AND ENVIRONMENTAL SYSTEM ENGINEERING

MAJOR : CIVIL AND ENVIRONMENTAL SYSTEM ENGINEERING

DATE OF ADMISSION : MARCH 01, 2008

DEGREE : Ph.D.

THIS IS TO VERIFY THAT THE ABOVE PERSON IS SCHEDULED TO RECEIVE THE DOCTOR'S DEGREE FROM THIS UNIVERSITY'S GRADUATE SCHOOL ON FEBRUARY 22, 2012

Kwon Jong Ho

KWON JONGHO

VICE PRESIDENT FOR ACADEMIC AFFAIRS

SEAL

제 12-D-128 호

KONKUK UNIVERSITY
1 HWAYANG-DONG, GWANGJIN-GU
SEOUL, 143-701, KOREA

OFFICIAL TRANSCRIPT

DECEMBER 08, 2011

Name in Full	: NORACHAN PRAMIN	School	: GRADUATE SCHOOL
Student Number	: 200881005	Department	: CIVIL AND ENVIRONMENTAL SYSTEM ENGINEERING
Gender	: MALE	Major	: CIVIL AND ENVIRONMENTAL SYSTEM ENGINEERING
Date of Birth	: DECEMBER 04, 1979	Date of Completion	: FEBRUARY 22, 2010
Date of Admission	: MARCH 01, 2008	Date of Graduation	:
Degree Program	: DOCTOR'S	Degree Received	:

TITLE OF COURSE	CR	GR
1st SEMESTER (2008)		
UNDERSTANDING OF KOREAN CULTURE & SOCIETY	2	P
FINITE ELEMENT METHOD	3	A+
WIND AND EARTHQUAKE ENGINEERING	3	A
ADVANCED SOIL MECHANICS	3	A
PSSD : 9 GPA : 4.16		
2nd SEMESTER (2008)		
FINITE ELEMENT METHOD I	3	A+
THEORY OF ELASTIC STABILITY	3	A+
COMPUTATIONAL AERODYNAMIC DESIGN	3	A+
PSSD : 9 GPA : 4.5		
3rd SEMESTER (2009)		
ADVANCED STRUCTURAL MECHANICS 1	3	A+
ADVANCED ENVIRONMENTAL CHEMISTRY	3	A+
STRUCTURAL DYNAMICS	3	A+
PSSD : 9 GPA : 4.5		
4th SEMESTER (2009)		
SPECIAL TOPICS IN CIVIL AND ENVIRONMENTAL SYSTEM	3	A+
CONTINUUM MECHANICS	3	A+
THEORY OF ELASTICITY	3	A
PSSD : 9 GPA : 4.33		

CREDITS EARNED	: 36
FULL MARKS	: 4.50
CUMULATIVE GPA	: 4.37
PERCENTAGE EQUIVALENT	: 97

TITLE OF COURSE	CR	GR

THESIS:

Remarks

1.Hours-Per-Week
One hour class work per week for 1 semester makes 1 credit.
(Two or more hours of laboratory work per week for 1 semester makes 1 credit.)

2.Weeks-Per-Year
16weeks make 1 semester and 2 semesters 1 academic year.

3.Grading System

A+ :4.5(100-95)	A :4.0(94-90)
B+ :3.5(89-85)	B :3.0(84-80)
C+ :2.5(79-75)	C :2.0(74-70)
D+ :1.5(69-65)	D :1.0(64-60)

4. Required Credits for Master's and Doctor's Degree : 24 ~ 36

SEAL

Kwon Jong Ho

KWON JONGHO
VICE PRESIDENT FOR ACADEMIC AFFAIRS
KONKUK UNIVERSITY

The Board of Trustees of the

Asian Institute of Technology

On the Recommendation of the Academic Senate
Has Conferred Upon

PRAMIN NORACHAN

The Degree of

Master of Engineering

With all of its Privileges and Obligations

Given this Twenty-seventh day of May 2005

President of the Institute

Chairman of the Board

Certified true copy
Laarni B Roa
Registry Officer

ASIAN INSTITUTE OF TECHNOLOGY
DEGREE OF MASTER

Issue Date: 14 May. 2005

Name Mr. Pramin Norachan	Previous Degree(s)/Institution B.Eng. King Mongkut's Inst. of Technology, North Bangkok, Thailand Year Awarded 2003
Date of Birth 04 December 1903 Country Thailand	
Registration No. 100572 Date Admitted to AIT 18 August 2003 Option Thesis	
School School of Civil Engineering	Credits/Institution Transferred
Field of Study Structural Engineering	Degree Awarded Master of Engineering
Notes	Date of Graduation 27 May 2005

Course No.	Descriptive Course Title	Total Hours Lab.	Total Hours Lec.	Credits	Grade	GPA	Cumulative GPA
	August Semester 2003						
CE72.11	Computer Methods of Structural Analysis	0	45	3.0	A		
CE72.21	Structural Dynamics	0	45	3.0	A		
CE72.31	Continuum Mechanics	0	45	3.0	B+		
CE72.41	Advanced Concrete Technology	0	45	3.0	B		
				12.0		3.63	3.63
	January Semester 2004						
CE72.12	Finite Element Methods in Engineering	0	45	3.0	B		
CE72.22	Wind and Earthquake Engineering	0	45	3.0	B		
CE72.42	Experimental Methods in Structural Engineering	45	30	3.0	C+		
CE72.9002	Selected Topic: Advanced Topic in Bridge Engineering	0	45	3.0	B+		
				12.0		3.00	3.31
	Inter-Semester 2004						
IN00.32	European Cultural Context	0	30	2.0	B		
				2.0			
	Coursework Credits Gained:			26.0			3.31
	Thesis Credits Gained:			22.0			
	Total Number of Credits Gained:			48.0			
	Thesis Examination:				Passed		

Certified true copy
Laarni B. Roa
Registry Officer

Note: The grades obtained on Institute-wide courses are not accounted for in the calculation of grade point average (IN00.xx codes).

Title of Thesis: Design Improvement of R/C Interior Beam-column Joints in Low to Moderate Seismic Risk Regions

Grade: Very Good

Program Committee:
1 Dr. Pennung Warnitchai (Chairman)
2 Dr. William Barry (Member)
3 Dr. Pichai Nimityongskul (Member)

Official transcript not valid without signature and seal of the Institute

Registry Officer

GRADING SYSTEM

A	=	4	-	Excellent
B+	=	3.5		
B	=	3	-	Good
C+	=	2.5		
C	=	2	-	Fair
D	=	1	-	Deficient
F	=	0	-	Fail
I	=	0	-	Incomplete

Grades received for all courses are used in the computation of cumulative averages, but only course grades of C or higher can be counted to satisfy the credit requirement.

Doctor Degree: The minimum credit requirement for the Degree of Doctor is 18 credits for those who earned their Master degree at AIT, and 24 credits for those who earned their Master degree elsewhere, of which not more than 6 credits are earned from special studies.

A doctoral student must complete a doctoral dissertation and defend it at an oral examination. The dissertation, which is not graded, must demonstrate scholarly distinction and show that, through the research performed during the program, the student has contributed to the advancement of knowledge in the chosen field of study. A satisfactory report from the external examiner selected by the Program Committee is also required for the doctoral degree. The required minimum cumulative grade point average for Doctoral Degree is 3.50.

Master Degree: The minimum credit requirement for the Master's Degree is 48 credits, which may include a thesis of 22 credits, a research study of 10 credits or a project of 6 credits. Thesis, research study and project are, if judged to be satisfactory, graded excellent, very good, good or fair; these grades, however, will not be included in the computation of the cumulative grade point average. Not more than six credits earned from special studies may be counted towards the credit requirement of the Master's program. The required minimum cumulative grade point average for Master's Degree is 2.75.

The Diploma program: This program requires a minimum of 24 credits of coursework, including 2-6 credits of special studies. The required minimum cumulative grade point average for AIT Diploma is 2.75.

Certificate of Advanced Studies: The minimum credit requirement for the CAS program is 18 credits for those who earned their Master degree at AIT, and 24 credits for those who earned their Master degree elsewhere, of which not more than 6 credits are earned from special studies. There is no minimum cumulative grade point average set for this non-degree program.

Certificate program: This program requires not less than 9 credits of coursework in a semester. There is no minimum cumulative grade point average set for this non-degree program.

Special program: This program is not normally directed towards completion of any of the above programs. Special program students register courses and are graded. No minimum credits and GPA requirement are set for this program.

English is the language of all Institute's academic and administrative communication.

The Registry
Asian Institute of Technology,
P.O. Box 4, Klongluang,
Pathumthani 12120, Thailand.
Fax: **(66-2) 524-6326**
Tel: **02-524-5034-7, 02-524-6322, 6325**
Email: **registry@ait.ac.th.**
http://www.ait.ac.th

FACULTY OF ENGINEERING

KING MONGKUT'S INSTITUTE OF TECHNOLOGY NORTH BANGKOK

BANGKOK 10800, THAILAND

To whom it may concern :

This is to certify that MR. PRAMIN NORACHAN was enrolled as a full-time undergraduate student in the Department of Civil Engineering, Faculty of Engineering, during 1999-2003. He completed all the requirements leading towards the degree of Bachelor of Engineering in Civil Engineering with first class honours on March 28, 2003

Given on July 22, 2003

(ASSOC.PROF. SIRISAK HARNCHOOWONG)

Dean

Faculty of Engineering

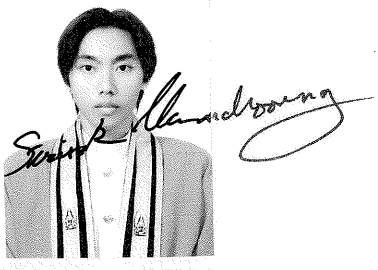

MR. PRAMIN NORACHAN

KING MONGKUT'S INSTITUTE OF TECHNOLOGY NORTH BANGKOK
BANGKOK THAILAND
OFFICIAL TRANSCRIPT OF RECORDS
FACULTY OF ENGINEERING

NAME IN THAI นายประมินทร์ นรชาญ

RECORD NO 42-1096-014-4 **NAME** Mr. PRAMIN NORACHAN

DATE OF BIRTH December 4, 1979 **PLACE OF BIRTH** BANGKOK METROPOLIS, THAILAND

PREVIOUS EDUCATION Vocational Education Certificate in Building Construction

DATE OF ADMISSION June 1, 999 **DATE OF GRADUATION** March 28, 2003

DEGREE CONFERRED Bachelor of Engineering in Civil Engineering (First Class Honours)

FIELD OF SPECIALIZATION ——

COURSE NO.	COURSE TITLES	CRD.	GRD.
	1st SEMESTER 1999		
101002	ENGINEERING DRAWING	2	A
111326	COMPUTER PROGRAMMING DESIGN	3	A
181070	TECHNOLOGY AND SOCIETY	1	B+
260111	ENG FOR SCIENCE & TECH I	3	C
263912	ART APPRECIATION	3	B+
421111	ENGINEERING MATHEMATICS I	3	A
431101	GENERAL PHYSICS I	3	B
431102	GENERAL PHYSICS LAB I	1	B+
SEM.	3.39	19	19	64.5
CUM.	3.39	19	19	64.5
	INDEX	ATTEMPTED	EARNED	POINTS
	2nd SEMESTER 1999		
181095	ENGINEERING STATICS	3	A
260112	ENG FOR SCIENCE & TECH II	3	C+
263857	VOLLEYBALL	1	B+
419008	CHEMISTRY FOR ENGINEERS	3	A
419009	CHEMISTRY LAB FOR ENGINEERS	1	B+
421112	ENGINEERING MATHEMATICS II	3	A
431103	GENERAL PHYSICS II	3	A
431104	GENERAL PHYSICS LAB II	1	B
450111	STAT FOR ENGR & SCIENTIST	3	B+
SEM.	3.61	21	21	76.0
CUM.	3.51	40	40	140.5
	INDEX	ATTEMPTED	EARNED	POINTS
	1st SEMESTER 2000		
102201	ENGINEERING DYNAMICS	3	C+
102401	THERMODYNAMICS I	3	B+
182001	SURVEYING I	3	B
182010	STRENGTH OF MATERIALS I	3	A
263510	INTRODUCTION TO ECONOMICS	3	B+
263856	BASKETBALL	1	B
421211	ENGINEERING MATHEMATICS III	3	B
SEM.	3.23	19	19	61.5
CUM.	3.42	59	59	202.0
	INDEX	ATTEMPTED	EARNED	POINTS

COURSE NO.	COURSE TITLES	CRD.	GRD.
	2nd SEMESTER 2000		
112120	ELECTRICAL ENGINEERING	3	B+
182002	SURVEYING II	3	A
182011	STRENGTH OF MATERIALS II	3	A
182015	STRUCTURAL ANALYSIS I	3	A
182045	INTRO TO CONST & ARCH	2	A
193110	ENGINEERING ECONOMY	3	A
263826	HUMAN RELATIONS	3	A
SEM.	3.92	20	20	78.5
CUM.	3.55	79	79	280.5
	INDEX	ATTEMPTED	EARNED	POINTS
	1st SEMESTER 2001		
183016	STRUCTURAL ANALYSIS II	3	B+
183030	ENGINEERING GEOLOGY	3	A
183040	CIVIL ENGR MATERIALS & TEST	3	C+
183060	HYDRAULICS	3	A
183090	NUMERICAL METHODS IN CE	3	B+
183099	SEMINAR IN CIVIL ENGINEERING	1	A
263331	ENGLISH CONVERSATION	3	B+
SEM.	3.52	19	19	67.0
CUM.	3.54	98	98	347.5
	INDEX	ATTEMPTED	EARNED	POINTS
	2nd SEMESTER 2001		
183020	REINFORCED CONCRETE DESIGN	4	A
183031	SOIL MECHANICS	3	B
183032	SOIL MECHANICS LABORATORY	1	B+
183050	TRANSPORTATION ENGINEERING	3	A
183065	HYDROLOGY	3	A
183075	ENVIRONMENTAL ENGINEERING	3	B
183091	COMPUTER APPLICATIONS IN CE	3	A
SEM.	3.67	20	20	73.5
CUM.	3.56	118	118	421.0
	INDEX	ATTEMPTED	EARNED	POINTS

A CUMULATIVE GRADE POINT AVERAGE OF 2.00 IS REQUIRED FOR GRADUATION.

NOT VALID WITHOUT SEAL **ISSUED ON May 9, 2003** **ACTING REGISTRAR** A. Vilaihong

(Mrs. AMPAIPUN VILAIHONG)

KING MONGKUT'S INSTITUTE OF TECHNOLOGY NORTH BANGKOK
BANGKOK THAILAND
OFFICIAL TRANSCRIPT OF RECORDS
FACULTY OF ENGINEERING

RECORD NO 42-1096-014-4 **NAME** Mr. PRAMIN NORACHAN

COURSE NO.	COURSE TITLES	CRD.	GRD.
	1st SEMESTER 2002		
184017	MATRIX ANALYSIS OF STRUCTURE	3	A
184023	TIMBER AND STEEL DESIGN	3	B+
184033	FOUNDATION ENGINEERING	3	A
184051	HIGHWAY ENGINEERING	3	A
184061	HYDRAULIC ENGINEERING	3	A
184062	HYDRAULICS LABORATORY	1	A
184080	CIVIL ENGINEERING PROJECT I	1	Ip

	INDEX	ATTEMPTED	EARNED	POINTS
SEM.	3.90	16	16	62.5
CUM.	3.60	134	134	483.5

	2nd SEMESTER 2002			
184021	PRESTRESSED CONCRETE DESIGN	3	B	
184046	CONSTRUCTION ENGR & MANAGE	3	B+	
184080	CIVIL ENGINEERING PROJECT I	1	A	
184081	CIVIL ENGINEERING PROJECT II	3	A	
184082	CIVIL ENGINEERING DESIGN	3	B+	

	INDEX	ATTEMPTED	EARNED	POINTS
SEM.	3.53	13	13	46.0
CUM.	3.60	147	147	529.5

COURSE REQUIREMENTS COMPLETED

COURSE NO.	COURSE TITLES	CRD.	GRD.

A CUMULATIVE GRADE POINT AVERAGE OF 2.00 IS REQUIRED FOR GRADUATION.

NOT VALID WITHOUT SEAL **ISSUED ON May 9, 2003** **ACTING REGISTRAR** A. Vilaihong

(Mrs. AMPAIPUN VILAIHONG)

Finite Elements in Analysis and Design 50 (2012) 70–85

Contents lists available at SciVerse ScienceDirect

Finite Elements in Analysis and Design

journal homepage: www.elsevier.com/locate/finel

A co-rotational 8-node degenerated thin-walled element with assumed natural strain and enhanced assumed strain

Pramin Norachan, Songsak Suthasupradit, Ki-Du Kim *

Department of Civil and Environmental System Engineering, Konkuk University, 1 Hwayang-dong, Gwangjin-gu, Seoul, Republic of Korea

ARTICLE INFO

Article history:
Received 10 December 2010
Received in revised form
8 June 2011
Accepted 26 August 2011
Available online 25 September 2011

Keywords:
8-Node solid element
Assumed natural strains
Enhanced assumed strains
Co-rotational method
Geometrical nonlinearity

ABSTRACT

In recent years, solid-shell elements with the absence of the rotational degrees of freedom have considerable attentions in analyzing thin structures. In this paper, the non-linear formulation of a co-rotational 8-node degenerated thin-walled element with no rotational degrees of freedom is presented to demonstrate the solutions of linear and geometrically non-linear analysis for plate and shell structures. The assumed natural strain (ANS) and enhanced assumed strain (EAS) are used to overcome various locking problems, while the co-rotational formulation is employed to remove rigid body rotations for solving geometrically non-linear problems. In addition, the element formulation here uses plane stress condition in order to fit to thin-walled and shell applications, and the global, local and natural coordinate systems are employed to conveniently model the thin-walled geometry. Several numerical examples are presented to demonstrate the performance of the present element and the results are in good agreement with the references.

© 2011 Elsevier B.V. All rights reserved.

1. Introduction

The low-order element formulations for bricks and tetrahedrals tend to be the most exploited for 3D non-linear analysis due to their combination of computational efficiency and robustness. For the 8-node solid element, several different formulations have been developed to maximize the accuracy and efficiency. However, this element cannot perform well in thin-walled problems. To fit three-dimensional continuum to thin-walled and shell applications, the degeneration concept can be used. The concept of element degeneration from three-dimensional field equations has been widely used in development of shell elements. Ahmad et al. [1] presented an 8-node shell element degenerated form of the 16-noded three-dimensional continuum elements. In a degenerated shell element, nodes are placed at the mid-surface of the element and the assumptions of shell elements are imposed. Kanok-Nukulchai [2] presented a simple, efficient and versatile finite element, which is developed based on a degeneration concept, and bi-linear functions are employed in conjunction with a reduced integration for the transverse shear energy. Kanok-Nukulchai and Sivakumar [3] also developed the finite element formulations of two degenerated thin-walled elements accounting for warping restraint. The element idealization of thin-walled structural members uses the degeneration concept.

To simulate thin-walled and shell structures, in addition, solid-shell elements with eight nodes are being widely used. They have only translational degrees of freedom in the nodes located at the top and the bottom surfaces, which alleviates the difficulties associated with complex shell formulations with nodal rotations. However, solid-shell elements also have serious drawbacks, which are directly related to several kinds of locking behaviors. Wilson et al. [4] proposed the addition of internal incompatible displacement modes of quadratic distribution to enhance the bending performance of quadrilateral elements. Taylor et al. [5] proposed modifications to Wilson's original formulation that allowed the satisfaction of the patch test for arbitrary configurations, usually referred to as QM6. This method is also called the incompatible displacement mode method. Although the solution of the incompatible solid element is not fully satisfactory, the formulation of this element provides the basic idea for the introduction of the enhanced assumed strain (EAS) method.

A systematic development of a class of assumed strain methods is presented by Simo and Rifai [6]. They provided the framework for the development of low-order elements possessing improved performance in bending dominant problems in the extent of small strains. Issues related to convergence and stability were also presented. It was also shown that the classical method of incompatible modes was included in the EAS as a special case. The concept of the EAS method has become widely used because the elements based on this concept perform very well in the incompressible limit as well as in bending situations. Further extensions were also made by Simo and Armero [7] in order to incorporate the geometrically

* Corresponding author. Tel.: +82 2 2049 6074; fax: +82 2 452 8619.
E-mail address: kimkd@konkuk.ac.kr (K.-D. Kim).

0168-874X/$ - see front matter © 2011 Elsevier B.V. All rights reserved.
doi:10.1016/j.finel.2011.08.023

non-linear case, but they were found to lock in the incompressible limit for three-dimensional hexagonal elements for both geometrically linear and non-linear problems. The improvement of the three-dimensional formulation was proposed by Simo et al. [8], which incorporated modifications to the tri-linear shape functions, additional enhanced modes and an increased quadrature rule. The resulting element yielded a locking free response in the incompressible limit and improved bending characteristics for both geometrically linear and non-linear problems. A non-linear formulation based on the quasi-conforming technique, which includes geometric and material linearity, was presented by Lomboy et al. [9]. The formulation was presented using co-rotational approach. In the derivation of the geometric stiffness matrix, the trial basis function for the non-linear strains is proposed to be made independent of its linear counterparts.

In terms of background contributions as a possible alternative to degenerated shell elements, the solid-shell elements introduced by Hauptmann and Schweizerhof [10] and Sze and Yao [11] have received considerable attentions since no rotational degrees of freedom are included in formulation. This is because the solid-shell elements are simpler and more efficient in formulation and modeling compared to the degenerated shell elements. However, their performances deteriorate rapidly due to the locking when the thickness becomes smaller. Consequently, the development of accurate, stable and robust solid-shell elements becomes more challenging and demanding than that of the degenerated shell elements.

Andelfinger et al. [12] developed two- and three-dimensional EAS elements, which overcome locking in the incompressible limit and behaved well in bending dominated regimes. The formulations which were developed require a minimum of 21 additional element parameters. Korelc and Wriggers [13] developed two- and three-dimensional EAS elements that yielded favorable results. With only nine element parameters, the efficiency of the element is improved. Hauptmann and Schweizerhof [10] developed a 'solid-shell' element for linear and non-linear analysis. The proposed element has locking free behavior by employing the assumed natural strain (ANS) method and the EAS method. Puso [14] presented a highly efficient hexahedral element. The novel enhanced strain fields do not require any matrix inversions to solve the internal element degrees of freedom. For most of the 8-node solid elements using reduced integration, the solution indicates inaccuracy when the element becomes very thin. For double curved and warped structures, these elements converge very slowly, a situation, which may be due to the assumption of constant Jacobian matrix. Areias et al. [15] presented a versatile 3D low-order element including a stabilizing term. To ensure the satisfaction of the Patch test, material averages are used, and the element consists of 18 internal variables of enhanced assumed strains.

A continuum based three-dimensional shell element for the non-linear analysis of laminated shell structures is presented by Klinkel et al. [16]. The basis of the element formulation is the standard 8-node brick element with assumed natural strain and enhanced assumed strain methods used to improve the relatively poor element behavior. The anisotropic material behavior of layered shells is modeled using a linear elastic orthotropic material law in each layer. Sze and Yao [11] developed a hybrid stress ANS solid-shell element and its generalization for smart structure modeling. The assumed natural strain (ANS) method is resorted to resolve the shear and trapezoidal lockings. Kim et al. [17] offered a resultant 8-node solid-shell element for geometrically non-linear analysis. The global, local and natural coordinate systems were used to accurately model the shell geometry. The assumed natural strain methods with plane stress concept were implemented to remove the various locking problems appearing in thin plates and shells. Cardoso et al. [18] presented the enhanced assumed strain (EAS) and assumed natural strain (ANS) methods for one-point quadrature solid-shell elements. In order to overcome shear locking, a modified assumed natural strain (ANS) method considering the top and the bottom surfaces of the element was incorporated for the transverse shear components.

The objective of this work is to apply the standard hexahedral element with both assumed natural strain (ANS) and enhanced assumed strain (EAS) techniques. The 11 enhanced assumed strain (EAS) parameters in the natural coordinate are used to increase the element performance. The element formulation here uses degeneration of three-dimensional continuum to fit to thin-walled and shell applications by employing plane stress condition, while co-rotational approach is included in order to deal with geometrically non-linear analysis. Additionally, the $2 \times 2 \times 2$ standard Gauss quadrature integration is used, and the element is defined as a co-rotational 8-node degenerated thin-walled element, XSOLID86.

2. Geometry and kinematics

In general, standard solid elements use only natural coordinate system (ξ,η,ζ) and global coordinate system (x–y–z). In the present element, a set of co-rotational local orthogonal coordinate systems (r–s–t) are added and set up at the center of each element. Thus, the present element shown in Fig. 1 can be described by the relation between global (x–y–z), local (r–s–t) and natural coordinates (ξ,η,ζ) using the shell geometry and

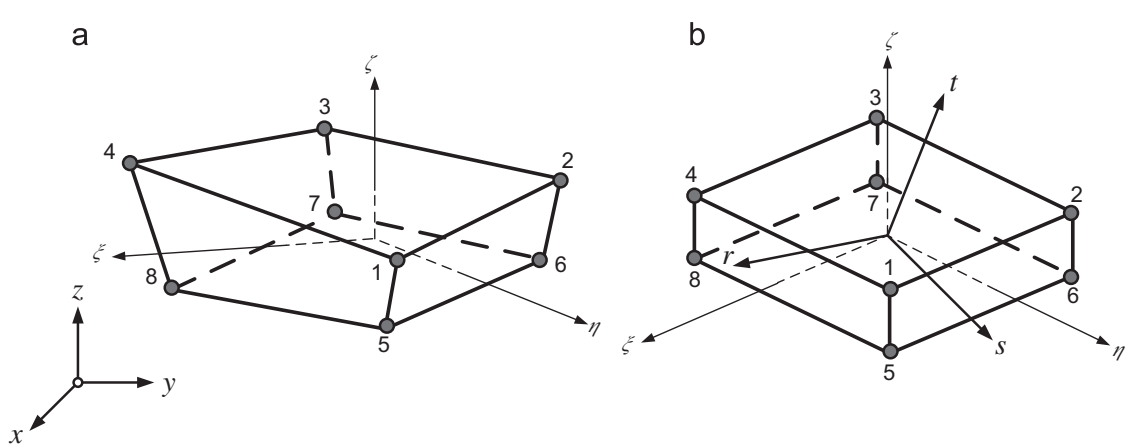

Fig. 1. Geometry of a typical 8-node solid element: (a) global coordinate system and (b) local and natural coordinate systems.

kinematics introduced by Kim et al. [17]. The origin of the natural coordinate system is set to the center of each element, and in general, this coordinate system is not always orthogonal for irregular element shapes.

In the global coordinate, the position vector **X** and the displacement vector **U** of a point inside the element can be, respectively, described as

$$\mathbf{X} = \sum_{i=1}^{8} N_i(\xi,\eta,\zeta)\mathbf{X}_i \tag{1}$$

$$\mathbf{U} = \sum_{i=1}^{8} N_i(\xi,\eta,\zeta)\mathbf{U}_i \tag{2}$$

where $\mathbf{X}_i$ is the nodal coordinate and $\mathbf{U}_i$ is the nodal displacement field in the global direction (x,y,z). For the 8-node isoparametric finite element, the shape functions are often defined as follows:

$$N_i(\xi,\eta,\zeta) = \frac{1}{8}(1+\xi_i\xi)(1+\eta_i\eta)(1+\zeta_i\zeta) \tag{3}$$

where (ξ_i,η_i,ζ_i) are the natural coordinates at the node i

The direction cosines of the new axes (r, s, t) with respect to the global axes (x, y, z) can be defined using the base vectors $(\mathbf{V}_r,\mathbf{V}_s,\mathbf{V}_t)$, which are parallel to the axes of the local coordinate as follows:

$$\begin{aligned}
\mathbf{V}_t &= \frac{\mathbf{V}_\xi \times \mathbf{V}_\eta}{|(\mathbf{V}_\xi \times \mathbf{V}_\eta)|}\\
\mathbf{V}_s &= \frac{\mathbf{V}_t \times \mathbf{V}_\xi}{|(\mathbf{V}_t \times \mathbf{V}_\xi)|}\\
\mathbf{V}_r &= \frac{\mathbf{V}_s \times \mathbf{V}_t}{|(\mathbf{V}_s \times \mathbf{V}_t)|}
\end{aligned} \tag{4}$$

where $\mathbf{V}_\xi$and $\mathbf{V}_\eta$ are the covariant base vectors at the centroid of element $(\xi=\eta=\zeta=0)$, tangential to ξ and η, respectively.

$$\begin{aligned}
\mathbf{V}_\xi &= \left.\frac{\partial \mathbf{X}}{\partial \xi}\right|_{(\xi=\eta=\zeta=0)} = \sum_{i=1}^{8} \frac{\partial N_i}{\partial \xi}\mathbf{X}_i\\
\mathbf{V}_\eta &= \left.\frac{\partial \mathbf{X}}{\partial \eta}\right|_{(\xi=\eta=\zeta=0)} = \sum_{i=1}^{8} \frac{\partial N_i}{\partial \eta}\mathbf{X}_i
\end{aligned} \tag{5}$$

For the transformation laws of Cartesian coordinate systems, the position vector **X** and the displacement vector **U** in the global coordinate system can be transformed into the position **x** and displacement **u** vectors in the local coordinate system by the relation:

$$\begin{aligned}
\mathbf{x} &= \mathbf{T}^T\mathbf{X}\\
\mathbf{u} &= \mathbf{T}^T\mathbf{U}
\end{aligned} \tag{6}$$

where a description of above position and displacement vectors can be given by

$$\begin{aligned}
&\mathbf{X} = [x \quad y \quad z]^T, \quad \mathbf{U} = [U \quad V \quad W]^T\\
&\mathbf{x} = [r \quad s \quad t]^T, \quad \mathbf{u} = [u \quad v \quad w]^T
\end{aligned} \tag{7}$$

The transformation matrix **T** between the local and the global coordinates is

$$\mathbf{T} = \begin{bmatrix} \mathbf{V}_r & \mathbf{V}_s & \mathbf{V}_t \end{bmatrix} \tag{8}$$

where $\mathbf{V}_r$, $\mathbf{V}_s$, $\mathbf{V}_t$ are the local coordinate vectors. It is important to note that $\mathbf{V}_t$ is normal to the mid-surface at the centroid of the element.

3. The Jacobian matrix

The Jacobian matrix based on the chain rule of differentiation is required to transform displacement derivatives from one system of axes to another. It is also necessary to impose the present element formulations on local orthogonal axes. The Jacobian matrix can be used to relate local orthogonal system (r,s,t) to the natural curvilinear system (ξ,η,ζ) as follows:

$$J_{ij} = \frac{\partial x_i}{\partial \xi_j} \tag{9}$$

Substituting Eqs. (6) and (8) into Eq. (9), the Jacobian matrix **J** can be expressed as

$$\mathbf{J} = \begin{bmatrix} \mathbf{V}_r^T \frac{\partial \mathbf{X}}{\partial \xi} & \mathbf{V}_s^T \frac{\partial \mathbf{X}}{\partial \xi} & \mathbf{V}_t^T \frac{\partial \mathbf{X}}{\partial \xi}\\ \mathbf{V}_r^T \frac{\partial \mathbf{X}}{\partial \eta} & \mathbf{V}_s^T \frac{\partial \mathbf{X}}{\partial \eta} & \mathbf{V}_t^T \frac{\partial \mathbf{X}}{\partial \eta}\\ \mathbf{V}_r^T \frac{\partial \mathbf{X}}{\partial \zeta} & \mathbf{V}_s^T \frac{\partial \mathbf{X}}{\partial \zeta} & \mathbf{V}_t^T \frac{\partial \mathbf{X}}{\partial \zeta} \end{bmatrix} \tag{10}$$

The component of the above Jacobian transformation matrix can be described using Eq. (1). The derivative forms are given by

$$\begin{aligned}
\frac{\partial \mathbf{X}}{\partial \xi} &= \sum_{i=1}^{8} \frac{\partial N_i}{\partial \xi}\mathbf{X}_i\\
\frac{\partial \mathbf{X}}{\partial \eta} &= \sum_{i=1}^{8} \frac{\partial N_i}{\partial \eta}\mathbf{X}_i\\
\frac{\partial \mathbf{X}}{\partial \zeta} &= \sum_{i=1}^{8} \frac{\partial N_i}{\partial \zeta}\mathbf{X}_i
\end{aligned} \tag{11}$$

It should be remarked that the Jacobian matrix in Eq. (10) reduces the computational effort and is much simpler than that proposed by Kim et al. [17], which has to be modified and neglects the high order terms of ζ. Belytschko et al. [19] were the first to suggest the way of improving the Jacobian matrix.

4. Linear strain–displacement relations

In this section, the strain–displacement relation for the present element will be presented by incorporating the commonly geometric assumptions in traditional 8-node solid element. As the material properties are defined in a local coordinate system (r, s, t), it is necessary to obtain the local physical strains as follows:

$$\begin{aligned}
\varepsilon_{rr} &= \frac{\partial u}{\partial r}\\
\varepsilon_{ss} &= \frac{\partial v}{\partial s}\\
\varepsilon_{tt} &= \frac{\partial w}{\partial t}\\
\gamma_{rs} &= \frac{\partial u}{\partial s} + \frac{\partial v}{\partial r}\\
\gamma_{rt} &= \frac{\partial u}{\partial t} + \frac{\partial w}{\partial r}\\
\gamma_{st} &= \frac{\partial v}{\partial t} + \frac{\partial w}{\partial s}
\end{aligned} \tag{12}$$

where the local strains defined above use local displacements, and the displacement derivatives with respect to local coordinate are

$$\frac{\partial}{\partial x_i} = J_{ij}^{-1}\frac{\partial}{\partial \xi_j} \tag{13}$$

5. Assumed natural strain (ANS) and enhanced assumed strain (EAS)

5.1. Assumed natural strain (ANS)

Many researchers have used both reduced integration and selective integration to overcome the locking behaviors in conventional elements. However, such methods have rank deficiency and zero energy modes. In order to overcome the transverse

shear, membrane locking problems and to keep the full integration, the assumed strain methods have been successfully used on finite element formulations. The assumed strain method in this work is used for the transverse shear strains ($\gamma_{\xi\zeta}$ and $\gamma_{\eta\zeta}$) and also for the normal thickness strain ($\gamma_{\zeta\zeta}$).

5.1.1. Assumed transverse shear strain

The assumed transverse shear strains ($\gamma_{\xi\zeta}$ and $\gamma_{\eta\zeta}$) in the natural coordinate can be calculated and interpolated at the tying points A_t, B_t, C_t and D_t located on the top and at the points A_b, B_b, C_b and D_b located on the bottom surfaces of the elements as illustrated in Fig. 2. These modified typing points are not usually conducted for the assumed natural strain (ANS) method. The detailed explanations for these typing points can be found in the many works [16,18,19–23]. However, numerical tests show that the use of the tying points on top and bottom surfaces of the elements increases the performance of the elements.

The shear strain at the sampling points can be obtained from

$$\begin{Bmatrix} \gamma_{rt} \\ \gamma_{st} \end{Bmatrix}^{A_{t,b},B_{t,b},C_{t,b},D_{t,b}} = \sum_{i=1}^{8} \begin{bmatrix} \frac{\partial N_i}{\partial t} & 0 & \frac{\partial N_i}{\partial r} \\ 0 & \frac{\partial N_i}{\partial t} & \frac{\partial N_i}{\partial s} \end{bmatrix} \begin{Bmatrix} u_i \\ v_i \\ w_i \end{Bmatrix} \tag{14}$$

where the displacement derivatives $\partial/\partial r$, $\partial/\partial s$ and $\partial/\partial t$ can be described using Eq. (13). The transverse shear strain components are converted to the natural coordinate system by the following relation:

$$\varepsilon_{mn} = \frac{\partial r^i}{\partial \xi^m} \frac{\partial r^j}{\partial \xi^n} \varepsilon_{ij} \tag{15}$$

where ε_{mn} is the strain tensor in the natural coordinate system and ε_{ij} is the strain tensor in the local coordinate system. Then, transverse shear strains of collocation points in the two coordinate systems can be expressed as follows:

$$\begin{Bmatrix} \gamma_{13} \\ \gamma_{23} \end{Bmatrix}^{A_{t,b},B_{t,b},C_{t,b},D_{t,b}} = \begin{bmatrix} J_{11}J_{33}+J_{31}J_{13} & J_{21}J_{33}+J_{31}J_{23} \\ J_{12}J_{33}+J_{32}J_{13} & J_{22}J_{33}+J_{32}J_{23} \end{bmatrix} \begin{Bmatrix} \gamma_{rt} \\ \gamma_{st} \end{Bmatrix}^{A_{t,b},B_{t,b},C_{t,b},D_{t,b}} \tag{16}$$

To avoid shear locking, the transverse shear strains are given using the interpolation functions introduced by Cardoso et al. [18] in the present element, as

$$\begin{Bmatrix} \gamma_{13} \\ \gamma_{23} \end{Bmatrix} = \frac{1}{2} \begin{bmatrix} (1+\eta)((1-\zeta)\gamma_{13}^{A_b}+(1+\zeta)\gamma_{13}^{A_t})+(1-\eta)((1-\zeta)\gamma_{13}^{C_b}+(1+\zeta)\gamma_{13}^{C_t}) \\ (1+\xi)((1-\zeta)\gamma_{23}^{D_b}+(1+\zeta)\gamma_{23}^{D_t})+(1-\xi)((1-\zeta)\gamma_{23}^{B_b}+(1+\zeta)\gamma_{23}^{B_t}) \end{bmatrix} \tag{17}$$

The relationship between the local shear strains and natural shear strains is

$$\begin{Bmatrix} \gamma_{rt} \\ \gamma_{st} \end{Bmatrix} = \begin{bmatrix} J_{11}^{-1}J_{33}^{-1}+J_{31}^{-1}J_{13}^{-1} & J_{21}^{-1}J_{33}^{-1}+J_{31}^{-1}J_{23}^{-1} \\ J_{12}^{-1}J_{33}^{-1}+J_{32}^{-1}J_{13}^{-1} & J_{22}^{-1}J_{33}^{-1}+J_{32}^{-1}J_{23}^{-1} \end{bmatrix} \begin{Bmatrix} \gamma_{13} \\ \gamma_{23} \end{Bmatrix} \tag{18}$$

where $J_{11}^{-1}, J_{12}^{-1}, \ldots, J_{33}^{-1}$ are the components of inverse Jacobian can be obtained in Eq. (10).

5.1.2. Assumed transverse normal strain

A locking effect due to artificial thickness strains has been observed by Ramm et al. in [24] for thin shell structures with bending dominated loading when using a direct interpolation of the director vector. To overcome this locking effect, an assumed natural strain of the thickness strain $\gamma_{\zeta\zeta}$ using bi-linear shape functions for 4-node shell elements has been proposed by Betsch and Stein in [25] and by Bischoff and Ramm in [26]. This efficient method is adapted for the present element, and the thickness strain is interpolated from four sampling points $L=M$, N, O, P located on the middle surface at the edges of the element as shown in Fig. 3.

The expression of the natural transverse normal strain for the mid-surface ($\zeta=0$) is

$$\varepsilon_t^L = \sum_{i=1}^{4} \begin{bmatrix} 0 & 0 & \frac{\partial N_i}{\partial t} \end{bmatrix} \begin{Bmatrix} u_i \\ v_i \\ w_i \end{Bmatrix} \tag{19}$$

The normal shear strain component is converted to the natural coordinate system by the following relation:

$$\varepsilon_{33}^L = (J_{33} \times J_{33})\varepsilon_t^L \tag{20}$$

The normal strain $\gamma_{\zeta\zeta}$ must be evaluated at these tying points and thereafter interpolated to the element's Gauss points according to the following interpolation scheme:

$$\varepsilon_{33} = \frac{1}{4}\sum_{i=1}^{4}(1+\xi_L\xi)(1+\eta_L\eta)\varepsilon_{33}^L \tag{21}$$

The corresponding local normal strain is

$$\varepsilon_t = (J_{33}^{-1} \times J_{33}^{-1})\varepsilon_{33} \tag{22}$$

5.2. Enhanced assumed strain (EAS)

In 1990, Simo and Rifai [6] introduced the enhanced strain formulation where usual displacement-based strain field is enhanced with a set of internal variables to overcome locking behavior and improve the response of traditional elements. For this method, the strain tensor obtained from the displacement vector is enhanced with a set of internal parameters. The variational basis of the finite element method with enhanced assumed

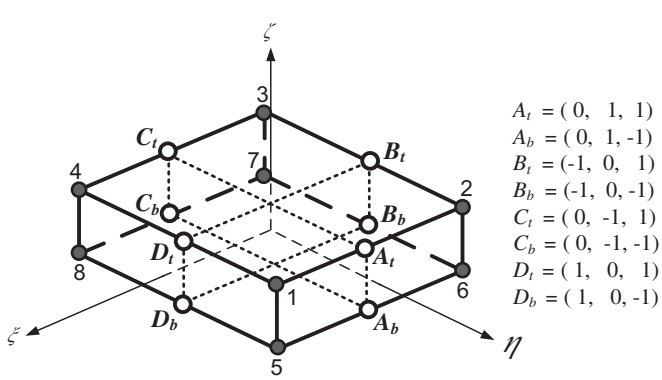

Fig. 2. Sampling points of the transverse shear strain interpolation.

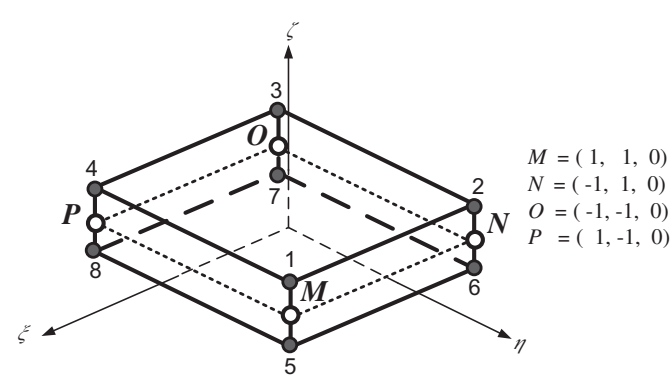

Fig. 3. Sampling points of the normal shear strain interpolation.

strain (EAS) fields is based on the principle of Hu-Washizu in the following:

$$\prod(\mathbf{u},\boldsymbol{\varepsilon},\boldsymbol{\sigma}) = \int_V \left[\frac{1}{2}\boldsymbol{\varepsilon}^T\mathbf{C}\boldsymbol{\varepsilon} - \boldsymbol{\sigma}^T(\boldsymbol{\varepsilon}-\boldsymbol{\varepsilon}^c)\right]\mathrm{d}V - \int_V \mathbf{u}^T\mathbf{b}\,\mathrm{d}V - \int_S \mathbf{u}^T\mathbf{t}\,\mathrm{d}S \tag{23}$$

where displacement field $\mathbf{u}$, strains $\boldsymbol{\varepsilon}$ and stresses $\boldsymbol{\sigma}$ are the free variables, $\mathbf{C}$ stands for the material stiffness matrix. Prescribed forces are also marked in bold, namely body force $\mathbf{b}$, and surface traction $\mathbf{t}$. In EAS method, the strain is approximated by two fields, such as the compatible and enhanced one via equation as follows:

$$\boldsymbol{\varepsilon} = \boldsymbol{\varepsilon}^c + \tilde{\boldsymbol{\varepsilon}} = \mathbf{B}\mathbf{u} + \mathbf{M}\boldsymbol{\alpha} \tag{24}$$

where $\boldsymbol{\varepsilon}^c$ is the compatible strain field, $\tilde{\boldsymbol{\varepsilon}}$ denotes the enhanced part of the strain, $\mathbf{B}$ is the standard strain operator, $\mathbf{M}$ is the interpolation operator for the additional strain field, which may be discontinuous across element edges, and $\boldsymbol{\alpha}$ is the vector of the internal strain parameters corresponding to the enhanced strain. By substituting Eq. (24) into Eq. (23) with three-field functional, we obtain

$$\prod(\mathbf{u},\tilde{\boldsymbol{\varepsilon}},\boldsymbol{\sigma}) = \int_V \left[\frac{1}{2}(\mathbf{B}\mathbf{u}+\tilde{\boldsymbol{\varepsilon}})^T\mathbf{C}(\mathbf{B}\mathbf{u}+\tilde{\boldsymbol{\varepsilon}}) - \boldsymbol{\sigma}^T\tilde{\boldsymbol{\varepsilon}}\right]\mathrm{d}V - \int_V \mathbf{u}^T\mathbf{b}\,\mathrm{d}V - \int_S \mathbf{u}^T\mathbf{t}\,\mathrm{d}S \tag{25}$$

In order to eliminate the statically admissible stress field from functional, the following condition has to be satisfied:

$$\int_V \boldsymbol{\sigma}^T\tilde{\boldsymbol{\varepsilon}}\,\mathrm{d}V = 0 \tag{26}$$

The enhanced assumed strain, defined in the global coordinate, is interpolated according to Eq. (24):

$$\tilde{\boldsymbol{\varepsilon}} = \mathbf{M}\boldsymbol{\alpha}$$

$$\mathbf{M} = \frac{\det\mathbf{J}_0}{\det\mathbf{J}}\mathbf{T}_0^{-T}\mathbf{M}_\xi \tag{27}$$

where det $\mathbf{J}$ denotes the determinant of the Jacobian matrix $\mathbf{J}$, det $\mathbf{J}_0$ is the determinant of the Jacobian matrix $\mathbf{J}_0 = \mathbf{J}|_{\xi=\eta=\zeta=0}$ at the element centroid in the natural coordinate and $\mathbf{T}_0^{-T}$ maps the polynomial shape functions of $\mathbf{M}_\xi$, defined in the natural coordinate into the global coordinate as follows:

$$\mathbf{T}_0 = \begin{bmatrix} J_{11}^2 & J_{21}^2 & J_{31}^2 & 2J_{11}J_{21} & 2J_{11}J_{31} & 2J_{21}J_{31} \\ J_{12}^2 & J_{22}^2 & J_{32}^2 & 2J_{12}J_{22} & 2J_{12}J_{32} & 2J_{22}J_{32} \\ J_{13}^2 & J_{23}^2 & J_{33}^2 & 2J_{13}J_{23} & 2J_{13}J_{33} & 2J_{23}J_{33} \\ J_{11}J_{12} & J_{21}J_{22} & J_{31}J_{32} & J_{11}J_{22}+J_{21}J_{12} & J_{11}J_{32}+J_{31}J_{12} & J_{21}J_{32}+J_{31}J_{22} \\ J_{11}J_{13} & J_{21}J_{23} & J_{31}J_{33} & J_{11}J_{23}+J_{21}J_{13} & J_{11}J_{33}+J_{31}J_{13} & J_{21}J_{33}+J_{31}J_{23} \\ J_{12}J_{13} & J_{22}J_{23} & J_{32}J_{33} & J_{12}J_{23}+J_{22}J_{13} & J_{12}J_{33}+J_{32}J_{13} & J_{22}J_{33}+J_{32}J_{23} \end{bmatrix} \tag{28}$$

The interpolation functions, assumed for the $\mathbf{M}_\xi$ matrix, are defined in isoparametric space. In the element formulation, the interpolations with 11 parameters are chosen as follows:

$$\mathbf{M}_\xi^{11} = \left[\begin{array}{cc|cccc|cc|ccc} \xi & 0 & 0 & 0 & 0 & 0 & 0 & 0 & \xi\eta & 0 & 0 \\ 0 & \eta & 0 & 0 & 0 & 0 & 0 & 0 & 0 & \xi\eta & 0 \\ 0 & 0 & 0 & 0 & 0 & 0 & 0 & 0 & 0 & 0 & 0 \\ 0 & 0 & \xi & \eta & 0 & 0 & 0 & 0 & 0 & 0 & \xi\eta \\ 0 & 0 & 0 & 0 & \xi & 0 & \xi\eta & 0 & 0 & 0 & 0 \\ 0 & 0 & 0 & 0 & 0 & \eta & 0 & \xi\eta & 0 & 0 & 0 \end{array}\right] \tag{29}$$

After intensive numerical tests, we found out that the use of 11 enhanced strain parameters is good enough to perform accurate results for analyzing thin-walled structures. Even though more terms of enhanced strain parameters are used in the element formulation, the element performance yields only minor improvements.

6. Convected displacements

Although thin structures can undergo large deflection with only small deformation, their rigid body motion constitutes the major part of the overall motion of the structure, which dominates the response. Therefore, non-linear analysis can be based on small strain, but finite rotation and displacements. In non-linear analysis, as in the case of linear analysis, it is essential to present rigid body motion accurately, irrespective of the geometry of the element. Obviously, failure to represent rigid body motion exactly will lead to self-straining and convergence towards the wrong solution [27–31].

For clarity, the motion is depicted using two points on a square object in the two-dimensional spaces r, s, but the physics of the actual three-dimensional motion is obtained by treating various vectors shown in the following figure.

The decomposition of the overall motion of the present element is illustrated in Fig. 4, and the physics of the actual three-dimensional motion is obtained by treating the various vectors. The portion of the reference line lying between the reference point p_i at the mid-surface of an element and the point at a typical node p_j is shown in three different configurations ${}^0C$, ${}^1C$, ${}^2C$ and C. In this way, the total motion is decomposed in accordance with the polar decomposition. It is clear that the transformation from the initial state (r,s,t) to the current state (r',s',t') must be considered in two stages, each involving a rigid Euler rotation. Therefore, the familiar direction cosine transformation can be applied as follows:

$${}^2\mathbf{x} = \mathbf{R}(\theta){}^0\mathbf{x} \tag{30}$$

where $\mathbf{R}(\theta)$, which is the orthogonal rotation matrix, corresponds to the rigid body rotation of the center of an element can be defined by

$$\mathbf{R}(\theta) = \begin{bmatrix} \mathbf{V}_{r'}^T\mathbf{V}_r & \mathbf{V}_{r'}^T\mathbf{V}_s & \mathbf{V}_{r'}^T\mathbf{V}_t \\ \mathbf{V}_{s'}^T\mathbf{V}_r & \mathbf{V}_{s'}^T\mathbf{V}_s & \mathbf{V}_{s'}^T\mathbf{V}_t \\ \mathbf{V}_{t'}^T\mathbf{V}_r & \mathbf{V}_{t'}^T\mathbf{V}_s & \mathbf{V}_{t'}^T\mathbf{V}_t \end{bmatrix} \tag{31}$$

Assuming that the current position vectors $(\mathbf{p}_i,\mathbf{p}_j)$ and the current displacement vector $(\mathbf{u}_i)$ at any node i are known. Then,

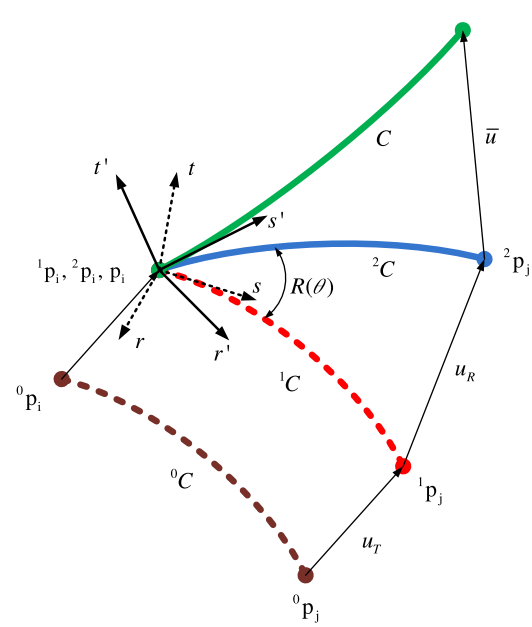

Fig. 4. Decomposition of the motion on the mid-surface of the present element.

the determination of the initial coordinates $(\mathbf{p}_i^0, \mathbf{p}_j^0)$ can be calculated:

$$\mathbf{p}_i^0 = \mathbf{p}_i - \mathbf{u}_i \tag{32}$$

with the purpose of calculating the pure deformation, the following vectors are introduced:

$$^0\mathbf{x} = {}^0\mathbf{p}_j - {}^0\mathbf{p}_i \tag{33}$$

$$\mathbf{x} = \mathbf{p}_j - \mathbf{p}_i \tag{34}$$

Substituting Eq. (33) into Eq. (30):

$$^2\mathbf{x} = \mathbf{R}(\theta)(\mathbf{p}_j^0 - \mathbf{p}_i^0) \tag{35}$$

The convected displacement at any node i is defined as the pure deformation components that remain after the removal of rigid body motion working from the initial configuration to the current configuration in Fig. 4 and can be written

$$\overline{\mathbf{u}} = \mathbf{x} - {}^2\mathbf{x} = (\mathbf{p}_j - \mathbf{p}_i) - \mathbf{R}(\theta)({}^0\mathbf{p}_j - {}^0\mathbf{p}_i) \tag{36}$$

Therefore, the above formulations are adequate to derive the convected displacement of the element formulations without violating rigid body motion criteria.

7. Non-linear strain–displacement relation and geometric stiffness matrix

In general, the non-linear parts of the strains can be written

$$\begin{aligned}
\Xi_r &= \frac{1}{2}\left[\left(\frac{\partial \overline{u}}{\partial r}\right)^2 + \left(\frac{\partial \overline{v}}{\partial r}\right)^2 + \left(\frac{\partial \overline{w}}{\partial r}\right)^2\right] \\
\Xi_s &= \frac{1}{2}\left[\left(\frac{\partial \overline{u}}{\partial s}\right)^2 + \left(\frac{\partial \overline{v}}{\partial s}\right)^2 + \left(\frac{\partial \overline{w}}{\partial s}\right)^2\right] \\
\Xi_t &= \frac{1}{2}\left[\left(\frac{\partial \overline{u}}{\partial t}\right)^2 + \left(\frac{\partial \overline{v}}{\partial t}\right)^2 + \left(\frac{\partial \overline{w}}{\partial t}\right)^2\right] \\
\Xi_{rs} &= \frac{\partial \overline{u}}{\partial r}\left(\frac{\partial \overline{u}}{\partial s}\right) + \frac{\partial \overline{v}}{\partial r}\left(\frac{\partial \overline{v}}{\partial s}\right) + \frac{\partial \overline{w}}{\partial r}\left(\frac{\partial \overline{w}}{\partial s}\right) \\
\Xi_{rt} &= \frac{\partial \overline{u}}{\partial r}\left(\frac{\partial \overline{u}}{\partial t}\right) + \frac{\partial \overline{v}}{\partial r}\left(\frac{\partial \overline{v}}{\partial t}\right) + \frac{\partial \overline{w}}{\partial r}\left(\frac{\partial \overline{w}}{\partial t}\right) \\
\Xi_{st} &= \frac{\partial \overline{u}}{\partial s}\left(\frac{\partial \overline{u}}{\partial t}\right) + \frac{\partial \overline{v}}{\partial s}\left(\frac{\partial \overline{v}}{\partial t}\right) + \frac{\partial \overline{w}}{\partial s}\left(\frac{\partial \overline{w}}{\partial t}\right)
\end{aligned} \tag{37}$$

The geometric nonlinearity arises from both the quadratic terms of the Green strain tensor and the kinematic relation themselves. The virtual work equation based on the updated Lagrangian description can be obtained as

$$\begin{aligned}
\int_V C_{ijkl}\,\mathrm{d}\varepsilon_{ij}\delta(\mathrm{d}\varepsilon_{ij})\mathrm{d}V + \int_V \tilde{\sigma}_{ij}\delta(\mathrm{d}\Xi_{ij})\mathrm{d}V &= \int_V F_{Bi}\delta(\mathrm{d}u_i)\mathrm{d}V \\
+ \int_A T_i\delta(\mathrm{d}u_i)\mathrm{d}A - \int_V \tilde{\sigma}_{ij}\delta(\mathrm{d}\varepsilon_{ij})\mathrm{d}V
\end{aligned} \tag{38}$$

To get the geometric stiffness, the matrix form for the second term in the left hand side of Eq. (38) is considered:

$$\begin{aligned}
\int_V \tilde{\sigma}_{ij}\delta(\mathrm{d}\Xi_{ij})\mathrm{d}V &= \int_V \delta\,\mathrm{d}\overline{\mathbf{u}}^T\mathbf{B}_{NL}^T\tilde{\boldsymbol{\sigma}}\mathbf{B}_{NL}\,\mathrm{d}\overline{\mathbf{u}}\,\mathrm{d}V \\
&= \delta\,\mathrm{d}\overline{\mathbf{u}}^T\int_V \mathbf{B}_{NL}^T\tilde{\boldsymbol{\sigma}}\mathbf{B}_{NL}\,\mathrm{d}V\,\mathrm{d}\overline{\mathbf{u}} \\
&= \delta\,\mathrm{d}\overline{\mathbf{u}}^T[\mathbf{K}_G]\mathrm{d}\overline{\mathbf{u}}
\end{aligned} \tag{39}$$

where $\overline{\mathbf{u}} = \left[\overline{u}_1\overline{v}_1\overline{w}_1 \cdots \overline{u}_8\overline{v}_8\overline{w}_8\right]^T$ are the nodal displacement fields. In this case, the geometric stiffness matrix $\mathbf{K}_G$ for the present element is expressed as

$$\mathbf{K}_{NL} = \int_V \mathbf{B}_{NL}^T\tilde{\boldsymbol{\sigma}}\mathbf{B}_{NL}\,\mathrm{d}V = \int_{-1}^{1}\int_{-1}^{1}\int_{-1}^{1}\mathbf{B}_{NL}^T\tilde{\boldsymbol{\sigma}}\mathbf{B}_{NL}|\mathbf{J}|\,\mathrm{d}\xi\,\mathrm{d}\eta\,\mathrm{d}\zeta \tag{40}$$

where the strain–displacement matrix $\mathbf{B}_{NL}$ and the stress matrix $\tilde{\boldsymbol{\sigma}}$ from Eq. (40) is also shown in Appendix A.

8. Constitutive relation

The continuum formulation is valid for any material constitutive law in which the stress $\boldsymbol{\sigma}$ is the function of the strain $\boldsymbol{\varepsilon}$. As the material properties of the present element is defined in a local coordinate system, all of the displacements, strains and stresses have to be considered in the same coordinate system. In addition, the element formulation here implies degenerating three-dimensional continuum to fit to thin-walled and shell applications by employing plane stress condition as follows:

$$\begin{aligned}
\boldsymbol{\sigma} &= \mathbf{C}\boldsymbol{\varepsilon} \\
\boldsymbol{\sigma} &= \left[\sigma_r \quad \sigma_s \quad \sigma_t \quad \sigma_{rs} \quad \sigma_{rt} \quad \sigma_{st}\right]^T \\
\boldsymbol{\varepsilon} &= \left[\varepsilon_r \quad \varepsilon_s \quad \varepsilon_t \quad \varepsilon_{rs} \quad \varepsilon_{rt} \quad \varepsilon_{st}\right]^T
\end{aligned} \tag{41}$$

The elastic plane-stress constitutive equation is given in the form:

$$\mathbf{C} = \begin{bmatrix} \lambda+2\mu & \lambda & 0 & 0 & 0 & 0 \\ \lambda & \lambda+2\mu & 0 & 0 & 0 & 0 \\ 0 & 0 & E & 0 & 0 & 0 \\ 0 & 0 & 0 & \mu & 0 & 0 \\ 0 & 0 & 0 & 0 & \mu & 0 \\ 0 & 0 & 0 & 0 & 0 & \mu \end{bmatrix} \tag{42}$$

where $\lambda = Ev/1-v^2$, $\mu = E/2(1+v)$, E is Young's Modulus and v is Poisson's ratio.

9. Finite element formulation

According to the weak form based on the well-known Hu–Washizu variational principle in Eq. (25), the linear equilibrium equations can be written in a form of matrix partition as

$$\begin{bmatrix} \mathbf{K}_{uu} & \mathbf{K}_{u\alpha} \\ \mathbf{K}_{\alpha u} & \mathbf{K}_{\alpha\alpha} \end{bmatrix}\begin{Bmatrix} \mathbf{u} \\ \boldsymbol{\alpha} \end{Bmatrix} = \begin{Bmatrix} \mathbf{F}^{ext} \\ 0 \end{Bmatrix} \tag{43}$$

The parameter $\boldsymbol{\alpha}$ can be eliminated by static condensation on element level. The condensed stiffness can be obtained as

$$\mathbf{K}_e^* = \mathbf{K}_{uu} - \mathbf{K}_{u\alpha}\mathbf{K}_{\alpha\alpha}^{-1}\mathbf{K}_{\alpha u} \tag{44}$$

Let

$$\tilde{\mathbf{u}} = \mathbf{T}_G^T\tilde{\mathbf{U}} \tag{45}$$

where $\tilde{\mathbf{U}}$ is the nodal displacement vector in the global coordinate. $\tilde{\mathbf{u}}$ is the nodal displacement vector in the local coordinate and the transformation matrix $\mathbf{T}_G$ is given in Appendix A. The element stiffness and force matrix can be obtained in the global coordinate as

$$\mathbf{K}_e = \mathbf{T}_G\mathbf{K}_e^*\mathbf{T}_G^T \tag{46}$$

$$\mathbf{F}_e = \mathbf{T}_G\mathbf{F}^{ext} \tag{47}$$

The nodal displacements $\tilde{\mathbf{u}}$ can be obtained by solving the following equation:

$$\sum_{e=1}^{N}(\mathbf{K}_e)\tilde{\mathbf{u}} = \sum_{e=1}^{N}(\mathbf{F}_e) \tag{48}$$

For the non-linear equations, since the formulation is based on the Updated Lagrangian method, all displacements in the following expressions are in incremental form as follows:

$$\begin{bmatrix} \mathbf{K}_{uu} & \mathbf{K}_{u\alpha} \\ \mathbf{K}_{\alpha u} & \mathbf{K}_{\alpha\alpha} \end{bmatrix}\begin{Bmatrix} \Delta\mathbf{u} \\ \Delta\boldsymbol{\alpha} \end{Bmatrix} = \begin{Bmatrix} \mathbf{F}^{ext} - \mathbf{F}^{\mathrm{int}} \\ 0 - \mathbf{h}_e \end{Bmatrix} \tag{49}$$

After eliminating the parameter $\Delta\boldsymbol{\alpha}$, the condensed force and stiffness can be derived as

$$\mathbf{F}_e^{\text{int}*} = \mathbf{F}^{\text{int}} + \mathbf{K}_{u\alpha}\mathbf{K}_{\alpha\alpha}^{-1}\mathbf{h}_e \tag{50}$$

$$\mathbf{K}_e^* = \mathbf{K}_{uu} - \mathbf{K}_{u\alpha}\mathbf{K}_{\alpha\alpha}^{-1}\mathbf{K}_{\alpha u} \tag{51}$$

All the matrices can be transformed to the global coordinate as

$$\mathbf{K}_e = \mathbf{T}_G\mathbf{K}_e^*\mathbf{T}_G^T \tag{52}$$

$$\mathbf{F}_e = \mathbf{T}_G\mathbf{F}^{ext} \tag{53}$$

$$\mathbf{F}_e^{int} = \mathbf{T}_G\mathbf{F}_e^{int*} \tag{54}$$

The incrementally nodal displacements can be calculated:

$$\sum_{e=1}^{N}(\mathbf{K}_e)\Delta\tilde{\mathbf{u}} = \sum_{e=1}^{N}(\mathbf{F}_e) - \sum_{e=1}^{N}(\mathbf{F}_e^{int}) \tag{55}$$

where all of the stiffness matrices and the force matrices are described as

$$\begin{aligned}
\mathbf{K}_{uu} &= \int_V \mathbf{B}^T\mathbf{C}\mathbf{B}\,\mathrm{d}V = \int_{-1}^{1}\int_{-1}^{1}\int_{-1}^{1}\mathbf{B}^T\mathbf{C}\mathbf{B}|\mathbf{J}|\,\mathrm{d}\xi\,\mathrm{d}\eta\,\mathrm{d}\zeta\\
\mathbf{K}_{u\alpha} &= \int_V \mathbf{B}^T\mathbf{C}\mathbf{M}\,\mathrm{d}V = \int_{-1}^{1}\int_{-1}^{1}\int_{-1}^{1}\mathbf{B}^T\mathbf{C}\mathbf{M}|\mathbf{J}|\,\mathrm{d}\xi\,\mathrm{d}\eta\,\mathrm{d}\zeta\\
\mathbf{K}_{\alpha u} &= \int_V \mathbf{B}^T\mathbf{C}\mathbf{B}\,\mathrm{d}V = \int_{-1}^{1}\int_{-1}^{1}\int_{-1}^{1}\mathbf{M}^T\mathbf{C}\mathbf{B}|\mathbf{J}|\,\mathrm{d}\xi\,\mathrm{d}\eta\,\mathrm{d}\zeta\\
\mathbf{K}_{\alpha\alpha} &= \int_V \mathbf{M}^T\mathbf{C}\mathbf{M}\,\mathrm{d}V = \int_{-1}^{1}\int_{-1}^{1}\int_{-1}^{1}\mathbf{M}^T\mathbf{C}\mathbf{M}|\mathbf{J}|\,\mathrm{d}\xi\,\mathrm{d}\eta\,\mathrm{d}\zeta\\
\mathbf{F}^{\text{int}} &= \int_V \mathbf{B}^T\boldsymbol{\sigma}\,\mathrm{d}V = \int_{-1}^{1}\int_{-1}^{1}\int_{-1}^{1}\mathbf{B}^T\boldsymbol{\sigma}|\mathbf{J}|\,\mathrm{d}\xi\,\mathrm{d}\eta\,\mathrm{d}\zeta\\
\mathbf{h}_e &= -\int_V \mathbf{M}^T\boldsymbol{\sigma}\,\mathrm{d}V = \int_{-1}^{1}\int_{-1}^{1}\int_{-1}^{1}\mathbf{M}^T\boldsymbol{\sigma}|\mathbf{J}|\,\mathrm{d}\xi\,\mathrm{d}\eta\,\mathrm{d}\zeta
\end{aligned} \tag{56}$$

where the matrix **B** is the compatible strain–displacement relation matrix. **M** is the interpolation operator for the additional strain field and **C** is the material stiffness matrix. The implementation of the present element XSOLID86 is straightforward and follows directly from Eq. (48) for the linear system and from Eq. (55) for the non-linear system.

10. Numerical examples

The finite element package FINAS was developed in Imperial College, London, for non-linear analysis of thin-walled structures in a UNIX environment. At present, XFINAS (an extended version of FINAS) for the general non-linear dynamic analysis has been developed in AIT (Asian Institute of Technology, Bangkok). The present co-rotational 8-node degenerated thin-walled element, named XSOLID86, is implemented in the XFINAS. Several linear and non-linear problems have been chosen in order to validate the performance of the present element in a wide range of situations. Firstly, several linear elastic tests are performed. After that, various classical problems with geometric non-linearities are presented. The results are compared with analytical solutions and results obtained from other elements. Most of the results presented here are normalized with the analytical solutions. A list of elements used for comparison with the proposed elements is outlined in Table 1.

10.1. Linear problems

The usefulness of the following tests lies in the inspection of the accuracy of the proposed element in the linear case. The suitability of the present element in situations that are typically analyzed with beam, plate and shell elements is verified. Some well-known solutions, from numerical and analytical sources, are used in the comparisons.

Table 1
List of the elements used for comparison.

Name	Element descriptions
MITC4	4-Node fully integrated shell element derived by Dvorkin and Bathe [32] The shear strains are determined using the assumed strain interpolation
Simo et al.	Bi-linear shell with mixed formulation used for the membrane and bending stresses and full 2×2 quadrature [33]
QUAD4	Quadrilateral shell element with selective reduced integration Transverse shear uses string-net approximation and shear flexibility [34]
QPH	Quadrilateral shell element with physical hourglass control by Belytschko and Leviathan [35]
RESS	Reduced enhanced solid-shell by Alves de Sousa et al. [36,37]
SOLID-EAS24	8-Node solid element with EAS24 terms following Appendix A
XSOLID85	8-Node solid-shell element with ANS proposed by Kim [17]
XSOLID86	Co-rotational 8-node degenerated thin-walled element with ANS and EAS

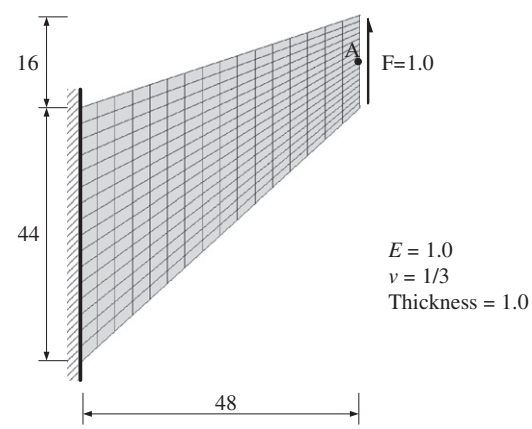

Fig. 5. Cook's membrane problem.

Table 2
The results of cook's membrane problem.

Mesh	Normalized solutions			
	XSOLID86	XSOLID85	SOLID-EAS24	Simo et al.
$2\times2\times1$	0.898	0.898	0.871	0.883
$4\times4\times1$	0.987	0.987	0.971	0.963
$8\times8\times1$	1.023	1.023	1.014	0.991
$16\times16\times1$	1.039	1.039	1.035	0.999

10.1.1. Cook's membrane problem

This example is performed to evaluate performances of the present element XSOLID86 in modeling the membrane deformation. The Cook's membrane problem shown in Fig. 5 is presented to test the sensitivity due to geometric distortion of the current element for a flat surface. The normalized displacement under load is presented in Table 2. When the structure is modeled using coarse meshes, the present element shows slightly more accuracy than the solid element SOLID-EAS24 and the shell element proposed by Simo et al. [33]. However, it tends to be slightly soft when finer meshes are used. For this problem, the present element do not show any in-plane membrane locking problems because 11 enhanced assumed strain (EAS) parameters included in the element formulation improve the element performance.

10.1.2. Bending of rectangular plate problem

A clamped square and rectangular plate subjected to a concentrated load at the center is analyzed to test shear locking by changing the aspect ratios. The problem description is shown in Fig. 6, and the convergence curves are shown in Fig. 7. The comparison results in Table 3 are normalized with the analytical solution from Timoshenko and Woinowsky-Krieger [38]. Two aspect ratios of $b/a=1$ and 5 were considered, and a quarter was modeled due to symmetry.

(a) *For the case of $b/a=1.0$*:
The reference vertical deflection at the center of the plate is 5.60×10^6. In Table 3, the numerical results obtained using different types of existing elements are listed.

(b) *For the case of $b/a=5.0$*:
The reference deflection at the center is 7.23×10^6. In Table 3, the numerical results obtained using different types of elements are listed.

The results of the clamped square plate obtained with the present element XSOLID86 and the reference results from solid-shell element XSOLID85, the solid element SOLID-EAS24 and the shell element QUAD4 are all presented in Fig. 7(a). There is a good agreement between the results obtained from the present element and the references for this case. Moreover, it is noticeable that the shell element QUAD4 presents apparently fast convergence, but in fact it converges to a higher value than theoretical solution.

For the clamped rectangular plate, the results obtained with the present element and the same references mentioned above are all illustrated in Fig. 7(b). The present element presents a lower level of convergence when compared with the shell element QUAD4 when using coarse meshes. However, for finer meshes, the XSOLID86 element shows good agreement with other references. In addition, the present element does not show any shear locking problems because the ANS interpolation improves the behavior of the present element.

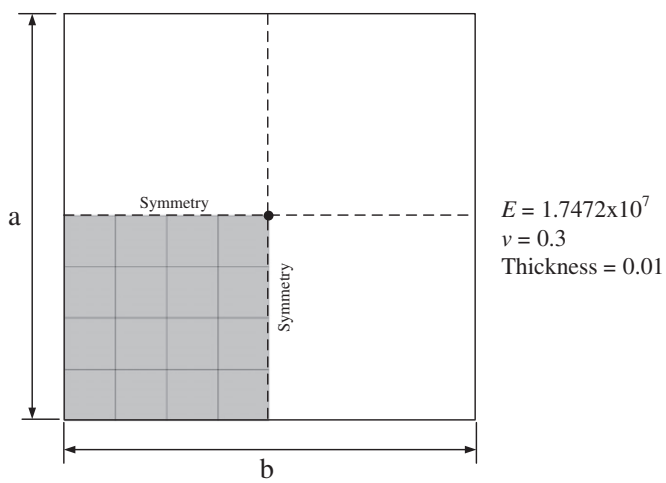

Fig. 6. Bending of clamped plate problem.

10.1.3. Curved beam problem under in-plane and out-of-plane shear

The curved beam problem was subjected to either the unit in-plane or out-of-plane shear tip force. Because there is an intrinsic mesh distortion, this problem can test the effect of slight irregularity in element geometry. The problem geometry and material properties are shown in Fig. 8; the reference result of the free end is 0.08734 for the in-plane problem and 0.5022 for the out-of-plane problem. The numerical results are listed in Table 4 and compared with the normalized results obtained by

Table 3
Normalized results for the clamped plate problem.

Mesh	Normalized solutions			
	XSOLID86	XSOLID85	SOLID-EAS24	QUAD4
(a) The case of $b/a=1.0$ ($W=5.60\times10^{-6}$)				
$2\times2\times1$	0.871	0.866	0.886	0.934
$4\times4\times1$	0.973	0.966	0.973	1.010
$6\times6\times1$	0.989	0.986	0.989	1.012
$8\times8\times1$	0.995	0.993	0.995	1.010
(b) The case of $b/a=5.0$ ($W=7.23\times10^{-6}$)				
$2\times2\times1$	0.321	0.319	0.321	0.519
$4\times4\times1$	0.850	0.826	0.850	0.863
$6\times6\times1$	0.927	0.912	0.928	0.940
$8\times8\times1$	0.957	0.947	0.957	0.972

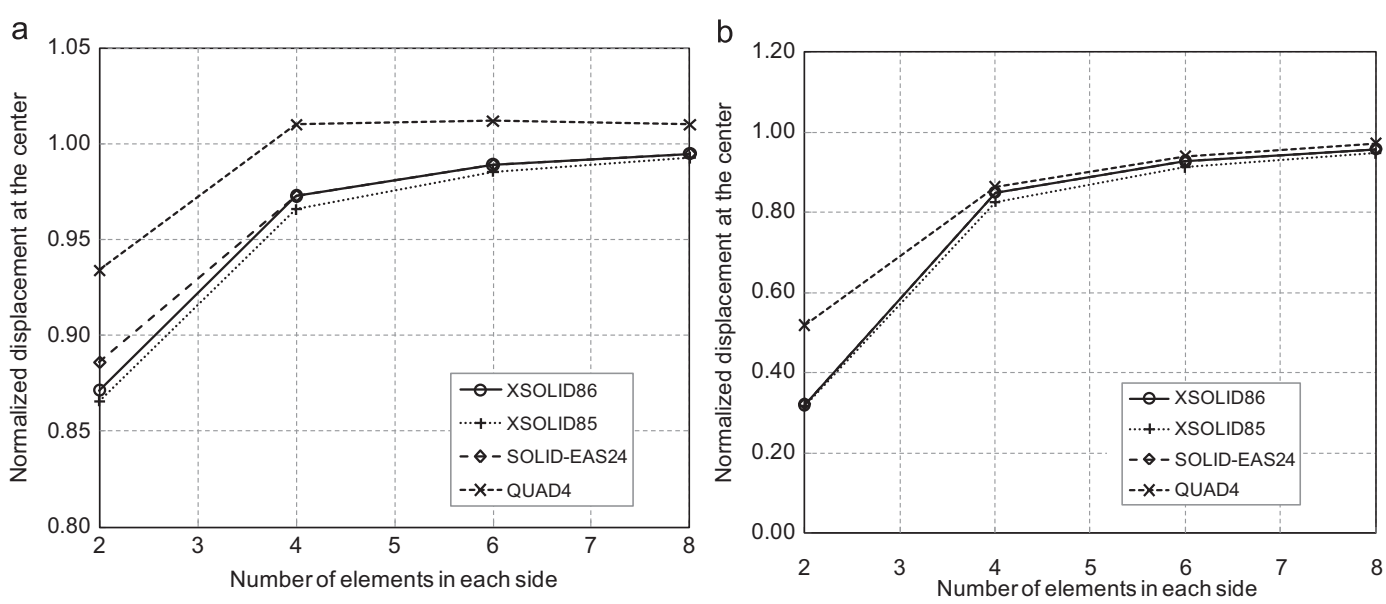

Fig. 7. The clamped plate problem: (a) case ($b/a=1.0$) and (b) case ($b/a=5.0$).

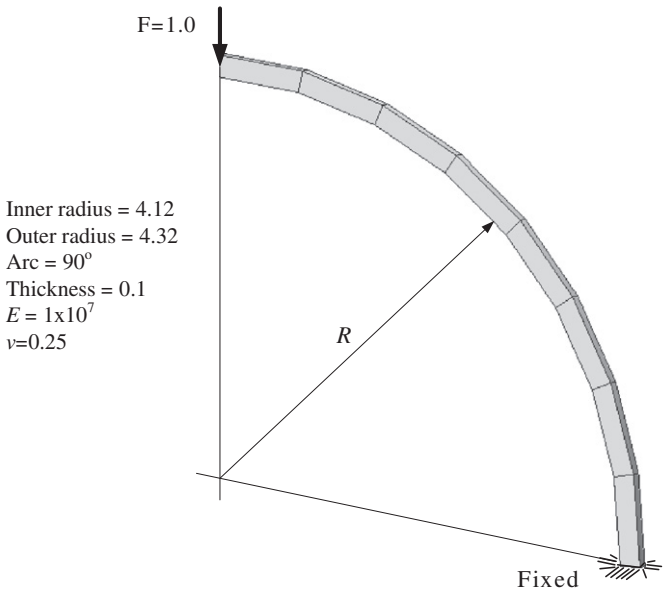

Fig. 8. Curved beam.

Table 4
Normalized results for the curved beam problem.

Mesh	Normalized solutions			
	XSOLID86	XSOLID85	SOLID-EAS24	QUAD4
In-plane shear (0.08734)				
$6\times1\times1$	0.887	0.887	0.880	0.833
$8\times1\times1$	0.968	0.968	0.964	–
$12\times1\times1$	1.003	1.003	0.999	–
Out-of-plane shear (0.5022)				
$6\times1\times1$	0.891	0.956	0.846	0.951
$8\times1\times1$	0.937	0.962	0.920	–
$12\times1\times1$	0.956	0.968	0.953	–

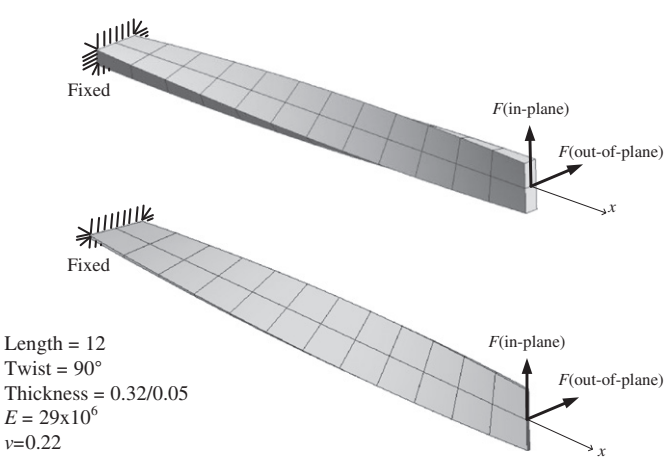

Fig. 9. Twisted beam problem.

other elements. It can be concluded that all the elements perform regularly, even for coarse meshes. The present element XSOLID86 shows accuracy compatible with the solid-shell element XSOLID85 and the solid element SOLID-EAS24. Moreover, the present element also provides convergence results for the case of in-plane shear and out-of-plane shear when the mesh requires a high aspect ratio.

Table 5
Normalized results for the twisted beam problem.

Mesh	Normalized results ($t=0.32$)				
	XSOLID86	XSOLID85	SOLID-EAS24	RESS	M-RESS
In-plane-shear (0.005424)					
$2\times12\times1$	0.992	0.997	0.998	1.088	1.002
$4\times24\times1$	1.002	1.005	1.000	0.996	1.001
$8\times48\times1$	1.004	1.005	1.001	0.997	1.000
Out-of-plane (0.0017541)					
$2\times12\times1$	0.993	0.990	0.991	0.936	1.022
$4\times24\times1$	0.995	0.998	0.997	0.979	1.006
$8\times48\times1$	0.999	1.002	0.999	0.992	1.003
Mesh	Normalized results ($t=0.05$)				
	XSOLID86	XSOLID85	SOLID-EAS24	RESS	MITC4
In-plane-shear (1.390)					
$2\times12\times1$	0.855	0.996	0.991	0.963	0.996
$4\times24\times1$	0.940	1.000	1.000	0.998	0.997
$8\times48\times1$	0.982	1.001	1.001	0.999	0.998
Out-of plane (0.3431)					
$2\times12\times1$	0.916	0.988	0.987	0.985	0.986
$4\times24\times1$	0.965	0.998	0.999	0.996	0.996
$8\times48\times1$	0.990	1.001	1.001	0.998	0.999

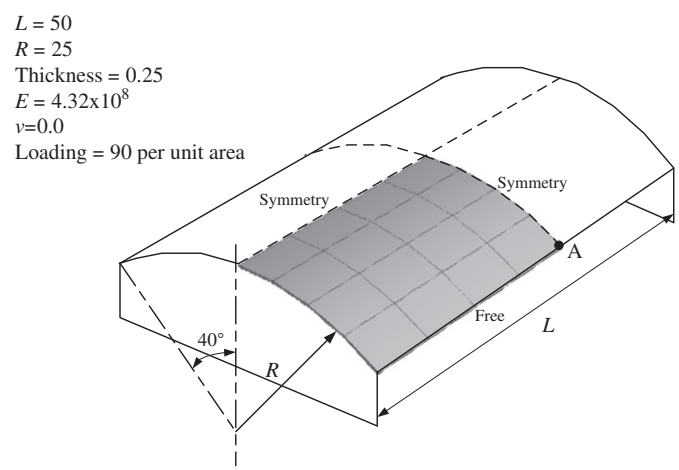

Fig. 10. Scordelis-Lo roof problem.

Table 6
Normalized results for the Scordelis-Lo roof problem.

Mesh	Normalized results					
	XSOLID86	XSOLID85	SOLID-EAS24	MITC4	QPH	Simo et al.
$4\times4\times1$	1.066	1.078	1.056	0.940	0.940	1.083
$8\times8\times1$	1.044	1.045	1.044	0.970	0.980	1.015
$16\times16\times1$	1.034	1.044	1.043	1.000	1.010	1.000

10.1.4. Twisted beam problem

The twisted beam problem is proposed to test the effect of element warping. The first version of the problem was introduced by MacNeal and Harder [34], who provided a reference solution for a thick beam. In Ref. [33] a 'more demanding version of the same problem' involving a thin twisted shell, which became a classical problem in shell elements evaluation, was adopted. A schematical representation of the modeled structure is presented in Fig. 9. The twisted beam has length $L=12$ in, width $W=1.1$ in and two thicknesses were considered: $t=0.32$ and 0.05 in for

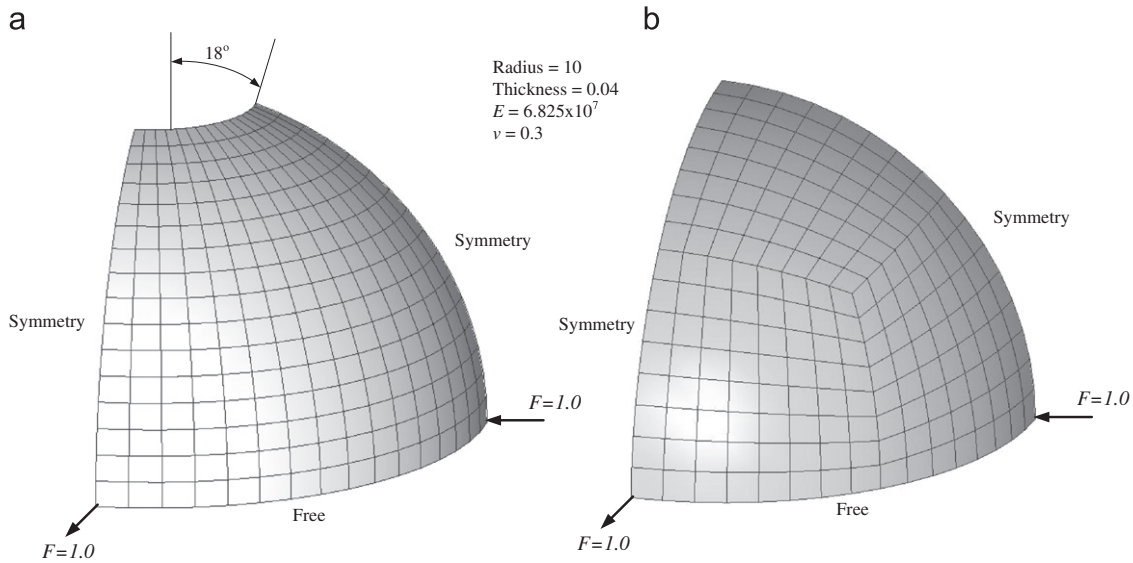

Fig. 11. (a) Hemispherical shell with 18° hole and (b) full hemispherical shell.

Table 7

(a) Normalized results for the hemispherical shell with 18° hole.

Mesh	Normalized results				
	XSOLID86	XSOLID85	SOLID-EAS24	Simo et al.	QUAD4
4 × 4 × 1	0.092	1.055	0.041	1.004	1.024
8 × 8 × 1	0.870	1.003	0.740	0.998	1.005
16 × 16 × 1	0.994	0.994	0.994	0.999	–

(b) Normalized results for the full hemispherical shell.

Mesh	Normalized results				
	XSOLID86	XSOLID85	SOLID-EAS24	QPH	MITC4
4 × 4 × 1	0.356	0.475	0.256	0.280	0.390
8 × 8 × 1	0.973	0.986	0.952	0.860	0.910
16 × 16 × 1	0.996	0.997	0.995	–	–

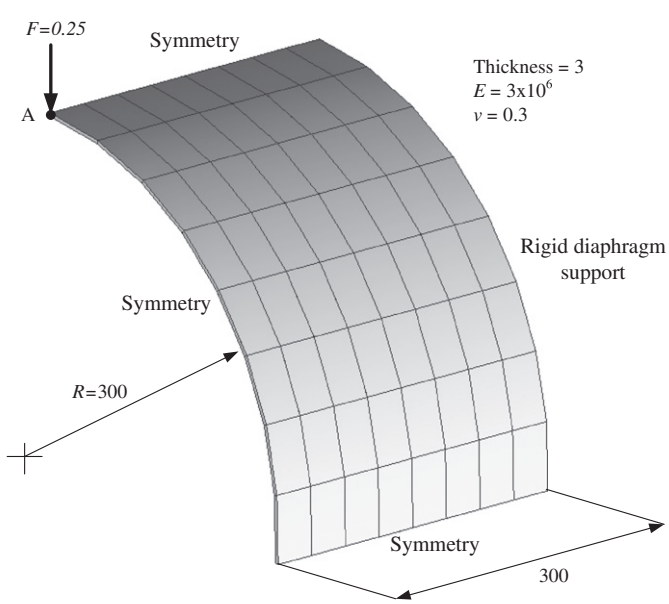

Fig. 12. Pinched cylinder with end diaphragm.

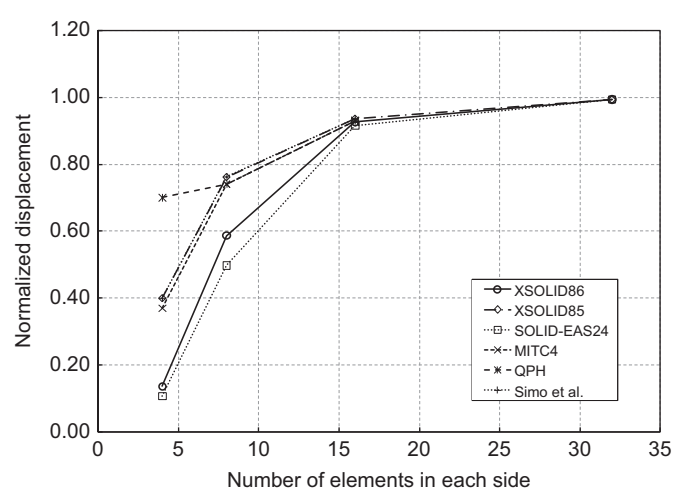

Fig. 13. Pinched cylinder with end diaphragm.

thick and thin beams, respectively. About the loading conditions, the twisted beams are investigated under in-plane and out-of-plane shear forces. The normalized displacement of the present

Table 8
Normalized results of the pinched cylinder with end diaphragm.

Mesh	Normalized results					
	XSOLID86	XSOLID85	SOLID-EAS24	MITC4	QPH	Simo et al.
$4\times4\times1$	0.137	0.399	0.107	0.370	0.700	0.399
$8\times8\times1$	0.586	0.762	0.498	0.740	0.740	0.763
$16\times16\times1$	0.926	0.936	0.916	0.930	0.930	0.935
$32\times32\times1$	0.993	0.993	0.993	–	–	–

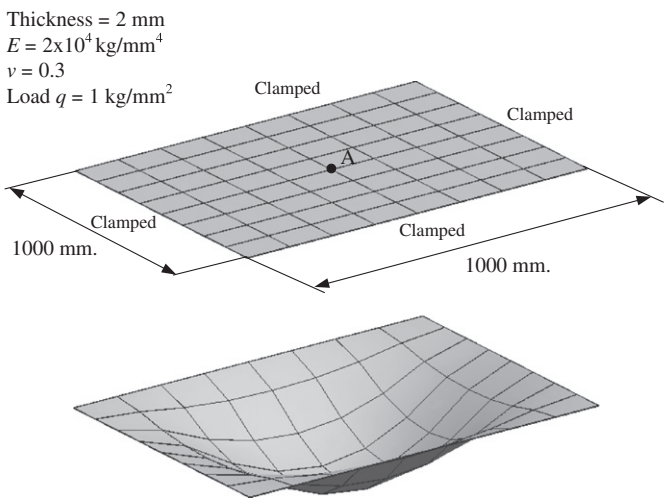

Fig. 14. Square clamped plate under uniform pressure.

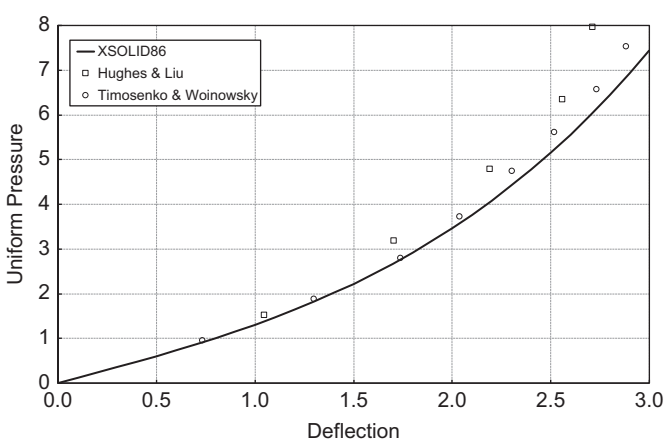

Fig. 15. Load–deflection curves at the middle point of the square clamped plate under uniform pressure.

element XSOLID86 for both cases are compared with the results obtained from the solid-shell element XSOLID85, the 8-node solid element SOLID-EAS24, the solid-shell element RESS and M-RESS [36,37] and the 4-node shell element MITC4 [32] as shown in Table 5. The present element presents good convergence ratio for the case of thick twisted beam when compared with the above references. For the thin twisted beam, when the structure is modeled using coarse meshes, the present element shows a lower level of convergence. However, the convergence of the present element can be achieved when finer meshes are used.

10.1.5. Scordelis-Lo roof problem

The Scordelis-Lo roof is a short cylinder section supported by rigid diaphragms at the edges shown in Fig. 10. Its load is only due to gravity force making it a membrane-dominated problem. Taking advantage of symmetry, only one-quarter is used in the analysis of the problem. As the membrane deformation contributes significantly to performance, this problem can be used to determine the capability of the element in modeling membrane states in curved shells. The reference solution of vertical deflection at point A is 0.3024. The normalized displacement of the present element XSOLID86 is compared with the results obtained from the solid-shell element XSOLID85, the solid element SOLID-EAS24 and the 4-node shell elements [32,33,35] as shown in Table 6. The present element shows accuracy compatible with XSOLID85 and SOLID-EAS24. However, when the results of the present element are compared with those of 4-node shell elements, it can be observed that the shell elements yield slightly better results than the present element when the mesh requires a high aspect ratio.

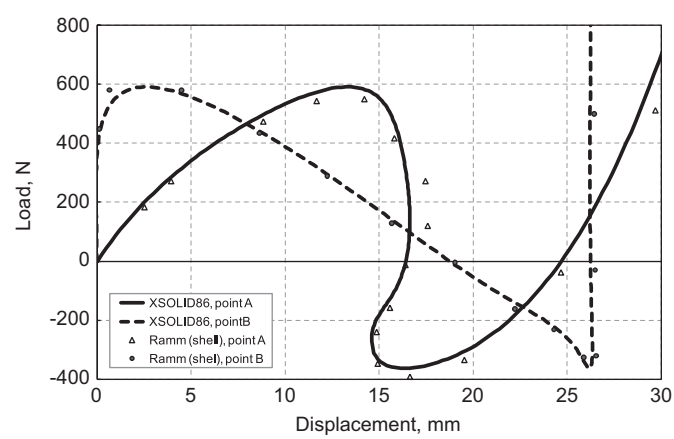

Fig. 17. Load–deflection curves at the middle point of the hinged cylindrical shell under a central point load.

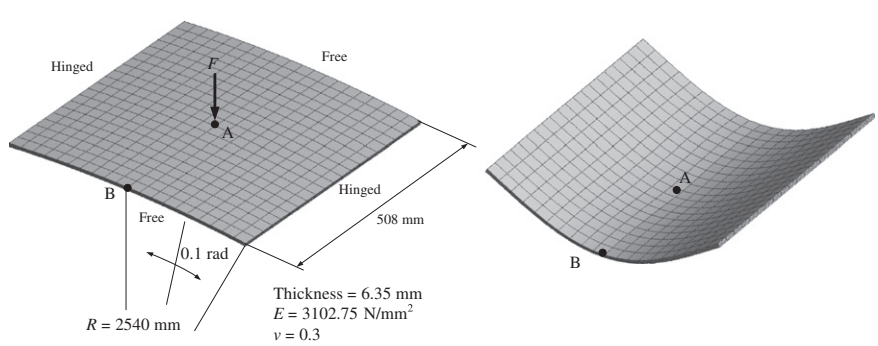

Fig. 16. Hinged cylindrical shell under a central point load.

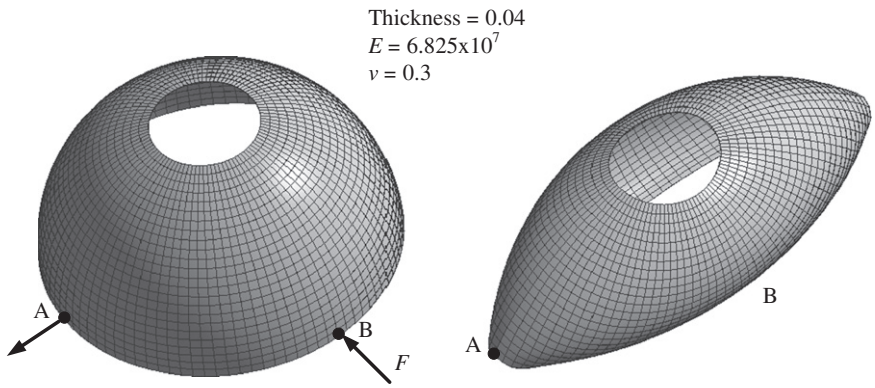

Fig. 18. Hemispherical shell loaded by pinching forces.

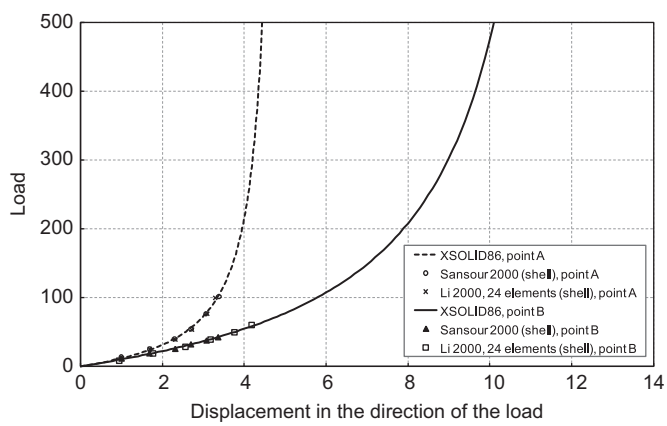

Fig. 19. Load–deflection curves at the points A and B of the hemispherical shell loaded by pinching forces.

10.1.6. Pinched hemispherical shell

Two geometries have been used for this problem: one is a hemispherical shell with an 18° hole shown in Fig. 11(a), and another is a full hemispherical shell illustrated in Fig. 11(b). Both shells have the same radius, thickness, material properties and loading conditions. The loads are two pairs of inward and outward point loads, 90° apart. The problem is modeled using only one-quarter of the hemisphere. The results for the hemispherical shell with a hole are normalized with 0.093 [33]. On the other hand, the value of the displacement at the loading point given by MacNeal and Harder [34] is 0.094. The convergence results of the present element XSOLID86 for the hemispherical shell with an 18° hole problem are compared with the references as shown in Table 7(a). When using coarse meshes, the present element shows better convergence result than the solid element SOLID-EAS24. However, for finer meshes, the present element presents the same result as the solid-shell element XSOLID85 and the solid element SOLID-EAS24, while the shell element proposed by Simo et al. [33] shows slightly better results than XSOLID86. The results of the present element for the full hemispherical shell compared with several references are illustrated in Table 7(b). The results of XSOLID86 presents more accurate convergence result than the shell element QPH and MITC4 for the $8 \times 8 \times 1$ mesh. Moreover, the present element also provides good convergence result when the mesh requires a high aspect ratio.

10.1.7. Pinched cylinder with end diaphragm

A short cylinder with rigid end diaphragms subjected to two pinching forces is analyzed as shown in Fig. 12. This is one of the most severe tests of an element's ability to model both inextensional bending and complex membrane states. Belytschko et al. [39] pointed out the difficulty in passing this test. The vertical deflection of point A was investigated, and the reference value is 1.8248×10^{-5}. The convergence rates between XSOLID86 and other references are illustrated in Fig. 13, and the results with different meshes and elements are presented in Table 8. When the results of the present element are compared with those of 4-node shell elements [32,33,35] for coarse meshes, it can be observed that the shell elements show better convergence results than the present element. Nevertheless, the present element can yield the same accurate results as other references when finer meshes are used.

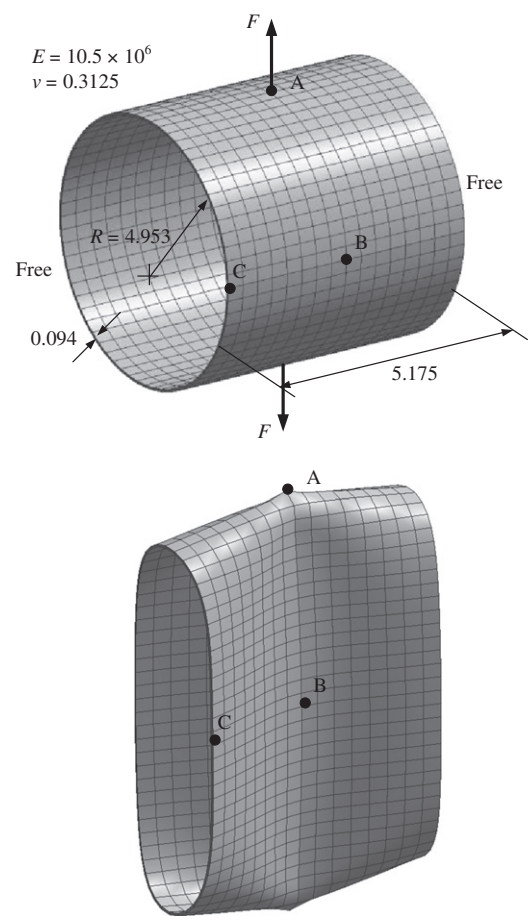

Fig. 20. Pinched cylinder with free edges.

10.2. Non-linear problems

10.2.1. Square clamped plate under uniform pressure

The result of the analysis of static non-linear problems is presented in the following example. The deflection of a square clamped plate subjected to a uniformly distributed increasing pressure was analyzed. In this problem presented in Fig. 14, an $8 \times 8 \times 1$ mesh was used to model one-quarter of the plate, and point A is monitored in terms of vertical displacement. For comparison purposes, the load–displacement curves are illustrated in Fig. 15. The curve of the present element XSOLID86 matches with that of the analytical solutions given by Timoshenko and Woinowsky-Krieger [38] and Hughes and Liu [40] during the beginning of analysis, while the load–displacement curve of the present element shows a slightly more soft behavior during the end of analysis. However, the present element presents the same tendency of the load–displacement curve as other references.

10.2.2. Hinged cylindrical shell under a central point load

This example constitutes a difficult test for finite element formulations, combining bending and membrane effects. Additionally, the test has been considered by Sabir and Lock [41] and latter by Ramm [42]. The snap through behavior of a cylindrical shell subjected to a point load at the center was analyzed, and the thickness used is 6.35 mm. The cylindrical shell is simply supported along the longitudinal boundaries but unsupported along the curved edges. The geometry, mesh and boundary conditions for the model are presented in Fig. 16. Only one-quarter of the problem was modeled using a $10 \times 10 \times 1$ mesh size. A comparison, in terms of load–displacement curves for points A and B, between the present formulation and the reference is presented in Fig. 17. The present element XSOLID86 shows good agreement with the shell element [42]. In addition, it is worth to remark that co-rotational formulation, which is included in the element formulation, improves the behavior of the present element in solving geometrically non-linear problems.

10.2.3. Hemispherical shell loaded by pinching forces

This example is a non-linear counterpart of the linear elastic open hemisphere example illustrated in Fig. 18. The shell suffers large displacements but strains and rotations are relatively small. The test is also very popular and has been studied in Refs. [43,44,46]. The non-linear version of this problem is more difficult to fully demonstrate that the formulation can undergo large displacements. The nodes A and B identified in the figure are monitored in terms of absolute radial displacement. The material is considered elastic with an elasticity modulus $E = 6.825 \times 10^7$ and a Poisson coefficient of $\nu = 0.3$. The radius is 10 consistent units and the thickness value is 0.04. Symmetry conditions with $24 \times 24 \times 1$ meshes are used in this example. The load–deflection curves for points A and B are depicted in Fig. 19. Excellent agreement is obtained between the present element XSOLID86

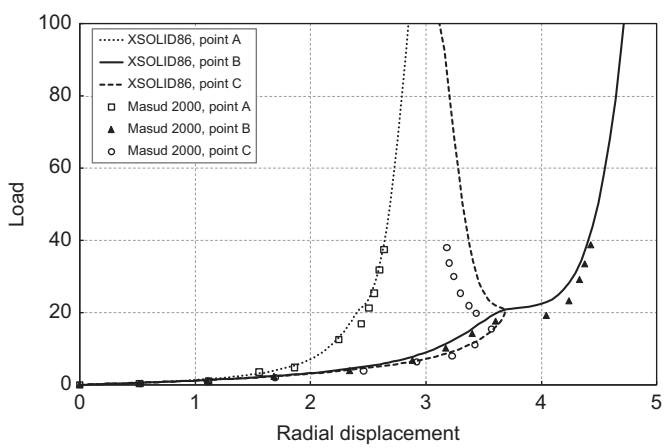

Fig. 21. Load–deflection curves at the points A, B and C of the pinched cylinder with free edges.

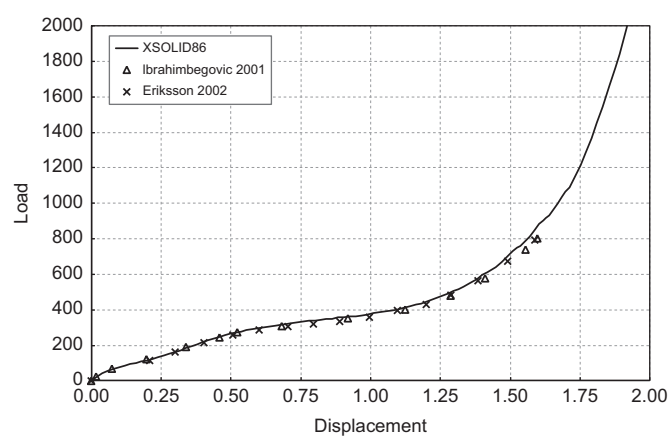

Fig. 23. Load–deflection curves of the pinching of a short clamped cylinder.

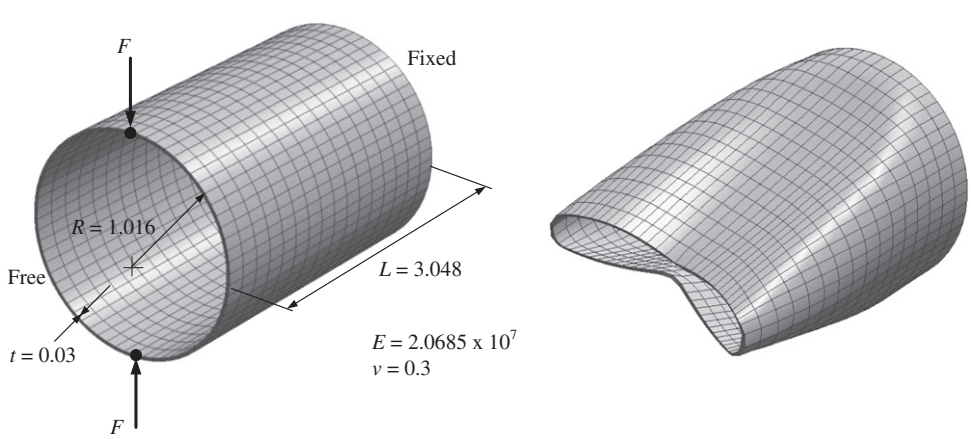

Fig. 22. Pinching of a short clamped cylinder.

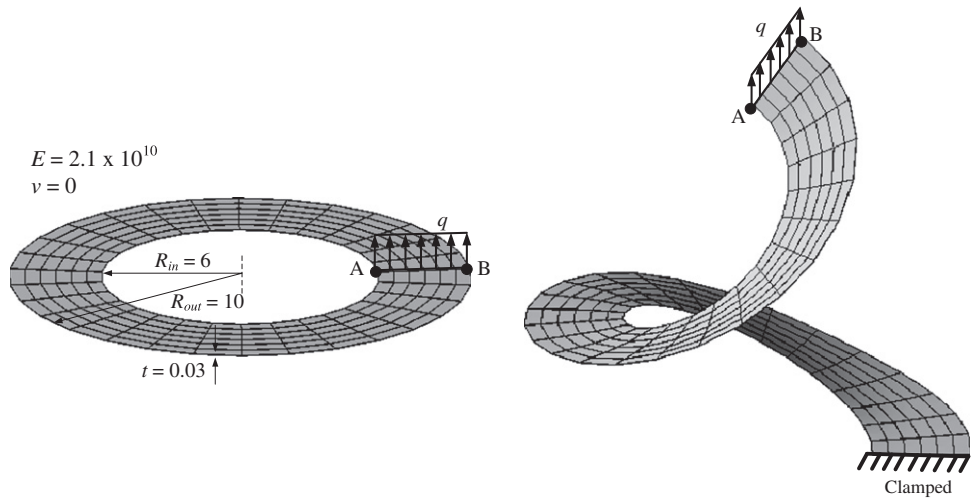

Fig. 24. Thin plate ring.

and the shell elements from both of the above references. Furthermore, it is clear that a much higher level of load can be achieved by the present element.

10.2.4. Pinched cylinder

This example constitutes a difficult test for finite element formulations, combining bending and membrane effects. The example consists of a cylinder shell with open ends, which is pulled in two diametrically opposite points through the application of point forces. The geometry, mesh and boundary conditions for one-eighth of the model are presented in Fig. 20. Points A, B and C are monitored in terms of absolute radial displacement. The material is considered elastic, with elasticity modulus $E=10.5\times10^6$ consistent units and Poisson coefficient $\nu=0.3125$, in agreement with the above references. A mesh with 16 elements along the circumferential direction, 8 elements along the longitudinal direction and 2 elements along the thickness is adopted. The absolute radial displacement for points A–C is compared with the values obtained by Masud et al. [45]. Very good agreement is obtained for the branches A and B, but branch C is slightly different from the references as shown in Fig. 21.

10.2.5. Pinching of a short clamped cylinder

The cylindrical shell is clamped at one end and subjected to two diametrically opposite forces in the other end. This test was carried out in Refs. [47,48] in the context of representing finite rotations in shell elements. The dimensions, material properties and boundary conditions for one-fourth of the geometry are illustrated in Fig. 22. A regular $16\times16\times2$ element mesh is employed. It is noticeable that this is a known test to verify the behavior of the element under inextensional deformations. The results of the present element XSOLID86 gives a very close agreement with those of the two references as shown in Fig. 23. In addition, it is clear that a much higher level of load can be achieved by the present element.

10.2.6. Thin plate ring

The test consists of the pulling of a thin circular ring containing a radial cut. The pulling is carried out resorting to a distributed load with fixed direction, applied on an edge. The opposite edge is clamped. This problem was first considered by Basar and Ding [49] to test formulations for finite shell rotations. The ring is considered elastic with an elasticity modulus of $E=2.1\times10^{10}$ and a Poisson coefficient of $\nu=0$. The geometry, mesh and boundary conditions are represented in Fig. 24. A regular $6\times30\times1$ element mesh is employed in modeling this problem. For comparison purposes, Ref. [44] is adopted. Fig. 25 shows the load–displacement curves. The present element XSOLID86 shows excellent agreement with the shell element of the reference for both points A and B. Furthermore, it should be noted that a much higher level of load can be achieved by the present element because the co-rotational formulation included in the element formulation improves the behavior of the present element.

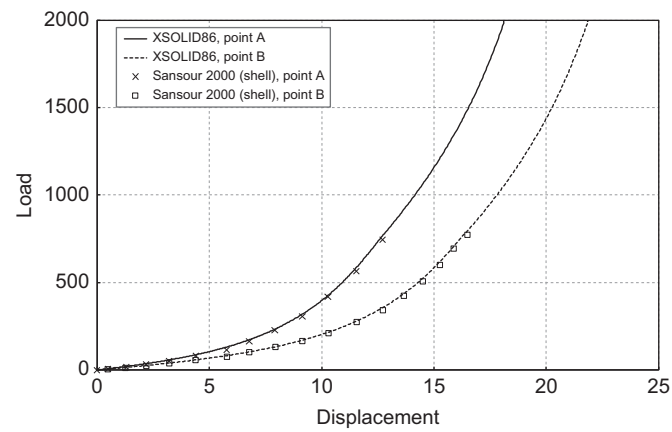

Fig. 25. Load–deflection curves at the points A and B of thin plate ring.

11. Conclusion

A co-rotational 8-node degenerated thin-walled element is developed and verified for various plate and shell problems. The global, local and natural coordinate systems are used to conveniently model the straight and curved thin-walled geometry. The formulation of the present element is different from that of the traditional solid-shell elements because there is no any modification in Jacobian. In contrast to shell elements with rotational degrees of freedom, the proposed formulation with no rotational degrees of freedom eliminates a tedious and complex shell element formulation. In addition, the present element considered here is also different from the standard 8-node solid elements

because the plane stress condition is used in the element formulation, which implies degeneration of three-dimensional continuum to fit to thin-walled and shell applications. The assumed natural strain (ANS) and 11 enhanced assumed strain (EAS) parameters are employed to overcome various locking problems, while the co-rotational formulation is used to remove rigid body rotations. Benchmark tests commonly employed for testing shear, membrane, thickness lockings have been conducted for linear problems. Based on the results of numerical problems, the present element has no locking behaviors and shows good performances of both membrane and bending behaviors in the linear analysis. For non-linear analysis, the proposed element presents good agreements with results close to the shell elements in a number of shell problems. Furthermore, co-rotational formulation improves the behavior of the present element in solving geometrically non-linear problems. Although the element formulation is simple, the results are good and suitable for the analysis of both linear and geometrically non-linear problems of thin structures.

Acknowledgment

This work was supported by the development of analysis of time-dependent response of nuclear reactor with bonded tendon using prestressed concrete solid-shell element of the Korea Institute of Energy Technology Evaluation and Planning (KETEP) grant funded by the Korea Government Ministry of Knowledge Economy (no. 2010T100101024).

Appendix A

According to Eq. (45), the nodal displacement vector in the global coordinate $\tilde{\mathbf{U}}$ can be transformed to the nodal displacement vector in the local coordinate $\tilde{\mathbf{u}}$ as follows:

$$\mathbf{T}_G = \begin{bmatrix} \mathbf{T} & & & & & & & \\ & \mathbf{T} & & & & & & \\ & & \mathbf{T} & & & & & \\ & & & \mathbf{T} & & & & \\ & & & & \mathbf{T} & & & \\ & & & & & \mathbf{T} & & \\ & & & & & & \mathbf{T} & \\ & & & & & & & \mathbf{T} \end{bmatrix} \tag{A.1}$$

where $\mathbf{T}$ is the transformation matrix between the local and global coordinates as shown in Eq. (8).

In order to calculate the geometric stiffness matrix, the non-linear strain–displacement matrix $\mathbf{B}_{NL}$ can be are expressed as follows:

$$\mathbf{B}_{NL} = \left[\begin{array}{ccc|ccc|c|ccc} \frac{\partial N_1}{\partial r} & 0 & 0 & \frac{\partial N_2}{\partial r} & 0 & 0 & \cdots & \frac{\partial N_8}{\partial r} & 0 & 0 \\ 0 & \frac{\partial N_1}{\partial r} & 0 & 0 & \frac{\partial N_2}{\partial r} & 0 & \cdots & 0 & \frac{\partial N_8}{\partial r} & 0 \\ 0 & 0 & \frac{\partial N_1}{\partial r} & 0 & 0 & \frac{\partial N_2}{\partial r} & \cdots & 0 & 0 & \frac{\partial N_8}{\partial r} \\ \frac{\partial N_1}{\partial s} & 0 & 0 & \frac{\partial N_2}{\partial s} & 0 & 0 & \cdots & \frac{\partial N_8}{\partial s} & 0 & 0 \\ 0 & \frac{\partial N_1}{\partial s} & 0 & 0 & \frac{\partial N_2}{\partial s} & 0 & \cdots & 0 & \frac{\partial N_8}{\partial s} & 0 \\ 0 & 0 & \frac{\partial N_1}{\partial s} & 0 & 0 & \frac{\partial N_2}{\partial s} & \cdots & 0 & 0 & \frac{\partial N_8}{\partial s} \\ \frac{\partial N_1}{\partial t} & 0 & 0 & \frac{\partial N_2}{\partial t} & 0 & 0 & \cdots & \frac{\partial N_8}{\partial t} & 0 & 0 \\ 0 & \frac{\partial N_1}{\partial t} & 0 & 0 & \frac{\partial N_2}{\partial t} & 0 & \cdots & 0 & \frac{\partial N_8}{\partial t} & 0 \\ 0 & 0 & \frac{\partial N_1}{\partial t} & 0 & 0 & \frac{\partial N_2}{\partial t} & \cdots & 0 & 0 & \frac{\partial N_8}{\partial t} \end{array}\right] \tag{A.2}$$

where the displacement derivatives $\partial/\partial r$, $\partial/\partial s$ and $\partial/\partial t$ can be described using Eq. (13), and the stress matrix $\tilde{\boldsymbol{\sigma}}$ can be written as

$$\tilde{\boldsymbol{\sigma}} = \begin{bmatrix} \sigma_{rr} & 0 & 0 & \sigma_{rs} & 0 & 0 & \sigma_{rt} & 0 & 0 \\ 0 & \sigma_{rr} & 0 & 0 & \sigma_{rs} & 0 & 0 & \sigma_{rt} & 0 \\ 0 & 0 & \sigma_{rr} & 0 & 0 & \sigma_{rs} & 0 & 0 & \sigma_{rt} \\ \sigma_{rs} & 0 & 0 & \sigma_{ss} & 0 & 0 & \sigma_{st} & 0 & 0 \\ 0 & \sigma_{rs} & 0 & 0 & \sigma_{ss} & 0 & 0 & \sigma_{st} & 0 \\ 0 & 0 & \sigma_{rs} & 0 & 0 & \sigma_{ss} & 0 & 0 & \sigma_{st} \\ \sigma_{rt} & 0 & 0 & \sigma_{st} & 0 & 0 & \sigma_{tt} & 0 & 0 \\ 0 & \sigma_{rt} & 0 & 0 & \sigma_{st} & 0 & 0 & \sigma_{tt} & 0 \\ 0 & 0 & \sigma_{rt} & 0 & 0 & \sigma_{st} & 0 & 0 & \sigma_{tt} \end{bmatrix} \tag{A.3}$$

In this study, the 8-node solid element with 24 enhanced isoperimetric strain terms named by SOLID-EAS24 is also implemented to compare performances with the present element. All of the interpolation parameters can be shown as follows:

$$\mathbf{M}_{\xi}^{24} = \left[\begin{array}{ccc|cccccc|cccccc|cccccc} \xi & 0 & 0 & 0 & 0 & 0 & 0 & 0 & 0 & 0 & 0 & 0 & 0 & 0 & 0 & \xi\eta & \xi\zeta & 0 & 0 & 0 & 0 & 0 & 0 \\ 0 & \eta & 0 & 0 & 0 & 0 & 0 & 0 & 0 & 0 & 0 & 0 & 0 & 0 & 0 & 0 & 0 & \xi\eta & \zeta\eta & 0 & 0 & 0 & 0 \\ 0 & 0 & \zeta & 0 & 0 & 0 & 0 & 0 & 0 & 0 & 0 & 0 & 0 & 0 & 0 & 0 & 0 & 0 & 0 & \xi\zeta & \eta\zeta & 0 & 0 \\ 0 & 0 & 0 & \xi & \eta & 0 & 0 & 0 & 0 & \xi\zeta & \eta\zeta & 0 & 0 & 0 & 0 & 0 & 0 & 0 & 0 & 0 & 0 & 0 & 0 \\ 0 & 0 & 0 & 0 & 0 & \xi & \zeta & 0 & 0 & 0 & 0 & \xi\eta & \zeta\eta & 0 & 0 & 0 & 0 & 0 & 0 & 0 & 0 & 0 & 0 \\ 0 & 0 & 0 & 0 & 0 & 0 & 0 & \eta & \zeta & 0 & 0 & 0 & 0 & \xi\eta & \xi\zeta & 0 & 0 & 0 & 0 & 0 & 0 & 0 & 0 \end{array}\right.$$

$$\left.\begin{array}{cccccc|ccc} \xi\eta & \xi\zeta & 0 & 0 & 0 & 0 & 0 & 0 & 0 \\ 0 & 0 & \xi\eta & \zeta\eta & 0 & 0 & 0 & 0 & 0 \\ 0 & 0 & 0 & 0 & \xi\zeta & \zeta\eta & 0 & 0 & 0 \\ 0 & 0 & 0 & 0 & 0 & 0 & \xi\eta & 0 & 0 \\ 0 & 0 & 0 & 0 & 0 & 0 & 0 & \xi\zeta & 0 \\ 0 & 0 & 0 & 0 & 0 & 0 & 0 & 0 & \zeta\eta \end{array}\right] \tag{A.4}$$

References

[1] S. Ahmad, B.M. Irons, O.C. Zienkiewicz, Analysis of thick and thin shell structures by curved finite elements, Int. J. Numer. Methods Eng. 2 (1970) 419–451.
[2] Worsak Kanok-Nukulchai, A simple and efficient finite element for general shell analysis, Int. J. Numer. Methods Eng. 14 (1979) 179–200.
[3] Worsak Kanok-Nukulchai, M. Sivakumar, Degenerate element for combined flexural and torsional analysis of thin-walled structures, J. Struct. Eng.—ASCE 114 (1988) 657–674.
[4] E.L. Wilson, R.L. Taylor, W.P. Doherly, J. Ghaboussi, Incompatible displacement models, in: S.J. Fenves, et al.et al.(Ed.), Numerical and Computer Methods in Structural Mechanics, Academic Press, New York, 1973.
[5] R.L. Taylor, P.J. Beresford, E.L. Wilson, A non-conforming element for stress analysis, Int. J. Numer. Methods Eng. 10 (1976) 1211–1219.
[6] J.C. Simo, M.S. Rifai, A class of mixed assumed strain methods and the methods of incompatible modes, Int. J. Numer. Methods Eng. 29 (1990) 1595–1638.
[7] J.C. Simo, F. Armero, Geometrically non-linear enhanced strain mixed methods and the method of incompatible modes, Int. J. Numer. Methods Eng. 33 (1992) 1413–1449.
[8] J.C. Simo, R. Armero, R.L. Taylor, Improved versions of assumed enhanced strain tri-linear elements for 3D finite deformation problems, Comput. Methods Appl. Mech. Eng. 110 (1993) 386–395.
[9] Gilson Rescober Lomboy, Songsak Suthasupradit, Ki-Du Kim, E. Oñate, Non-linear formulations of a four-node quasi-conforming shell element, Arch. Comput. Methods Eng. 16 (2009) 189–250.
[10] R. Hauptmann, K. Schweizerhof, A systematic development of solid-shell element formulations for linear and non-linear analysis employing only displacement degrees of freedom, Int. J. Numer. Methods Eng. 42 (1998) 49–69.
[11] K.Y. Sze, L.Q. Yao, A hybrid stress ANS solid-shell element and its generalization for smart structure modeling, Part I: solid-shell element formulation, Int. J. Numer. Methods Eng. 48 (2000) 545–564.
[12] U. Andelfinger, E. Ramm, D. Roehl, 2D- and 3D-enhanced assumed strain element and their application in plasticity, in: D. Owen, E. Onate, E. Hinton (Eds.), Computational Plasticity: Proceedings of the Fourth International Conference, Pineridge Press, Swansea, UK, 1996, pp. 1992–2007.

[13] J. Korelc, P. Wriggers, Improved enhanced strain four-node element with Taylor expansion of the shape functions, Int. J. Numer. Methods Eng. 40 (1997) 406–421.
[14] M.A. Puso, A highly efficient enhanced assumed strain physically stabilized hexahedral element, Int. J. Numer. Methods Eng. 49 (2000) 1029–1064.
[15] P.M.A. Areias, J.M.A. Cesar de Sa, C.A. Conceicao Antonio, A.A. Fernandes, Analysis of 3D problems using a new enhanced strain hexahedral element, Int. J. Numer. Methods Eng. 58 (2003) 1637–1682.
[16] S. Klinkel, F. Gruttmann, W. Wagner, A continuum based three-dimensional shell element for laminated structures, Comput. Struct. 71 (1998) 43–62.
[17] K.D. Kim, G.Z. Liu, S.C. Han, A resultant 8-node solid-shell element for geometrically nonlinear analysis, Comput. Mech. 35 (2005) 315–331.
[18] Rui P.R. Cardoso, Jeong Whan Yoon, M. Mahardika, S. Choudhry, R.J. Alves de Sousa1, R.A. Fontes Valente, Enhanced assumed strain (EAS) and assumed natural strain (ANS) methods for one-point quadrature solid-shell elements, Int. J. Numer. Methods Eng. 75 (2008) 156–187.
[19] T. Belytschko, B.L. Wong, H. Stolarski, Assumed strain stabilization procedure for the 9-node lagrange shell element, Int. J. Numer. Methods Eng. 28 (1989) 385–414.
[20] E.N. Dvorkin, K.J. Bathe, A continuum mechanics based four-node shell element for general nonlinear analysis, Eng. Comput. 1 (1984) 77–88.
[21] L. Vu-Quoc, X.G. Tan, Optimal solid shells for non-linear analyses of multilayer composites. I. Statics, Comput. Methods Appl. Mech. Eng. 192 (2003) 975–1016.
[22] R.P.R. Cardoso, J.W. Yoon, One point quadrature shell elements for sheet metal forming analysis, Arch. Comput. Methods Eng. 12 (2005) 3–66.
[23] R.P.R. Cardoso, J.W. Yoon, R.A. Fontes Valente, A new approach to reduce membrane and transverse shear locking for one point quadrature shell elements: linear formulation, Int. J. Numer. Methods Eng. 66 (2005) 214–249.
[24] E. Ramm, M. Bischoff, M. Braun, Higher order nonlinear shell formulations-a step back into three dimensions, in: K. Bell (Ed.), From Finite Elements to the Troll Platform, Department of Structural Engineering, Norwegian Institute of Technology, Trondheim, 1994, pp. 65–88.
[25] P. Betsch, E. Stein, An assumed strain approach avoiding artificial thickness straining for a nonlinear 4-node shell element, Commun. Numer. Methods Eng. 11 (1995) 899–909.
[26] M. Bischoff, E. Ramm, Shear deformable shell elements for large strains and rotations, Int. J. Numer. Methods Eng. 40 (1997) 4427–4449.
[27] David Nicholas Bates, The Mechanics of Thin Walled Structures with Special Reference to Finite Rotations, Doctoral Thesis, Department of Civil Engineering, Imperial College of Science and Technology, London, 1987.
[28] Seyed Hassan Seyed-Kesari, Innovative Design of Underintegrated Lagrangian Finite Elements, Dotoral Thesis, Department of Civil Engineering, Imperial College of Science, Technology and Medicine, London, 1989.
[29] K.D. Kim, G.R. Lomboy, A co-rotational quasi-conforming 4-node assumed strain shell element for large displacement of elasto-plastic analysis, Comput. Methods Appl. Mech. Eng. 195 (2006) 6502–6522.
[30] G.R. Lomboy, K.D. Kim, Eugenio Onate, A co-rotational 8-node resultant shell element for progressive nonlinear dynamic failure analysis of laminated composite structures, Mech. Adv. Mater. Struct. 14 (2) (2007) 89–105.
[31] Ki-Du Kim, Sung-Cheon Han, Songsak, Geometrically nonlinear analysis of laminated composite structures using a 4-node co-rotational shell element with enhanced strain terms, Int. J. Nonlinear Mech. 42 (6) (2007) 864–881.
[32] E.N. Dvorkin, K.J. Bathe, A continuum mechanics based four-node shell element for general non-linear analysis, Eng. Comput. 1 (1984) 77–88.
[33] J.C. Simo, D.D. Fox, Rifai MSm, On stress resultant geometrically exact shell model, Part II: the linear theory; computational aspects, Comput. Methods Appl. Mech. Eng. 73 (1989) 53–92.
[34] R.H. MacNeal, R.L. Harder, A proposed standard set of problems to test finite element accuracy, Finite Elem. Anal. Des. 1 (1985) 3–20.
[35] T. Belytschko, I. Leviathan, Physical stabilization of the 4-node shell element with one point quadrature, Comput. Methods Appl. Mech. Eng. 113 (1994) 321–350.
[36] R.J. Alves de Sousa, R.P.R. Cardoso, R.A. Fontes Valente, J.W. Yoon, J.J. Grácio, R.M. Natal Jorge, A new one point quadrature enhanced assumed strain solid-shell element with multiple integration points along thickness. Part I—geometrically linear applications, Int. J. Numer. Methods Eng. 62 (2005) 952–977.
[37] R.J. Alves de Sousa, R.P.R. Cardoso, R.A. Fontes Valente, J.W. Yoon, J.J. Grácio, R.M. Natal Jorge, A new one-point quadrature enhanced assumed strain solid-shell element with multiple integration points along thickness. Part II—nonlinear applications, Int. J. Numer. Methods Eng. 67 (2006) 160–188.
[38] S. Timoshenko, S. Woinowsky-Krieger, Theory of Plates and Shells, McGraw-Hill, Inc., Singapore, 1959.
[39] T. Belytschko, H. Stolarski, W.K. Liu, N. Carpenter, J.S.J. Ong, Stress projection for membrane and shear locking in shell finite elements, Comput. Methods Appl. Mech. Eng. 51 (1985) 221–258.
[40] T.J.R. Hughes, W.K. Liu, Nonlinear finite element analysis of shells, Part I: three-dimensional shells, Comput. Methods Appl. Mech. Eng. 26 (1981) 331–362.
[41] A.B. Sabir, A.C. Lock, The application of finite elements to the large deflection geometrically nonlinear behaviour of cylindrical shells, in: Variational Methods in Engineering, University Press, Southampton, 1972, pp. 766–775.
[42] E. Ramm, The Riks/Wempner approach—an extension of the displacement control method in nonlinear analyses, in: Recent Advances in Non-linear Computational Mechanics, Pineridge Press Limited, Swansea, UK, 1982, pp. 63–86 (Chapter 3).
[43] M. Li, F. Zhan, The finite deformation theory for beam, plate and shell, Part 5: the shell element with drilling degree of freedom based on biot strain, Comput. Methods Appl. Mech. Eng. 189 (2000) 743–759.
[44] C. Sansour, F.G. Kollmann, Families of 4-node and 9-node finite elements for a finite deformation shell theory. An assessment of hybrid stress, hybrid strain and enhanced strain elements, Comput. Mech. 24 (2000) 435–447.
[45] A. Masud, C.L. Tham, W.K. Liu, A stabilized 3D co-rotational formulation for geometrically nonlinear analysis of multi-layered composite shells, Comput. Mech. 26 (2000) 1–12.
[46] C. Sansour, H. Buer, An exact finite rotation shell theory, its mixed variational formulation and its finite element implementation, Int. J. Numer. Methods Eng. 34 (1992) 73–115.
[47] A. Eriksson, C. Pacoste, Element formulation and numerical techniques for stability problems in shells, Comput. Methods Appl. Mech. Eng. 191 (2002) 3775–3810.
[48] A. Ibrahimbegovĭc, B. Brank, P. Courtois, Stress resultant geometrically exact form of classical shell model and vector-like parameterization of constrained finite rotations, Int. J. Numer. Methods Eng. 52 (2001) 1235–1252.
[49] Y. Basar, Y. Ding, Finite rotation shell elements for the analysis of finite rotation shell problems, Int. J. Numer. Methods Eng. 34 (1992) 165–169.

Analysis of Segmentally Constructed Prestressed Concrete Bridges Using Hexahedral Elements with Realistic Tendon Profiles

Pramin Norachan[1]; Ki-Du Kim[2]; and Eugenio Oñate, M.ASCE[3]

Downloaded from ascelibrary.org by ASIAN INSTITUTE OF TECHNOLOGY on 09/12/14. Copyright ASCE. For personal use only; all rights reserved.

Abstract: The paper presents a systematically numerical procedure based on the finite-element method for three-dimensional analysis of segmentally constructed prestressed concrete bridges using hexahedral elements including realistic tendon profiles. The enhanced assumed strain (EAS) is used in the formulation of the hexahedral element in order to improve the element performances. Both the geometric nonlinearity and time-dependent effects due to creep, shrinkage, and aging of the concrete and relaxation of the prestress are taken into account, while variations of the structural configuration due to changes of the structural geometry and boundary conditions during the construction process are also incorporated. To include realistic tendon profiles, the idealized prestressing tendon is represented by a system of piecewise linear prestressing segments. Several numerical examples in a wide range of prestressed concrete structures are presented to demonstrate the validity and efficiency of the proposed procedure. Finally, application to the erection of a segmentally erected prestressed concrete bridge is discussed at the end of the paper. **DOI: 10.1061/(ASCE)ST.1943-541X.0000923.** *© 2014 American Society of Civil Engineers.*

Author keywords: Hexahedral element; Enhanced assumed strains; Construction stage analysis; Prestressed concrete bridges; Analysis and computation.

Introduction

In recent years, segmentally constructed prestressed concrete bridges have been widely used because they are economical and attractive construction alternatives in situations where continuously supported formwork is impractical or too expensive. During the construction process, significant variations of the structural geometry, material properties, and support conditions can take place. The variations substantially influence the distribution of internal forces, displacements, and reactions. These affect the serviceability and safety conditions not only during the construction stage but also during the service life of the structure. Moreover, the time-dependent effects due to creep, shrinkage, aging of the concrete and relaxation of the prestress can lead to excessive vertical deflection in the long term. These effects may cause cracking or even failure due to loss of serviceability, durability, or safety of the bridges.

Several research works dealing with numerical procedures based on the finite-element method for the nonlinear analysis of prestressed concrete structures were proposed during the past decades (Kang et al. 1977, 1980; Scordelis 1983, 1984, 1988). The contribution of prestressing steel is incorporated, while the material and geometric nonlinear analysis of plane prestressed concrete frames including the time dependent effects due to load history, temperature history, creep, shrinkage, and aging of concrete and relaxation of prestress were also considered. For the construction stage analysis, many sophisticated computer programs for the analysis of segmentally erected prestressed concrete bridges considering the time-dependent effects of concrete has been developed to predict the bridge response (Ketchum 1986; Cruz et al. 1991, 1994, 1998; Mari et al. 1984, 2000, 2003; Bishara et al. 1990). Changes in structural configuration and the structural effects of the load and temperature histories, materials nonlinear behavior, creep, shrinkage, aging of concrete and relaxation of prestressing steel were taken into account. Prestressing tendons may be stressed, restressed, and removed, while a traveling formwork can be modeled. However, most computer programs have some limitations in wide use because of complexities in practical applications.

In general, box-girder bridges are traditionally modeled by using frame elements where the cross sections are assumed to remain plane. Frame elements cannot, however, capture the deformation of box-girder bridges and the shear lag effects accurately. To including these effects, shell elements are used to model cross sections of bridges. The formulation of a quasi-conforming shell element and its application to the prestressed concrete box girder bridge analysis were proposed by considering the nonlinear behavior of the steel and the time-dependent behavior of the concrete (Kim et al. 2007b), while the analysis of the stepwise cast-in-place construction of a balanced cantilever bridge modeled by using shell elements was carried out to investigate the structural responses including time-dependent effects (Malm et al. 2010).

As seen in the previous literature, numerical procedures based on the finite-element method using frame and shell elements have been proposed to analyze prestressed concrete bridges. When frame elements are employed to model bridges, they are not able to represent structural behaviors accurately and efficiently. Some examples that contribute to this viewpoint: (1) frame elements cannot accurately capture the effect of shear lag, which causes a nonlinear distribution of normal stresses over the top and bottom slabs of box girders; (2) transverse tendons typically placed in the top and

[1]Senior Structural Engineer, AIT Consulting, Asian Institute of Technology, P.O. Box 4, Klong Luang, Pathumthani 12120, Thailand.

[2]Professor, Dept. of Civil and Environmental System Engineering, Konkuk Univ., 1 Hwayang-dong, Gwangjin-gu, Seoul 143-701, Republic of Korea (corresponding author). E-mail: kimkd@konkuk.ac.kr

[3]Professor, International Center for Numerical Methods in Engineering (CIMNE), Universidad Politecnica de Cataluna, Edificio C1 Campus Nord, 08032 Barcelona, Spain.

Note. This manuscript was submitted on October 12, 2012; approved on August 6, 2013; published online on August 8, 2013. Discussion period open until August 13, 2014; separate discussions must be submitted for individual papers. This paper is part of the ***Journal of Structural Engineering***, © ASCE, ISSN 0733-9445/04014028(17)/$25.00.

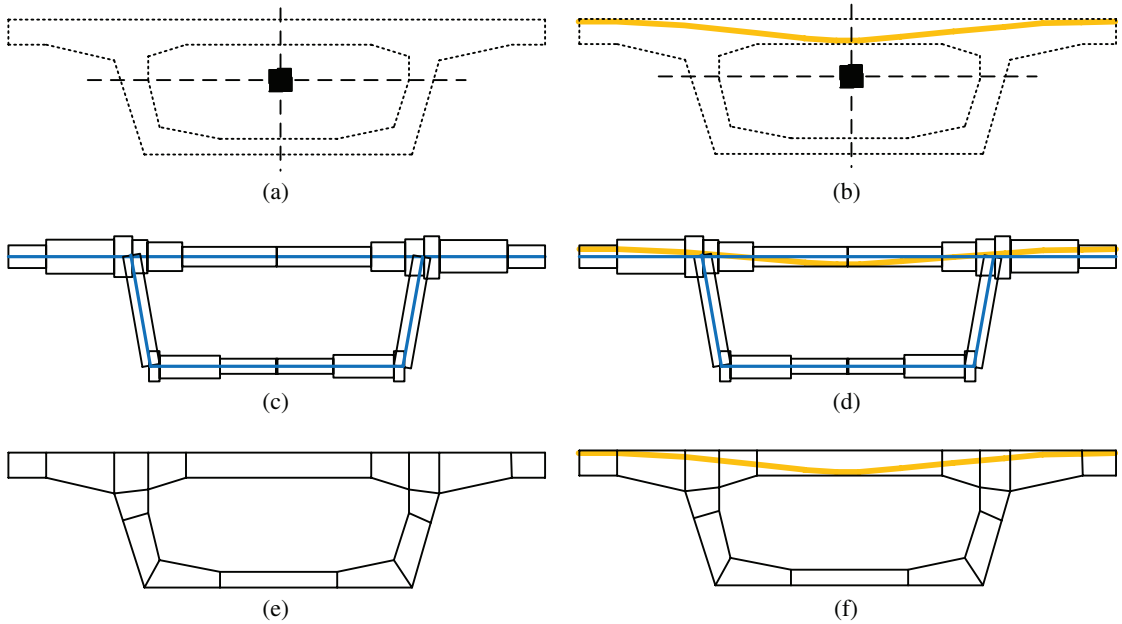

Fig. 1. (Color) A box girder cross section modeled using frame, shell, and solid elements

bottom slabs of bridge cross sections to control deformations cannot be modeled with frame elements, as illustrated in Fig. 1(b); and (3) it is necessary to adjust the finite-element model to obtain the reactions correctly when frame elements are used to model curved bridges.

Furthermore, when shell elements are used in modeling the bridges, there are also some issues that have to be discussed: (1) shell element cannot model the geometry of a bridge cross section exactly, due to its constant thickness, as shown in Fig. 1(c); (2) when shell elements with six degrees of freedom for each node are employed to model bridges, there are some difficulties in assigning boundary conditions; and (3) the calculation of offset from the shell middle surface, which causes complex and tedious work during implementation of the program, is required when a tendon is modeled with shell elements, as illustrated in Fig. 1(d).

Instead of using frame and shell elements, solid elements can also be used to model sophisticated and complex structures accurately and efficiently because they are able to represent the real behavior of the structures. Many different formulations of brick elements have been developed to maximize the accuracy and efficiency. However, it has been found that low-order element formulations for solid elements have serious drawbacks directly related to several kinds of locking behaviors.

To enhance the performance of traditional brick elements, the EAS method, in which usual displacement based strain field is enhanced with a set of internal variables, has become widely used, because the elements based on this concept perform very well in bending situations as well as in modeling thin structures (Simo et al. 1990, 1992, 1993). Two-dimensional and three-dimensional EAS elements which overcome locking in the incompressible limit and behave well in bending-dominated regimes were developed with a minimum of 21 additional element parameters (Andelfinger et al. 1996), while other of two-dimensional and three-dimensional EAS element approaches yielded favorable results with only nine element parameters (Korelc et al. 1997). In addition, the EAS method was successfully implemented to alleviate shear locking appearing in shell and solid-shell elements in membrane strains (Kim et al. 2005, 2007a; Hauptmann et al. 2001; Cardoso et al. 2008; Pramin et al. 2012).

In addition, the use of brick elements in modeling prestressed concrete bridges for three-dimensional analysis has increased recently. A study which was mainly focused on numerical modeling of a bridge using solid elements has been carried out (Ates 2011), and an analysis considering segmental construction stages, time-dependent material properties of concrete and steel, and geometric nonlinearities was performed by using SAP2000. Another interesting numerical procedure for three-dimensional analysis performed using *ABAQUS* was presented to evaluate excessive long-time deflections of prestressed box girders. The bridge was modeled by using hexahedral elements, while the construction sequences and the time-dependent effects due to creep and shrinkage were also taken into account (Bažant et al. 2012a, 2012b; Yu et al. 2012). However, these papers are conducted based on commercial finite-element software. To demonstrate the overall picture in developing a computer program based on finite-element methods for the analysis of segmentally constructed prestressed concrete bridges, the systematically numerical procedure should be presented.

The purpose of this paper is to develop a general step-by-step procedure for the three-dimensional finite-element analysis of segmentally constructed prestressed concrete bridges. The hexahedral element, including the enhanced assumed strain technique, is employed to improve the element performances. Structural effects caused by realistic tendon profiles, load history, changes of the bridge geometry, and support movement are taken in account, while long-term effects such as creep, shrinkage, and aging of the concrete, as well as relaxation of the prestressing steel, are also incorporated. Finally, several numerical examples are presented to demonstrate the capabilities of the proposed procedure.

Formulation of the Present Element

Geometry and Kinematics

In this study, the traditional hexahedral element with three translational degrees of freedom per node is employed. Fig. 2 shows the relation between global (x-y-z) and natural coordinate systems (ξ, η, ζ) using the present geometry and kinematics. The origin of the natural coordinate system is set at the centroid of each element.

Downloaded from ascelibrary.org by ASIAN INSTITUTE OF TECHNOLOGY on 09/12/14. Copyright ASCE. For personal use only; all rights reserved.

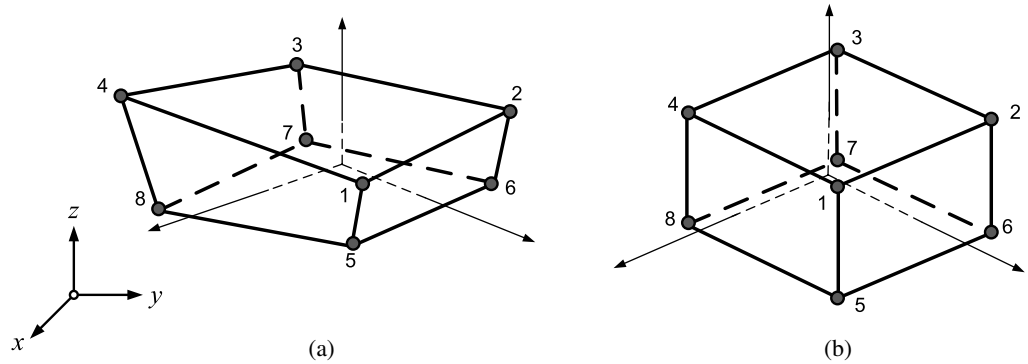

Fig. 2. Geometry of a typical hexahedral element: (a) global coordinate system; (b) natural coordinate systems

In the global coordinate system, the position vector $\mathbf{X}$ and the displacement vector $\mathbf{U}$ of a point inside the element can respectively be described as

$$\mathbf{X} = \sum_{i=1}^{8} N_i(\xi, \eta, \zeta)\mathbf{X_i} \tag{1}$$

$$\mathbf{U} = \sum_{i=1}^{8} N_i(\xi, \eta, \zeta)\mathbf{U_i} \tag{2}$$

where $\mathbf{X_i}$ is the nodal coordinate and $\mathbf{U_i}$ is the nodal displacement field in the global direction (x, y, z). The shape functions of the eight-node isoparametric finite elements are often defined as follows:

$$N_i(\xi, \eta, \zeta) = \frac{1}{8}(1 + \xi_i\xi)(1 + \eta_i\eta)(1 + \zeta_i\zeta) \tag{3}$$

where (ξ_i, η_i, ζ_i) are the natural coordinates of node i.

The formulation of the present element is based upon the conversion of the global displacement values to the local coordinate system and then interpolation using eight-point Gaussian quadrature. The strain-displacement relationships can be obtained from the derivatives of the shape functions with respect to the reference coordinates, while geometric nonlinearity arises from both the quadratic terms of the Green strain tensor and the kinematic relationship. The virtual work equation can be formulated based on the updated Lagrangian description and both the element and geometric stiffnesses can be obtained by following standard procedures.

Enhanced Assumed Strain (EAS)

The enhanced strain formulation where the usual displacement-based strain field is enhanced with a set of internal variables to overcome locking behavior and improve the performance of traditional elements was introduced by Simo et al. (1990). The strain is approximated by two fields, such as the compatible and enhanced one via the following equation:

$$\varepsilon = \varepsilon^c + \tilde{\varepsilon} = \mathbf{Bu} + \mathbf{M}\boldsymbol{\alpha} \tag{4}$$

where $\boldsymbol{\varepsilon}^c$ = compatible strain field; $\tilde{\boldsymbol{\varepsilon}}$ = enhanced part of the strain; $\mathbf{B}$ = standard strain operator; $\mathbf{M}$ = interpolation operator for the additional strain field, which may be discontinuous across element edges; and $\boldsymbol{\alpha}$ = vector of the internal strain parameters corresponding to the enhanced strain. The enhanced assumed strain, defined in the global coordinate system, is interpolated according to Eq. (4).

$$\tilde{\boldsymbol{\varepsilon}} = \mathbf{M}\boldsymbol{\alpha} \tag{5}$$

$$\mathbf{M} = \frac{\det \mathbf{J}_0}{\det \mathbf{J}} \mathbf{T}_0^{-T} \mathbf{M}_\xi \tag{6}$$

where $\det \mathbf{J}$ denotes the determinant of the Jacobian matrix $\mathbf{J}$ and $\det \mathbf{J}_0$ is the determinant of the Jacobian matrix $\mathbf{J}_0 = \mathbf{J}|_{\xi=\eta=\zeta=0}$ at the element centroid in the natural coordinate system, and $\mathbf{T}_0^{-T}$ maps the polynomial shape functions of $\mathbf{M}_\xi$, defined in the natural coordinate into the global coordinate.

Several papers published recently presented the element formulations with different terms of enhanced strain parameters (Simo et al. 1992, 1993; Andelfinger et al. 1996; Korelc et al. 1997). However, after intensive numerical tests, it was found that the use of 24 enhanced strain parameters is sufficient to obtain accurate results for the analysis of box-girder bridges. Despite the fact that more enhanced strain parameters are used in the element formulation, the element performance yields only minor improvements (Pramin et al. 2012). The enhanced isoperimetric strain terms which are chosen are shown as follows:

$$\mathbf{M}_\xi = \left[\begin{array}{ccc|ccccccc|cccccc|cccccc|ccc}
\xi & 0 & 0 & 0 & 0 & 0 & 0 & 0 & 0 & 0 & 0 & 0 & 0 & 0 & 0 & \xi\eta & \xi\zeta & 0 & 0 & 0 & 0 & 0 & 0 & 0 \\
0 & \eta & 0 & 0 & 0 & 0 & 0 & 0 & 0 & 0 & 0 & 0 & 0 & 0 & 0 & 0 & 0 & \xi\eta & \zeta\eta & 0 & 0 & 0 & 0 & 0 \\
0 & 0 & \zeta & 0 & 0 & 0 & 0 & 0 & 0 & 0 & 0 & 0 & 0 & 0 & 0 & 0 & 0 & 0 & 0 & \xi\zeta & \zeta\eta & 0 & 0 & 0 \\
0 & 0 & 0 & \xi & \eta & 0 & 0 & 0 & 0 & \xi\zeta & \eta\zeta & 0 & 0 & 0 & 0 & 0 & 0 & 0 & 0 & 0 & 0 & \xi\eta & 0 & 0 \\
0 & 0 & 0 & 0 & 0 & \xi & \zeta & 0 & 0 & 0 & 0 & \xi\eta & \zeta\eta & 0 & 0 & 0 & 0 & 0 & 0 & 0 & 0 & 0 & \xi\zeta & 0 \\
0 & 0 & 0 & 0 & 0 & 0 & 0 & \eta & \zeta & 0 & 0 & 0 & 0 & \xi\eta & \xi\zeta & 0 & 0 & 0 & 0 & 0 & 0 & 0 & 0 & \zeta\eta
\end{array}\right] \tag{7}$$

Downloaded from ascelibrary.org by ASIAN INSTITUTE OF TECHNOLOGY on 09/12/14. Copyright ASCE. For personal use only; all rights reserved.

Downloaded from ascelibrary.org by ASIAN INSTITUTE OF TECHNOLOGY on 09/12/14. Copyright ASCE. For personal use only; all rights reserved.

Time-Dependent Concrete Material Properties

In the development of the time-dependent material properties based on finite-element analyses, the evolution of creep, shrinkage and aging of concrete are implemented according to the CEB-FIP and ACI-209 model codes (CEB-FIP 1990; ACI 1982). The total strain in the concrete may be considered as a superposition of several independent components caused by different phenomena. Thus, the total concrete strain $\boldsymbol{\varepsilon}(t)$ at any time t is assumed to be composed of the mechanical strain $\boldsymbol{\varepsilon}^m(t)$ caused by short-term service loads and the nonmechanical strain $\boldsymbol{\varepsilon}^{nm}(t)$ consisting of creep strain $\boldsymbol{\varepsilon}^c(t)$, shrinkage strain $\boldsymbol{\varepsilon}^s(t)$ and aging strain $\boldsymbol{\varepsilon}^a(t)$

$$\boldsymbol{\varepsilon}(t) = \boldsymbol{\varepsilon}^m(t) + \boldsymbol{\varepsilon}^{nm}(t) \tag{8}$$

$$\boldsymbol{\varepsilon}^{nm}(t) = \boldsymbol{\varepsilon}^c(t) + \boldsymbol{\varepsilon}^s(t) + \boldsymbol{\varepsilon}^a(t) \tag{9}$$

Due to the increase of the elastic modulus of the concrete over time, the aging strain $\boldsymbol{\varepsilon}^a(t)$, which is a fictitious stress-originated strain, can be defined as the decrease in mechanical strain. Under constant stress, the aging strain increment $\Delta\varepsilon^a(t)$ occurring between time t_{n-1} and t_n may be expressed as

$$\Delta\varepsilon^a(t) = \sigma\left[\frac{1}{E(t_{n-1})} - \frac{1}{E(t_n)}\right] \tag{10}$$

Shrinkage strain can be evaluated directly by utilizing the shrinkage model proposed in the design codes, since it is defined as the volume change which occurs independently of imposed stresses, while creep is defined as the increase in strain under a sustained stress. In general, the creep strain can also be determined by using design codes, but in order to calculate the creep for the entire history of loading the quantity of data storage would be excessive. Therefore a first-order recursive algorithm based on the expansion of creep compliance has been adopted because the model can simulate the stress history effectively in spite of its simplicity of application (Kabir 1976; Mari 1984; Ketchum 1986; Abbas et al. 1993):

$$\Delta\varepsilon_n^c = \sum_{i=1}^{m} A_{i_{n-1}}(1 - e^{-\Delta t_n/\Gamma_i}) \tag{11}$$

$$A_{i_n} = A_{i_{n-1}} e^{-\Delta t_n/\Gamma_i} + a_i(\tau)\Delta\sigma_n \tag{12}$$

where $\Delta\varepsilon_n^c$ = incremental creep strain; Γ_i = retardation; $a_i(\tau)$ are creep compliance coefficients which depend on the age of loading τ; = m number of time steps; and A_i = hidden state variables which are updated during each time step. The initial values are $A_{i_1} = a_i(t_1)\Delta\sigma_n$ at step $n = 1$.

Before the calculation of creep strain using Eq. (11), parameters such as, m, $a_i(\tau)$, and Γ_i must be determined. The values of $a_i(\tau)$ are determined by the method of least squares using Kabir's Dirichlet series creep compliance:

$$J(t_j, \tau) = \sum_{i=1}^{m} a_i(\tau)[1 - e^{-(t_j-\tau)/\Gamma_i}] \tag{13}$$

In order to obtain the creep compliance coefficients $a_i(\tau)$, a best-fit approximation of the test data using a degenerate kernel can be evaluated by the following procedure. After choosing m and Γ_i, $(i = 1, 2, \ldots, m)$ on a trial basis, a particular loading age τ and various observation times t_j, $(j = 1, 2, \ldots, n)$ need to be set. The creep function $J(t_j, \tau)$ can then be calculated by following the model proposed in the design codes. After setting all of the initial values, the following system of equations is set up:

$$\begin{bmatrix} 1 - e^{-(t_1-\tau)/\Gamma_1} & 1 - e^{-(t_1-\tau)/\Gamma_2} & \cdots & 1 - e^{-(t_1-\tau)/\Gamma_m} \\ 1 - e^{-(t_1-\tau)/\Gamma_2} & 1 - e^{-(t_1-\tau)/\Gamma_2} & \cdots & 1 - e^{-(t_1-\tau)/\Gamma_m} \\ \vdots & \vdots & & \vdots \\ 1 - e^{-(t_n-\tau)/\Gamma_2} & 1 - e^{-(t_n-\tau)/\Gamma_2} & \cdots & 1 - e^{-(t_n-\tau)/\Gamma_m} \end{bmatrix} \begin{bmatrix} a_1(\tau) \\ a_2(\tau) \\ \vdots \\ a_m(\tau) \end{bmatrix} = \begin{bmatrix} J(t_1, \tau) \\ J(t_2, \tau) \\ \vdots \\ J(t_n, \tau) \end{bmatrix} \tag{14}$$

For the matrix form, the above equation can be written

$$\mathbf{Ea} = \mathbf{b} \tag{15}$$

The method of least-squares is applied to solve the overdeterminate system of equations for the values of $\mathbf{a}$ as follows:

$$\mathbf{a} = (\mathbf{E}^{\mathrm{T}}\mathbf{E})^{-1}(\mathbf{E}^{\mathrm{T}}\mathbf{b}) \tag{16}$$

To obtain a best-fit value, different values of m and Γ_i should be tried, and the calculation steps repeated. Once sufficient combinations have been trialed, the optimization of m and Γ_i can be evaluated. After the numerical tests were performed, it was found that $m = 4$ and $\Gamma_i = 5$, 50, 500, and 5,000 are sufficient to provide accurate results. For efficient and realistic creep analysis, in addition, some researchers have recently presented numerical procedures for predicting excessive long-term deflection of prestressed box girders (Bažant et al. 2012a, b), while the other revealed that the creep analysis based on a rate-type creep law obtained by Laplace transform inversion using simple Widder's formula, which can capture various nonlinear and drying effects as well as changes in structural system and a complex load history, is necessary for large creep-sensitive structures, such as box-girder bridges and super-tall buildings (Yu et al. 2012). However, the integral-type approach is used here not because it would be realistic, but because it is the simplest to check the correctness of programming with the references.

Finite-Element Formulation

Since the formulation of the nonlinear equations is based on the Updated Lagrangian method, all of the displacements are in incremental form. As a result of the application of the EAS method, the condensation approach is employed to obtain the force vector and stiffness matrix

$$\begin{bmatrix} \mathbf{K}_{uu} & \mathbf{K}_{u\alpha} \\ \mathbf{K}_{\alpha u} & \mathbf{K}_{\alpha\alpha} \end{bmatrix} \begin{Bmatrix} \Delta\mathbf{U} \\ \Delta\alpha \end{Bmatrix} = \begin{Bmatrix} \mathbf{F}^{\mathrm{ext}} - \mathbf{F}^{\mathrm{int}} \\ 0 - \mathbf{h} \end{Bmatrix} \tag{17}$$

After eliminating $\Delta\boldsymbol{\alpha}$, the condensed force and stiffness matrices can be derived from

$$\mathbf{R}^{\mathrm{int}} = \mathbf{F}^{\mathrm{int}} + \mathbf{K}_{u\alpha}\mathbf{K}_{\alpha\alpha}^{-1}\mathbf{h} \tag{18}$$

$$\mathbf{K}_E = \mathbf{K}_{uu} - \mathbf{K}_{u\alpha}\mathbf{K}_{\alpha\alpha}^{-1}\mathbf{K}_{\alpha u} \tag{19}$$

All of these stiffness matrices and force vectors are described by

$$\mathbf{K}_{uu} = \int_V \mathbf{B}^T\mathbf{D}\mathbf{B}\mathrm{d}V \qquad \mathbf{K}_{u\alpha} = \int_V \mathbf{B}^T\mathbf{D}\mathbf{M}\mathrm{d}V$$
$$\mathbf{K}_{\alpha u} = \int_V \mathbf{B}^T\mathbf{D}\mathbf{B}\mathrm{d}V \qquad \mathbf{K}_{\alpha\alpha} = \int_V \mathbf{M}^T\mathbf{D}\mathbf{M}\mathrm{d}V$$
$$\mathbf{F}^{\mathrm{int}} = \int_V \mathbf{B}^T\boldsymbol{\sigma}\mathrm{d}V \qquad \mathbf{h} = -\int_V \mathbf{M}^T\boldsymbol{\sigma}\mathrm{d}V \tag{20}$$

where the matrix $\mathbf{B}$ is the compatible strain-displacement relation matrix; $\mathbf{M}$ is the interpolation operator for the additional strain field; and $\mathbf{D}$ is the material stiffness matrix. The geometric stiffness matrix $\mathbf{K}_G$ for the hexahedral element is expressed as

$$\mathbf{K}_G = \int_V \mathbf{B}_{NL}^T\boldsymbol{\sigma}\mathbf{B}_{NL}dV \tag{21}$$

where the strain-displacement matrix $\mathbf{B}_{NL}$ and the stress matrix $\boldsymbol{\sigma}$ can be obtained by following standard procedures.

Formulation of the Prestressing Tendon

Tendon Segment Displacement Fields

To include realistic tendon profiles, in other commercial finite-element software, the individual prestressing bar generally modeled as two-node line element have to be directly attached to nodes of concrete elements modeled by using frame, shell or solid elements. However, in the proposed procedure, the individual prestressing bar can be randomly modeled inside hexahedral elements. Each tendon segment is assumed to be under a constant axial stress, while its stiffness and load contributions are obtained from the nodal variables of each tendon element inside the hexahedral elements. A global coordinate system and geometry is set during the generation of the three-dimensional space as shown in Fig. 3(a).

Each tendon segment is associated with the hexahedral elements as illustrated in Fig. 3(b). Points a and b are located inside the hexahedral elements m and n, respectively. Tendon point a is rigidly linked to the nodes of hexahedral element m and tendon point b is directly linked to the nodes of hexahedral element n. For an isoparametric finite element, the relationship between the nodal and inner displacements of an element is given by Eq. (2). To find any tendon points located inside an element, a search algorithm is initiated by dividing the structure into groups of solid elements. After dividing the groups, the algorithm which is based on the Newton-Raphson method will search for the position and record the element number for each tendon point. For tendon displacements, the global displacement $\bar{\mathbf{U}}$ can be transformed to the local displacement $\tilde{\mathbf{U}}$ as follows:

$$\tilde{\mathbf{U}} = \mathbf{T}\bar{\mathbf{U}} \tag{22}$$

where the components of the displacement vectors $\bar{\mathbf{U}}$ and $\tilde{\mathbf{U}}$ are given by

$$\tilde{\mathbf{U}} = [\,\tilde{u}_a \quad \tilde{u}_b\,]^T, \qquad \bar{\mathbf{U}} = [\,u_a \quad v_a \quad w_a \quad u_b \quad v_b \quad w_b\,]^T \tag{23}$$

The transformation matrix $\mathbf{T}$ between the local and global coordinates is

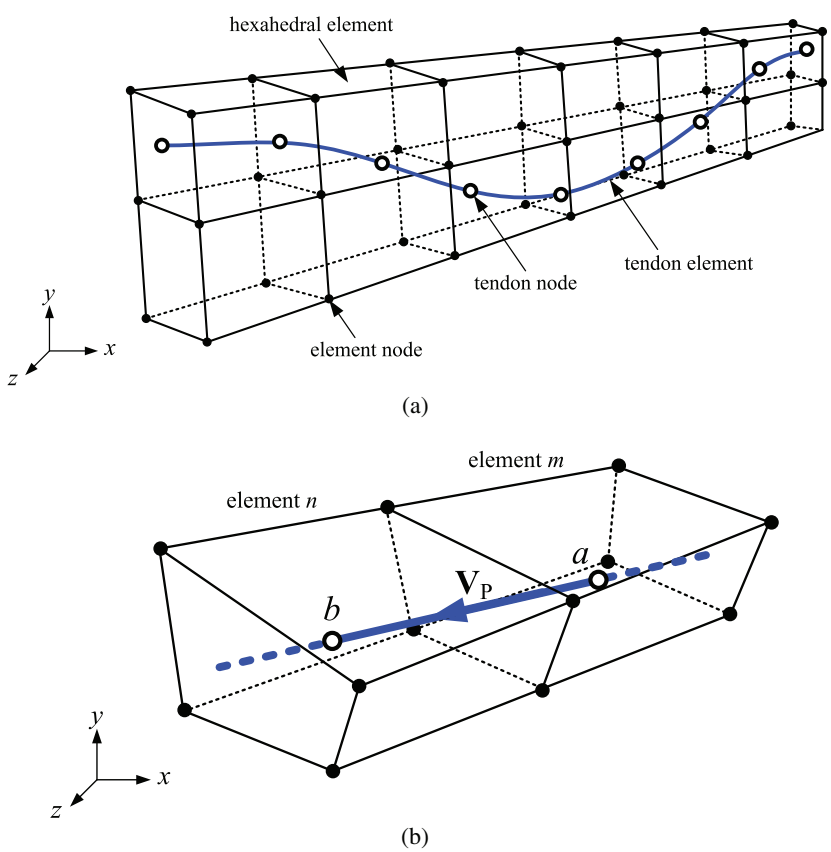

Fig. 3. (Color) Descriptions of tendon segments

Downloaded from ascelibrary.org by ASIAN INSTITUTE OF TECHNOLOGY on 09/12/14. Copyright ASCE. For personal use only; all rights reserved.

$$\mathbf{T} = \begin{bmatrix} V_{p1} & V_{p2} & V_{p3} & 0 & 0 & 0 \\ 0 & 0 & 0 & V_{p1} & V_{p2} & V_{p3} \end{bmatrix} \tag{24}$$

where V_{p1}, V_{p2}, and V_{p3} are the components of the unit vector $\mathbf{V}_P$ from point a to point b. Using the concept of mapping variables, both the stiffness and nodal load of the tendon element contribute to those of the hexahedral element. The variables of the tendon segment at point a are converted to nodal variables of the hexahedral element m, and the variables from point b contribute to the nodal variables of element n in the same manner. Thus, the relationship of the displacement variables between the tendon and the hexahedral element can be obtained as follows:

$$\bar{\mathbf{U}} = \mathbf{H}\mathbf{U} \tag{25}$$

where $\mathbf{U}$ contains the global displacements of the associated elements m and n and $\mathbf{H}$ is the transformation matrix relating the displacements of the two tendon points to the nodal displacements of the hexahedral elements. All of the components of the above vectors can be defined by

$$\mathbf{U} = [\ u_{m1} \quad v_{m1} \quad w_{m1} \quad \cdots \quad u_{m8} \quad v_{m8} \quad w_{m8} \mid \ u_{n1} \quad v_{n1} \quad w_{n1} \quad \cdots \quad u_{n8} \quad v_{n8} \quad w_{n8}\ ]^T \tag{26}$$

$$\mathbf{H} = \begin{bmatrix} \bar{\mathbf{H}} & 0 \\ 0 & \bar{\mathbf{H}} \end{bmatrix} \tag{27}$$

where the transformation matrix $\bar{\mathbf{H}}$ is defined as follows:

$$\bar{\mathbf{H}} = \left[\begin{array}{ccc|c|ccc} N_1 & 0 & 0 & & N_8 & 0 & 0 \\ 0 & N_1 & 0 & \cdots & 0 & N_8 & 0 \\ 0 & 0 & N_1 & & 0 & 0 & N_8 \end{array}\right] \tag{28}$$

Tendon Stiffness and Load Computations

In this section, the principle of virtual work, which is known as the principle of virtual displacements, can be formulated to obtain both the tendon stiffness matrix and the load vector.

Based on the Updated Lagrangian method, the virtual work equation can be written as

$$\int_V D_{ijkl}\Delta e_{kl}\delta(\Delta e_{ij})dV + \int_V \sigma_{ij}\delta(\Delta\eta_{ij})dV = R - \int_V \sigma_{ij}\delta(\Delta e_{ij})dV \tag{29}$$

By substitution of Eq. (25) into Eq. (29) and rearrangement, the formulation of the tendon element with the incremental form of the displacement can be written in standard matrices with only the internal force of the prestressing tendon:

$$(\mathbf{H}^T\mathbf{T}^T\mathbf{K}_p\mathbf{T}\mathbf{H})\Delta\mathbf{U} = \mathbf{H}^T\mathbf{T}^T\mathbf{F}_p \tag{30}$$

where the total tendon stiffness matrix $\mathbf{K}_p$ consists of the tendon elastic stiffness matrix $\mathbf{K}_e$ and the tendon geometric stiffness matrix $\mathbf{K}_g$ and $\mathbf{F}_p$ is the tendon load vector in the local coordinates of the tendon segment.

$$\mathbf{K}_p = \mathbf{K}_e + \mathbf{K}_g \tag{31}$$

$$\mathbf{K}_e = \frac{E_pA}{L}\begin{bmatrix} 1 & -1 \\ -1 & 1 \end{bmatrix}, \qquad \mathbf{K}_g = \frac{P}{L}\begin{bmatrix} 1 & -1 \\ -1 & 1 \end{bmatrix} \tag{32}$$

$$\mathbf{F}_p = P\begin{Bmatrix} -1 \\ 1 \end{Bmatrix} \tag{33}$$

where A is the cross-sectional area of the segment, L = segment length; E_p = stress-strain modulus; and P = prestressing force in the tendon segment. By considering the metric terms of Eq. (30), the tendon stiffness matrix $\mathbf{K}_{TD}$ with dimensions of 48×48 and the tendon load vector $\mathbf{F}_{TD}$ having dimensions of 48×1 can be defined as follows:

$$\mathbf{K}_{TD} = \mathbf{H}^T\mathbf{T}^T\mathbf{K}_p\mathbf{T}\mathbf{H} \tag{34}$$

$$\mathbf{F}_{TD} = \mathbf{H}^T\mathbf{T}^T\mathbf{F}_p \tag{35}$$

As a result of Eq. (35), the tendon nodal loads are directly transferred to the equivalent nodal loads of the hexahedral element in which the tendon segment is located. In addition, these equivalent nodal loads from tendons are various during changes of strain due to elastic shortening and time-dependent effects. An algorithm based on iteration is implemented to correct the tendon force due to these effects.

Losses in the Prestressing Tendon

1. Friction loss: Losses due to friction are assumed to apply only to posttensioned members. The initial tendon force P_x at a distance x from the jacking end can be described by the following commonly used expression:

$$P_x = P_0 e^{-(\mu\alpha + kx)} \tag{36}$$

where P_0 = tendon force at the jacking end; x = distance along the tendon; α = cumulative angle; μ = curvature friction coefficient; and k = wobble friction coefficient. According to the concept of the piecewise linear tendon discretization (Mari 1984; Ketchum 1986) the force in the tendon P_i at each tendon point i is evaluated by direct application of the friction loss relationship.

$$P_i = P_0 e^{-(\mu\sum_{i=1}^{n}\alpha_i + k\sum_{i=1}^{n}L_i)} \tag{37}$$

where P_0 = tendon force at the jacking end; and L_i = tendon segment length. The angle change α, which is modeled as discrete deviations in θ at the interior tendon points over the length x, is defined by

$$\alpha_i = (\theta_i + \theta_{i+1})/2 \tag{38}$$

2. Anchor slip loss: In order to include the effect of anchorage slip, it is necessary to obtain the value of the prestressing loss at the anchorage point ΔP_0 and the length of the affected

Downloaded from ascelibrary.org by ASIAN INSTITUTE OF TECHNOLOGY on 09/12/14. Copyright ASCE. For personal use only; all rights reserved.

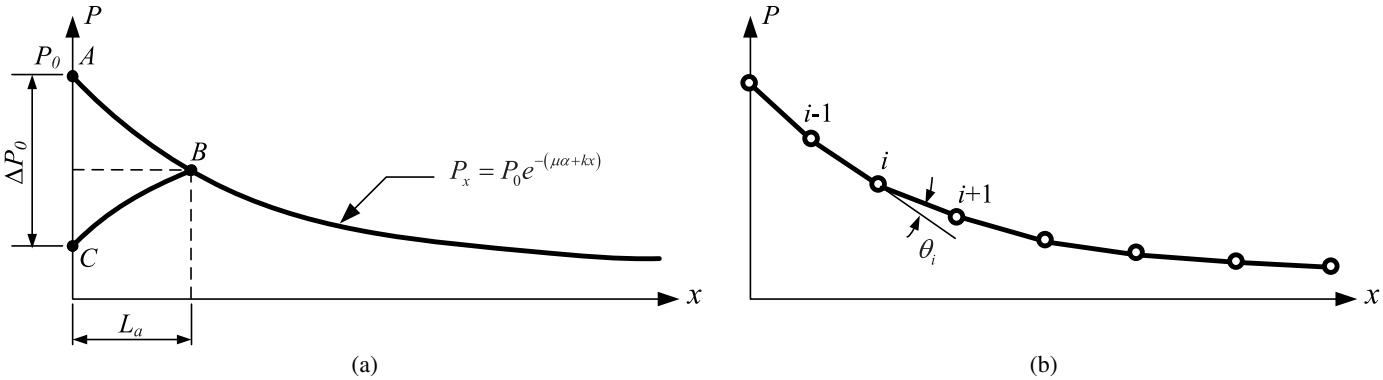

Fig. 4. Prestressing force variation due to friction and anchor slippage

zone L_a. The anchor slip displacement, which is equal to the integral of the change in strain over the slip distance L_a, can be obtained as

$$\Delta l = \int_0^{L_a} \frac{P(x)}{E_p A_p} dx \tag{39}$$

where E_P and A_P are the elastic modulus of the prestressing steel and the cross-sectional area of the prestressing tendon, respectively. Since the area ABC of the tendon force diagram, as shown in Fig. 4(a), is equal to the anchor slip displacement multiplied by $E_p A_p$, the anchor slip displacement can also be written

$$\Delta l = \frac{1}{E_p A_p} \text{Area}(ABC) \tag{40}$$

After the area ABC has been calculated using the geometry of the tendon profile, the numerical solution for the length L_a can be obtained by starting at the jacking end and locating the point C which satisfies the above condition.

3. Tendon stress relaxation: Relaxation is a phenomenon similar to creep and is defined as the decrease in stress over time under a constant strain. The following equation is used for the calculation of tendon stress relaxation:

$$\frac{f_s}{f_{si}} = 1 - \frac{\log_{10} t}{10} \left\{ \frac{f_{si}}{f_y} - 0.55 \right\} \tag{41}$$

where f_s = prestress at a time t; f_{si} = initial steel stress; and $f_y = 0.001$ offset yield stress of the prestressing steel. In order to capture the structural responses in numerical examples presented in the last section, the relaxation which is implemented here is based on only the ACI approach.

Construction Stage Analysis

Construction stage analysis can be defined as the numerical procedures for simulating complicated changes of structural system during actual construction (Ketchum 1986; Bishara 1990; Abbas 1993; Cruz 1994; Khaloo 2007; Malm 2010). In this study, there are some construction activities are defined and done at any construction stage to simulate the actual construction sequence such as installing or removing structural members and travelers, stressing tendons, and assigning or removing loads and supports. In the forward stage during construction, to ensure continuity of the deflection curve, continuity of the structure can be achieved by installing a new segment to the segment which has already been constructed in the

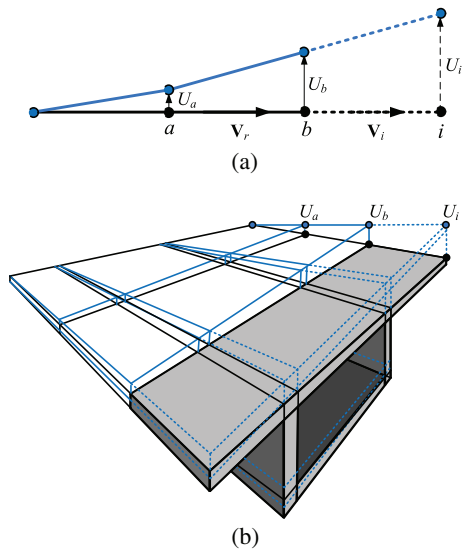

Fig. 5. (Color) Tangential installation of a new segment

tangential direction. The updated position for installing a new segment in one dimension is illustrated in Fig. 5(a). Similarly, the position of a new element in three-dimensional space can be evaluated by adopting the one-dimensional concept as shown in Fig. 5(b).

The following algorithm is here developed for determining the coordinate of a newly installed segment. The nodal coordinate of the target point i can be determined using the following relationships:

$$\mathbf{V}_r = [x_b - x_a \quad y_b - y_a \quad z_b - z_a]^T \tag{42}$$

$$\mathbf{V}_i = [x_i - x_a \quad y_i - y_a \quad z_i - z_a]^T \tag{43}$$

By using a linear equation, the new position of the displacements can be obtained as follows:

$$\begin{Bmatrix} u_i \\ v_i \\ w_i \end{Bmatrix} = \frac{|\mathbf{V}_i|}{|\mathbf{V}_r|} \begin{Bmatrix} u_b - u_a \\ v_b - v_a \\ w_b - w_a \end{Bmatrix} + \begin{Bmatrix} u_b \\ v_b \\ w_b \end{Bmatrix} \tag{44}$$

where $|\mathbf{V}_r|$ denotes the magnitude of the reference vector and $|\mathbf{V}_i|$ is the magnitude of the newly installed vector. The updated position of the installed segmental element can be found as follows:

J. Struct. Eng. 2014.140.

Downloaded from ascelibrary.org by ASIAN INSTITUTE OF TECHNOLOGY on 09/12/14. Copyright ASCE. For personal use only; all rights reserved.

$$\begin{Bmatrix} x_i \\ y_i \\ z_i \end{Bmatrix} = \begin{Bmatrix} x_o \\ y_o \\ z_o \end{Bmatrix} + \begin{Bmatrix} u_i \\ v_i \\ w_i \end{Bmatrix} \tag{45}$$

where the nodal displacements in the updated configuration u_i, v_i, w_i are combined with the nodal coordinates in the original configuration x_o, y_o, z_o to obtain the nodal coordinates in an updated configuration x_i, y_i, z_i.

Numerical Solution Strategy

The numerical solution for the analysis of structures undergoing time-dependent behavior is performed within a finite-element framework with a forward integration scheme in the time domain. The stresses, strains, and displacements of a structure are known at the beginning of each time step. External loads are incrementally applied and the resulting displacements, stresses, and strains are assumed to vary linearly within the time step. The new displacements, stresses, and strains are known at the end of each time step. For each solution step, the equilibrium equations may be expressed in matrix form as follows:

$$\mathbf{K}\Delta\mathbf{U} = \Delta\mathbf{R} \tag{46}$$

where the tangent stiffness matrix $\mathbf{K}$ of structure is a combination of the elastic stiffness matrix $\mathbf{K}_E$ and the geometric stiffness matrix $\mathbf{K}_G$ of the hexahedral elements and the stiffness matrix $\mathbf{K}_{TD}$ of the tendon elements as follows:

$$\mathbf{K} = \mathbf{K}_E + \mathbf{K}_G + \mathbf{K}_{TD} \tag{47}$$

The unknown incremental displacement $\Delta\mathbf{U}$ and the incremental total load $\Delta\mathbf{R}$ are obtained at each time from the relationship

$$\Delta\mathbf{R} = \Delta\mathbf{R}^{\text{ext}} + \mathbf{R}^{\text{int}} + \Delta\mathbf{R}^{nm} \tag{48}$$

where the incremental nodal load $\Delta\mathbf{R}^{\text{ext}}$ consists of an external load and a dead load. The internal force vector $\mathbf{R}^{\text{int}}$ can be obtained from the internal stresses in all of the elements, while the incremental load due to the nonmechanical strains $\Delta\mathbf{R}^{nm}$ is calculated based on changes in the time-dependent materials over the time step. To provide in more numerical details, furthermore, the scheme of the program is schematically demonstrated in Fig. 6.

Numerical Examples

The finite-element package *FINAS* was developed in Imperial College, London, for nonlinear analysis of general structures in a *UNIX* environment. At present, *XFINAS*, which is an extended version of *FINAS* for the general nonlinear dynamic analysis, has been developed at Asian Institute of Technology (AIT) and Konkuk University. *XFINAS* runs on the personal preprocessor and postprocessor software *GID 10* (2011) developed by International Center for Numerical Methods in Engineering (CIMNE) in Spain. The proposed procedure is implemented in the *XFINAS*. Several examples of prestressed concrete structures are chosen in order to demonstrate the validity and efficiency of the proposed procedure, while the numerical solution of a three-span segmental prestressed concrete bridge is carried out at the end of the paper.

Arc-Shaped Shell Structure

An arc-shaped cantilever shell structure with an angle of 45° and a radius of 30 is presented in order to verify the displacements obtained from the present procedure. A prestressing force of 150 is applied to each tendon and the additional external concentrated loads are simultaneously applied at the tip as illustrated in Fig. 7. The structure is modeled with an elastic modulus for the concrete of $E_c = 3 \times 10^6$ and a Poisson's ratio for the concrete of $\nu = 0.18$. A mesh with eight elements along the circumferential direction, eight elements along the edge, and two elements along the thickness is adopted. The numerical results are shown in Table 1. It can be seen from these that the tip displacements at point A from the present element in XFINAS match with those from the eight-node shell element in the finite-element program DIANA and from the nine-node PSC shell element in the other reference (Oh et al. 2005). Moreover, this numerical example demonstrates that the tendon element can perform well with the present element.

Horizontally Curved Prestressed Bridges

In this problem, four single-span box girder bridges with different radii of curvatures were selected to observe vertical displacements at the middle span and to evaluate performances of prestressing tendon included in the present hexahedral element (Khaloo et al. 2007). All four bridges are 54 m in length. Curvature angles of 0°, 30°, 60°, and 90° are considered, and the corresponding radii of curvatures are infinity, 103.1, 51.6, and 34.4 m, respectively. Geometry and layout of these bridges are illustrated in Fig. 8. Support conditions simulate a simple span with fixed torsion behavior about the longitudinal axis. Horizontal movements are free at both ends along the curved axis, while the vertical displacements are completely constrained. The two ends of the bridges are closed by a 30-cm-thick concrete diaphragm in order to reduce local effects and provide uniform distribution of the large support reactions. Prestressing tendons are distributed at nine slab positions. Each prestressing tendon is subdivided into 200 elements connected rigidly to the nodes of the hexahedral elements, while each bridge model includes 1,648 hexahedral elements. The typical finite-element bridge models with various angles are shown in Fig. 9. A 500-kN tension force is imposed on each tendon. The gravity loading which includes dead and live loads is modeled by a 25 kN/m^2 uniformly distributed load, which acts vertically and downward on the top of the slab surface.

All of the curved bridges were analyzed by *XFINAS* using the present eight-node solid element and another commercial program SAP2000 using four-node shell element. The vertical displacements at the middle span from both finite programs were compared and shown in Table 2 and Fig. 10. For the numerical results, it can be concluded that an increase in the angle of curvature significantly increases the vertical displacements at the middle span in all of load cases. In addition, the displacement results from the present hexahedral element including realistic tendon profiles show good agreement with those of the other finite-element program using shell element.

Concrete Cantilever Beam under Step Loading

A cantilever beam which is found in *MIDAS* verification examples (MIDAS 1989) is presented to validate the implemented creep model functions of CEB-FIP (1990) as shown in Fig. 11(a). This beam has the following parameters: a beam cross section of 1.0×1.0 m; a beam length of $L = 10$ m, elastic modulus of $E_c = 3.63 \times 10^6$ ton/m^2; a Poisson's ratio of $\nu = 0.18$; a compressive strength for the concrete at the age of 28 days of 4000 ton/m^2; a relative humidity of 70%; a notational size of member of 0.5; normal or rapid hardening cement. The step load acts on the tip of the beam as illustrated in Fig. 11(b). For this example, the cantilever beam subjected to four axial loads at the tip was modeled

Downloaded from ascelibrary.org by ASIAN INSTITUTE OF TECHNOLOGY on 09/12/14. Copyright ASCE. For personal use only; all rights reserved.

Downloaded from ascelibrary.org by ASIAN INSTITUTE OF TECHNOLOGY on 09/12/14. Copyright ASCE. For personal use only; all rights reserved.

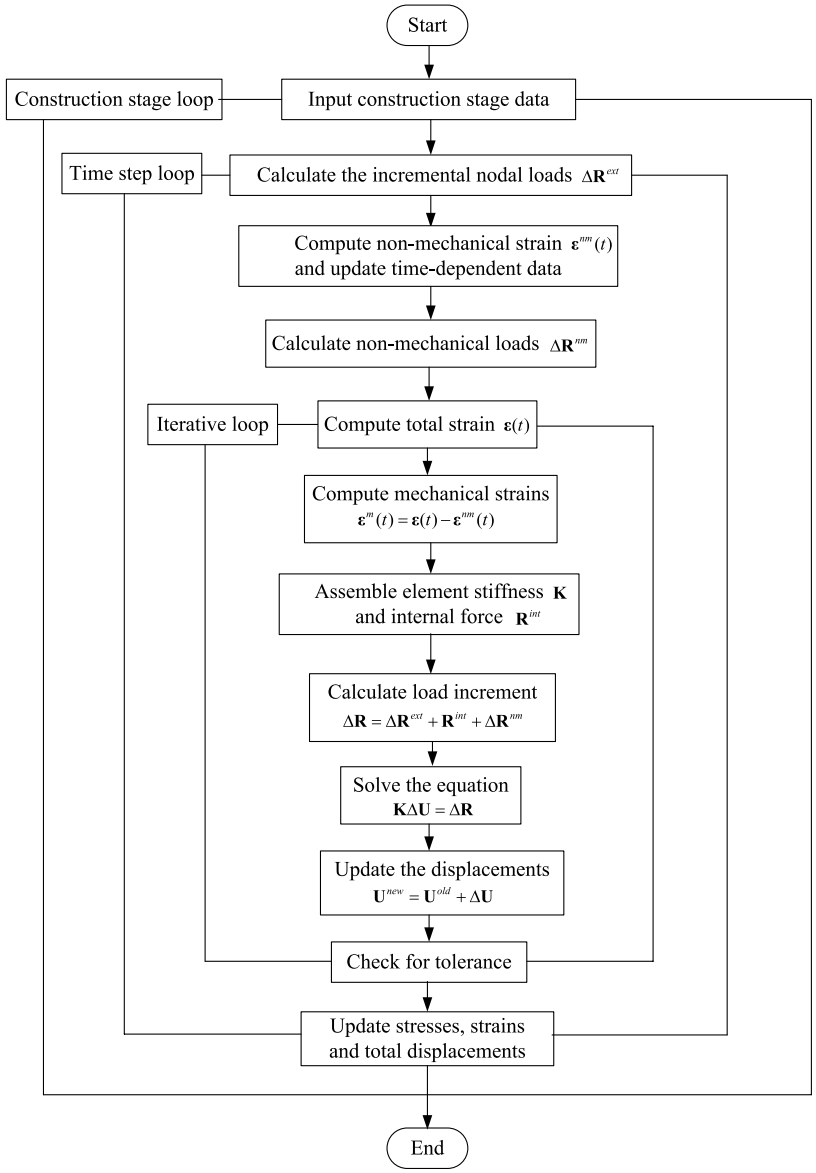

Fig. 6. Flow chart for implementation

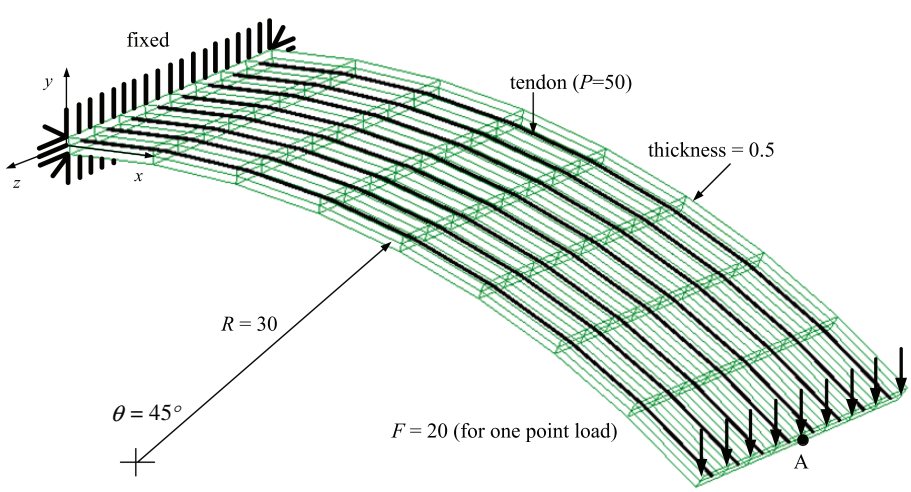

Fig. 7. (Color) Arc-shaped shell structure

using a $1 \times 1 \times 10$ mesh size as shown in Fig. 11(c). A comparison of the results from *XFINAS* using the present element and from *MIDAS* using frame element is shown in Fig. 12. The elastic shortening displacement is 0.0275 cm, with the total displacements affected by creep being normalized by this value. The displacement obtained from the beam modeled using the present element show good agreement with that from the reference using frame element. Therefore, it is proved that the implementation of creep analysis under changes of load history has adequate accuracy.

Cantilever Beam under an Imposed Shear Load

To verify the creep recovery, a cantilever beam under an imposed shear load is presented, while shrinkage and temperature effects are not included (Kechum 1986). The beam is 3.05 m (120 in.) long, 0.56 m (22 in.) deep and 0.23 m (9 in.) wide, as shown in Fig. 13. The concrete's 28th day strength is 34.48 MPa (5,000 psi), the unit weight is 2,403 kg/m^3 (150 pcf), and the humidity is set at 70%. The ultimate creep used for the ACI model is 3.00 and the casting date of concrete is made to be day 0. The beam boundary conditions for this case are fixed at one end and free at the other with an imposed load of $F = 44.48$ kN (10,000 lb). The load is applied on day 30 and removed on day 630, this applies a constant stress to the beam over the duration of the loading.

In this study, the cantilever beam is modeled with 20 hexahedral elements. The results of the vertical displacement at the tip of the beam from the present element and from the reference are illustrated in Fig. 14. During the time period when applying the load, very good agreement of the vertical displacements from both studies is obtained. Moreover, a comparison of the tip displacements for the two element types during the creep recovery phase also shows good agreement.

Three Span Cantilever Box Girder Bridge

This example demonstrates the capabilities of the proposed procedure for analysis of a three-span segmentally erected prestressed concrete bridge (Ketchum 1986). The girder segments are cast in situ using a travelling formwork, while the girders near the abutments are erected conventionally. The structural behavior of the bridge under the dead load, construction loads and prestressing is traced through the construction phase and over a 27-year service period thereafter.

The bridge geometry and details are as shown in Fig. 15(a). The center span is 137.16 m (450 ft) long, with the two side spans being 86.87 m (285 ft) long. The girders are single-cell, haunched box sections with wide cantilever slabs, while the depth varies from 7.30 m (24 ft) at the piers to 2.75 m (9 ft) at the midspan and abutments. The bottom slab thickness varies from 1.07 m (3.5 ft) at the piers to 0.23 m (0.75 ft) at midspan. The variations of these dimensions over the length of the bridge are summarized in Figs. 15(b and c). The bottom slab width varies from 8.84 m (29 ft) at midspan and at the abutments to 7.32 m (24 ft) at the piers.

The typical profiles of the cantilever prestressing tendons are shown in Fig. 16(a). A total of 64 prestressing tendons, each of 20.73 cm^2, are stressed with an initial force of 2835.6 kN from both

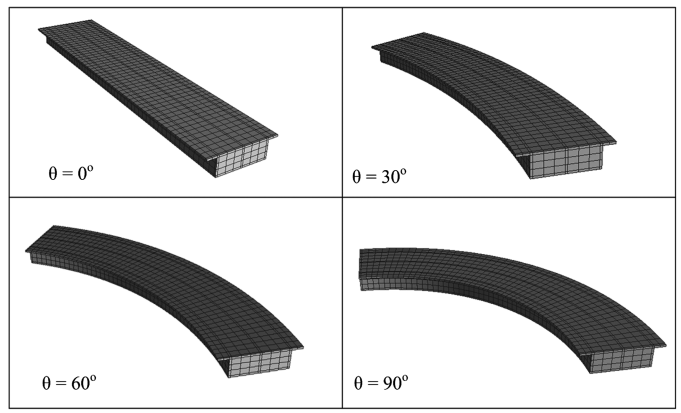

Fig. 9. Finite-element models of the curved bridges with 0°, 30°, 60°, and 90°

Table 1. Comparison of the Tip Displacements

Name	x-direction	y-direction	z-direction
Oh et al. (2005)	−1.0020	−1.6763	0
DIANA	−0.9591	−1.6150	0
XFINAS	−0.9016	−1.6928	0

Table 2. Comparison of the Middle Displacements under Different Angles of Curvature

		Bottom deflection at middle span (m)		
Name	Angle	Gravity	Prestressing	Gravity and prestressing
SAP2000	0	−0.0660	0.0050	−0.0610
	30	−0.0730	0.0061	−0.0669
	60	−0.1030	0.0058	−0.0972
	90	−0.1790	0.0070	−0.1720
XFINAS	0	−0.0671	0.0049	−0.0594
	30	−0.0744	0.0050	−0.0663
	60	−0.1042	0.0055	−0.0951
	90	−0.1761	0.0065	−0.1645

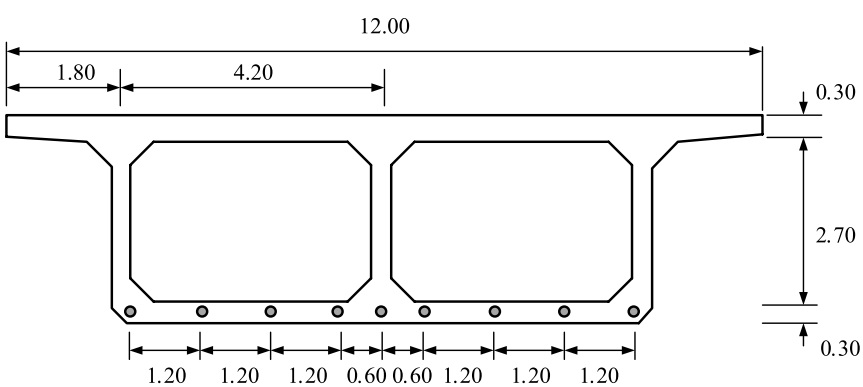

Fig. 8. Cross section and tendon position of the curved bridge

Downloaded from ascelibrary.org by ASIAN INSTITUTE OF TECHNOLOGY on 09/12/14. Copyright ASCE. For personal use only; all rights reserved.

ends and anchored at the end of each girder segment during the construction phase as illustrated in Fig. 16(b). Fig. 16(c) shows eight continuity prestressing tendons which are stressed after the bridge has been made continuous with the midspan closure. There are 12 local tendons placed in the center span and eight local tendons provided in the side spans. All local tendons are stressed after the bridge is made continuous as shown in Fig. 16(d). Moreover, in this study, a total of four transverse tendons are also placed on the top slab of each girder segment to reduce the deflection of the flange for each box girder as shown in Fig. 16(f). The diameter of each transverse tendon is 0.0127 m (0.5 in).

The time-dependent development of creep, shrinkage and aging utilize the ACI 209R-92 (ACI 1982) recommendation parameters. The concrete has an ultimate strength of $f_c'(28) = 34.47$ MPa (5,000 psi), an ultimate creep factor of $C(\infty) = 3.00$, an ultimate shrinkage strain of $\varepsilon(\infty) = 0.0008$, and a unit weight $W = 2{,}482.86$ kg/m^3 (155 pcf). The prestressing steel has an elastic modulus of $E_{ps} = 1.93 \times 10^5$ MPa (2.8×10^7 psi), a yield strength of $f_{py} = 1{,}862$ MPa (2.6×10^5 psi), an ultimate strength of $f's = 1{,}900$ Mpa (2.7×10^5 psi), a relaxation coefficient of $R = 10$, a curvature friction coefficient of $\mu = 0.25$/radian, a wobble coefficient of $k = 0.001312$/m (0.0004/ft), and an anchorage slip of 0.00635 m (1/4 in).

Only one-quarter of the bridge is modeled as a result of symmetry as shown in Fig. 17. The bridge model consists of 898 of the present hexahedral elements, while the prestressing tendons which are modeled using tendon elements are subdivided into 300 elements for each tendon with no slip. Sufficiency of mesh fineness has been validated based on checking the elastic response. The loads applied to the bridge consist of the structural dead load and a superimposed dead load of 36.5 kN/m (2.5 kips/ft). The superimposed dead load is added after the midspan closure and is sustained for the 27-year service period. Construction sequence activities of the segmental prestressed concrete bridge are demonstrated in Table 3. The traveling formwork which is used in this example is modeled using frame elements. The travelers may be moved around the structure and are therefore not subjected to time-dependent effects.

The comparison of the average of the top and bottom vertical displacements of the web during construction and at the completion of cantilevering are made between the numerical results obtained from the frame element proposed by Ketchum and from the present

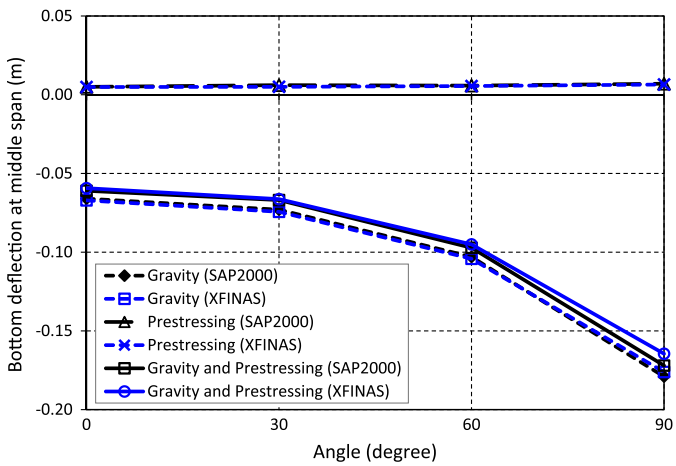

Fig. 10. Vertical displacements at the middle span of the curved bridges with 0°, 30°, 60°, and 90°

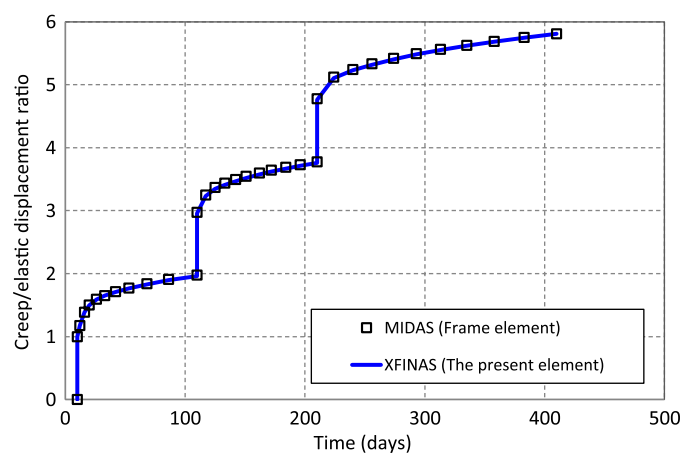

Fig. 12. Comparison of the results for the present element and the reference

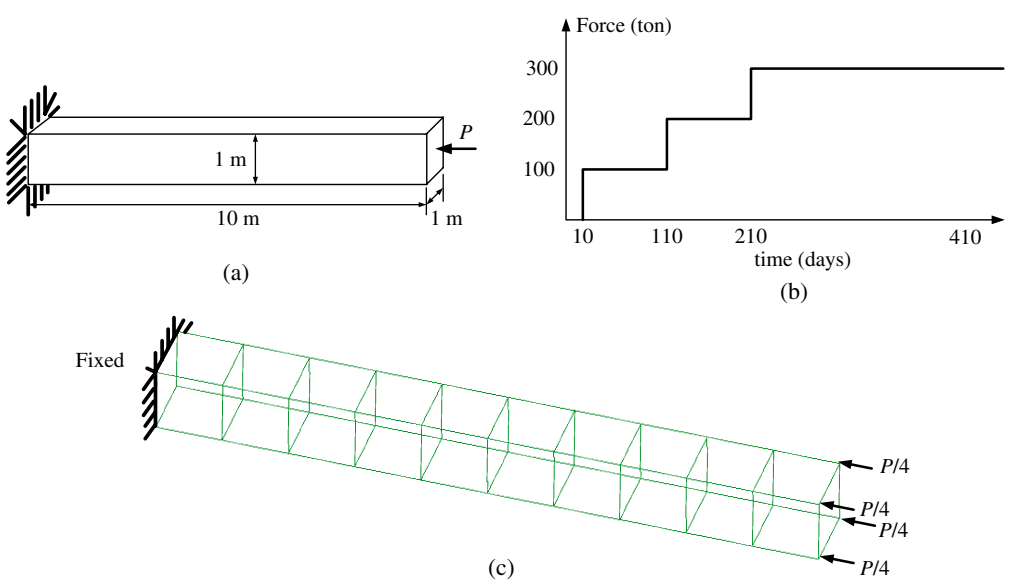

Fig. 11. Pure creep under axial step loadings

Downloaded from ascelibrary.org by ASIAN INSTITUTE OF TECHNOLOGY on 09/12/14. Copyright ASCE. For personal use only; all rights reserved.

Downloaded from ascelibrary.org by ASIAN INSTITUTE OF TECHNOLOGY on 09/12/14. Copyright ASCE. For personal use only; all rights reserved.

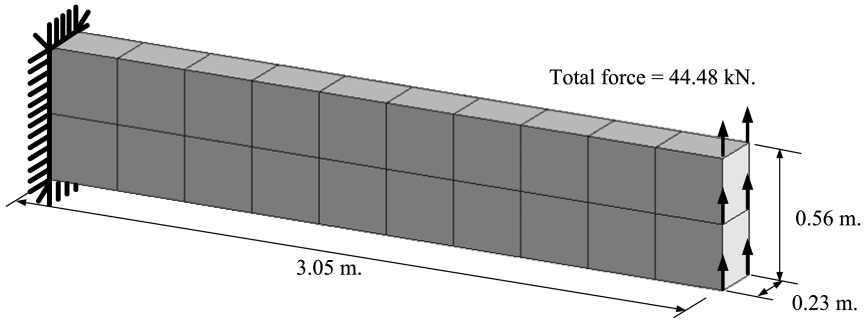

Fig. 13. Cantilever beam under an imposed shear load

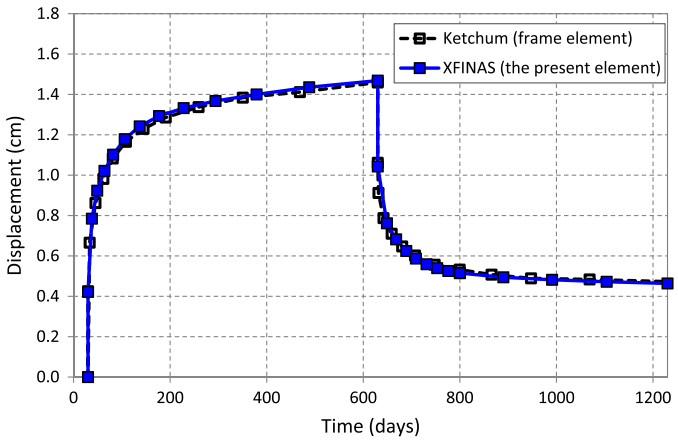

Fig. 14. History of the tip deflection of the cantilever beam under an imposed shear load

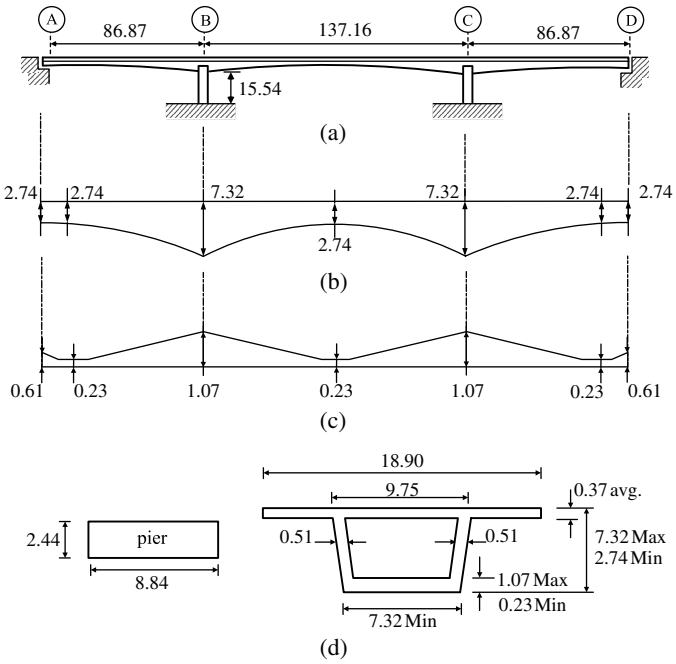

Fig. 15. Three span cantilever bridge geometry

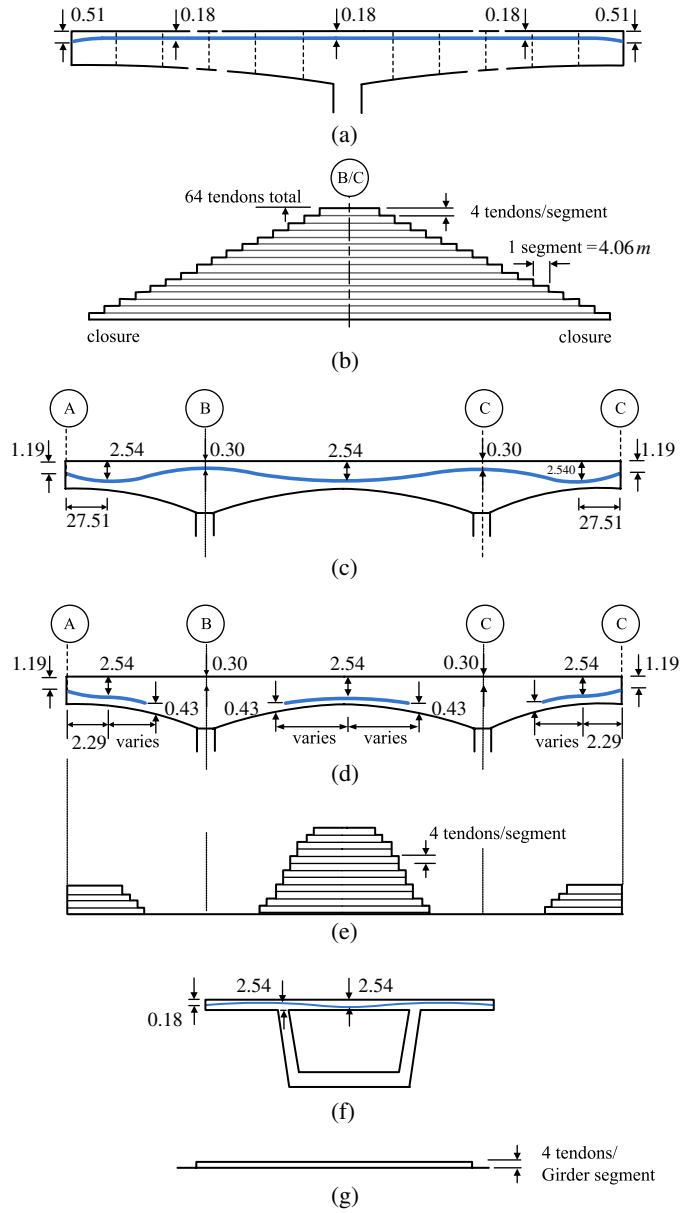

Fig. 16. Prestressing tendon layout

hexahedral element based on the proposed procedure as illustrated in Fig. 18. For both construction phases, it can be observed that the displacements are approximately symmetrical about the pier as a result of the structural symmetry. However, the displacements obtained from the solid element model are larger than those obtained from the frame element model.

Fig. 19 shows a comparison of the average of the top and bottom vertical displacements of the web at the completion of construction and after 27 years. The displacements about the pier are not

Downloaded from ascelibrary.org by ASIAN INSTITUTE OF TECHNOLOGY on 09/12/14. Copyright ASCE. For personal use only; all rights reserved.

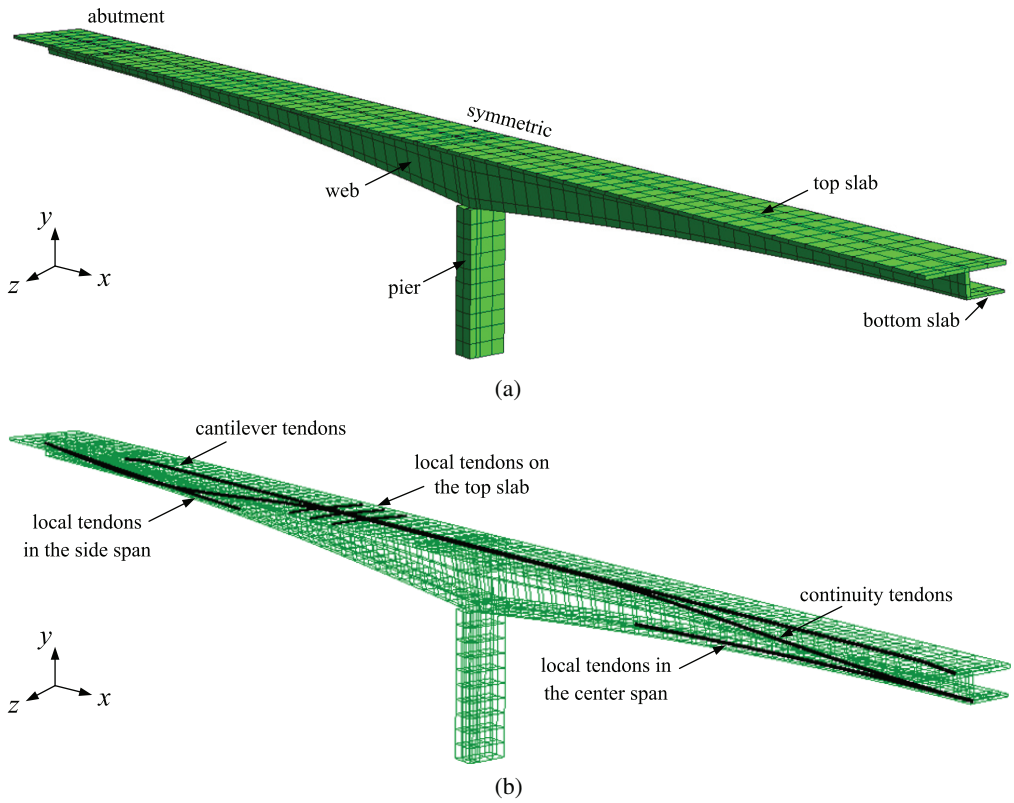

Fig. 17. (Color) Finite-element mesh of the quarter bridge model

Table 3. Construction Sequence Activities

Day	Construction activities
0–63	Build pier and starting girder segments, and stress the corresponding transverse tendon
63–168	Build cantilever girder segments, stress and cantilever and transverse tendons, with a seven day for each set of segment
100	Build approach girder segments, stress the corresponding transverse tendons
168	Close side span with closure girder segment, stress the corresponding transverse tendons
175	Stress local tendons in side span
182	Close center span with closure girder segment, stress the corresponding transverse tendons
189	Stress local tendons in center span and remove travelers
196	Stress continuity tendons and add superimposed dead load

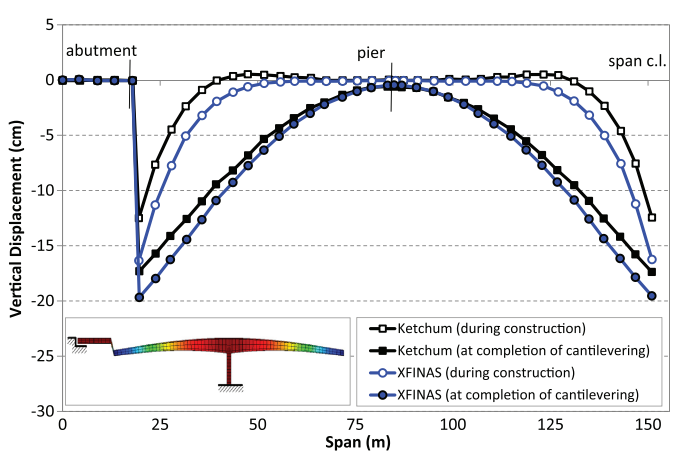

Fig. 18. (Color) Deflections during construction and at completion of cantilevering

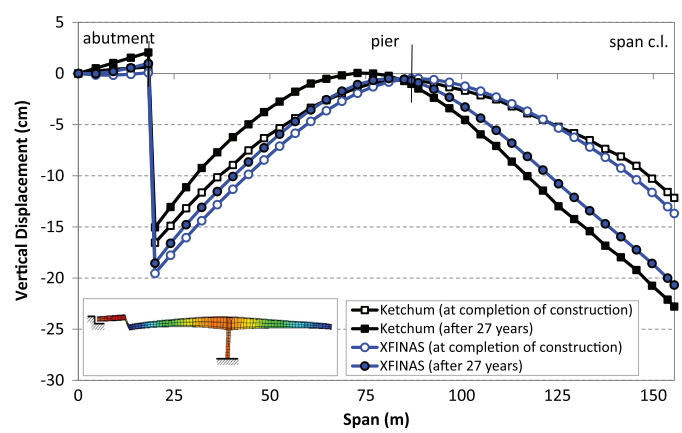

Fig. 19. (Color) Deflections at completion of construction and after 27 years

symmetrical due to the effects of the supports. The long-term displacements in the short span are vertically upwards because the length of the main span is longer. The time-dependent effects due to creep, shrinkage and relaxation play an important role by causing downward deflection at midspan after the 27 years when compared with that at the completion of construction phase. The long-term deflection after the 27 years obtained from the present model increases approximately 51% of that at the state of completion of construction. Therefore, it is necessary to include the time-dependent effects in the design of prestressed concrete bridges to avoid excessive deflection. In addition, the deflections of the bridge modeled by the present element at various time steps is shown in Fig. 20, while the deformation shape of the full model of the segmental prestressed concrete bridge after 27 years is illustrated in Fig. 21.

As shown in Fig. 18, 19, and 20, there is an abrupt jump of deflection at the closure girder segment connecting between abutment and cantilever segments. In this analysis, the girder displacements are obtained without applying pre-camber. This results in large discontinuities of the girder profile at the closure segments when the bridge is complete. During construction, in general, these displacements are compensated by cambering the girder so that it will not have such discontinuities and the girder profile will be at a specified elevation when the bridge is completed. However, the construction process is used here not because it would be realistic as the actual construction, but because it is the simplest to check the correctness of programming with the reference.

For the deformation of the bridge cross section, comparisons of the displacements of the top and bottom decks located at the sample distance of 156 m (512 ft) in the x-direction are summarized and illustrated in Fig. 22. This is an advantage of using brick elements

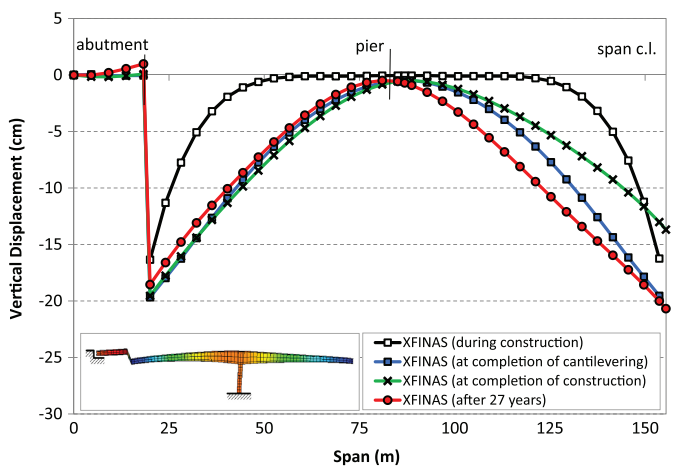

Fig. 20. (Color) Deflections of the bridge obtained from the present model at various times

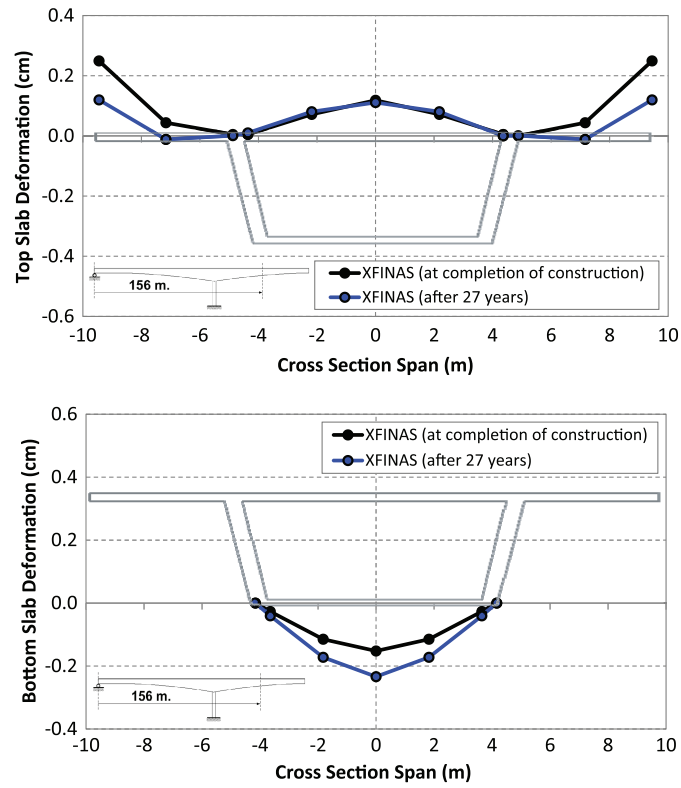

Fig. 22. (Color) Average deflections along top and bottom slabs at 156 m in the x-direction

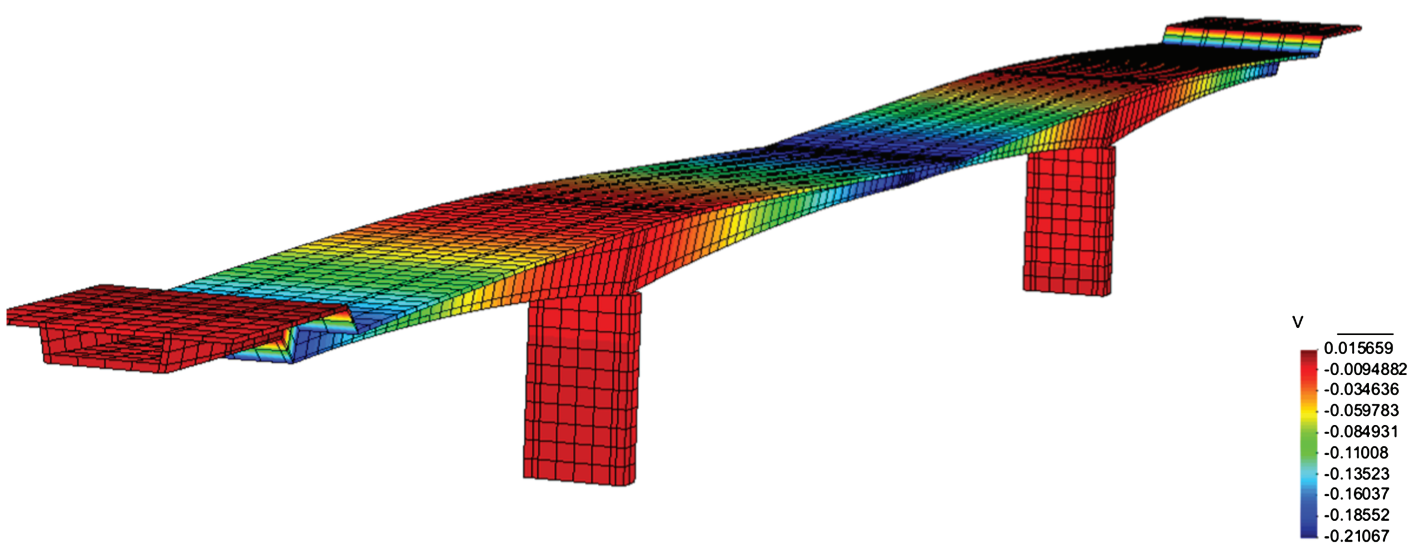

Fig. 21. (Color) Deformation shape of the bridge after 27 years

Downloaded from ascelibrary.org by ASIAN INSTITUTE OF TECHNOLOGY on 09/12/14. Copyright ASCE. For personal use only; all rights reserved.

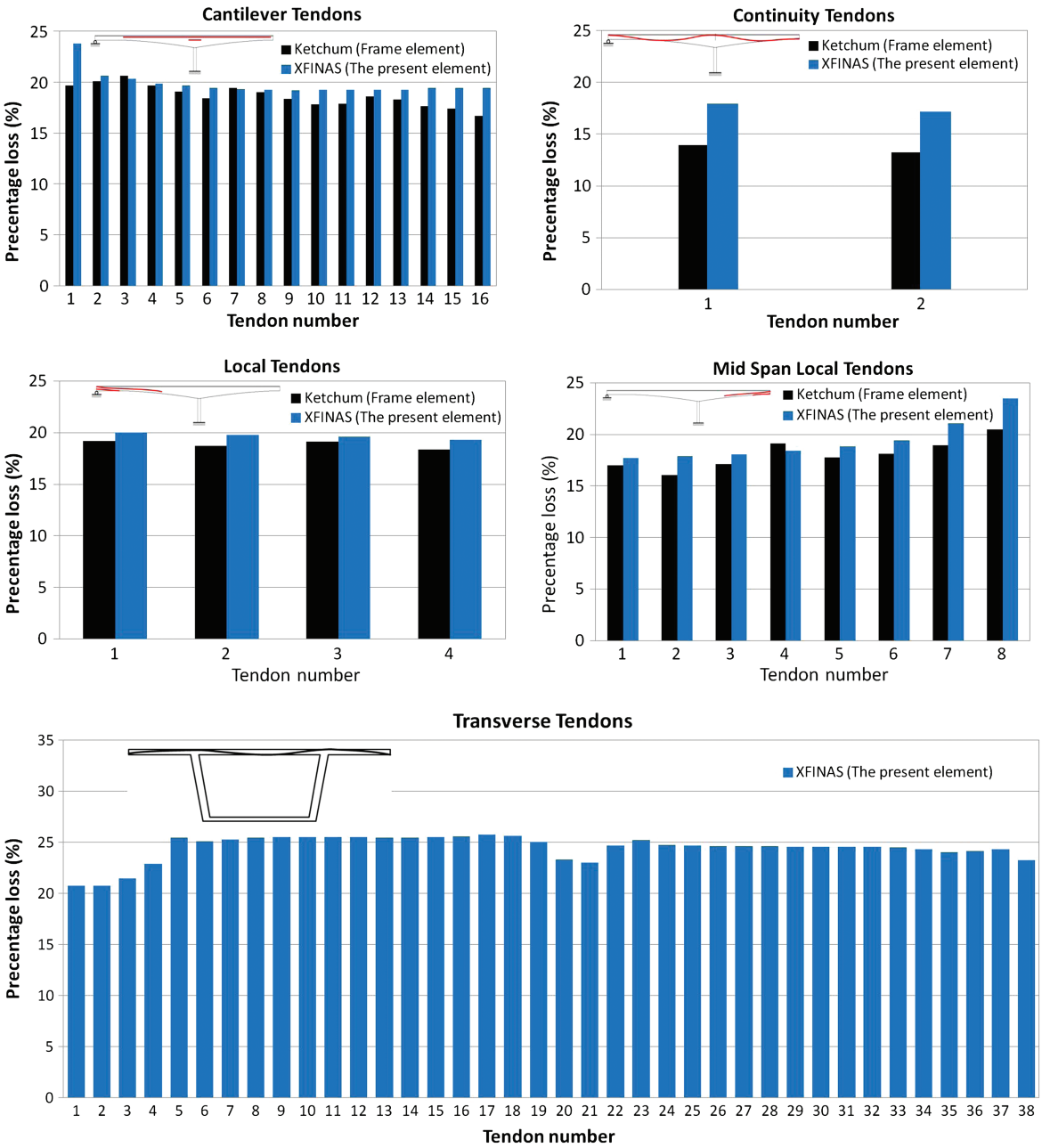

Fig. 23. (Color) Prestress losses in the tendons after 27 years

in modeling the bridge, because the transverse deformation used for the design of the bridge cross section can be obtained.

According to the results mentioned above, however, the trend of the displacements obtained from the present element show some differences from those obtained from the frame element. There are four significant reasons contributed to these results as follows: (1) the stiffness formulation used for the frame element proposed by Ketchum neglects the effect of shear deformation, while the present element includes shear deformation in its formulation; (2) the geometric nonlinearity is taken into account in the present study—however, this nonlinear effect was not included in the analysis using frame element; (3) the supports for the frame model are assigned at the centroid of the cross section, while the boundary conditions for the present model are assigned by following the realistic support profile of the bridge; and (4) the prestressing loss in the present model is slightly different from that occurring in the frame element due to the differences of the finite-element modeling and element formulations used in both studies, as illustrated in Fig. 23. The total average loss obtained from the cantilever, continuity, local, and midspan local tendons of the present model reaches 19%, while the one of the frame model is approximately 17%. Moreover, the total average loss in the transverse tendons located in the top slab of the present model using hexahedral element is around 24%.

Conclusion

In this paper, a step-by-step numerical procedure for three-dimensional analysis of segmentally constructed prestressed concrete bridges using the hexahedral element with 24 enhanced assumed strain (EAS) parameters has been presented. The geometric

J. Struct. Eng. 2014.140.

Downloaded from ascelibrary.org by ASIAN INSTITUTE OF TECHNOLOGY on 09/12/14. Copyright ASCE. For personal use only; all rights reserved.

nonlinearity and time-dependent effects due to creep, shrinkage and aging of the concrete and relaxation of the prestress have been taken in account, while possible changes to the structural configuration and load histories during the construction process have also been incorporated. In order to include realistic tendon profiles, the prestressing tendon has been developed based on a system of piecewise linear prestressing segments.

Several numerical examples of prestressed concrete structures have been carried out to demonstrate the validity and efficiency of the proposed procedure. The results of the present procedure show good agreement with those from the references. At the end of the paper, the analysis of the segmental prestressed concrete bridge has been successfully performed to predict the structural responses at each construction stage and at the long-term periods. The numerical results of the analysis using hexahedral element present similar tendency with those of the reference using frame element, while the time-dependent effects due to creep, shrinkage, and relaxation show a significant impact on the long-term response of the bridge. Based on these numerical results, complex responses from the three-dimensional analysis of segmentally constructed prestressed concrete bridges can be realistic captured by the proposed procedure.

Acknowledgments

This work was supported by Konkuk University.

References

ABAQUS [Computer software]. Dassault Systèmes/SIMULIA, Providence, Rhode Island.

Abbas, S., and Scordelis, A. C. (1993). "Nonlinear geometric, material and time-dependent analysis of segmentally erected three-dimensional cable stayed bridges." *UCB/SEMM-93/09*, Univ. of California at Berkeley, Berkely, CA.

American Concrete Institute (ACI). (1982). "Prediction of creep, shrinkage, and temperature effects in concrete structures." *ACI 209R-82, ACI Committee 209*, Detroit, MI.

Andelfinger, U., Ramm, E., and Roehl, D. (1996). "2D-and 3D-enhanced assumed strain element and their application in plasticity." *Proc., Computational Plasticity 4th Int. Conf.*, D. Owen, E. Onate and H. Hinton, eds., Pineridge Press, Swansea, U.K., 1992–2007.

Ates, S. (2011). "Numerical modelling of continuous concrete box girder bridges considering construction stages." *App. Math. Model.*, 35(8), 3809–3820.

Bažant, Z. P., Yu, Q., and Li, G.-H. (2012a). "Excessive long-term deflections of prestressed concrete box girders. I. Record-span bridge in Palau and other paradigms." *J. Struct. Eng.*, 10.1061/(ASCE)ST.1943-541X.0000487, 676–686.

Bažant, Z. P., Yu, Q., and Li, G.-H. (2012b). "Excessive long-term deflections of prestressed concrete box girders. II. Numerical analysis and lessons learned." *J. Struct. Eng.*, 10.1061/(ASCE)ST.1943-541X.0000375, 687–696.

Bishara, A. G., and Papakonstantinou, N. G. (1990). "Analysis of cast-in-place concrete segmental cantilever bridges." *J. Struct. Eng.*, 10.1061/(ASCE)0733-9445(1990)116:5(1247), 1247–1268.

Cardoso, R. P. R., Yoon, J. W., Mahardika, M., Choudhry, S., Alves de Sousa1, R. J., and Fontes Valente, R. A. (2008). "Enhanced assumed strain (EAS) and assumed natural strain (ANS) methods for one-point quadrature solid-shell elements." *Int. J. Numer. Methods Eng.*, 75(2), 156–187.

Cruz, P. J. S. (1991). "Nonlinear analysis of planar reinforced concrete frames." M.S. thesis, Univ. of Porto, Porto, Portugal.

Cruz, P. J. S. (1994). "A model for the nonlinear and time-dependent analysis of sequentially constructed reinforced, prestressed and composite concrete structures." Ph.D. thesis, Technical Univ. of Catalonia, Barcelona, Spain.

Cruz, P. J. S., Mari, A. R., and Roca, P. (1998). "Nonlinear time-dependent analysis of segmentally concreted structures." *J. Struct. Eng.*, 10.1061/(ASCE)0733-9445(1998)124:3(278), 278–287.

DIANA [Computer software]. Delft, Netherlands, TNO Building and Construction Research.

Euro-International Committee for Concrete, and International Federation for Prestressing (CEB-FIB). (1990). *Model code for concrete structures*, Thomas Telford, London.

GID 10 [Computer software]. Barcelona, Spain, International Center for Numerical Methods in Engineering.

Hauptmann, R., Doll, S., Harnau, M., and Schweizerhof, K. (2001). "Solid-shell elements with linear and quadratic shape functions at large deformations with nearly incompressible materials." *Comput. Struct.*, 79(18), 1671–1685.

Kabir, A. F. (1976). "Non-linear Analysis of Reinforced Concrete Panels, Slabs and Shells for Time Dependent Effects." *UC-SEEM 76-6*, Univ. of California, Berkeley, CA.

Kang, Y. J. (1977). "Nonlinear geometric, material, and time dependent analysis of reinforced and prestressed concrete frames." *UC-SESM 77-1*, Univ. of California, Berkeley, CA.

Kang, Y. J., and Scordelis, A. C. (1980). "Nonlinear analysis of prestressed concrete frames." *J. Struct. Div.*, 106(2), 445–462.

Ketchum, M. A. (1986). "Redistribution of stresses in segmentally erected prestressed concrete bridges." *UCB-SEMM 86/07*, Univ. of California, Berkeley, CA.

Khaloo, A. R., and Kafimosavi, M. (2007). "Enhancement of flexural design of horizontally curved prestressed bridges." *J. Bridge. Eng.*, 10.1061/(ASCE)1084-0702(2007)12:5(585), 585–590.

Kim, K. D., Byun, Y. J., Kim, H. K., Lomboy, G. R., Suthasupradit, S., and Kim, Y. H. (2007a). "Development of quasi-conforming shell element for the three dimensional construction stage analysis of PSC bridge." *J. Comput. Struct. Eng. Ins. Korea.*, 20(3), 329–338.

Kim, K. D., Han, S. C., and Suthasupradit, S. (2007b). "Geometrically nonlinear analysis of laminated composite structures using a 4-node co-rotational shell element with enhanced strain terms." *Int. J. Nonlin. Mech.*, 42(6), 864–881.

Kim, K. D., Liu, G. Z., and Han, S. C. (2005). "A resultant 8-node solid-shell element for geometrically nonlinear analysis." *Comput. Mech.*, 35(5), 315–331.

Korelc, J., and Wriggers, P. (1997). "Improved enhanced strain fournode element with Taylor expansion of the shape functions." *Int. J. Numer. Methods Eng.*, 40(3), 407–421.

Malm, R., and Sundquist, H. (2010). "Time-dependent analyses of segmentally constructed balanced cantilever bridges." *Eng. Struct.*, 32(4), 1038–1045.

Mari, A. R. (1984). "Nonlinear geometric, material, and time dependent analysis of three-dimensional reinforced and prestressed concrete frames." *UC-SESM 84-10*, Univ. of California, Berkeley, CA.

Mari, A. R. (2000). "Numerical simulation of the segmental construction of three dimensional concrete frames." *Eng. Struct.*, 22(6), 585–596.

Mari, A. R., Mirambell, E., and Estrada, I. (2003). "Effects of construction process and slab prestressing on the serviceability behaviour of composite bridges." *J. Constr. Steel. Res.*, 59(2), 135–163.

MIDAS Information Technology. (1989). *MIDAS/Civil verification examples*, Seoul, Korea.

Oh, B. H., and Jeon, S. J. (2005). "An advanced FE analysis of PSC shell structures incorporating tendon-induced deformation-dependent loads." *Finite. Elem. Anal. Des.*, 41(9–10), 834–849.

Pramin, N., Songsak, S., and Kim, K.-D. (2012). "A co-rotational 8-node degenerated thin-walled element with assumed natural strain and enhanced assumed strain." *Finite Elem. Anal. Des.*, 50, 70–85.

SAP2000 [Computer software]. Berkeley, CA, Computers and Structures.

Scordelis, A. C. (1983). "Analytical models for nonlinear material, geometric, and time- dependent effects." *Int. Symp. on Nonlinearity and Continuity in Prestressed Concrete, Preliminary Publication*, Univ. of Waterloo, ON, 25–43.

Scordelis, A. C. (1984). "Computer models for nonlinear analysis of reinforced and prestressed concrete structures." *PCI J.*, 29(6), 116–135.

Downloaded from ascelibrary.org by ASIAN INSTITUTE OF TECHNOLOGY on 09/12/14. Copyright ASCE. For personal use only; all rights reserved.

Scordelis, A. C. (1988). "Recent developments at Berkeley in non-linear analysis of prestressed concrete structures." *Proc., of the Int. Federation for Prestressing (FIP) Symp.*, Jerusalem, 369–376.

Simo, J. C., and Armero, F. (1992). "Geometrically non-linear enhanced strain mixed methods and the method of incompatible modes." *Int. J. Numer. Methods Eng.*, 33(7), 1413–1449.

Simo, J. C., Armero, R., and Taylor, R. L. (1993). "Improved versions of assumed enhanced strain tri-linear elements for 3D finite deformation problems." *Comput. Meth. Appl. Mech. Eng.*, 110(3–4), 359–386.

Simo, J. C., and Rifai, M. S. (1990). "A class of mixed assumed strain methods and the methods of incompatible modes." *Int. J. Numer. Methods Eng.*, 29(8), 1595–1638.

XFINAS 3.0 [Computer software]. Seoul, Korea, Konkuk Univ.

Yu, Q., Bažant, Z. P., and Wendner, R. (2012). "Improved algorithm for efficient and realistic creep analysis of large creep-sensitive concrete structures." *ACI Struct. J.*, 109(5), 665–676.

Downloaded from ascelibrary.org by ASIAN INSTITUTE OF TECHNOLOGY on 09/12/14. Copyright ASCE. For personal use only; all rights reserved.

Performance-Based Seismic Design of a High-Rise Hybrid Building

Pramin Norachan
Coordinator, Civil and Structural Engineering Unit
AIT Solutions, Asian Institute of Technology, Thailand
Pathumthani, Thailand
pramin.aitc@ait.asia

Govinda Khanal
Structural Engineer, Civil and Structural Engineering Unit
AIT Solutions, Asian Institute of Technology, Thailand
Pathumthani, Thailand
govinda@ait.asia

Naveed Anwar
Executive Director
AIT Solutions, Asian Institute of Technology, Thailand
Pathumthani, Thailand
nanwar@ait.ac.th

Abstract*—A systematically procedure of performance-based seismic design of a high-rise hybrid building is presented in this paper as an alternative to the prescriptive design codes. This 37-story residential building consists of both cast-in-place reinforced concrete (RC) and precast concrete (PC) structures. The cast-in-place RC shear walls are used as the primary lateral force-resisting system, while the PC load-bearing walls and PC slabs are employed for all residential areas. Fiber modeling technique are used to simulate the nonlinear behavior of structural walls, while lumped plastic moment or shear hinges are employed to capture the nonlinear actions of frame components. The performance-based seismic evaluation under MCE earthquake level using nonlinear time-history analysis (NLTHA) based on 7 pairs of ground motions are mainly carried out in order to correcting deficiencies of structural system to satisfy the selected performance level of Collapse Prevention (CP). The performance of the building is assessed by using several response indicators both in terms of global and local responses such as base shears, story drifts, energy dissipations, and the strength and deformation actions against capacities of primary structural components. The results show not only vertical elements of the lateral force-resisting systems perform in inelastic range, but the floor systems also play a very critical role in the seismic responses.

***Keywords*—hybrid building, precast load-bearing walls, performance-based seismic design, maximum considered earthquake, nonlinear time-history analysis**

I. INTRODUCTION

Over the past decade, hybrid structure system which is a combination of cast-in-place reinforced concrete (RC) and precast concrete (PC) structural systems has been increasingly developed and utilized to build low-rise, mid-rise and high-rise buildings in Thailand. The precast concrete system which is also known as prefabricated construction has several advantages, such as rapid construction, cost effectiveness, business competition and good quality control. However, the connections between the PC members become very critical and needs to play careful attention for design. There are two main types of PC structural systems which are frame and bearing wall are commonly used with welded and cast-in-place connections.

However, based on recent seismic hazard studies in Thailand, there are many regions especially northern and western parts of the country have high risk from damaging ground motions [1]. Even Bangkok is located at the center of the country and is far away from seismic sources, Bangkok is still at risk from damaging ground motions induced by distant large earthquakes [2]. The recent Thai seismic design codes for structures have been also included theses seismic effects. Therefore, the buildings must be designed to resist not only gravity and wind loads, but also seismic loads as wells. Especially, for the PC structures in seismic regions, the seismic-resisting system needs to be provided, which can be related to these different systems: (1) moment frames; (2) structural walls; and (3) floor diaphragm [3]. In general, the buildings are designed by using conventional code-based design as prescriptive codes which are intended to provide the minimum safety requirement and for the general types of buildings. As a result of these board applicability, the prescriptive codes contain many requirements that are not specifically applicable to tall buildings and may result in designs that are less than optimal for both of cost and safety perspectives. Therefore, in this paper, in order to assess more accurate responses of this high-rise hybrid building under an extreme earthquake events, the performance-based seismic design which is more rational approach will be carried out.

II. OVERVIEW OF BUILDINGS

The 37-story high-rise residential building including 5-story of car parking is located near Bangkok with seismic zone of 4. The building is approximately 126 m tall above the ground level. The building supported by both mat foundations at shear wall location and pile caps at column locations is a hybrid structure which consists of both cast-in-place reinforced concrete (RC) and precast concrete (PC) systems. The cast-in-place concrete shear walls used as the primary lateral force-resisting system continue from mat the foundations to the top roof. The typical plans and elevation of the building are shown in Fig. 1. The car parking floor starting from the 1st level to 5th level are RC structures with columns and post-tensioned slab system. The transfer beams using RC structures is located at 6th floor with the depth of the members of 2.5 m. The RC structural walls are casted before installing PC bearing wall system at 7th floor. The PC bearing walls and slabs are used from the 8th floor to 36th floor. Then, the RC structures are again used at the top few floors of the building.

III. PERFORMANCE-BASED SEISMIC DESIGN

A. Design Criteria

As code provisions contain many requirements that are not specifically applicable to tall buildings. Advances in performance-based design methodologies and maturity of capacity design principles now permit a more direct, nonprescriptive, and rational approach to analysis and design of tall buildings [4] and [5]. A performance level describes a

XXX-X-XXXX-XXXX-X/XX/$XX.00 ©20XX 7ACEE

limiting damage condition which may be considered satisfactory for a given building or part of the building for a given ground motion. The limiting condition is described by the physical damage within the structure, the threat to life safety of the building's occupants created by the damage and the post-earthquake serviceability and repair of the building.

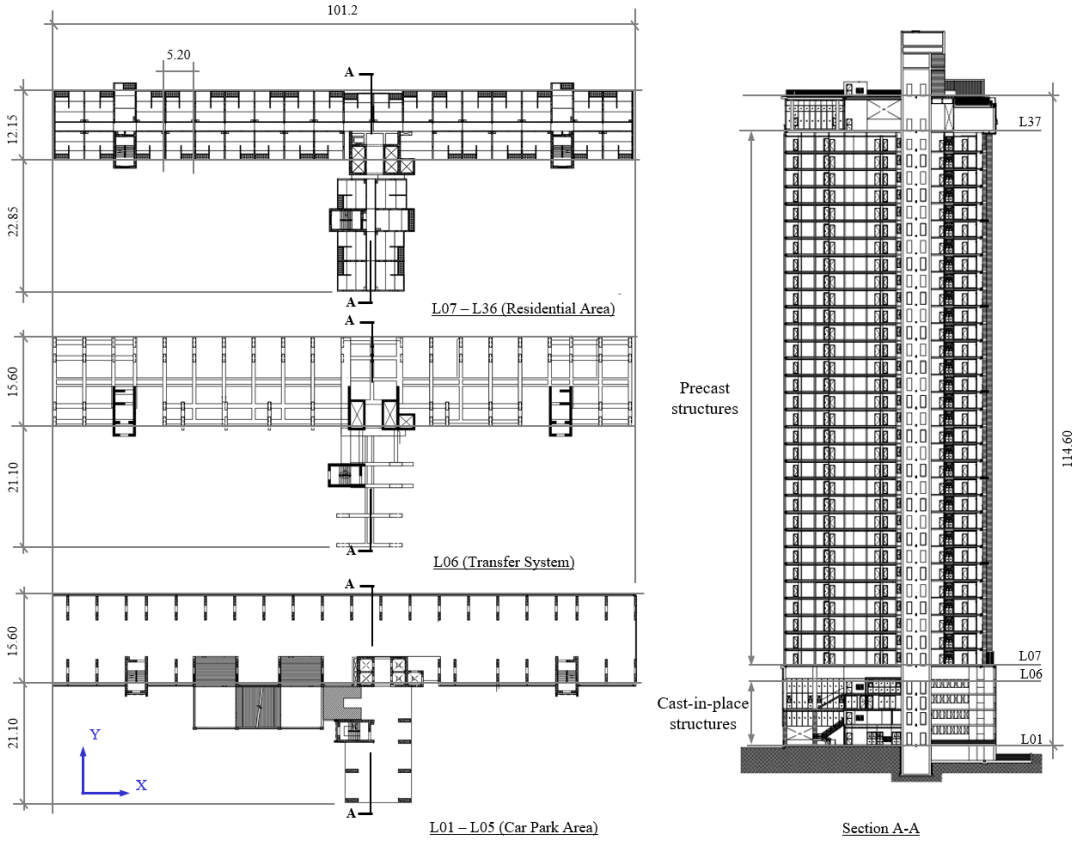

Fig. 1. *Typical floor plans and elevation*

TABLE 1: *ACCEPTANCE CRITERIA FOR MAXIMUM CONSIDERED EARTHQUAKE (MCE)*

Structural Responses	Acceptance Criteria
Peak transient drift	Maximum of mean values shall not exceed 3.0%. Maximum drift shall not exceed 4.5%.
Residual drift	Maximum of mean values shall not exceed 1.0%. Maximum drift shall not exceed 1.5%.
Coupling beam plastic rotation	Table 10-19 and 10-20, ASCE 41-13
Column (Axial-flexural interaction and shear)	Remain elastic.
Shear wall reinforcement axial strain	≤0.05 in tension and ≤0.02 in compression, taken as average of response history results.
Shear wall concrete axial strain	≤0.003 (Unconfined concrete)
Shear wall shear	Remain elastic.
Girder plastic rotation	Table 10-7, ASCE 41-13
Girders shear	Remain elastic.

Structural performance levels include Immediate Occupancy (IO), Life Safety (LS) and Collapse Prevention (CP) as discrete damage states and are used directly in the evaluation and retrofit procedure. However, in this study, the CP performance level against the maximum considered earthquake (MCE) level is only presented as the highest seismic force level. The structural evaluation actions can be classified into deformation controlled and force controlled actions as shown below. Moreover, the acceptance criteria at MCE level is also illustrated in Table 1.

1) Deformation-controlled actions: Deformation capacities were calculated using expected material properties and strength reduction factor of 1.0. The deformation demands obtained from the mean values of seven sets of ground motion records under MCE level, while the defromation limit of CP performance level detaermined from ASCE 41-13 [6].

2) Force-controlled actions: Force-controlled actions can be classified as critical and non-critical actions. The demand forces of the force-controlled critical action are determined using 1.5 times of the mean value, such as shear of primary elements., while the demand forces of the force-controlled non-critical actions are calculated using the mean value, such as flexure of members which are intentionally designed to remain elastic, such as flexure of foundation.

B. *Seismic Hazard*

As shown in Fig 2, the selected seven pairs of ground motions scaled to MCE level response spectra were used to check the performance under the earthquakes with an approximate return period of 2475 years (2% probability of exceedance in 50 years). The MCE target response spectrum

was calculated by scaling up 1.5 times of the DBE level which was directly determined from the Thai seismic design code (DPT 1302-52).

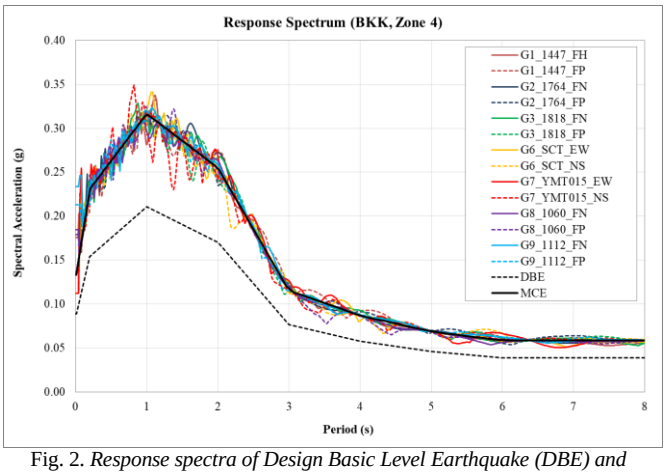

Fig. 2. *Response spectra of Design Basic Level Earthquake (DBE) and Maximum Considered Level Earthquake (MCE)*

C. Modeling

The model which consist of elastic and inelastic components was created using CSI PERFORM-3D and is illustrated in Fig. 3. Brittle action of the primary elements which were assumed to remain elastic were modeled with elastic properties, such as shear, while ductile action of those elements that were anticipated to perform beyond their elastic limits were modeled including inelastic behaviors, such as flexure of shear walls, PC walls, columns, and PC slabs. The detailed procedures and modeling approach for the nonlinear model are described in following sections.

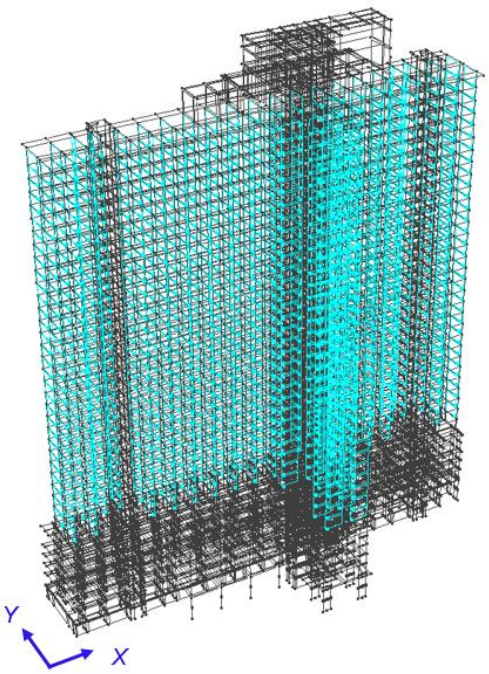

Fig. 3. *Nonlinear modeling using PERFROM 3D*

1) Material properties: Expected material strengths of concrete with 1.3 times of nominal strength were used for MCE analysis. The effect of confinement was taken into account for the compressive strength and ductility of concrete. Mander's confinement model [7] was used to determine the confinement effect. The concrete material was modeled with tri-linear backbone curve. The tensile strength of concrete was neglected. The expected material strength of reinforcing steel was used in the MCE analysis. The steel material was modeled using the tri-linear backbone curve. Expected yield strength was taken as 1.17 times nominal yield strength and the ultimate strength was estimated as 1.5 times expected yield strength.

2) Shear wall modeling: Fiber modeling technique [8] was used to model the flexural behavior of the core wall as shown in Fig. 4. Shear wall element was used to model the nonlinear behavior of shear wall. The shear behavior of the wall was modeled as elastic with the modified stiffness value of $0.2E_cA_g$ assuming that there will be significant cracks during MCE level. Furthermore, the out-of-plane bending and shear were also modeled as elastic. The out-of-plane stiffness of the wall was reduced to one-fourth value in order to consider the effect of concrete cracking.

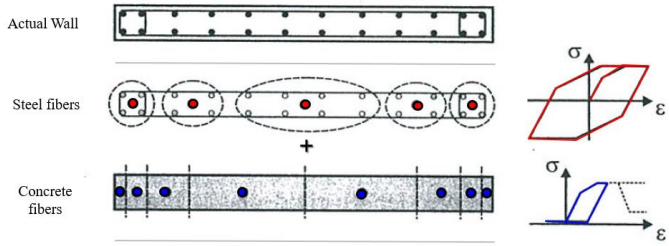

Fig. 4. *Structural Walls with Fiber Modeling*

3) Column modeling: The shell element was used to model columns including nonlinear behavior. Fiber modeling technique was used to model the axial combined with flexural behavior of the columns under the transfer girder system, while shear behaviour of columns was modeled to remain elastic.

4) RC and PC bearing wall modeling: Before starting PC bearing walls for residentail floors, the RC walls were strated first above the transfer beams. The PC splicing system with concrete grout was employed as the connection between walls to walls to provid the continuity of the vertical reinforcement. Fiber modeling technique was used to model the flexural behavior of the RC and PC bearing walls using sheall elements, while the out-of-plane stiffness of the wall was reduced to one-fourth value in order to consider the effect of concrete cracking. The shear behavior of the wall was modeled as elastic with the modified stiffness value of $0.2E_cA_g$.

5) Coupling beams: The coupling beams which were dominated by flexure behavior with span to depth ratio (l/h) >2 were modeled as elastic beam elements including two nonlinear moment-rotation hinge at the both end, while those that were dominated by shear behavior with span to depth ratio <2 were modeled as elastic beam elements with a nonlinear shear hinge at the mid-span. The capacities of the shear hinge were calculated based on the diagonal reinforcements using formula provided in ACI 318-11 [9]. The ultimate point is taken as the 1.13 times of the yielding capacity. The elastic stiffness of the deep beams is reduced to 0.2EIg.

6) Transfer beams: Transfer beams located at the 6th floor were modeled using frame elements. The transfer beams dominated by flexure were modelled including nonlinear moment hinges at both ends, while those conttroled by shear were modeled using shear hinge at the middle span. The elastic stiffness of the transfer girder are reduced to $0.35I_g$.

7) Floor slabs: The floor slabs under the transfer beams were modeled as a shell element with in-plane stiffness modified to $0.5I_g$. For the slab system above the transfer beams, in order to capture the inelastic behaviour, the PC slabs were modeled using equivalent slab beams including nonlinear moment hinges at both ends.

8) Supports: Pin supports were assigned to the base of the reinforced concrete shear walls and retaining walls, while fixed supports were assigned to base of columns.

9) Dampings: The 2.4% modal damping and 0.1% Rayleigh damping was used for the MCE analysis to obtain the target damping of 2.5%. The Rayleigh damping ratios are provided as below.

TABLE 2: *RAYLEIGH DAMPLING RATIOS*

Period ratio T/T1	Damping %
0.25	0.1
1.5	0.1

D. Nonlinear Time-History Analysis

Seven pairs of ground motions were selected and scaled to be matched with the target response spectrum at MCE level of Bangkok zone 4 and geologic condition at the site. Nonlinear time-history analysis (NLTHA) based on these ground motions were performed. The averaged responses obtained from the analyses were used as the demands for evaluation of the building performances.

IV. RESULTS

This section presents the seismic evaluation results obtained from the nonlinear time-history analysis. Structural responses of the building under MCE earthquake level were mainly presented and evaluated by using the several response indicators which can be defined as structural and component responses, such as base shear, story drift, lateral displacements, and strength and deformation capacity of structural members. Demand over capacity (DC) ratio which is the ratio of member force to the member strength was also employed for evaluation of the component performance. If the DC ratio is less than 1.0, the member capacity is sufficient in resisting the demand force. However, if the DC ratio is greater than 1.0, the member capacity needs to be enhanced to satisfy with the demand force.

A. Structural (Global) Responses

1) Base shears: The base shear from different types of analysis were compared above ground level as shown in Table 3 and Fig. 5. The service level earthquake (SLE) base shears with the return period of 225 years were obtained from response spectrum analysis using the elastic model. Under MCE earthquake level, the base shears obtained from the nonlinear time-history analysis (NLTHA) based on 7 pairs of ground motions using the inelastic model were compared to those obtained from the linear time-history analysis (LTHA) using the elastic model in order to observe the inelastic effect which results in the reduction of base shear. It was found that the computed MCE inelastic base shears in percentage are about 6.2 and 9.2 above the ground level which are lower than the computed MCE elastic base shear in X and Y directions with the reduction values approximately 1.3 times in both X and Y directions. Based on these low reduction values, it indicates that most of structural components still remains elastic under the MCE earthquake level.

TABLE 3: *COMPARISON OF BASE SHEAR (ABOVE GROUND LEVEL)*

Load Cases	Analysis	Base Shear	
		(KN)	%
SLE-RSA-X	Response Spectrum	17,746	2.3
SLE-RSA-Y	Response Spectrum	21,888	2.9
MCE-LTHA-X	Linear Time-History	62,970	8.2
MCE-LTHA-Y	Linear Time-History	89,822	11.7
MCE-NLTHA-X	Nonlinear Time-History	47508	6.2
MCE-NLTHA-Y	Nonlinear Time-History	70,199	9.2

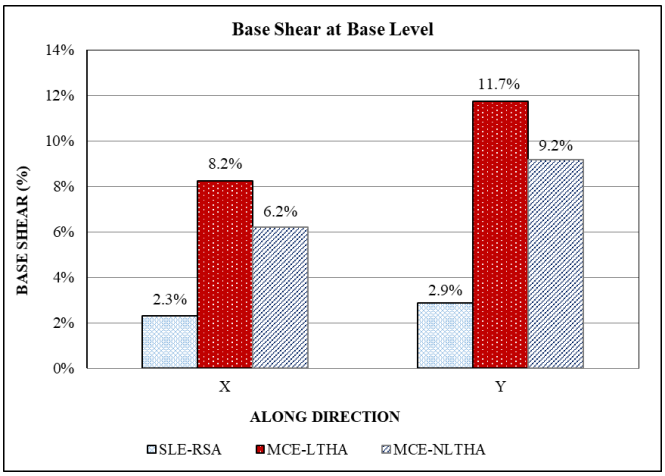

Fig. 5. *Base shear percentage in terms of seismic weight of building above ground level*

2) Story shear: The story shears of 7 ground motions and their averages in X and Y directions obtained from NLTHA under MCE are shown in Fig.6 and 7. The results of the story shear show contribution of higher mode effects.

3) Story drift: Under MCE level earthquakes, for the transient drifts, the mean values from 7 sets of ground motions were checked against the limit of 0.03. The maximum story drift ratio of thses ground motions was checked against the limit of 0.045. A point of the building corner along the hight was used for reporting the drifts. In term of global responses, the building generally perfroms witin the drift limts at the Collasp Prvention (CP) perfromance level as shown in Fig. 9 and 9.

4) Energy dissipation: To determine which members in the building contribute the most to the inelastic dissipated energy, the energy balance results can be investigated. The energy dissipated by inelastic effects is about 26% of overall

building energy, while overall structure remains elastic approximately 74% as shown in Fig. 10. As illustrated in Fig. 11, the PC slabs contributes the most (67%) to the inelastic dissipated energy. The coupling beams, transfer beams, PC walls and RC Walls contribute about 19%, 10%, 1% and 1.5% of the inelastic dissipated energy, respectively, while shear walls and columns below the transfer systems seem to remain in elastic.

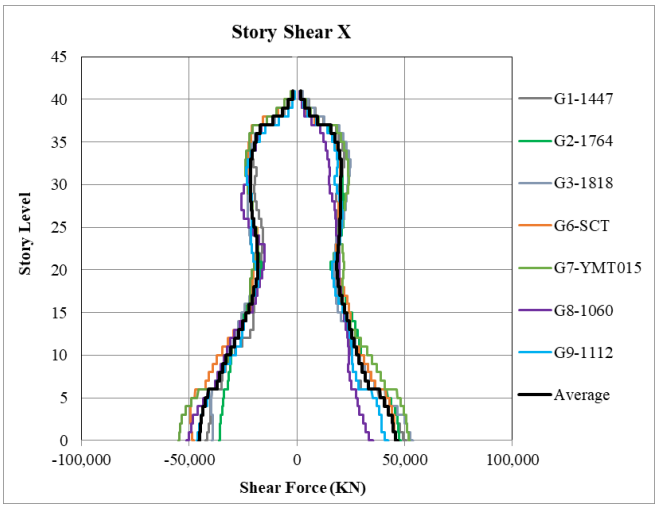

Fig. 6. *Story shears based on MCE in X*

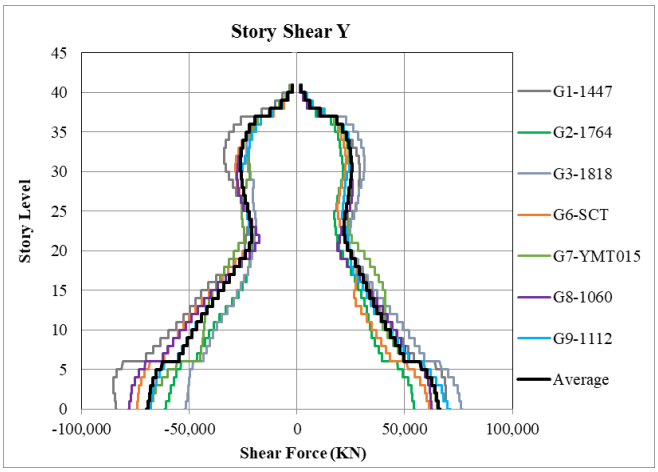

Fig. 7. *Story shears based on MCE in Y*

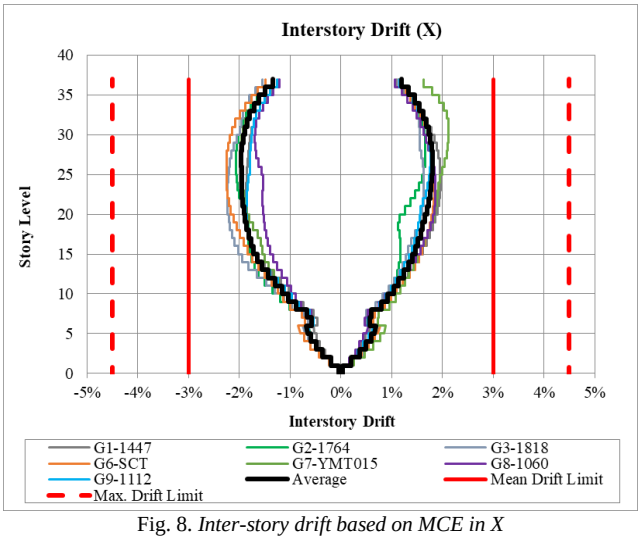

Fig. 8. *Inter-story drift based on MCE in X*

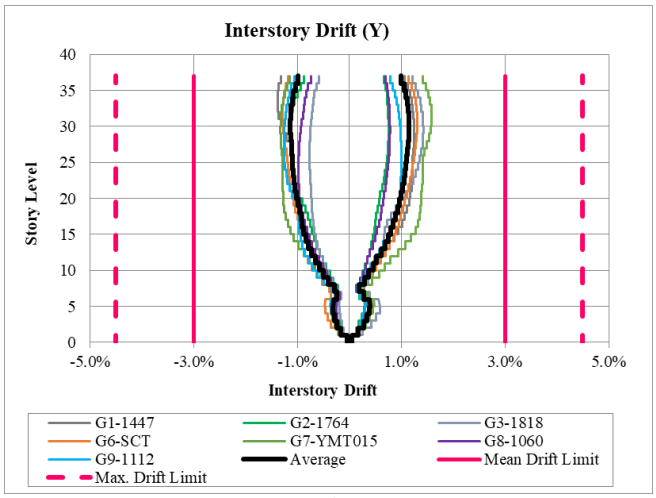

Fig. 9. *Inter-story drift based on MCE in Y*

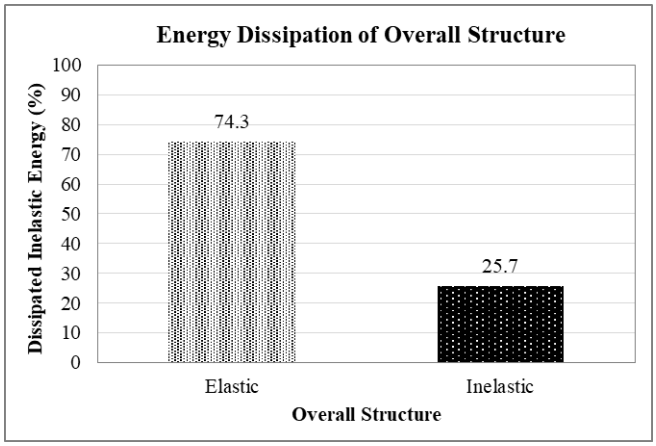

Fig. 10. *Energy balance of overall structure under MCE Level*

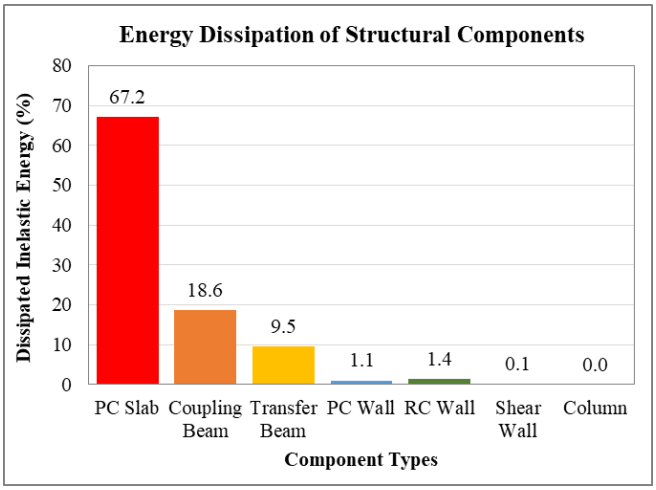

Fig. 11. *Energy balance of element groups under MCE Level*

B. *Component (Local) Responses*

1) Shear walls: The flexural response of the shear walls were investigated in terms of the tensile and compressive strains obtained from assigned starin gages at the edges or corners of the walls as shown in Fig.12. The yielding steel strain is approximate 0.002, while the ultimate steel strain is 0.05. The crushing strain for unconfined concrete crushing is 0.003. It was found that strains in both concrete and steel reinforcing bar were within the acceptable strain limits. The shear walls generally remain elastic under extreme

earthquakes, except few locations which shown yielding of reinfoceing bars. For shear wall shear, the shear capacity of each shear wall leg was checked and plotted against the averaged shear demands multipied with the factor of 1.5 for the brittle action as illustrated in Fig. 13. If shear force of any wall leg for particular floor level is greter than shear wall capacity, the shear capacity of the wall leg need to be increasaed. And, if shear force of the wall leg is grether than maximum limit of section, the section dimension needs to be increased in order to satisfy with the forces. However, if shear force is smaller than both shear capacity and limt capacity, the section is satisfied in resisting forces under MCE level.

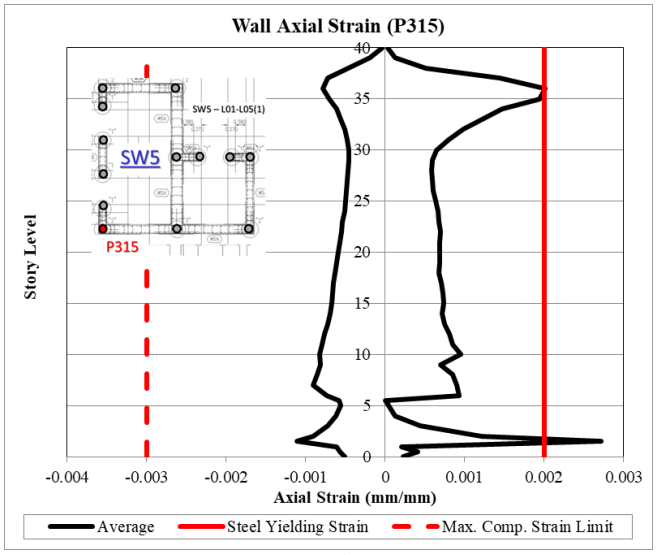

Fig. 12. *Axial Strain of Shear Wall (P315)*

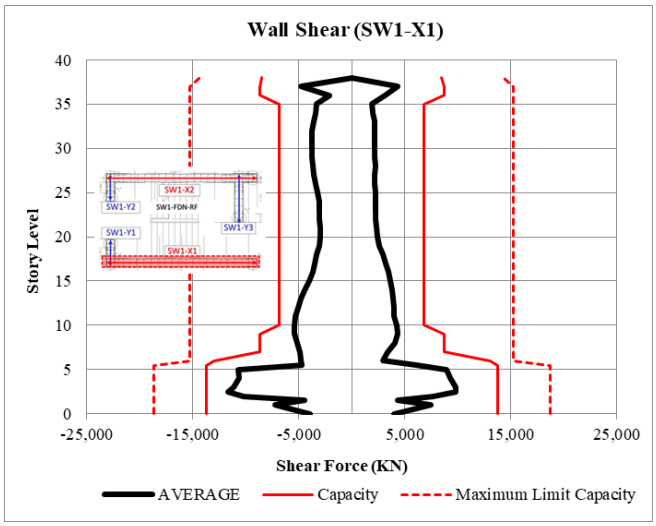

Fig. 13. *Shear wall shear (SW1-X1)*

2) Columns: The axial combined with flexural response of the columns under the transfer system was investigated similarly shear wall strains. It was found that strains in both concrete and reinforcing steel were within the acceptable limits. In addition, for the column shear, the DC ratio was employed to evaluate the member performance. if the column shear DC ratio is grether than 1.0, the column shear capacity needs to be enhanced for its capacity. However, if DC ratio is smaller than 1.0, the column shear capacity is able to resist the shear force. For this building, all columns have sufficient capacities in resisting the demand forces under MCE level as illustrated in the table 4.

TABLE 4: COLUMN SHEAR

Criteria	DC Ratio	
	Number	%
DC < 0.5 (Low to Moderate Stressed)	347	78.2
0.5 < DC < 1.0 (High Stressed)	97	21.8
1.0 < DC < 1.5 (Overstressed)	-	-
DC > 1.5 (Severe Overstressed)	-	-
Total	444	100.0
Acceptable	444	100.0
Unacceptable	-	-

3) RC and PC walls: The axial combined with flexural response of the RC and PC walls were also evaluated in terms of the tensile and compressive strains. It was found that there were some yieling of vertical rebars, but all yeilding strains were within the ultimate tensil strain. Very high tensile and compressive strains were observed above the transfer beams as the base of RC and PC wall systems. For RC and PC wall shear, the shear forces againts capacities cab be plotted in the same manner of shear wall shear. If the provided shear capacity of the members are not sufficient, the recommendation to increase shear capcity of the sections will be provided in order to satify with the shear demand at MCE level.

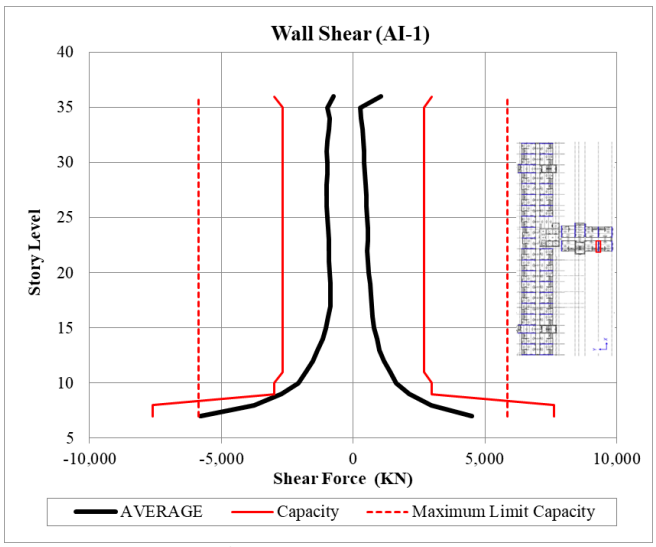

Fig. 14. *Shear force against horizontal PC wall connection*

4) Horizontal and vertical PC wall connections: To confirm the sufficient connection capacities bewteen PC members under the extreme erthquake event, the base connections of PC walls which is named as horizontal PC connection, and the vertical connections between PC wall to PC wall which is defined as vertical PC connection were checked based on the shear friction concept. For the horizontal PC wall connections, the horizontal shears at each base PC wall connection were checked against the

shear friction capacities calculated from the contribution of concrete and provided vertical reinforcing bars. A sample plots of the PC wall horizontal shear demand against capacity along the building height shown in Fig. 14. The results showed all shear forces of PC wall horizontal connection were within the shear friction capacities. For the vertical PC wall connection which its connection details shown in Fig. 15, the vertical shear forces between PC wall to PC wall connection which were calculated in term of shear flow were checked against the vertical shear friction capacities calculated from the contribution of concrete and provided horizontal reinforcing bars linked within connection. A sample plot of the PC wall vertical shear demand against capacity are shown in Fig. 16. The results showed that the shear demands of all PC wall vertical connections were within the vertical shear friction capacities.

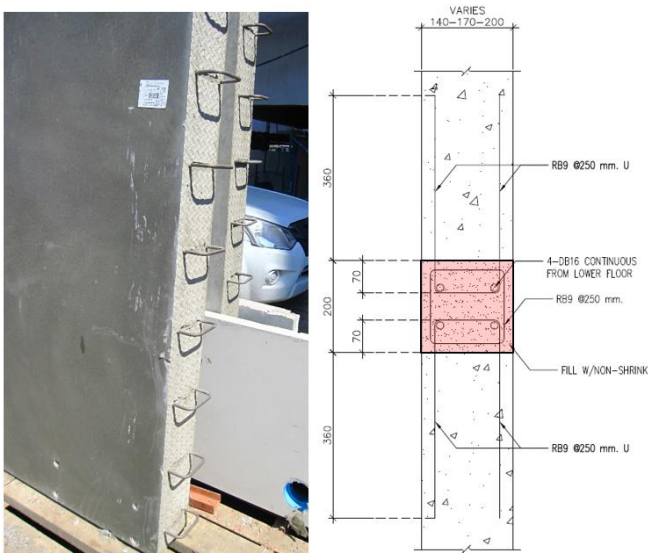

Fig. 15. *Vertical PC wall connection detail*

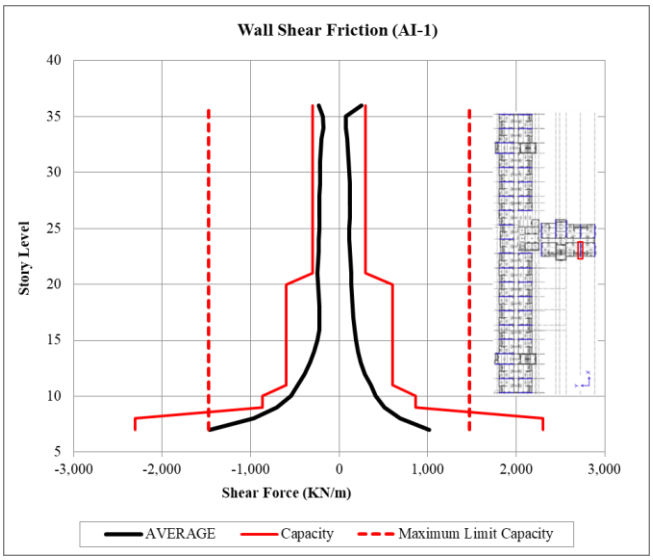

Fig. 16. *Shear force against capacity of vertical PC wall connection*

5) Transfer beams: In term of beam flexure defined as ductile action, the plastic rotation demands were checked against the plastic rotation limit at collapse prevention (CP). The evaluation results show that most of the beam rotation (78%) remain in elastic range, while some of beam rotation (22%) were in plastic ranges as illustarted in Table 5. However, all of plastic beam rotation were within the plastic rotation limits at the CP performance level. For beam shear as shown in Table 6, the evaluation results show that the shear DC ratios of all transfer beams are smaller than 1.0 which indicate that all beams have sufficient shear capcities in resisting shear forces at MCE level.

TABLE 5: PLASTIC ROTATION OF TRANSFER BEAMS

Criteria	DC Ratio	
	Number	%
DC < 0.0 (Elstic range)	82	78.1%
0.0 < DC < 1.0 (Plastic range)	23	21.9%
1.0 < DC < 1.5	0	0.0%
DC > 1.5	0	0.0%
Total	105	100.0%
Acceptable	105	100.0%
Unacceptable	0	0.0%

TABLE 6: TRNASFER BEAM SHEAR

Criteria	DC Ratio	
	Number	%
DC < 0.5 (Low to Moderate Stressed)	159	58.0%
0.5 < DC < 1.0 (High Stressed)	115	42.0%
1.0 < DC < 1.5 (Overstressed)	0	0.0%
DC > 1.5 (Severe Overstressed)	0	0.0%
Total	274	100.0%
Acceptable	274	100.0%
Unacceptable	0	0.0%

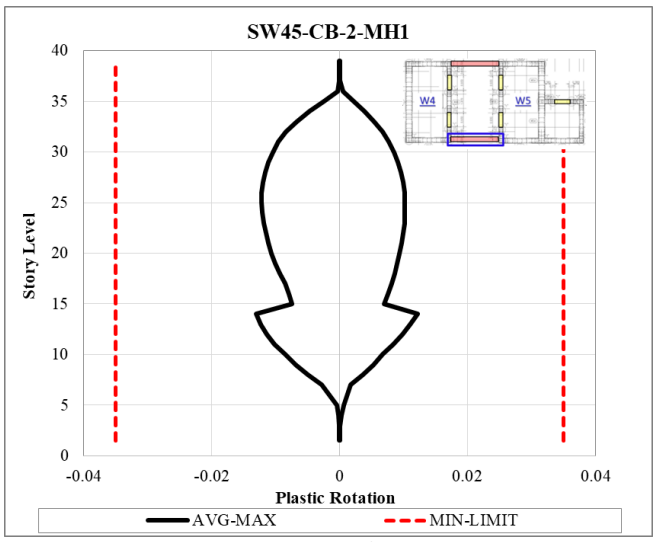

Fig. 17. *Plastic Rotation of Coupling Beams*

6) Coupling beams: A sample plot of the plastic rotations against plastic rotation limits of a coupling beam is shown in Fig. 17. The result shows that all plastic rotation demands of the coupling beam was within the plastic

rotation limit at collapse prevention (CP) under MCE level. There is a drop of plastic rotation at floor level 15 due to increasing coupling beam section and reinforcement results in obtaining smaller the plastic rotation demand.

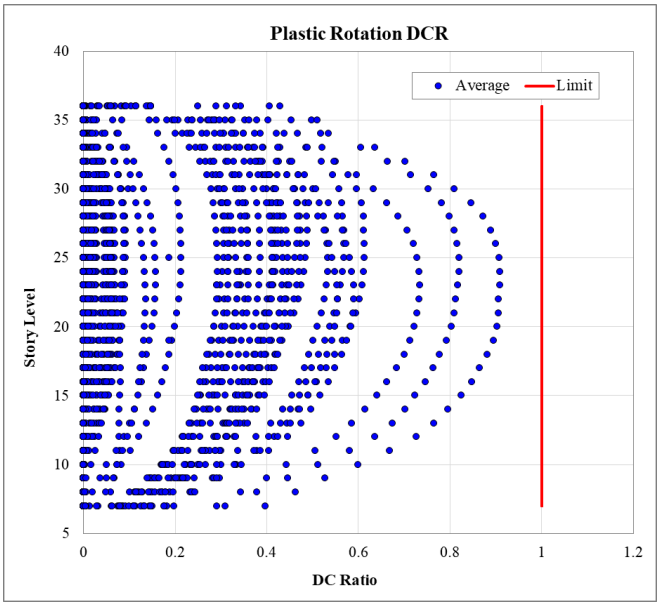

Fig. 18. *Plastic Rotation of PC Slabs (Equivalent-Slab Beams) under MCE Level*

7) PC slabs: The plastic rotation demands obtained from moment hings assigned at both ends of the PC equivalent slab frame were summarized and plotted against plastic rotation limit in term of DC ratio as shown in Fig. 20. It was observed that the maximum plastic rotatio occurred approximately the 20th floor to 25th floor with very high DC ratio, but still within the plastic rotation limit. Based on the slab sections, the corridor PC slabs with the thickness of 14 cm. shown lager plastic rotation than the residential PC slabs with the thickness of 16 cm. The corridor PC slabs located between the PC walls which are the position for large lateral load transferring similarly to coupling beam action. This result also corresponds to the energy dissipation which shows that the PC slabs contributes the most to the inelastic dissipated energy. Based on thses large defromation, to prevent the progressive collapse during or after this extreme earthquake event, the additional supports or reinforcements can be recommned for carrying the gravity load.

8) Diaphragms: Diaphragms transmit lateral forces from the floor system (PC slabs) to the vertical elements (Shear, RC and PC walls) of the structural system. They also tie the vertical elements together and thereby stabilize these elements and transmit forces among them [10] and [11]. As reported in the previous section, the PC slabs of this building also seem to significantly perform in inelastic range. Therefore, floor diaphragms are the essential part of the structural system and require design attention to ensure the continuous load path in trasferring seismic loads, especially PC structural system.

a) Diaphragm chords and shear: Under membrane load acting to the diaphragms (PC slabs) due to inertia forces, the diaphragm act like a beam spanning between supports (vertical elements or shear walls). The diaphragm forces were obtained by using the section cuts provided in the software. Sample diaphragm chord reinforcements were designed and provided as shown in Fig. 19.

b) Collectors: Collectors are tension and compression elements that gather (collect) shear forces from diaphragms and deliver the force to vertical elements, such as shear walls. Sample details of collector reinforcements which were designed against the loads at MCE level are shown in Fig. 20.

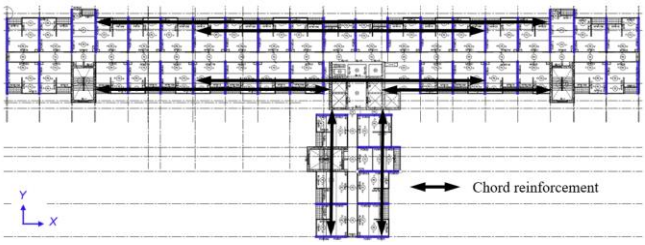

Fig. 19. *Diaphragm chord reinforcements*

Fig. 20. *Collectors*

c) Shear frictions: Shear friction is defined as the force transfer between diaphragm and vertical elements or shear walls. To provide a continuous load path to transmit seismic forces from the diaphragm to vertical element, the shear friction design also need to be carried out. The shear friction reinforcements are normally provided surrounding shear walls.

V. CONCLUSIONS

The purpose of this paper is to present the performance-based seismic evaluation of a high-rise hybrid building which is a combination of cast-in-place reinforced concrete (RC) and precast concrete (PC) structural systems as an alternative to the prescriptive design codes in Thailand. Nonlinear time-history analysis (NLTHA) based on 7 pairs of ground motions was mainly performed as the highest lateral load demands acting on the building to satisfy with Collapse Prevention (CP) performance level. The structural analysis and evaluation results under Maximum Considered Earthquake (MCE) were carried out by using the several response indicators such as base shear, story drift, lateral displacements, and strength and deformation capacity of structural components. Demand over capacity (DC) ratio which is the ratio of member force to the member strength was employed for evaluating deficiencies of structural components.

The results show not only vertical lateral force resisting systems perform in inelastic range, but the floor systems also perform in inelastic range with very high DC ratio under this extreme earthquake event, especially PC slabs which shown very large plastic rotation demands. Therefore, it needs to

carefully design for PC slab system to provide the continuous load path to the vertically seismic force-resisting system.

REFERENCES

[1] T. Ornthammarath, P. Warnitchai, K. Worakanchana, S. Zaman, R. Sigbjörnsson, and C. G. Lai, "Probabilistic seismic hazard assessment for Thailand," Bull Earthquake Eng, vol. 9, pp. 367–394, 2011.

[2] Pennung Warnitchai, "Development of seismic design requirements for buildings in Bangkok againt the Effects of Distant Large Earthquakes," 13th World Conference on Earthquake Engineering, Vancouver, B.C., Canada, Paper No. 744, August 2004.

[3] Y. C. Kurama, S. Sritharan, R. B. Fleischman, J. I. Restrepo, R. S. Henry, N. M. Cleland, S. K. Ghosh, and P. Bonelli, "Seismic-resistant precast concrete structures: state of the art," J. Struct. Eng., vol. 144(4), 2018.

[4] TBI 2010, "Tall buildings initiative, Guidelines for Performance-Based Seismic Design of Tall Buildings, " Pacific Earthquake Engineering Research Center (PEER), 2010.

[5] LATBSDC 2014, "Alternative procedure for seismic analysis and design of Tall Buildings Located in the Los Angeles Region, " Los Angeles Tall Buildings Structural Design Council, 2014.

[6] ASCE 41-13, "Seismic evaluation and retrofit of existing buildings, " American Society of Civil Engineerings (ASCE), 2013.

[7] J. B. Mander, M. J. N. Priestley, and R. Park, "Theoretical stress‐strain model for confined concrete, " Journal of Structural Engineering, vol. 114, Issue 8, September 1988.

[8] G. H. Powell, "Modeling for structural analysis, behaviour and basics," Compupers and Structures, Inc., Berkeley, California, USA, 2010.

[9] ACI 318-11, "Building code requirements for structural concrete," American Concrete Institue (ACI), 2011.

[10] J. P. Moehle, J. D. Hooper, T. R. Meyer, "Seismic design of cast-in-place concrete diaphragm, chords, and collectors, a guide for practicing engineers," NIST GCR 16-917-42, 2016.

[11] S. K. Ghosh, Ned. M. Cleland, "Seismic design of precast concrete diaphragms, a guide for practicing engineerrs," NIST GCR 17-917-47, 2017.

Case Study: Challenges of a Super Hall Dome

Naveed Anwar, Pramin Norachan, Thaung Htut Aung

AIT Consulting, Asian Institute of Technology, Bangkok, Thailand

Contact: nanwar@ait.asia

Abstract

This paper presents the challenges and studies involved in the structural design of a super hall dome. The geometry of the dome is not conventional dome-shaped with largest diameter. The dome is "Inverted monk bowl" in shape with the largest diameter around the mid-height. The dome is used as temple. It is a single-layer latticed steel dome, resting on the reinforced concrete structure. The dome is approximately 65 m in diameter at the base, while the diameter at mid-height is about 86 m. Wind tunnel test was conducted to determine the wind pressure on the surface of the dome which is located in the open terrain. High Frequency Pressure Integration (HFPI) technique was applied in the overall wind load study. Linear response history analysis was conducted to determine the response of the structure under wind load, while response spectrum analysis was conducted for seismic load. Staged construction analysis was performed in order to evaluate the performance of the structural components under construction. The structural components and construction loads are added in accordance with the actual construction sequences to determine the design forces.

Keywords: Single-layer latticed steel dome; High Frequency Pressure Integration technique (HFPI); linear response history analysis.

1 Introduction

In recent years, single-layer reticulated structures are widely used due to their capacity to cover large areas with an immense variety of shapes, light weight and without intermediate support. The single layer structures also present an undeniable attractiveness for their lightness as well as for their beauty. The span of reticulated dome has increased gradually in decades. For example, the diameter of the Formosa plastics storage facility dome in Taiwan is about 122 m. The diameter of the roof of the Walkup Sky dome in Northern Arizona University is 153 m, and the diameter of Nagoya Dome, which is supported on the frame column on stands is approximate 187 m.

However, they are several difficulties from complexity of structural analysis and design which are affected by diverse factors such as static stability of structures, realistic wind loads acting on the large dome, rigidity of support and joint, and geometric changes due to the construction. Therefore, the designers should pay attention for analysis and design of single-layer dome structures which are significantly different from those of conventional structures.

In this study, structural analysis and design reviews of the single-layer super reticulated steel domes with a span of 86 m supported by reinforcement concrete (RC) frame structure which is used to be the Buddha image super hall located in Saraburi, Thailand are presented as shown in Figure 1.

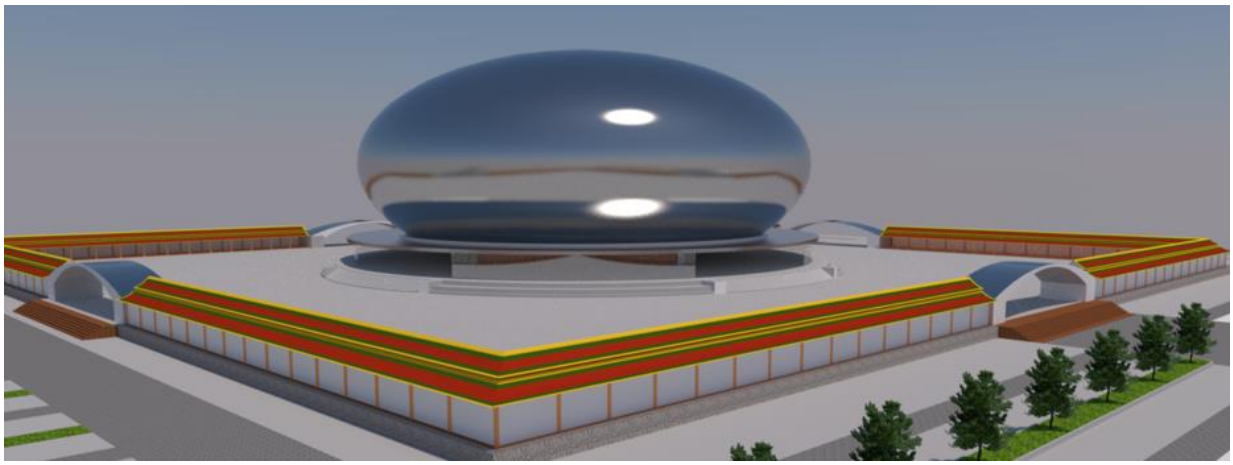

Figure 1. 3D view of the dome

2 Overall Structural Review Criteria

In this study, gravity load case is evaluated based on the nonlinear staged construction analysis including P-Delta effect. The staged construction analysis is also performed to check the performances of structural members during construction. Wind load case is evaluated based on linear time-history analysis using direct integration approach in order to find the dynamic responses of the structure. The response spectrum analysis for earthquake load based on DBE earthquake level with R equal to 1.0 is employed. Finally, all load cases are combined as appropriate load combinations for evaluate the performance of structural components.

The performance of the redesigned structure is assessed by using several response indicators such as natural periods, mode shapes, base shear and displacements. For the performance of the redesigned components such as the girders, columns, foundations and steel frames, the demand over capacity (D/C) ratios of PMM, flexure and shear are evaluated.

2.1 Structural geometry

The Buddha image super hall which is a single-layer steel dome structure is located in Saraburi, Thailand. As shown in Figure 2, the diameter of the circular RC base structure supporting the steel dome is 65 m., while the diameter at the middle of the steel dome is 86m. The total height of the whole structure is 40 m.

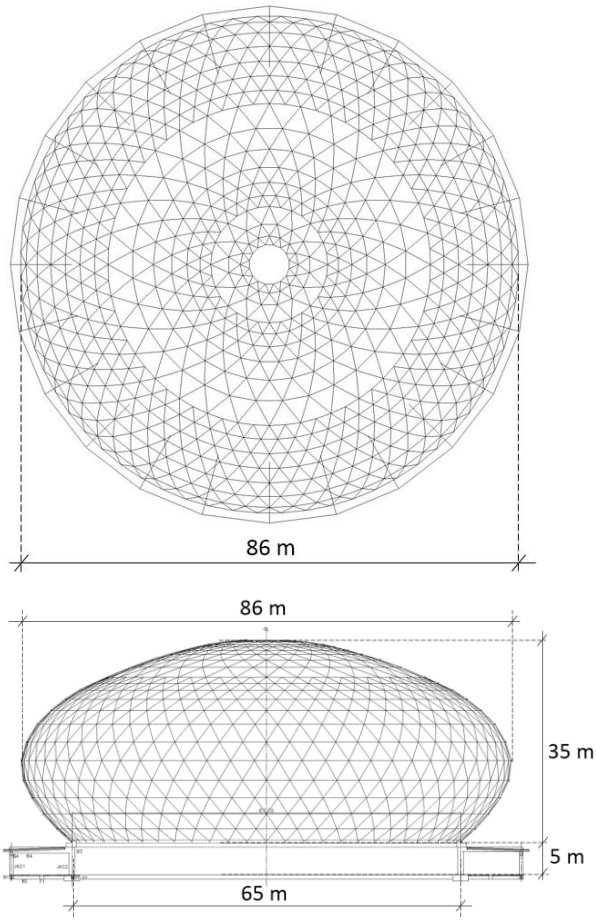

Figure 2. Overall dimension of the dome

2.2 Staged construction load

Staged construction analysis is performed in order to evaluate the performance of the structure components during construction. The structural components, shoring support and construction loads are added and removed following the actual

construction sequences to capture the demand forces under gravity load. The construction stages can be summarized in Table 1 and Figure 3.

Table 1. The principal activities of construction sequence

Stages	Construction Activities
1	Build RC circular base structure including piles, foundations, columns, beams, and slabs
2	Construct the bottom part of the super steel dome supported by using steel frame shoring
3	Install a set of steel cells until completing the first ring of the top part of the super steel dome
4	Repeat the stage 3 until fishing the top part of the super steel dome
5	Remove the steel frame shoring from the bottom part of the super steel dome
6	Install cladding throughout the super steel dome

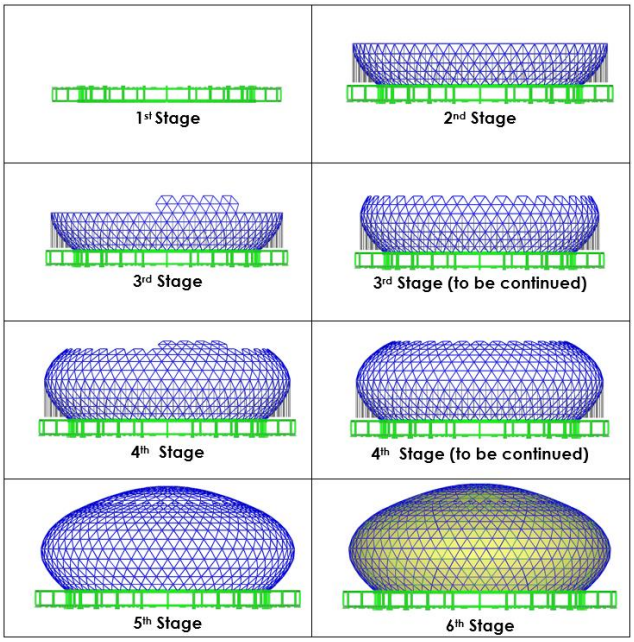

Figure 3. Principal activities of construction sequence

2.3 Wind Loads

Wind load action on this structure was evaluated based on design gridlines and wind tunnel test.

2.3.1 Wind load based on design guidelines

Before obtaining the wind pressure from the wind tunnel test, the structural performance of the dome was checked against the wind loads obtained from design guidelines in order to carry out the preliminary structural design. External wind pressure applied to the dome structure is calculated based on Thai wind calculation guideline (1311-50) and ASCE-05 as shown in Figure 4 and 5.

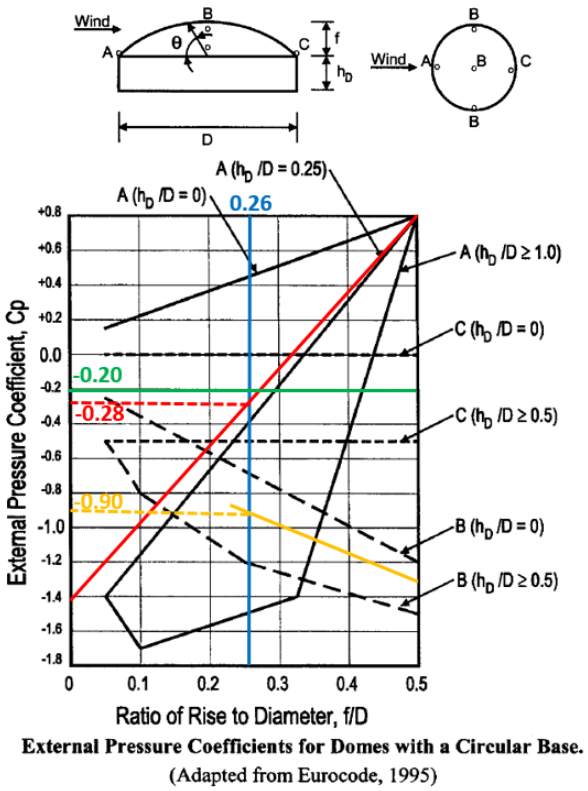

Figure 4. External pressure coefficients

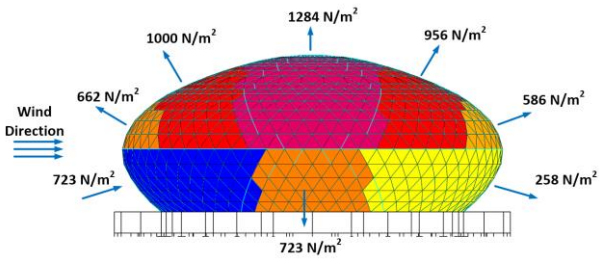

Figure 5. Wind external pressure

2.3.2 Wind load based on wind tunnel test

In order to capture more accurate result under wind load, the dome structure was tested in the wind tunnel to obtain the wind pressure acting on the structure. A 1:300 scaled model of the dome

was constructed based on the architectural drawings. The surrounding area of dome building was mainly car parking or open area; therefore, only main structure of dome was modelled with open terrain surrounding area. Beyond the area of the surrounding model, the influence of the upwind terrain on the atmospheric boundary layer was simulated by appropriate roughness on the wind tunnel floor and a flow conditioning grid at the upwind end of the working section for each wind direction. The following parameters is used in the wind tunnel test.

- Wind speed (z = 40 m) = 40.67 m/s (146.41 km/hr.) for 1,000 year return period
- Wind condition = Open terrain

In this study, the wind load obtained from a wind tunnel test were measured on a direction by direction basis for 36 directions at 10 degree intervals on scaled model exposed to an approaching wind. The measured data were converted into wind pressure. The 79 measurement points of time-history pressure on the surface of scaled model were assigned to the finite element software SAP2000 in order to evaluate the dynamic response under the actual wind pressure acting on the structure during a certain time. Due to symmetry of the steel dome, only one wind direction is applied to the structure. The scaled model in the wind tunnel test and the sample time-history pressure patterns are illustrated in Figure 6 to Figure 9.

Figure 6. 1:300 scaled model

Figure 7. The scaled model in TU-AIT Boundary-Layer wind tunnel

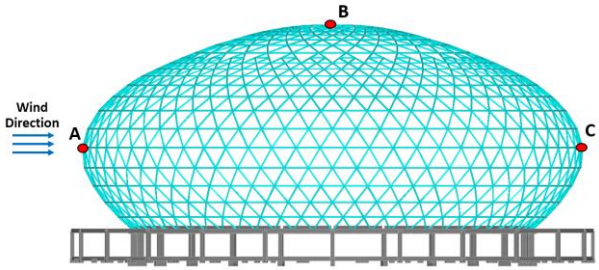

Figure 8. Sampling pressure measurement points on the dome

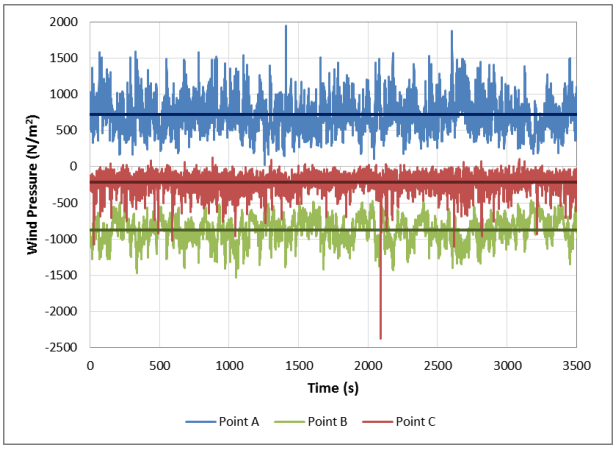

Figure 9. Time-history pressure at the sampling measurement points

2.4 Earthquake Loads

Seismic load was obtained from Thai seismic calculation guideline (1302-52). The response spectra at the design basis earthquake level (DBE) for 475-year return period (10% of probability of exceedance in 50 years) was used in this evaluation with the importance factor (I=1.25) and the response modification factor (R=1). The DBE elastic response spectra is illustrated in Figure 10.

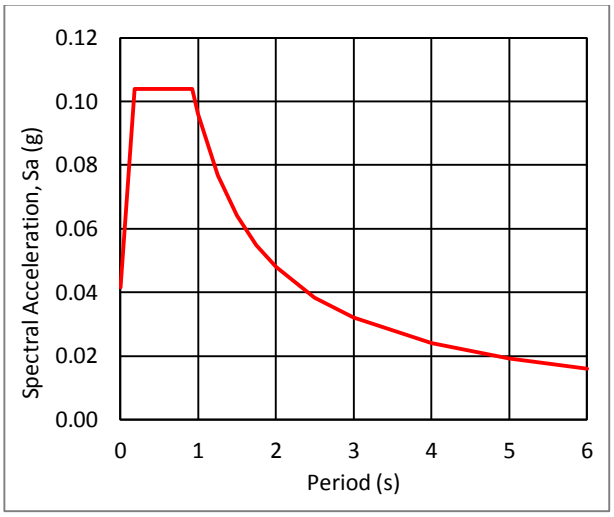

Figure 10. Response spectra for DBE earthquake level

3 Finite Element Modelling

Three-dimensional finite element model was created for evaluation as shown in Figure 11. SAP2000 V14.2.4 was used as analysis tool. For the RC circular base of the structure, the foundation system was modelled by using frame elements, while soil springs which represent piles were assigned below the foundation to include the behavior of soil structure interaction during the analysis. The RC beams which are connected to the columns were modelled as linearly elastic members using frame element. Moreover, all RC columns were also assigned as linear frame elements. The RC slabs were modelled as linear-elastic shell elements. For the steel dome, the steel pipes were modelled by using frame elements, while the cladding areas were modelled by using shell elements with modification of stiffness in order to transfer only loads to the surrounding steel pipes without contributing any stiffness.

4 Analysis Procedures

The analysis procedures used for each load case are presented in this section. Gravity load case was run based on the nonlinear staged construction analysis including P-Delta effect. Wind load cases were run for both linear static and linear time-history analyses. Direct integration approach was employed to find the dynamic responses of the structure for the linear time-history analysis. The total time step of 27,201 and the step size of 0.133 second were used to capture the wind loads acting on the structure within 1 hr. For earthquake loading assignment, the response spectrum analysis based on DBE level with R equal to 1 was used in order to provide higher force to the structure. Finally, all load cases are combined as load combinations.

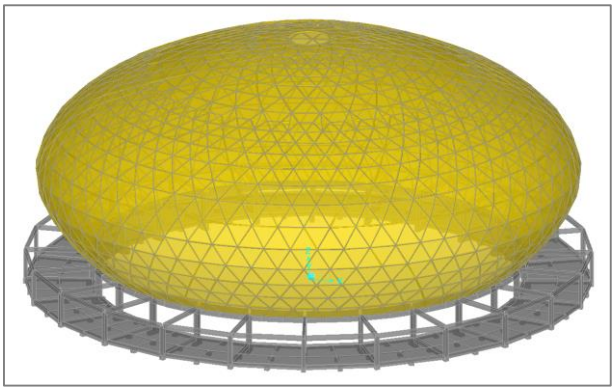

Figure 11. 3D finite element model

5 Overall Structural Design Review

This section discusses the structural performance of the building under the gravity and lateral loads. For gravity load response, construction sequence analysis including P-Delta effect was conducted to check the response of the vertical resisting system. For the lateral load response, the wind pressure obtained from design codes and wind tunnel test and the earthquake at DBE level were accounted for checking the response of lateral resisting system. Global responses of the structure were presented and the capacities of primary structural elements were checked against the demand forces under loads mentioned above.

5.1 Modal analysis

Modal analysis was performed to determine the vibration modes of the structure under dynamic forces as well as to understand the behavior of the structure. A combination of mass from 100% of dead load and superimposed dead load plus 25% of live load was considered in modal analysis. Forty modes were considered to achieve more than 90% of the total participating mass in each orthogonal direction. The first two modes are pure translation in X and Y direction, respectively due to symmetrical configuration of the structure as expected. The third mode is vertical vibration,

while the fourth mode performs in twisting. After the fifth mode, it is found that the steel dome structure starts to vibrate with the local vibration in various patterns. The modal participation mass ratios and the modal deformation shapes are shown in Figure 12.

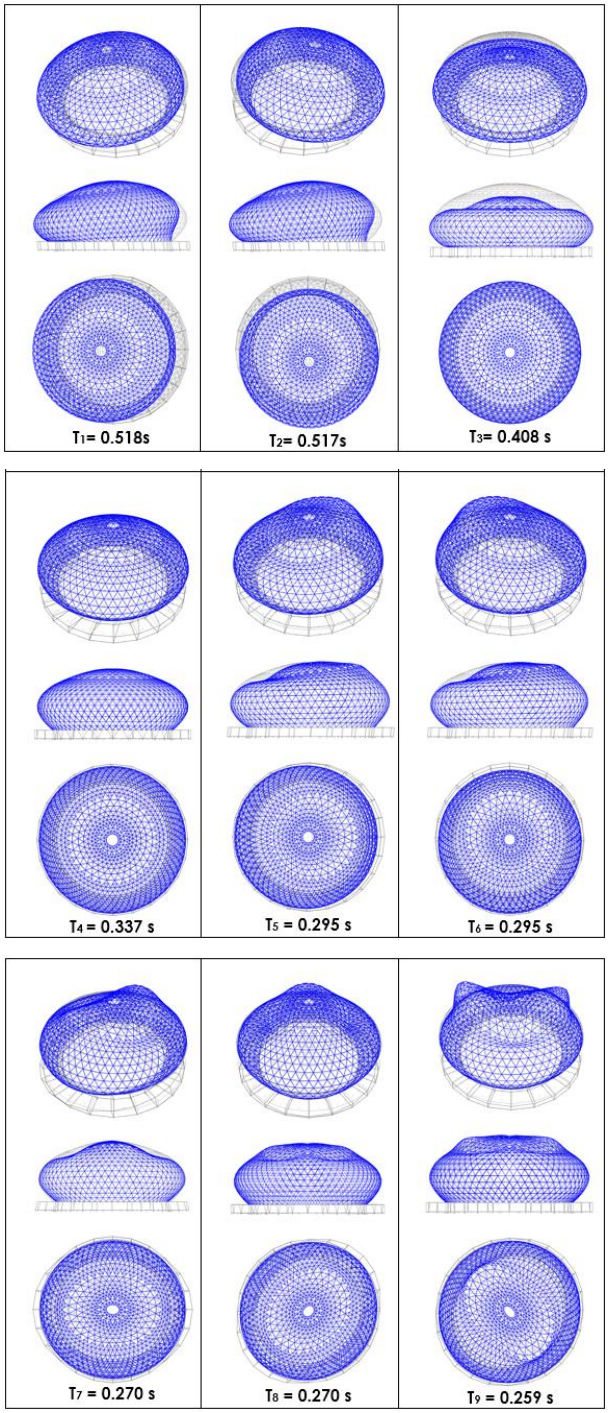

Figure 12. First nine vibration modes

5.2 Base shear

Base shear resulting from different load cases are summarized in Figure 13. Elastic base shear resulting from wind loads based on the design codes and wind tunnel test as well as elastic base shear resulting from response spectrum analysis (RSA) at DBE are compared.

At the beginning state, the structure is designed to resist the wind loads based on the design codes and seismic load at DBE level. After obtaining the wind tunnel test results, the design of structure was re-checked. At the ground level, the computed elastic base shear from wind tunnel test is approximately 5.7% of the seismic weight of the building (DL+0.25LL = 23613 kN) in both X and Y directions. The base shear for both directions are same due to symmetrical configuration of the structure. It is also found that the elastic base shear obtained from wind tunnel test is slightly lower than that obtained from wind design codes and from response spectrum analysis at DBE.

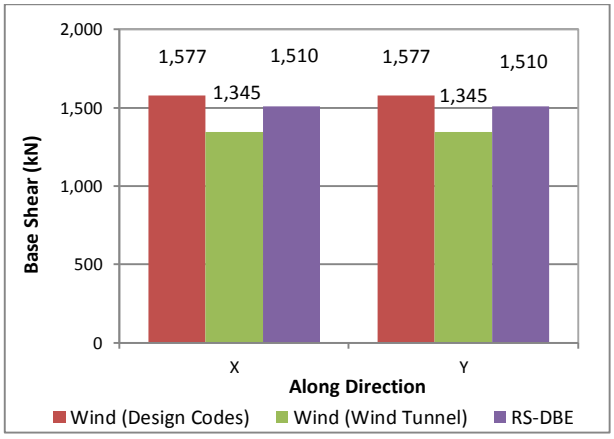

Figure 13. Comparison of base shear percentage at the ground

5.3 Deformations and Displacements

The deformation shapes under wind pressure obtained from wind tunnel test at a time step are illustrated in Figure 14 and 15. As expected, the results shows that the upward deformation can be observed at the top of the dome due to the suction pressure at this region, while pushing pressure can be observed at the surface that directly resist wind load.

As shown in Figure 16, the maximum story displacements under gravity loads based on

nonlinear staged construction analysis, wind load based on linear time history analysis and earthquake load based on response spectrum analysis were carried out. It is found that the maximum lateral displacements is approximate 3.6 cm which is less than the limit 20 cm (H/200 =40x100/200), while the maximum vertical displacements at the top of the dome is about 6.1 cm which is within the limit 17.9 cm (L/480 = 86x100/480).

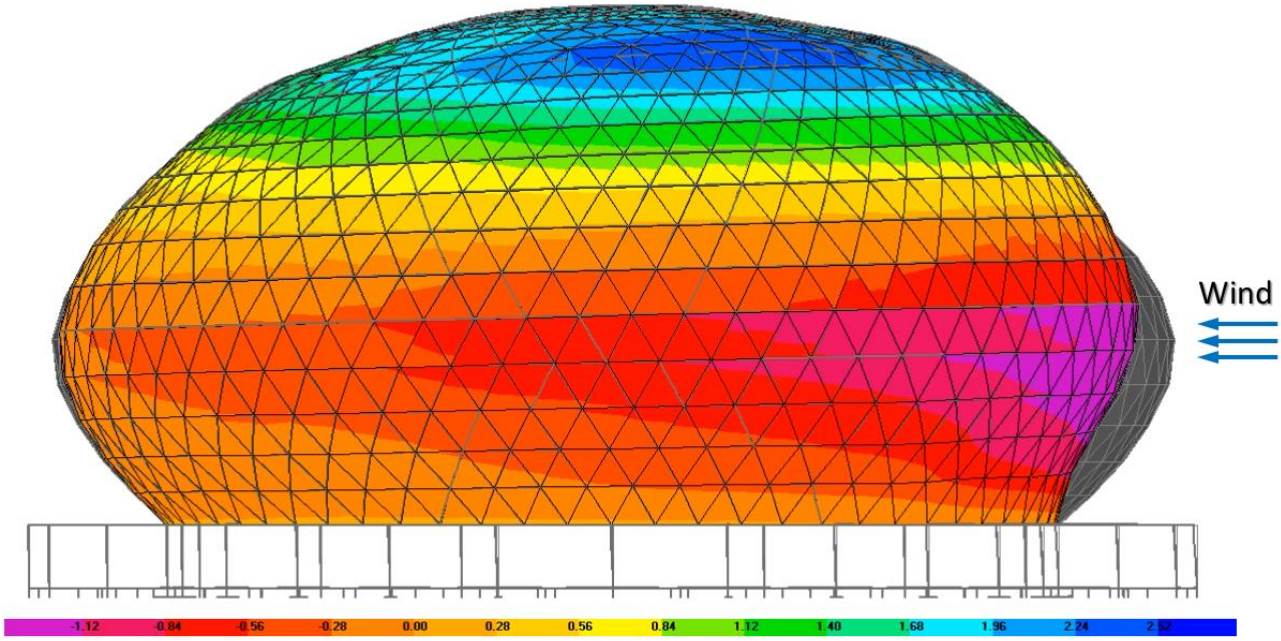

Figure 14. Elevation view of deformation of the dome under wind pressure

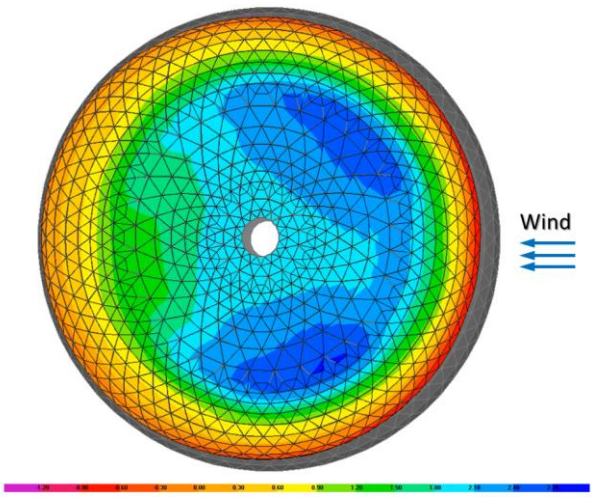

Figure 15. Top view of deformation of the dome under wind pressure

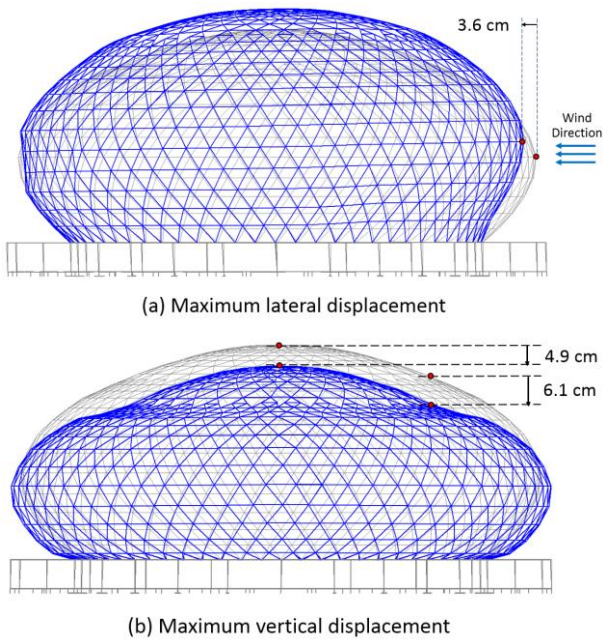

Figure 16. Maximum displacement

5.4 Design review of structural members

The demand over capacity (D/C) ratios of structural components such as the foundations, columns, and steel frames were carried out to evaluate structural performances of members in this section.

5.4.1 Piles and foundations

Based on the load combinations, the maximum demand axial force acting on the pile is less than the pile capacity with the demand over capacity (D/C) ratio of 0.67. Moreover, the foundation is also safe to resist the demand forces for both bending moment and shear with the demand over capacity (D/C) ratio of 0.94 and 0.88 respectively.

5.4.2 Columns and beams

The PMM results of the original columns exceed their capacities limit with the demand over capacity (D/C) ratio of 1.02 and 1.19, respectively, while the axial and shear forces are less than their capacities. To increase the capacities of columns, the column jacketing approach was proposed. After revising the original columns, the maximum PMM D/C ratio of the jacketing columns are less than 1.0. The demand over capacity (D/C) ratios for PMM, axial and shear are reduced due to increment of column dimensions and additional longitudinal and transverse reinforcements. The detail of column jacketing is illustrated in Figure 17.

After checking the performances of beams, it found that some beams cannot resist the demand forces. In order to increase the beam capacities, some beams are revised by increasing the amount of reinforcement for both longitudinal and transverse reinforcements.

5.4.3 Steel pipes

As illustrated in Figure 18, the 10 inch steel pipes with thickness 4.5 and 6.0 mm are used to be the primary components of the single-layer steel dome structure. The performances of these steel members, such as PMM, axial tension, axial compression, moment and shear were evaluated against the load combinations. Based on the results, the PMM demand over capacity D/C ratio provides the highest value of 0.61 when compared with the other D/C ratio. Thus, the steel pipes based on the previous design seem to have sufficient capacities to resist the demand forces.

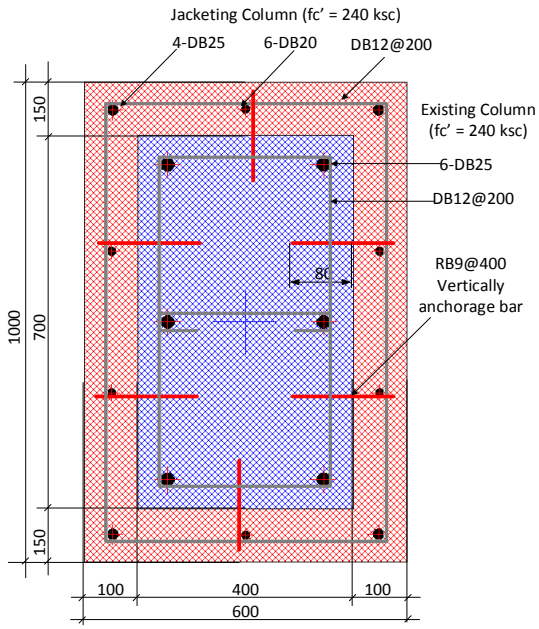

Figure 17. Details of jacketing column

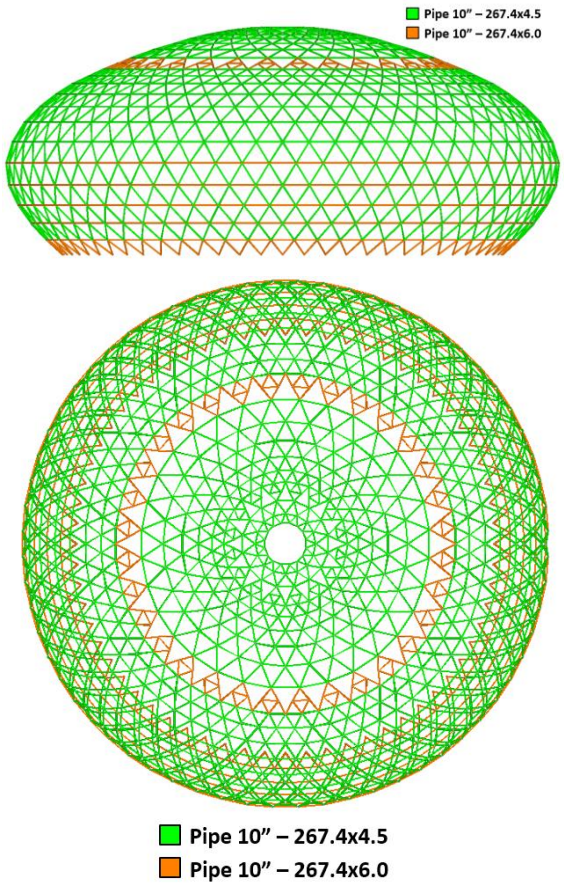

Figure 18. Elevation and plan views of dome structure

6 Conclusions

Three-dimensional finite element model using SAP2000 V14.2.4 was created for the structural design review of Buddha image super hall, a single-layer steel dome structure. Gravity load case was performed based on the nonlinear staged construction analysis including P-Delta effect. Wind load case was evaluated based on design codes and wind tunnel test. In order to find the dynamic responses of the structure under wind obtained from wind tunnel test, linear time-history analysis using direct integration approach was employed. The response spectrum analysis for earthquake load based on DBE level with R equal to 1 was used. Finally, all load cases were combined as load combinations for evaluate the performance of structural components.

Based on the analysis results, the performance of the structure was assessed by using several response indicators such as natural periods, mode shapes, base shear, displacements, flexural and shears capacities of the girders, columns, foundations and steel frames. Following conclusions can be drawn from this study:

- Due to symmetrical configuration of the structure, the analysis result of modal analysis shows that the first two modes are pure translation in X and Y direction, respectively. The third mode is vertical vibration, while the fourth mode performs in twisting. After the fifth mode, it is found that the steel dome structure starts to vibrate with the local vibration in various patterns.
- The elastic base shear obtained from wind tunnel test is lower than that obtained from wind design codes and from response spectrum analysis at DBE.
- The maximum displacements under the gravity and lateral loads are within the acceptable limit.
- The maximum demand axial force acting on the pile is less than the pile capacity, and the foundation is also safe to resist the demand forces for both bending moment and shear.
- To increase the capacities of columns, the column jacketing approach was proposed. The demand over capacity (D/C) ratios for PMM, axial and shear are significantly reduced due to increment of column dimensions and additional longitudinal and transverse reinforcements.
- After revising their reinforcement details of some beams, the demand over capacities are less than 1.0. Therefore, all beams seem to have sufficient capacities to resist the demand forces.
- The steel pipes which is the main component of the single-layer steel dome structure seem to have sufficient capacities to resist the demand forces.

After revising details of the some structural components, it can be concluded that the overall performance of the structure was improved in terms of global structural response as well as local member performances under both wind and earthquake.

7 References

[1] Portela G., and Godoy L.A. Wind Pressure and Bucking of Cylindrical Steel Tanks with a Dome Roof. *Journal of Constructional Steel Research*. 2005; 61: 808-824.

[2] Anuj C. Analysis and Design of Steel Dome using Software. *International Journal of Research in Engineering and Technology*. 2014; **3**(3): 2321-7308.

[3] ACI 318-08 (2008). Building Code Requirements for Structural Concrete (ACI 318-08) and Commentary (ACI 318R-08). American Concrete Institute: Farmington Hills, MI.

[4] ASCE 7-10 (2010). Minimum Design Loads for Buildings and Other Structures. American Society of Civil Engineers, Reston, VA.

[5] Thai Standard for Calculation of Wind Loads and Responses of Buildings 1311-50 (2007). Department of Public Works and Town & Country Planning.

[6] Thai Standard for Design of Buildings Resisting Earthquakes 1302-52 (2009). Department of Public Works and Town & Country Planning.

Finite Element Analysis of Offshore Wind Turbines under Environmental Loadings

Pramin Norachan[1)] and *Ki-Du Kim[2)]

[1), 2)] Department of Civil and Environmental System Engineering, Konkuk University,
1 Hwayang-dong, Gwangjin-gu, Seoul, Korea
[2)] kimkd@konkuk.ac.kr,

Abstract

A numerical analysis of offshore wind turbines based on finite element method is described in this paper. In order to simulate wave forces on offshore structural members, Stokes' fifth order wave theory, which are widely used in ocean engineering, is adopted in developing a program. Based on the Morison equation, the velocity and acceleration terms are converted into resultant forces acting on vertical and arbitrarily oriented structural members. Furthermore, other environmental loadings due to currents, wind are also included in the analysis of offshore wind turbines. Finally, the numerical analysis of an offshore wind turbine is then presented to demonstrate the performances of the proposed finite element code. The numerical results from the simulation of environmental loadings show that the developed program is able to predict the responses of the offshore structure with satisfactory accuracy and efficiency.

Keywords: offshore wind turbines, Stokes' fifth order wave theory, Morison's equation, wave and current forces.

1. Introduction

Offshore wind energy generation is the fastest growing source of renewable energy. Many technological developments in wind energy design have contributed to the significant advances in wind energy utilization in order to get optimum power from available winds. Offshore wind turbines are an efficient solution for this renewable energy. Offshore wind turbines are relatively complex structural and mechanical systems located in a highly demanding environment (Francesco, Hui and Franco, 2010). It is essential for all offshore structural analysts to estimate the forces generated by fluid loading given the description of the wave and current environment (Borthwick and Herbert, 1988). In order to provide engineering solutions, the use of regular wave theories is common because regular wave theories yield good mathematical models of long crested periodic waves, which are components of an irregular sea (Witz, Lyons, Patel, and Brown, 1994). For one of the regular wave theories, the Stokes' wave theory which has been widely used in offshore structural engineering was extended to fifth order (Skjelbreia and Hendrickson, 1961). The order of solution depends on the number of Taylor series terms included. Furthermore, all the significant loadings that the structure is likely to experience in the ocean environment, such as wind, currents and severe storm condition, is necessary to be estimate before analyzing offshore structures (Dawson, 1983). The objective of this paper is to present numerical analysis using a finite element program (XFINAS) to predict the responses of offshore wind turbines.

2. Wave Theories

Ocean waves are random in nature which can be defined as regular or irregular. However, in order to provide engineering solutions, the use of regular wave theories is common. Regular waves have a fixed profile with respect to an axis system translating at the wave celerity and can provide useful results in offshore analysis. In order to develop the wave theories, it is necessary to define the coordinate system and the terminology that will be used as illustrated in Figure 1.

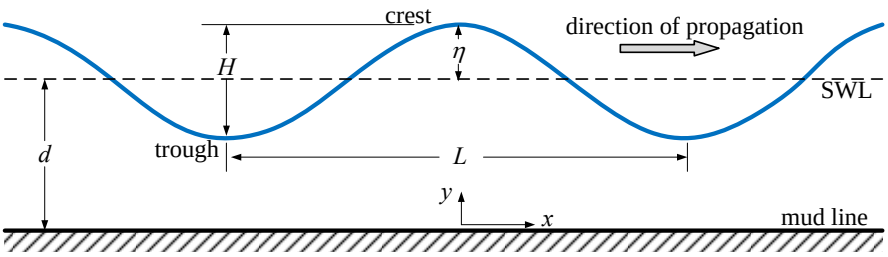

Figure 1. Definition of wave parameters

[1)] Graduate Student
[2)] Professor

In this study, Stokes' fifth order wave theory is applied for estimation of wave load acting on offshore structural members. The concept of this wave theory is to expand the wave solution in Taylor series approximations. The coefficients of the individual terms are determined to satisfy the appropriate hydrodynamic equation for finite-amplitude wave. Before evaluating wave forces, the velocities and accelerations of the water particles need to be calculated. The horizontal water velocity u and the vertical water velocity v caused by the free-surface wave propagation over water of depth d are expressible as

$$u = \frac{\omega}{k}\sum_{n=1}^{5} G_n \frac{\cosh nky}{\sinh nkd}\cos n(kx-\omega t) \tag{1}$$

$$v = \frac{\omega}{k}\sum_{n=1}^{5} G_n \frac{\sinh nky}{\sinh nkd}\sin n(kx-\omega t) \tag{2}$$

The horizontal acceleration a_x and vertical acceleration a_y of the water particles can be respectively determined from the equations

$$a_x = \frac{kc^2}{2}\sum_{n=1}^{5} R_n \sin n(kx-\omega t) \tag{3}$$

$$a_y = \frac{-kc^2}{2}\sum_{n=1}^{5} S_n \cos n(kx-\omega t) \tag{4}$$

where the coefficients G_n, R_n and S_n are determined based on the wave properties.

3. Prediction of Wave Forces

According to the offshore standard DNV (2004) and API (2007), Morison's equation is recommended to evaluate wave loads when the dimension of the structure is small relative to the wave length (D/L<0.2). The wave force per unit length on a body in an unsteady viscous flow can be determined using Morrison's equation, which is a combination of an inertial term and a drag term.

$$f = \frac{1}{2}\rho C_D D|u|u + \rho C_M \frac{\pi D^2}{4} a_x \tag{5}$$

where ρ denotes water density, C_D and C_M denotes drag and inertia coefficients, D is the diameter of the member, u and a_x denote the horizontal velocity and acceleration of the water associated with the wave.

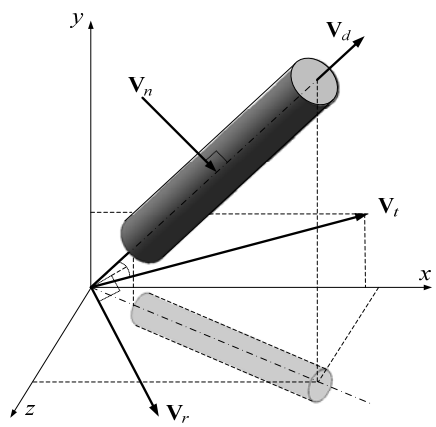

Figure 2. Definition of sketch for an inclined member

In addition, the application of the Morison equation to a cylinder member oriented in a random direction is here discussed. The direction of wave force normal to the cylinder may conveniently be resolved into horizontal and vertical components. To define the system, a fixed cylinder arbitrarily is inclined to axes *x, y* and *z* as shown in Figure 2. Assuming that the wave is propagation in the *x*-direction, the resulting water motion will have horizontal and vertical velocities *u, w* and *v* and horizontal and vertical accelerations a_x, a_z and a_y. The wave velocity $\mathbf{V}_t$ can be defined by

$$\mathbf{V}_t = \begin{bmatrix} u & v & w \end{bmatrix}^T \tag{6}$$

The water velocity $\mathbf{V}_n$ normal to the cylinder axis can be obtained as:

$$\mathbf{V}_r = \mathbf{V}_t \times \mathbf{V}_d \tag{7}$$

$$\mathbf{V}_n = \mathbf{V}_d \times \mathbf{V}_r \tag{8}$$

where the components of the water velocity $\mathbf{V}_n$ normal to the cylinder are u_{nx}, u_{ny}, and u_{nz}, respectively. By using the same way as the normal water velocity, the components of the normal water acceleration are a_{nx}, a_{ny}, and a_{nz}, respectively. With these relations, the components of the force per unit of cylinder length acting in the *x, y,* and *z* directions are given by the generalized Morison equations:

$$\begin{Bmatrix} f_x \\ f_y \\ f_z \end{Bmatrix} = \frac{1}{2}\rho C_D \left|\mathbf{V}_n\right| \begin{Bmatrix} u_{nx} \\ u_{ny} \\ u_{nz} \end{Bmatrix} + \rho C_M \frac{\pi D^2}{4} \begin{Bmatrix} a_{nx} \\ a_{ny} \\ a_{nz} \end{Bmatrix} \tag{9}$$

where $\left|\mathbf{V}_n\right|$ denotes the magnitude of the normal wave velocity. The total forces in each direction are calculated along the distance s of the member axis.

$$F_x = \int_s f_x ds, \qquad F_y = \int_s f_y ds, \qquad F_z = \int_s f_z ds \tag{10}$$

4. Current Velocity

Generally, the common currents considered in offshore structural analysis are tidal and wind drift currents (Dawson, 1983). Both of them are usually regarded as horizontal and varying with depth. The tidal current velocity profile at any vertical distance from the seabed may be determined as:

$$U_T(y) = U_{oT}\left(\frac{y}{d}\right)^{1/7} \tag{11}$$

and the wind drift current velocity profile may be determined as:

$$U_w(y) = U_{ow}\left(\frac{y}{d}\right) \tag{12}$$

where, *d* denotes the water depth, *y* is the vertical distance from the seabed, U_{oT} and U_{oW} denote the tidal and wind drift current velocity at the water surface respectively. For regular design waves and a horizontal current of arbitrary depth variation, the force exerted on an offshore structure is normally calculated by directly adding the horizontal water velocity caused by the waves to that component of current velocity.

5. Wind Speed

Since the wind acts as an external force to the upper structure, above sea level, the wind velocity is determined to estimate the wind generated force (Lee, 1989). The wind climate represented by the 10 minute mean wind speed U_{10} should be preferably based on statistical data. The mean wind velocity profile within atmospheric boundary layer could be described by the power law.

$$u(z) = U_{10}(H)\left(\frac{z}{H}\right)^{\alpha} \tag{13}$$

where $u(z)$ is the mean wind speed at height z above the ground, $U_{10}(H)$ the reference height, and α = 0.12 the power law exponent for rough sea is used in this study.

6. The Numerical Example

A numerical analysis of an offshore wind turbine which is as shown in Figure 3(a) is presented to demonstrate the performance of the finite element program (XFINAS). The environmental loads based on 50-year return period are considered in this numerical example (Pasin, 2011). The Stokes' fifth order wave theory is used in simulation of wave acting on the offshore structural members. Wind-generated loads on the rotor and the tower is also included. The direct wind-generated loads consist of aerodynamic blade loads and aerodynamic drag forces on tower and nacelle. Table 1 shows the estimate of forces and moments generated by the rotor blade form 5.5MW GE Energy turbine. Figure 3(b) illustrates the directions of forces and moments acting at the rotor (Ven der Tempel, 2006). The static analysis of fixed offshore wind turbine is separated into two load cases as follows:
Load case 1: 1.35 (Wave load)
Load case 2: 1.35 (Wave load + Wind load + Current load)

Table 1. Estimated load at the top of the tower

Fx (KN)	Fy (KN)	Fz (KN)	Mx (KN)	My (KN)	Mz (KN)
128	348	210	4250	124	820

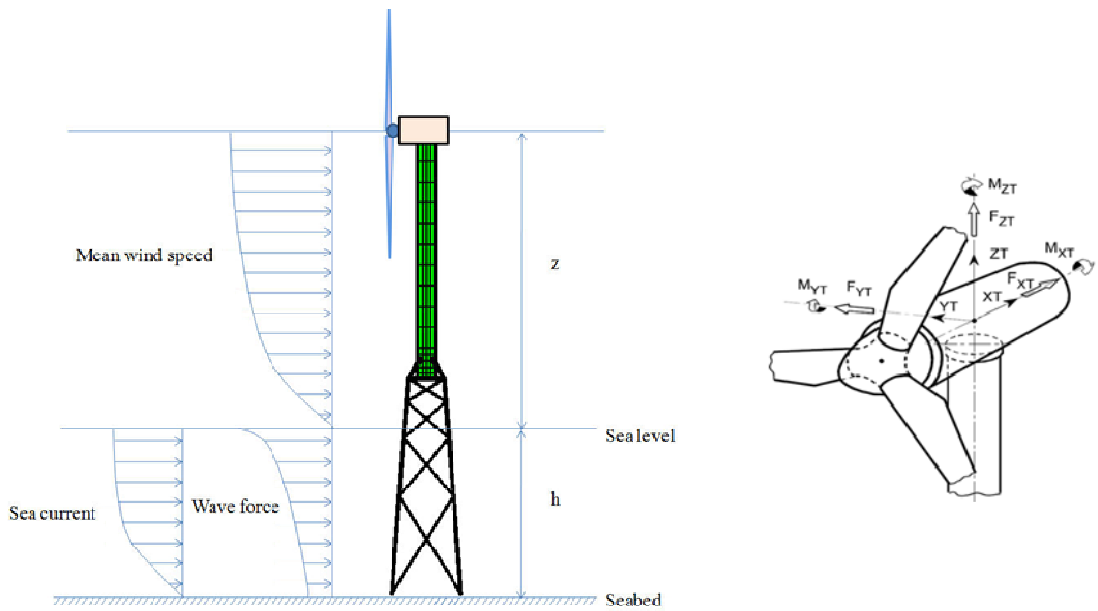

(a) Environmental loads (b) The estimated load of rotor blade

Figure 3. All loads on the offshore wind turbine

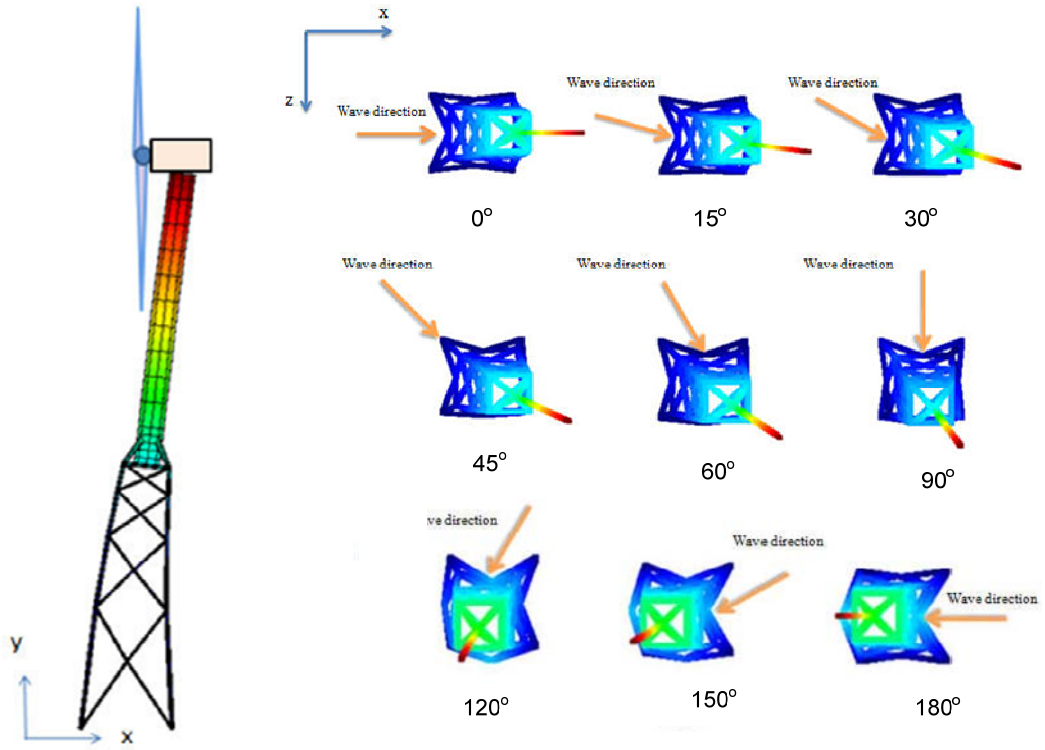

(a) Structural deformation (b) Deformed shapes with various wave angles

Figure 4. Deformation shape of wave propagation from 0 to 180 degrees with respect to *x*-direction

Figure 4(a) depicts a deformed shape due to the effects of wave and wind loads. To investigate the wave angle producing the maximum displacement at the top, the wave direction is rotated around the offshore wind turbine. In this study, only the wave direction attacking to the offshore wind turbine is changed, while the wind direction is fixed at 0 degree. The deformed shapes with various wave angles from 0 to 180 degrees with respect to *x*-direction are illustrated in Figure 4(b). In the first load combination, the top displacement caused by only wave load with various wave angles is illustrated in Figure 5. The maximum displacement which occurs at 0 degree is 0.105 m. In addition, the result of the top displacement of the second load case is plotted in Figure 6. It can be observed that the maximum displacement occurs at 0 degree because wave and wind have the same direction. The maximum displacement of the second load case which is the combinations of wave, wind, and current loads is 0.233 m. provides the higher value than the first case. It is clearly that extreme environmental loads for design load combinations and rotation of wave direction attacking to the offshore wind turbine have to be considered to obtain the maximum response.

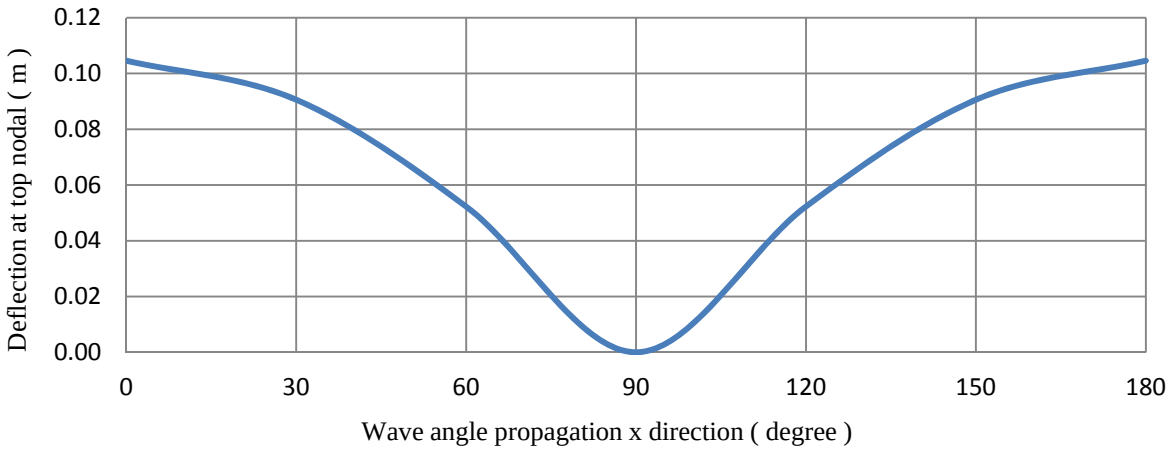

Figure 5. The top displacement with various wave angles (load combination 1)

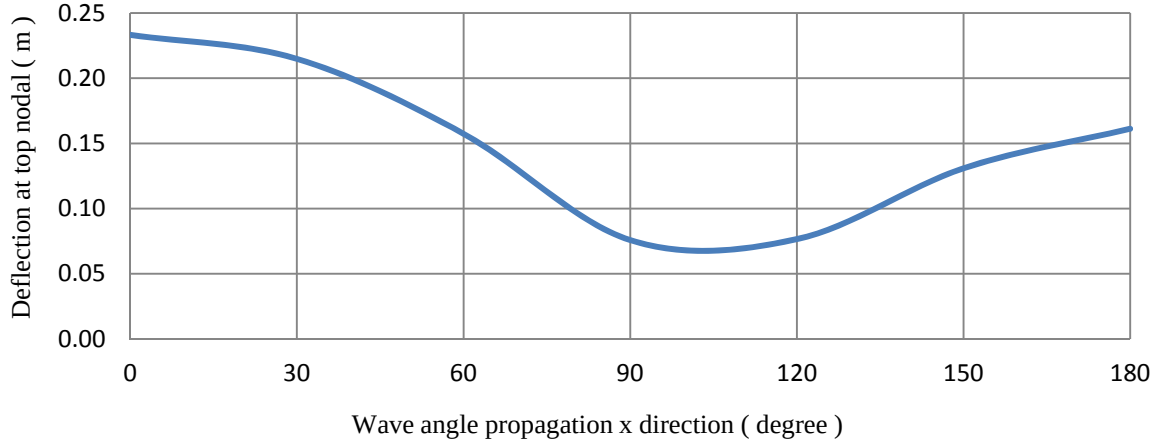

Figure 6. The top displacement with various wave angles (load combination 2)

7. Conclusion

In this paper, a numerical analysis of wind turbine offshore structures based on finite element method is presented. Stokes' fifth order theory, which are commonly used in offshore structural engineering, are employed in simulation of ocean surface waves. The velocity and acceleration terms are converted into resultant forces based on the Morison equation. Furthermore, other environmental loadings due to currents, wind are also included in analysis of offshore wind turbines. A numerical example of the offshore wind turbine is then carried out to demonstrate the performances of the proposed finite element program. From the simulations of environmental loadings, the results show that the developed program is able to predict the responses of the offshore wind turbine efficiency.

References

Francesco Petrini, Hui Li and Franco Bontempi. (2010) Basis of Design and Numerical Modeling of Offshore Wind Turbines, Structural Engineering and Mechanics, Vol. 36, No. 5, pp. 599-624.

Borthwick, A.G.L., and Herbert, D.M. (1988) Loading and Response of a Small Diameter Flexibly Mounted Cylinder in Waves. Journal of Fluids and Structures, Academic Press Limited, pp. 479-501.

Witz, J., Lyons, G., Patel, M.H., and Brown, D. (1994). Advanced Offshore Engineering. Offshore Engineering Handbook Series. book edition. Bentham Press, London, UK.

Skjelbreia, L., and Hendrickson, J.A. (1961) Fifth Order Gravity Wave Theory. Proceedings of 7th Coastal Eng. Conf., The Hague, pp. 184-196.

Dawson, T.H. (1983) Offshore Structural Engineering. book edition. Prentice Hall, Englewood Cliffs, N.J., USA, total number of pages.

DNV, Det Norske Veritas. (2004) DNV-OS-J101 Offshore Standard. Design of Offshore Wind Turbine Structures, June 2004.

API (2007). Recommended Practice for Planning, Designing and Constructing Fixed Offshore Platforms – Load and Resistance Factor Design, RP 2A-LRFD, American Petroleum Institute.

Lee Kang Su. (2002) Effects of Various Stiffeners on Offshore Steel Jacket Strength. A Master's thesis, INAH University of korea.

Pasin Plodpradit. (2011) Response of a Wind Turbine Offshore Structure under Environmetal Loading including Soil-structure interaction. Master Thesis, Asian institute of Technology.

Jan Van Der Tempel. (2006) Design of support structure for wind turbines. Offshore Engineering report 2006.OE.009.

Time-Dependent Analysis of PWR Prestressed Concrete Containment Considering Realistic Tendon Profile

*Pramin Norachan[1)], Ki-Du Kim[2)] and Kyung-Chul Kim[3)]

[1), 2)] *Department of Civil and Environmental System Engineering, Konkuk University, 1 Hwayang-dong, Gwangjin-gu, Seoul, Korea*
[3)] *Kolon Construction Company, Research & Development Center*
[1)] min_krub@hotmail.com,

ABSTRACT

Time-dependent analysis of a PWR prestressed concrete containment based on finite element method using the standard 8-node solid element is discussed in this paper. The enhanced assumed strain (EAS) is included in the formulation of the present element to overcome various locking problems that appear in solving structures. For the prestressing tendon, its idealization is based on representing the actual curved geometry of a tendon by a system of piecewise linear prestressing segments intersecting at tendon points. All variables of the tendon points are directly converted to those of the nodes of solid element. In addition, the time dependent effects due to creep, shrinkage and relaxation are also considered in analysis of prestressed concrete containment. Finally, numerical examples are employed to predict the long-term responses of the prestressed concrete containment.

1. INTRODUCTION

In order to analyze a sophisticated and complex prestressed concrete structures accurately and efficiently, solid elements have been employed because they can represent the real behavior of the prestressed concrete structures. In general, the 8-node solid elements have serious drawbacks, which are directly related to several kinds of locking behaviors. (Simo 1990) introduced the enhanced assumed strain (EAS) method to overcome locking behavior and improve the response of traditional elements. In the analysis of prestressed concrete containments, the realistic tendon profile should be considered to obtain accurate results. In general, the ultimate analysis is carried out to predict the failure mode of the prestressed concrete containment (Hsuan 2006). However, the effects of time-dependent behavior on this kind of structures have received little attention. For time-dependent analysis, deformations of prestressed concrete structures will considerably increase due to creep, shrinkage. As the result, it is necessary to consider these effects to control the long-term deformations of the prestressed concrete structures for serviceability which is an important criterion in design. The objective of this paper is to present numerical analysis using the XFINAS finite element program to investigate the long-term responses of the PWR prestressed concrete containment.

2. FORMULATION OF THE SOLID ELEMENT

2.1. Enhanced assumed strain (EAS)

In this study, the standard 8-node solid element with three degrees of freedom per node in translation is employed. To overcome various locking problems and improve the performances of traditional elements, the enhanced strain formulation is used in the present

---

[1)] Graduate Student
[2)] Professor

solid element formulation. In EAS method, the interpolation functions, assumed for the $\mathbf{M}_{\xi}$ matrix with 24 parameters, are chosen as follows:

$$\mathbf{M}_{\xi} = \left[\begin{array}{ccc|ccccccc|cccccc|cccccc|ccc}
\xi & 0 & 0 & 0 & 0 & 0 & 0 & 0 & 0 & 0 & 0 & 0 & 0 & 0 & 0 & \xi\eta & \xi\zeta & 0 & 0 & 0 & 0 & 0 & 0 & 0 \\
0 & \eta & 0 & 0 & 0 & 0 & 0 & 0 & 0 & 0 & 0 & 0 & 0 & 0 & 0 & 0 & 0 & \xi\eta & \zeta\eta & 0 & 0 & 0 & 0 & 0 \\
0 & 0 & \zeta & 0 & 0 & 0 & 0 & 0 & 0 & 0 & 0 & 0 & 0 & 0 & 0 & 0 & 0 & 0 & 0 & \xi\zeta & \zeta\eta & 0 & 0 & 0 \\
0 & 0 & 0 & \xi & \eta & 0 & 0 & 0 & 0 & \xi\zeta & \eta\zeta & 0 & 0 & 0 & 0 & 0 & 0 & 0 & 0 & 0 & 0 & \xi\eta & 0 & 0 \\
0 & 0 & 0 & 0 & 0 & \xi & \zeta & 0 & 0 & 0 & 0 & \xi\eta & \zeta\eta & 0 & 0 & 0 & 0 & 0 & 0 & 0 & 0 & 0 & \xi\zeta & 0 \\
0 & 0 & 0 & 0 & 0 & 0 & 0 & \eta & \zeta & 0 & 0 & 0 & 0 & \xi\eta & \xi\zeta & 0 & 0 & 0 & 0 & 0 & 0 & 0 & 0 & \zeta\eta
\end{array}\right] \tag{1}$$

After intensive numerical tests, we found out that the use of 24 enhanced strain parameters performs accurate results for analyzing structures. Even though more terms of enhanced strain parameters are used in the element formulation, the element performance yields only minor improvements.

2.2 Time-dependent concrete material properties

An important assumption in studying and predicting the time-dependent behavior of concrete structures is that the total strain in the concrete may be considered as a superposition of several independent components caused by different phenomena. The total concrete strain $\varepsilon(t)$ at any time t is assumed to be composed of the mechanical strain $\varepsilon^{m}(t)$ caused by short-term service loads and the non-mechanical strain $\varepsilon^{nm}(t)$ consists of creep strain $\varepsilon^{cr}(t)$ and shrinkage strain $\varepsilon^{sh}(t)$.

$$\begin{aligned}\varepsilon(t) &= \varepsilon^{m}(t) + \varepsilon^{nm}(t) \\ &= \varepsilon^{m}(t) + \varepsilon^{cr}(t) + \varepsilon^{sh}(t)\end{aligned} \tag{2}$$

Shrinkage strain can be evaluated directly by utilizing the shrinkage model proposed in design codes, but creep is defined as the increase in strain under sustained stress. Therefore, the first-order recursive algorithm based on the expansion of creep compliance has been adopted because the model can simulate the stress history effectively in spite of its simplicity in application (Kabir 1976 and Ketchum 1986).

$$\Delta\varepsilon_{n}^{c} = \sum_{i=1}^{m} A_{i_{n-1}}(1 - e^{-\Delta t_n/\Gamma_i}) \tag{3}$$

$$A_{i_n} = A_{i_{n-1}} e^{-\Delta t_n/\Gamma_i} + a_i(\tau)\Delta\sigma_n \tag{4}$$

where $\Delta\varepsilon_{n}^{c}$ is the incremental creep strain; Γ_i is the retardation; $a_i(\tau)$ are creep compliance coefficients which depend on the age of loading τ; m is the number of time steps; A_i is the hidden state variables and are updated during each time step. Initial values are $A_{i_1} = a_i(t_1)\Delta\sigma_n$ at $n = 1$. The values of $a_i(\tau)$ are determined by the method of least squares using Kabir's Dirichlet series creep compliance.

$$J(t_j, \tau) = \sum_{i=1}^{m} a_i(\tau)[1 - e^{-(t_j - \tau)/\Gamma_i}] \tag{5}$$

In this study, $m = 4$ is used, and the assumed corresponding retardation times Γ_i are 5, 50, 500 and 5000.

3. FORMULATION OF THE PRESTRESSING TENDON ELEMENT

3.1 Tendon segment stiffness and load computation

The tendon is idealized using a series of straight segments connected at tendon points, where each tendon segment is assumed to be under constant axial stress, and its stiffness and load contributions are obtained from nodal variables of each tendon element inside solid elements. A global coordinate system and geometry is defined in the generation of the three-dimensional space as shown in Fig. 1.

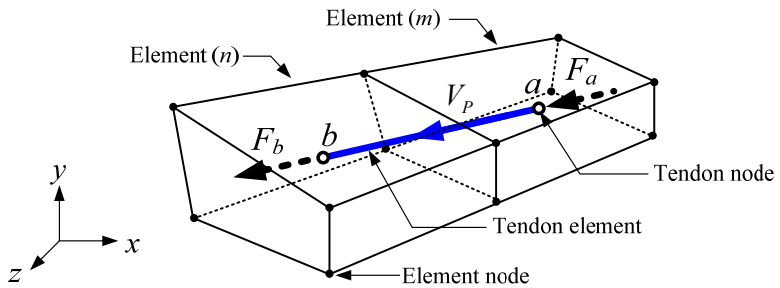

Fig. 1 Coordinate systems and geometry of tendon element associated solid elements

Points *a* and *b* are located inside the solid element *m* and *n* respectively. The association of tendon point *a* is rigidly linked to the nodes of solid element *m*, and tendon point *b* is directly linked to the nodes of solid element *n* in the same manner. To find any tendon point inside an element, the algorithm based on Newton-Raphson method will be operated to search the position and record the element number for each tendon point. By using the concept of mapping variables and following the same procedure as truss element, the tendon stiffness matrix K_{TD} and the load vectors F_{TD} can be obtained as follows:

$$K_{TD} = H^T T^T K_e T H \tag{6}$$

$$F_{TD} = H^T T^T F_e \tag{7}$$

where the stiffness matrix K_e, the force vector F_e in local coordinates of the tendon element are given by

$$K_e = \frac{E_p A}{L}\begin{bmatrix} 1 & -1 \\ -1 & 1 \end{bmatrix}, \text{ and } \quad F_e = \begin{Bmatrix} F_a \\ F_b \end{Bmatrix} \tag{8}$$

The transformation matrix H between the displacements of two tendon points to the nodal displacements of the associated solid elements, can be defined by

$$H = \begin{bmatrix} \bar{H} & 0 \\ 0 & \bar{H} \end{bmatrix}, \text{ and } \bar{H} = \left[\begin{array}{ccc|c|ccc} N_1 & 0 & 0 & & N_8 & 0 & 0 \\ 0 & N_1 & 0 & \cdots & 0 & N_8 & 0 \\ 0 & 0 & N_1 & & 0 & 0 & N_8 \end{array}\right] \tag{9}$$

3.2 Tendon stress relaxation

Relaxation is a phenomenon similar to creep and is defined as the decrease in stress over time under constant strain. The following equation is used for the calculation of tendon stress relaxation.

$$\frac{f_s}{f_{si}} = 1 - \frac{\log_{10} t}{10}\left\{\frac{f_{si}}{f_y} - 0.55\right\} \tag{10}$$

where f_s is the prestress at a time t, f_{si} is the initial steel stress and f_y is the 0.001 offset yield stress of prestressing steel.

4. FINITE ELEMENT FORMULATION

For the non-linear equations, since the formulation is based on the Updated Lagrangian method, all displacements are in incremental form. Due to apply the EAS method, the condensation approach is employed to obtain the force vector and stiffness matrix. In addition, the stiffness matrix $\mathbf{K}_{TD}$ of tendon element is combined with the elastic stiffness matrix $\mathbf{K}_E$ and geometric stiffness matrix $\mathbf{K}_G$ of solid element to obtain the total stiffness $\mathbf{K}_T$ as follows:

$$\mathbf{K}_T = \mathbf{K}_E + \mathbf{K}_{TD} + \mathbf{K}_G \tag{11}$$

In this study, the finite element package XFINAS for the general non-linear dynamic analysis is used to investigate the time-dependent effects of the prestressed concrete containment.

5. NUMERICAL EXAMPLES

5.1 Concrete cantilever beam

A cantilever beam which can be found in MIDAS/Civil Verification Examples is presented to validate the implemented creep model functions of CEB-FIP 1990. This beam which shown in Fig. 2(a) is considered with the following parameters: the beam cross-section is 1.0 × 1.0 m; beam length L = 10 m; E_c = 3.63×10^6 ton/m^2; Poisson's ratio ν = 0.18; Compressive strength of concrete at the age of 28 days 4000 ton/m^2; Relative Humidity 70 %, Notational size of member 0.5, Type of cement: Normal or rapid hardening cement. The step load acts on the tip of the beam is illustrated in Fig. 2(b). There are two load cases that the beam has to carry. First, the cantilever beam will be subjected an axial load as shown in Fig. 2(c). In the other case, prestressed force will be applied on the beam instead of the axial load as shown in Fig. 2(d).

For this example, comparison of the results from XFINAS using the present element and from MIDAS using frame element and analytical solutions obtained from the hand-calculated results are shown in Fig. 3. The elastic shortening displacement is 0.000275 m, and the total displacements affected by creep are normalized by this value. The trends of the tip displacement in both load cases from the present element show an acceptable match with that from the analytical solution. This example, moreover, can prove that the prestressed tendon works well with the present element because there is slightly difference between the results from the beams is applied axial force and the beam is subjected by prestressed force.

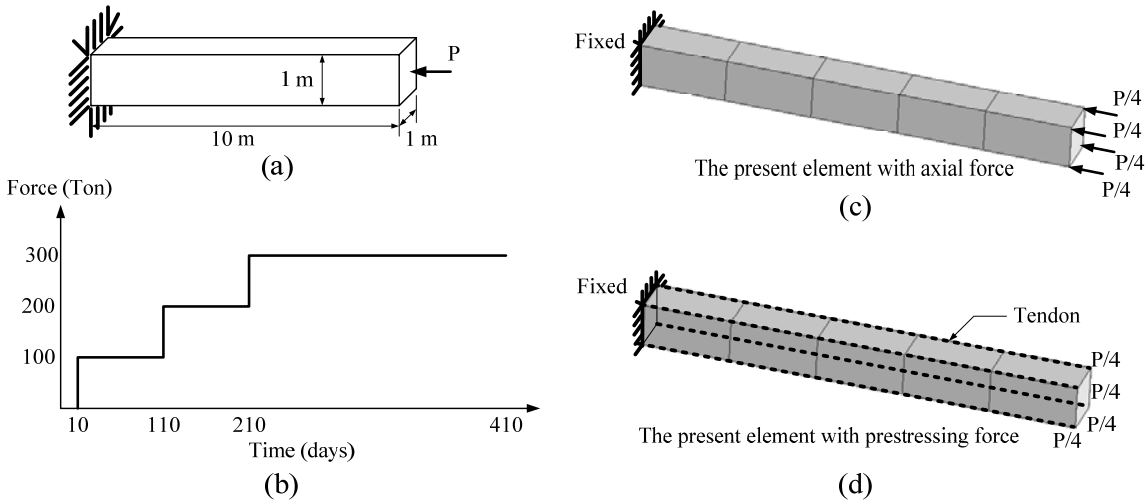

Fig. 2 Pure creep under the step load

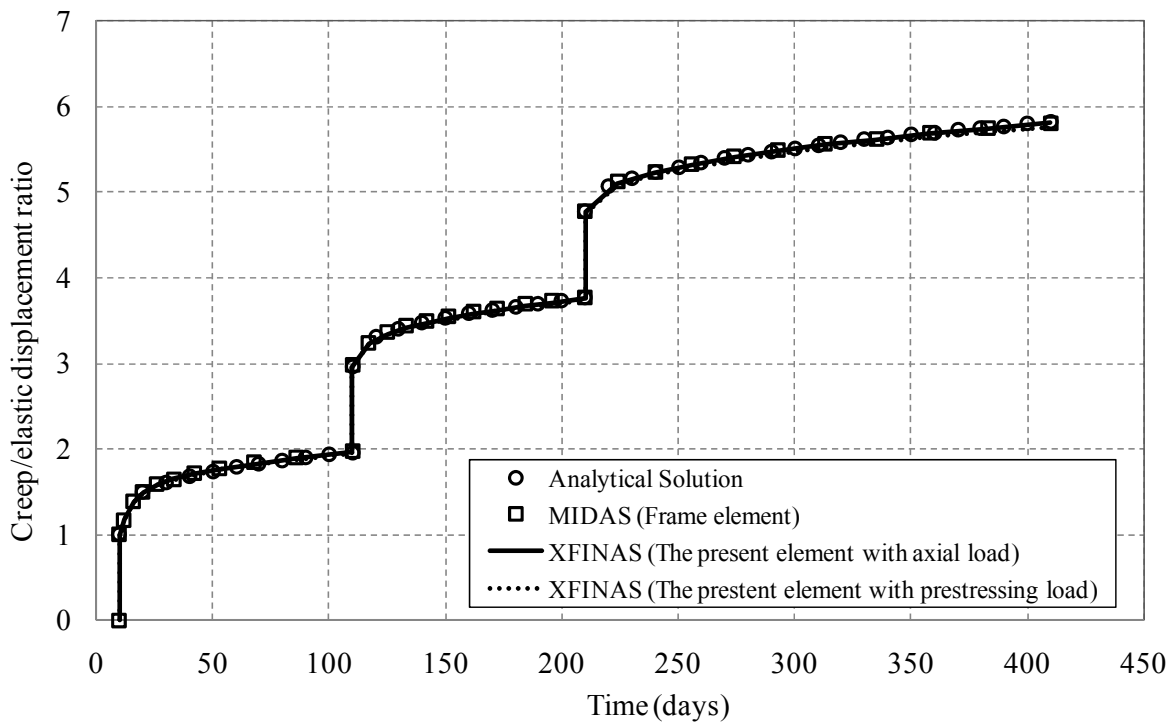

Fig. 3 Comparison the results between the present element and other references

5.2 Prestressed concrete containment

A PWR prestressed concrete containment is composed of a circular base slab, an upright cylinder and a hemispherical dome as shown in Fig. 4(a). To simplify the analysis, the structural geometry is assumed to be axisymmetric. At the cylinder wall, the prestressing tendons are placed in the meridional and circumferential directions of the containment as illustrated in Fig. 4(b). For simplicity, only 1/4 part of the structure is analyzed and the boundary conditions imposed on the symmetry planes are displacements in the circumferential direction. In the numerical simulation, the present element is used to model the structure. The containment is composed of 250 tendons with the diameter of each strand 1.52 cm. The average tensile force is 190 kN for each tendon. The containment including its self-weight load was stressed at 56 days after casting as illustrated in Fig. 4(c). At 112 days,

the design pressure load of 476 kPa is applied to the internal surface of the containment and this pressure load is kept up to 500 days. Material properties of concrete, steel, and prestressing tendon are assumed and shown in Fig 4(d). To observe the time-dependent effect with higher pressure, the design pressure load is further multiplied by a factor 1.25 to obtain a higher pressure of 595 kPa. The creep and shrinkage parameters recommended by the ACI committee 209 are used as follows: ultimate creep factor $C(\infty) = 2.35$, ultimate shrinkage $\varepsilon(\infty) = 0.0008$, and relative humidity 70 %.

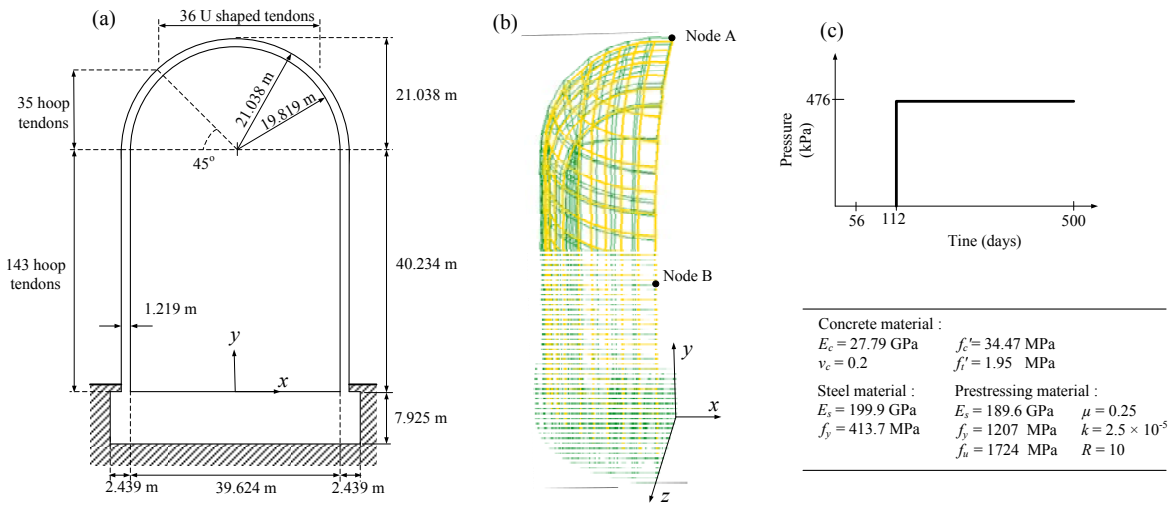

Fig. 4 Geometry, applied loads, and material properties of the prestressed concrete containment

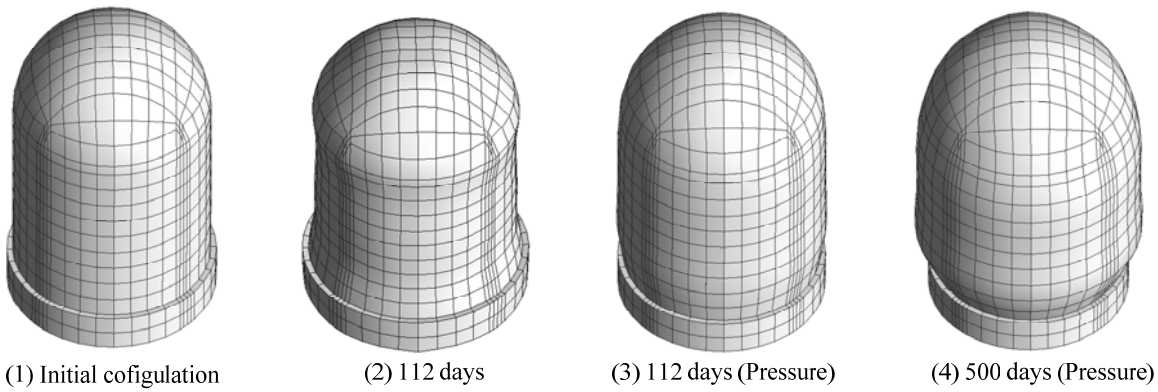

Fig. 5 Deformed configurations of the prestressed concrete containment

The deformations at several loading times are illustrated in Fig. 5. For results of analysis, Fig. 6(a) shows the displacement of node A in the *y*-direction versus various times by considering different pressure 0, 1.00*P*, and 1.25*P*. At 56 days after casting, the instantaneous elastic displacement at node A in the *y*-direction due to the applied dead load plus prestressing force is 0.24 cm downward, and it increases continuously due to creep and shrinkage effects to 0.73 cm at 112 days. The application of the design pressure load of 476 kPa (1.00*P*), which is added to the internal surface of the containment at 112 days, causes an upward displacement. After the containment has carried the loads up to 500 days, the upward displacement at this point increases up to the value of 0.32 cm. At this state, the developed

displacement with the factor 1.25 of pressure is 0.69 cm upward, while the displacement with no pressure load is 1.15 cm downward. For the enveloped curve of the displacement at node B in the *z*-direction, the trends of deflection curves are quite similar to that of point A as illustrated in Fig. 6(b). At 500 days, the displacement with the design pressure is 0.812 cm, while the displacement with the factor 1.25 of pressure is 1.078 cm, and the displacement with no pressure load is -0.254 cm. By comparing the displacements between node A and B in both load cases of pressure , It can be observed that most of the deformations take place in the wall of the containment based on the geometry and material properties of this example.

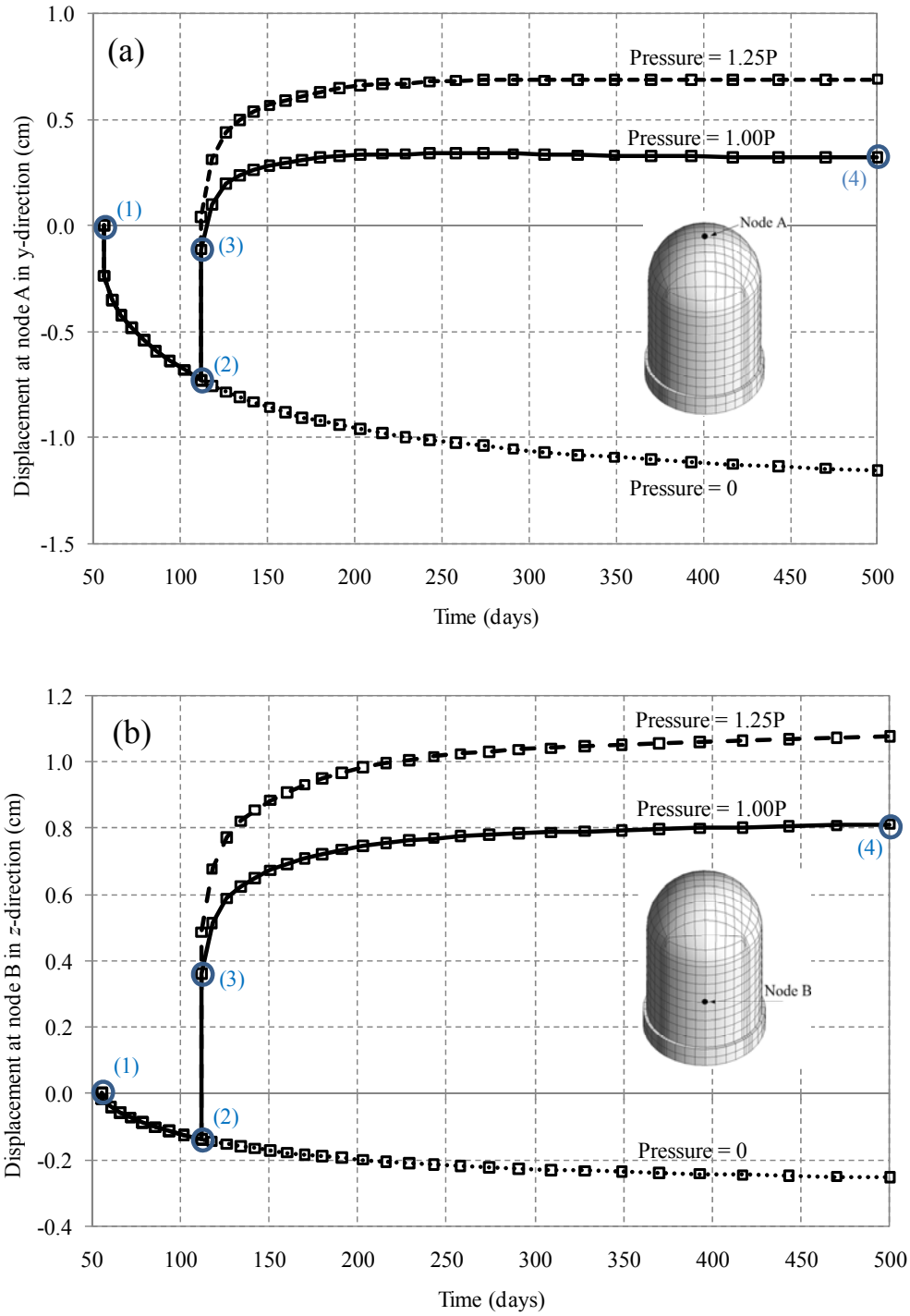

Fig. 6 Displacement-time histories of the prestressed concrete containment

CONCLUSION

In this paper, the standard 8-node solid element is developed in the analysis for prestressed concrete containment. To overcome the various locking problems that occur in solving structures, 24 enhanced assumed strain (EAS) parameters are presented in the formulation of the present element. In general, prestressing tendons are frequently arranged inside the prestressed concrete containment with some eccentrics. Therefore, the combination of the realistic tendon profile improves displacement filed of the prestressed concrete containment. To predict long-term behaviors, relaxation effect of tendon is considered, and creep and shrinkage effects following the ACI and CEB-FIP concrete codes are also included in analyzing prestressed concrete containment. The numerical results of time-dependent analysis demonstrated that the present element has the potential to predict the response of prestressed concrete contaiment to investigate the long-term deformations for serviceability being an important criterion in design.

ACKNOWLEDGEMENT

This work was supported by the Development of analysis of time-dependent response of nuclear reactor with bonded tendon using Prestressed concrete solid-shell element of the Korea Institute of Energy Technology Evaluation and Planning (KETEP) grant funded by the Korea government Ministry of Knowledge Economy. (No.2010T100101024)

REFERENCES

Simo JC, Rifai MS. (1990). “A class of mixed assumed strain methods and the methods of incompatible modes”, Int. *J. Numer. Meth. Eng*., Vol. **29**, 1595–1638.

Byung Hwan Oh, Se Jin Jeon. (2005). “An advanced FE analysis of PSC shell structures incorporating tendon-induced deformation-dependent loads”, *Finite Elem. Anal. Des*., Vol. **41**, 834-849.

Saleem Akhtar, K.K. Pathak, S.S. Bhadauria, N. Ramakrishnan. (2008). “Finite element analysis of prestressed concrete beams considering realistic cable profile”, *Int. J. Appl. Eng. Res*., Vol. **3**(1), 121-138.

CEB-FIB. (1993). *Model Code for Concrete Structures*, Euro-International Committee for Concrete (CEB) & International Federation for Prestressing (FIP), Thomas Telford.

ACI Committee 209. (2008). *Prediction of Creep, Shrinkage, and Temperature Effects in Concrete Structures*, American Concrete Institute, Report No. ACI 209R-92.

Kabir AF. (1976). “Non-linear analysis of reinforced concrete panels, slabs and shells for time dependent effects”, University of California, Berkeley, CA, Report no. UC-SEEM 76-6.

Ketchum MA. (1986). “Redistribution of stresses in segmentally erected prestressed concrete bridges”, University of California, Berkeley, CA, Report no. UCB-SEMM 86/07.

MIDAS Information Technology Co., Ltd. (1989). MIDAS/Civil Verification Examples, Seoul, Korea.

Hsuan-The Hu and Yu-Hon Lin. (2006). “Ultimate analysis of PWR prestressed concrete containment subjected to internal pressure”, *Int. J. Pres. Ves. Pip*., Vol. **83**, 161-167.

Z. Hora and B. Patzak. (2007). “Analysis of long-term behavior of nuclear reactor containment”, *Nucl. Eng. Des*., Vol. **237**, 253-259

Nan Zhang, Chung C. Fu, Huimin Che. (2011). “Experiment and numerical modeling of prestressed concrete curved slab with spatial unbonded tendons.” *Eng. Struct*., Vol. **33**, 747-756.

เทคโนโลยีการเสริมกำลัง โครงสร้างอาคาร เพื่อรับแรงแผ่นดินไหว

1 - 4 ตุลาคม 2558
โรงแรม เมอร์เคียว เชียงใหม่

Sponsored by TEMASEK Foundation

AIT Asian Institute of Technology · NANYANG TECHNOLOGICAL UNIVERSITY

01 ตุลาคม

8:00
ลงทะเบียน ณ ห้องประชุม Paris ชั้น 2 โรงแรมเมอร์เคียว

8:45
กล่าวเปิดการอบรมและวัตถุประสงค์ของงาน
TMS/NTU/CMU/AIT/KMUTT

9:00
ความเข้าใจเรื่องแผ่นดินไหวและความเสี่ยงในการเกิดแผ่นดินไหวของประเทศไทย
ศ. ดร. เป็นหนึ่ง วานิชชัย

11:00
ความรู้พื้นฐานด้านวิศวกรรมโครงสร้างต้านทานแผ่นดินไหว
ผศ. ดร. ชยานนท์ หรรษภิญโญ

13:00
ผลกระทบของแผ่นดินไหวต่อโครงสร้างและมาตรฐานการออกแบบที่เกี่ยวข้อง
ผศ. ดร. ชยานนท์ หรรษภิญโญ

14:30
ความรู้พื้นฐานด้านวิธีการและข้อคำนึงต่างๆสำหรับการเสริมกำลังของโครงสร้างต้านทานแผ่นดินไหว
รศ. ดร.สุทัศน์ ลีลาทวีวัฒน์

02 ตุลาคม

9:00
การสร้างแบบจำลอง การวิเคราะห์โครงสร้างแบบไม่เชิงเส้นโดยใช้โปรแกรมคอมพิวเตอร์
ดร. ประมินทร์ นรชาญ

10:45
ตัวอย่างของการประเมินกำลังและการเสริมกำลังของโครงสร้างต้านทานแผ่นดินไหว
ดร. ประมินทร์ นรชาญ

13:00
การทดสอบการเสริมกำลังโครงสร้างต้านทานแผ่นดินไหวของต่างประเทศ 1*
Assoc. Prof. Li Bing

14:45
การทดสอบการเสริมกำลังโครงสร้างต้านทานแผ่นดินไหวของต่างประเทศ 2*
Assoc. Prof. Li Bing

*บรรยายเป็นภาษาอังกฤษ และสรุปเนื้อหาเป็นภาษาไทย

03 ตุลาคม

8:00
นัดรวมตัวที่ Lobby โรงแรมเมอร์เคียว

9:00
ดูงานโครงสร้างอาคารโรงเรียนบ้านหนองโค้ง
ผศ. ดร. ชยานนท์ หรรษภิญโญ และ AIT

10:45
ดูงานโครงสร้างอาคารโรงเรียนสันกำแพง
ผศ. ดร. ชยานนท์ หรรษภิญโญ และ AIT

13:00
การเสริมกำลังโครงสร้างด้วยวิธี FRP
ศ. ดร. อมร พิมานมาศ

14:45
การเสริมกำลังโครงสร้างด้วยวิธี Concrete Jacketing
ศ. ดร. อมร พิมานมาศ

04 ตุลาคม

9:00
การเสริมกำลังด้วยโครงสร้างกำแพง
รศ. ดร. ไพบูลย์ ปัญญาคะโป

10:45
การเสริมกำลังด้วยโครงสร้างเหล็ก
รศ. ดร.สุทัศน์ ลีลาทวีวัฒน์

13:00
การสรุปองค์ความรู้ทั้งหมดและการประเมินผลการอบรม/การปิดการอบรม
กิจกรรมกลุ่ม

หมายเหตุ:
รับประทานอาหารกลางวัน ณ ห้อง Citrus โรงแรมเมอร์เคียว

ติดต่อผู้ประสานงาน
มือถือ : 090-319-3544 E-mail : ait.acecoms@gmail.com

CPD/PDU 18 หน่วย

สมาคมคอนกรีตแห่งประเทศไทย
Thailand Concrete Association

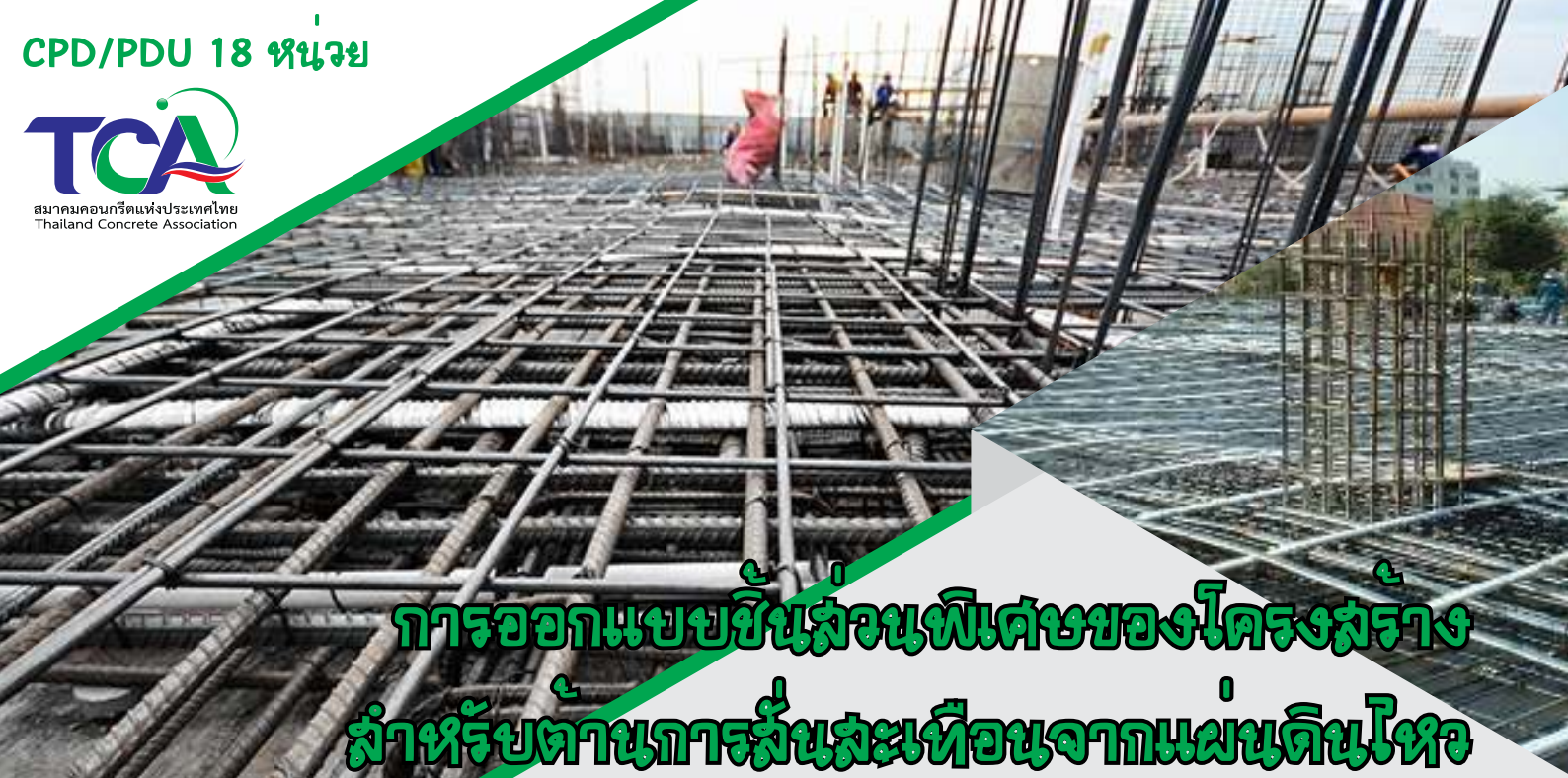

การออกแบบชิ้นส่วนพิเศษของโครงสร้าง สำหรับต้านการสั่นสะเทือนจากแผ่นดินไหว

(Designing of Special Structural Members for Earthquake Resistance)

วันพฤหัสบดีและวันศุกร์ที่ 13-14 มิถุนายน พ.ศ. 2562

เวลา 8.30 - 16.30 น. ห้องสัมมนา ชั้น 3 อาคาร วสท.

ผศ.ดร.ภาณุวัฒน์ จ้อยกลัด

รศ.ดร.ไพบูลย์ ปัญญาคะโป

ดร.ประมินทร์ นรชาญ

รศ.ดร.สุทัศน์ ลีลาทวีวัฒน์

ดร.อัศวิน วาณิชย์ก่อกุล

ดร.เมธี เชี่ยววณิชย์กร

ผศ.ดร.ปรีดา ไชยมหาวัน

หลักการและเหตุผล

เนื่องจากรูปแบบอาคารสูงในปัจจุบันมีความซับซ้อนมากขึ้นมาก อีกทั้งเมื่อต้องออกแบบอาคารเหล่านั้นให้ต้านการสั่นสะเทือนจากแผ่นดินไหว การวิเคราะห์และดำเนินการจึงต้องอาศัยหลักวิชาความรู้ขั้นสูงและมีความทันสมัย

หลักสูตรพิเศษที่นำเสนอนี้จะนำวิศวกรโครงสร้างเข้าสู่โหมดการออกแบบองค์อาคารพิเศษที่มีอยู่ในอาคารสูงทั่วไป ซึ่งมีพฤติกรรมซับซ้อนและไม่สามารถออกแบบได้ด้วยหลักการโดยทั่วไป การคัดเลือกชิ้นส่วนในหลักสูตรนี้เน้นการทำงานจริง ซึ่งในครั้งนี้ได้มีการรวบรวมวิทยากรที่มีความรู้ความสามารถทั้งที่เกี่ยวข้องในฐานะผู้ร่างมาตรฐานการออกแบบ นักวิจัย และวิศวกรนักปฏิบัติ ไว้มากมาย โดยสมาคมฯหวังว่าผู้เข้ารับการอบรมจะได้รับความรู้ที่ทันสมัย และสามารถนำไปใช้ในการออกแบบอาคารในประเทศไทยได้อย่างมั่นใจ

วัตถุประสงค์

1. เพื่อให้ผู้เข้ารับการอบรมมีความรู้ความเข้าใจในหลักการของการออกแบบองค์อาคารพิเศษภายใต้แรงแผ่นดินไหวที่มีอยู่ในอาคารขนาดใหญ่ที่มีความซับซ้อน
2. เพื่อให้ผู้เข้ารับการสัมมนาได้รับความรู้จากประสบการณ์การทำงานจริงของผู้เชี่ยวชาญ ในการคำนวณและออกแบบอาคารต้านแผ่นดินไหว
3. เพื่อให้เกิดความร่วมมือในการพัฒนาองค์ความรู้ด้านการคำนวณออกแบบโครงสร้างซึ่งมีความทันสมัยและเกิดความมั่นใจในการทำงานมากขึ้น

สอบถามข้อมูลเพิ่มเติมที่ สมาคมคอนกรีตแห่งประเทศไทย (สคท.)

ชั้น 3 อาคาร วสท. 487 ซอยรามคำแหง 39 (ซอยเทพลีลา) ถนนรามคำแหง แขวงพลับพลา เขตวังทองหลาง กรุงเทพฯ 10310

โทรศัพท์ 02-935-6593 โทรสาร 02-935-6538 E-mail : thaitca@gmail.com website : http://thaitca.or.th เลขประจำตัวผู้เสียภาษี / TAX ID : 0-9930-00131-266

CPD/PDU 18 หน่วย

การออกแบบชิ้นส่วนพิเศษของโครงสร้างสำหรับต้านการสั่นสะเทือนจากแผ่นดินไหว

(Designing of Special Structural Members for Earthquake Resistance)

วันพฤหัสบดีและวันศุกร์ที่ 13-14 มิถุนายน พ.ศ. 2562 เวลา 8.30 - 16.30 น. ห้องสัมมนา ชั้น 3 อาคาร วสท.

กำหนดการ

วันพฤหัสบดีที่ 13 มิถุนายน พ.ศ.2562

08.30 - 09.00 น. ลงทะเบียน

09.00 - 10.30 น. การออกแบบโครงดัดให้มีความเหนียวพิเศษ
(Design of Special Moment Frames)
โดย ผศ.ดร.ภาณุวัฒน์ จ้อยกลัด
มหาวิทยาลัยศรีนครินทรวิโรฒ

10.30 - 10.45 น. พักรับประทานอาหารว่าง

10.45 - 12.15 น. การออกแบบกำแพงเฉือน
(Design of Shear Wall)
โดย ดร.อัศวิน วาณิชย์ก่อกุล
บริษัท ออเรคอน คอนซัลติ้ง (ประเทศไทย) จำกัด

12.15 - 13.15 น. พักรับประทานอาหารกลางวัน

13.15 - 14.45 น. การออกแบบคานเชื่อม
(Design of Coupling Beam)
โดย ดร.เมธี เชี่ยววณิชย์กร
บริษัท ไมนฮาร์ท (ประเทศไทย) จำกัด

14.45 - 15.00 น. พักรับประทานอาหารว่าง

15.00 - 16.30 น. การออกแบบฐานราก
(Design of Foundations)
โดย รศ.ดร.ไพบูลย์ ปัญญาคะโป
มหาวิทยาลัยศรีปทุม

วันศุกร์ที่ 14 มิถุนายน พ.ศ.2562

08.30 - 09.00 น. ลงทะเบียน

09.00 - 10.30 น. การออกแบบไดอะแฟรม คอร์ด และคอลเล็กเตอร์
(Design of Diaphragm, Chord and Collector)
โดย ดร.ประมีนทร์ นรชาญ
AIT Solutions

10.30 - 10.45 น. พักรับประทานอาหารว่าง

10.45 - 12.15 น. การออกแบบแผ่นพื้นคอนกรีตอัดแรง
(Design of Post-Tensioned Concrete Slab)
โดย รศ.ดร.สุทัศน์ ลีลาทวีวัฒน์
มหาวิทยาลัยเทคโนโลยีพระจอมเกล้าธนบุรี

12.15 - 13.15 น. พักรับประทานอาหารกลางวัน

13.15 - 14.45 น. การออกแบบจุดต่อแผ่นพื้นและกำแพง
(Design of Slab-Column/Slab-Wall Connection)
โดย ผศ.ดร.ภาณุวัฒน์ จ้อยกลัด
มหาวิทยาลัยศรีนครินทรวิโรฒ

14.45 - 15.00 น. พักรับประทานอาหารว่าง

15.00 - 16.30 น. การออกแบบจุดต่อคาน-เสา
(Design of Beam-Column Connections)
โดย ผศ.ดร.ปรีดา ไชยมหาวัน
มหาวิทยาลัยพะเยา

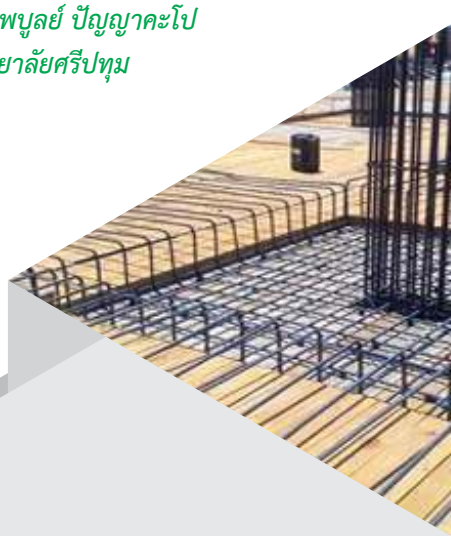

TCA
สมาคมคอนกรีตแห่งประเทศไทย
Thailand Concrete Association

สอบถามข้อมูลเพิ่มเติมที่ สมาคมคอนกรีตแห่งประเทศไทย (สคท.)

ชั้น 3 อาคาร วสท. 487 ซอยรามคำแหง 39 (ซอยเทพลีลา) ถนนรามคำแหง แขวงพลับพลา เขตวังทองหลาง กรุงเทพฯ 10310

โทรศัพท์ 02-935-6593 โทรสาร 02-935-6538 E-mail : thaitca@gmail.com website : http://thaitca.or.th เลขประจำตัวผู้เสียภาษี / TAX ID : 0-9930-00131-266

CPD/PDU 18 หน่วย

การออกแบบชิ้นส่วนพิเศษของโครงสร้างสำหรับต้านการสั่นสะเทือนจากแผ่นดินไหว

(Designing of Special Structural Members for Earthquake Resistance)

วันพฤหัสบดีและวันศุกร์ที่ 13-14 มิถุนายน พ.ศ. 2562 เวลา 8.30 - 16.30 น. ห้องสัมมนา ชั้น 3 อาคาร วสท.

ที่อยู่ในการออกใบกำกับภาษี / ใบเสร็จรับเงิน

ชื่อ - นามสกุล.....

หมายเลขสมาชิก TCA.....

หน่วยงาน (บริษัท/บ้าน.....

เลขที่อาคาร.....ชั้น.....หมู่.....ซอย.....

ถนน.....ตำบล/แขวง.....อำเภอ/เขต.....

จังหวัด.....รหัสไปรษณีย์.....โทรศัพท์.....

โทรสาร.....มือถือ.....E-mail.....

Tax ID (หมายเลขประจำตัวผู้เสียภาษี).....

เลขสมาชิกสภาวิศวกร (ในกรณีต้องการคะแนน CPD / PDU).....

หากต้องการรับประทานอาหารอิสลามหรือมังสวิรัติกรุณาแจ้ง.....

หมายเหตุ

1. อัตรานี้รวมภาษีมูลค่าเพิ่ม 7% เอกสารอบรม อาหารกลางวัน อาหารว่าง เครื่องดื่ม และวุฒิบัตร สามารถหักภาษี ณ ที่จ่าย 3%
2. ข้าราชการ พนักงานรัฐวิสาหกิจ ที่ได้รับอนุญาตจากต้นสังกัด สามารถเบิกจ่ายได้ตามระเบียบกระทรวงการคลัง
3. นักศึกษาโปรดแนบสำเนาบัตรนักศึกษามาพร้อมใบลงทะเบียน
4. กรณีที่ท่านไม่สามารถเข้าร่วมการอบรมได้ โปรดนำหนังสือแจ้งยกเลิกการอบรมล่วงหน้าก่อนการอบรมโดยมีรายละเอียดการคืนเงินดังต่อไปนี้
   - 4.1 แจ้งยกเลิกก่อนวันจัดอบรม / สัมมนา 7 วัน คืนเงิน 50 % ของค่าลงทะเบียน
   - 4.2 แจ้งยกเลิกน้อยกว่า 7 วันก่อนวันจัดอบรม / สัมมนา ไม่คืนเงินค่าลงทะเบียน
5. กรณี สคท. ยกเลิกการจัดอบรม / สัมมนา / ศึกษาดูงาน เนื่องจากสาเหตุใดก็ตาม สคท. จะคืนเงินให้ท่านเต็มจำนวน

การชำระเงิน

เงินสด สามารถชำระได้ที่ สมาคมคอนกรีตแห่งประเทศไทย (สคท. ชั้น 3 อาคาร วสท. วังทองหลาง กรุงเทพฯ)

เช็ค สั่งจ่ายในนาม **สมาคมคอนกรีตแห่งประเทศไทย**

โอนเงิน เข้าบัญชีเงินฝากประเภทออมทรัพย์ **ชื่อบัญชี สมาคมคอนกรีตแห่งประเทศไทย**

ธนาคารไทยพาณิชย์ สาขาสี่แยกศรีวรา เลขบัญชี 140-2-55084-3

*กรณีโอนเงิน กรุณาแนบสำเนาหลักฐานการชำระเงินพร้อมใบลงทะเบียน ส่งโทรสารมาตามเบอร์โทรสารสมาคมฯหรือสแกนส่ง E-mail และกรุณาช่วยโทรแจ้งกับเจ้าหน้าที่สมาคมฯ ด้วย ขอบคุณค่ะ

* ค่าลงทะเบียน *

ประเภท	ชำระภายในวันที่ 15 พฤษภาคม 2562	ชำระหลังวันที่ 15 พฤษภาคม 2562
นักศึกษา	2,400.00	2,800.00
สมาชิก TCA	3,100.00	3,400.00
ข้าราชการ / พนง.รัฐวิสาหกิจ	3,300.00	3,700.00
บุคคลทั่วไป	3,700.00	3,900.00

สมาคมคอนกรีตแห่งประเทศไทย
Thailand Concrete Association

สอบถามข้อมูลเพิ่มเติมที่ สมาคมคอนกรีตแห่งประเทศไทย (สคท.)

ชั้น 3 อาคาร วสท. 487 ซอยรามคำแหง 39 (ซอยเทพลีลา) ถนนรามคำแหง แขวงพลับพลา เขตวังทองหลาง กรุงเทพฯ 10310

โทรศัพท์ 02-935-6593 โทรสาร 02-935-6538 E-mail : thaitca@gmail.com website : http://thaitca.or.th เลขประจำตัวผู้เสียภาษี / TAX ID : 0-9930-00131-266

สมาคมคอนกรีตแห่งประเทศไทย
Thailand Concrete Association

CPD/PDU 9 หน่วย

แนวทางใหม่สำหรับการออกแบบโครงสร้างเพื่อต้านการสั่นสะเทือนจากแผ่นดินไหว

(New Approaches of Structural Design for Earthquake Resistance)

หลักการและเหตุผล

เนื่องจากรูปแบบอาคารสูงในปัจจุบันมีความซับซ้อนมากขึ้นมาก อีกทั้งเมื่อต้องออกแบบอาคารเหล่านั้นให้ต้านการสั่นสะเทือนจากแผ่นดินไหว การวิเคราะห์และดำเนินการจึงต้องอาศัยหลักวิชาความรู้ขั้นสูงและมีความทันสมัย

หลักสูตรพิเศษที่นำเสนอนี้จะนำท่านไปทำความเข้าใจกับสาระการเปลี่ยนแปลงของมาตรฐาน มยผ.1302 ตัวใหม่ รวมถึงสร้างภาพรวมให้เข้าใจถึงแนวทางการออกแบบอาคารต้านแผ่นดินไหวในประเทศไทยผ่านการเปรียบเทียบกับกฎกระทรวงฯ ที่มี อีกทั้งยังนำเสนอแนวทางการประเมินอาคารที่มีอยู่เดิมว่ามีความสามารถรองรับการสั่นสะเทือนจากแผ่นดินไหวได้หรือไม่ สุดท้ายยังมีการเสนอแนวทางการออกแบบอาคารในเชิงสมรรถนะ ซึ่งสามารถอธิบายพฤติกรรมของโครงสร้างภายใต้การสั่นสะเทือนจากแผ่นดินไหวได้อย่างครบวงจร

กำหนดการอบรม

08.30 – 09.00 น.	ลงทะเบียน
09.00 – 10.30 น.	แนวทางการออกแบบตาม มยผ.1302 ตัวใหม่ *โดย ศาสตราจารย์ ดร.เป็นหนึ่ง วานิชชัย* *สถาบันเทคโนโลยีแห่งเอเชีย*
10.30 – 10.45 น.	พักรับประทานอาหารว่าง
10.45 – 12.15 น.	ภาพรวมสำหรับมาตรฐานการออกแบบโครงสร้างต้านแผ่นดินไหวสำหรับประเทศไทย *โดย ผู้ช่วยศาสตราจารย์ ดร.ภาณุวัฒน์ จ้อยกลัด* *มหาวิทยาลัยศรีนครินทรวิโรฒ*
12.15 – 13.15 น.	พักรับประทานอาหารกลางวัน
13.15 – 14.45 น.	การประเมินเพื่อการเสริมกำลังโครงสร้างภายใต้แผ่นดินไหว *โดย ดร.ประวีณ ชูศิลป์* *บริษัท ไมนฮาร์ท (ประเทศไทย) จำกัด*
14.45 – 15.00 น.	พักรับประทานอาหารว่าง
15.00 – 16.30 น.	การออกแบบเชิงสมรรถนะ (Performance Based Design) *โดย ดร.ประมีนทร์ นรชาญ* *AIT Solutions*

วันพฤหัสบดีที่ 16 เดือน พฤษภาคม พ.ศ. 2562
เวลา 8.30-16.30 น. ณ ห้องสัมมนา ชั้น 3
อาคารวิศวกรรมสถานแห่งประเทศไทย ฯ

ศาสตราจารย์ ดร.เป็นหนึ่ง วานิชชัย

ผู้ช่วยศาสตราจารย์ ดร.ภาณุวัฒน์ จ้อยกลัด

ดร.ประวีณ ชูศิลป์

ดร.ประมีนทร์ นรชาญ

วัตถุประสงค์

1. เพื่อให้ผู้เข้ารับการอบรมมีความรู้ความเข้าใจในหลักการของการออกแบบอาคารต้านแผ่นดินไหวภายใต้มาตรฐานการออกแบบและระเบียบข้อบังคับที่เป็นปัจจุบัน
2. เพื่อให้ผู้เข้ารับการสัมมนาได้รับความรู้จากประสบการณ์การทำงานจริงของผู้เชี่ยวชาญ ในการคำนวณและออกแบบอาคารต้านแผ่นดินไหว
3. เพื่อให้เกิดความร่วมมือในการพัฒนาองค์ความรู้ด้านการคำนวณออกแบบโครงสร้างซึ่งมีความทันสมัยและเกิดความมั่นใจในการทำงานมากขึ้น

สอบถามข้อมูลเพิ่มเติมที่ สมาคมคอนกรีตแห่งประเทศไทย (สคท.)
ชั้น 3 อาคาร วสท. 487 ซอยรามคำแหง 39 (ซอยเทพลีลา) ถนนรามคำแหง แขวงพลับพลา เขตวังทองหลาง กรุงเทพฯ 10310
โทรศัพท์ 02-935-6593 โทรสาร 02-935-6538 E-mail : thaitca@gmail.com website : http://thaitca.or.th เลขประจำตัวผู้เสียภาษี / TAX ID : 0-9930-00131-266

สมาคมคอนกรีตแห่งประเทศไทย
Thailand Concrete Association

CPD/PDU 9 หน่วย

แนวทางใหม่สำหรับการออกแบบโครงสร้างเพื่อต้านการสั่นสะเทือนจากแผ่นดินไหว

(New Approaches of Structural Design for Earthquake Resistance)

วันพฤหัสบดีที่ 16 เดือน พฤษภาคม พ.ศ. 2562 ณ ห้องดัมมนา ชั้น 3 อาคารวิศวกรรมสถานแห่งประเทศไทย ฯ

ที่อยู่ในการออกใบกำกับภาษี / ใบเสร็จรับเงิน

ชื่อ - นามสกุล.....

หมายเลขสมาชิก TCA.....

หน่วยงาน (บริษัท/บ้าน.....

เลขที่อาคาร.....ชั้น.....หมู่.....ซอย.....

ถนน.....ตำบล/แขวง.....อำเภอ/เขต.....

จังหวัด.....รหัสไปรษณีย์.....โทรศัพท์.....

โทรสาร.....มือถือ.....E-mail.....

Tax ID (หมายเลขประจำตัวผู้เสียภาษี).....

เลขสมาชิกสภาวิศวกร (ในกรณีต้องการคะแนน CPD / PDU).....

หากต้องการรับประทานอาหารอิสลามหรือมังสวิรัติกรุณาแจ้ง.....

* ค่าลงทะเบียน *

ประเภท	ชำระภายในวันที่ 15 เมษายน 2562	ชำระหลังวันที่ 15 เมษายน 2562
นักศึกษา	☐ 2,000.00	☐ 2,200.00
สมาชิก TCA	☐ 2,200.00	☐ 2,400.00
ข้าราชการ / พนง.รัฐวิสาหกิจ	☐ 2,600.00	☐ 2,800.00
บุคคลทั่วไป	☐ 2,800.00	☐ 3,000.00

หมายเหตุ

1. อัตรานี้รวมภาษีมูลค่าเพิ่ม 7% เอกสารอบรม อาหารกลางวัน อาหารว่าง เครื่องดื่ม และวุฒิบัตร สามารถหักภาษี ณ ที่จ่าย 3%
2. ข้าราชการ พนักงานรัฐวิสาหกิจ ที่ได้รับอนุญาตจากต้นสังกัด สามารถเบิกจ่ายได้ตามระเบียบกระทรวงการคลัง
3. นักศึกษาโปรดแนบสำเนาบัตรนักศึกษามาพร้อมใบลงทะเบียน
4. กรณีที่ท่านไม่สามารถเข้าร่วมการอบรมได้ โปรดนำหนังสือแจ้งยกเลิกการอบรมล่วงหน้าก่อนการอบรมโดยมีรายละเอียดการคืนเงินดังต่อไปนี้
   - 4.1 แจ้งยกเลิกก่อนวันจัดอบรม / สัมมนา 7 วัน คืนเงิน 50 % ของค่าลงทะเบียน
   - 4.2 แจ้งยกเลิกน้อยกว่า 7 วันก่อนวันจัดอบรม / สัมมนา ไม่คืนเงินค่าลงทะเบียน
5. กรณี สคท. ยกเลิกการจัดอบรม / สัมมนา / ศึกษาดูงาน เนื่องจากสาเหตุใดก็ตาม สคท. จะคืนเงินให้ท่านเต็มจำนวน

การชำระเงิน

เงินสด สามารถชำระได้ที่ สมาคมคอนกรีตแห่งประเทศไทย (สคท. ชั้น 3 อาคาร วสท. วังทองหลาง กรุงเทพฯ)

เช็ค สั่งจ่ายในนาม **สมาคมคอนกรีตแห่งประเทศไทย**

โอนเงิน เข้าบัญชีเงินฝากประเภทออมทรัพย์ **ชื่อบัญชี สมาคมคอนกรีตแห่งประเทศไทย**
ธนาคารไทยพาณิชย์ สาขาสี่แยกศรีวรา เลขบัญชี 140-2-55084-3

*กรณีโอนเงิน กรุณาแนบสำเนาหลักฐานการชำระเงินพร้อมใบลงทะเบียน ส่งโทรสารมาตามเบอร์โทรสารสมาคมฯหรือสแกนส่ง E-mail และกรุณาช่วยโทรแจ้งกับเจ้าหน้าที่สมาคมฯ ด้วย ขอบคุณค่ะ

สอบถามข้อมูลเพิ่มเติมที่ สมาคมคอนกรีตแห่งประเทศไทย (สคท.)
ชั้น 3 อาคาร วสท. 487 ซอยรามคำแหง 39 (ซอยเทพลีลา) ถนนรามคำแหง แขวงพลับพลา เขตวังทองหลาง กรุงเทพฯ 10310
โทรศัพท์ 02-935-6593 โทรสาร 02-935-6538 E-mail : thaitca@gmail.com website : http://thaitca.or.th เลขประจำตัวผู้เสียภาษี / TAX ID : 0-9930-00131-266

<u>หลักการและเหตุผล</u>

ในช่วง 10 ปีที่ผ่านมา อาคารสูงและอาคารที่มีรูปทรงลักษณะพิเศษได้เกิดขึ้นมากในประเทศไทย ด้วยความสูงของอาคารที่มีมากกว่า 300 เมตร หลายอาคารในใจกลางกรุงเทพฯมหานคร และล่าสุดประเทศไทยจะมีอาคารที่สูงมากกว่า 615 เมตร หรือติดอันดับ 1 ใน 10 ของโลกในอนาคต ด้วยกระแสความต้องการพื้นที่ใช้สอยของอาคารที่มีมากขึ้น ในขณะที่พื้นที่ใจกลางของกรุงเทพฯเริ่มคับแคบ ประกอบกับราคาที่ดินที่สูงมาก จึงส่งผลให้นักลงทุนมีความต้องการที่จะก่อสร้างอาคารสูงหรืออาคารขนาดใหญ่และคาดว่าอีก 10 ปีข้างหน้า อาคารสูงและอาคารขนาดใหญ่ของประเทศไทยต้องเกิดขึ้นอีกมากมาย ดังนั้น ทางสมาคมคอนกรีตแห่งประเทศไทยได้เล็งเห็นความสำคัญในเรื่องนี้ จึงจัดอบรมดังกล่าวขึ้นเพื่อให้ผู้ที่เกี่ยวข้องมีความรู้ความเข้าใจที่ถูกต้องถึงสิ่งสำคัญในการก่อสร้างอาคารสูงและอาคารขนาดใหญ่

คณะกรรมการวิชาการ
สาขาคอนกรีต วัสดุและการก่อสร้าง
สมาคมคอนกรีตแห่งประเทศไทย

<u>กำหนดการอบรม</u> (วันแรก)

<u>วันเสาร์ที่ 29 กันยายน 2561</u>

08.30 – 09.00 น. ลงทะเบียน

09.00 – 10.30 น. ความท้าทายทางด้านวิศวกรรมของงานอาคารสูงในประเทศไทย
โดย รศ.ดร.การุญ จันทรางศุ

10.30 – 10.45 น. พักรับประทานอาหารว่าง

10.45 – 12.15 น. ผลกระทบของแผ่นดินไหวและแรงลมต่ออาคารสูง
โดย ศ.ดร.เป็นหนึ่ง วานิชชัย

12.15 - 13.15 น. พักรับประทานอาหารกลางวัน

13.15 – 14.30 น. หลักการวิเคราะห์โครงสร้างอาคารสูง ด้วยโปรแกรมคอมพิวเตอร์
โดย ดร.สมพร อรรถเศรณีวงศ์

14.30 – 15.45 น. การตรวจวัดพฤติกรรมการสั่นสะเทือนของอาคารสูง เพื่อการเฝ้าระวังและประเมินสภาพ
โครงสร้าง
โดย ดร.ปั้นเจตน์ ธรรมรักษ์

15.45 – 16.00 น. พักรับประทานอาหารว่าง

16.00 – 17.15 น. การประเมินโครงสร้างเชิงสมรรถนะของอาคารสูง
โดย ดร.ประมีนทร์ นรชาญ

17.15 – 18.30 น. การควบคุมคุณภาพคอนกรีต Zero Bleeding ในการก่อสร้างเสาเข็มเจาะ
ลึก 100 เมตร
โดย คุณทวีศักดิ์ อัศวชัยวรรณ

<u>กำหนดการอบรม</u> (วันที่สอง)

<u>วันอาทิตย์ที่ 30 กันยายน 2561</u>

08.30 – 09.00 น. ลงทะเบียน ณ อาคารวิศวกรรมศาสตร์ มหาวิทยาลัยรามคำแหง

09.40 – 11.40 น. เยี่ยมชม การก่อสร้างอาคารสูง โครงการ The Residences at Mandarin Oriental, Bangkok (Icon Siam)
บริษัท แมกโนเลีย ควอลิตี้ ดีเวล็อปเม้นต์ คอร์ปอเรชั่น จำกัด
รับประทานอาหารบนรถตู้

12.20 – 17.00 น. เยี่ยมชม เทคนิคการก่อสร้างกำแพงกันดินและระบบฐานรากขนาดใหญ่ โครงการ MRT Orange Line Contract E1 & E2
SEAFCO Public Company Limited
เดินทางกลับถึงมหาวิทยาลัยรามคำแหง เวลาประมาณ 17.40 น.

AIT
Asian Institute of Technology

Office of the Vice President
Academic Affairs

Postal Address:
P.O. Box 4, Klong Luang
Pathumthani 12120
Thailand

Street Address:
Km. 42, Paholyothin Highway
Klong Luang, Pathumthani 12120
Thailand

(For local calls, dial 02 before the tel./fax nos.)
Tel : +(66-2) 524-6001
Fax: +(66-2) 524-8000
http://www.ait.asia

PERSONAL & CONFIDENTIAL
Our Ref.: HRP-AFL7/2016
11 April 2016

Dr. Pramin Norachan
Manager
AIT Solutions
Asian Institute of Technology

Dear Dr. Pramin,

Upon the recommendations of the Dean of the School of Engineering & Technology and the Field of Study Coordinator, I am pleased to offer you the opportunity of conducting academic lectures for CE72.32 "Tall Buildings" in the Structural Engineering Field of Study as well as any other academic duties that may be assigned to you by the School Dean.

This appointment which is for the period as of **1 January 2016 to 30 June 2016** is subject to the continuation of your primary appointment as Manager in the AIT Solutions. You can be listed as an **Affiliated Faculty** member in the School of Engineering & Technology.

An Affiliated Faculty member participates in the specific academic activities, as assigned, while holding a non-teaching appointment in our Institute. You will not receive additional remuneration for teaching duties.

I hope that you will be able to accept this appointment so that the students of the School of Engineering & Technology will benefit from your expertise.

Yours sincerely

Professor Sivanappan Kumar
Vice President for Academic Affairs

cc : Dean, SET

ที่ ศธ.๐๕๘๐.๑๑๔/๑๑๔๒

มหาวิทยาลัยเทคโนโลยีราชมงคลตะวันออก
วิทยาเขตอุเทนถวาย
๒๒๕ ถนนพญาไท เขตปทุมวัน
กรุงเทพฯ ๑๐๓๓๐

๑๐ กันยายน ๒๕๕๘

เรื่อง ขอเชิญเป็นอาจารย์พิเศษ

เรียน ดร.ประมีน นรชาญ

ด้วยในภาคการศึกษาที่ ๑ ปีการศึกษา ๒๕๕๘ คณะวิศวกรรมศาสตร์และสถาปัตยกรรมศาสตร์ มีความประสงค์ขอเชิญ ดร.ประมีน นรชาญ เป็นอาจารย์พิเศษสอนวิชา ๐๗-๑๒-๖๑๐ หัวข้อพิเศษทางด้านวิศวกรรมโยธา ในวันเสาร์ เวลา ๙.๐๐-๑๒.๐๐ น. ให้แก่นักศึกษาหลักสูตรวิศวกรรมศาสตรมหาบัณฑิต สาขาวิชาวิศวกรรมโยธา ปริญญาโท คณะวิศวกรรมศาสตร์และสถาปัตยกรรมศาสตร์ ตั้งแต่วันที่ ๒๙ สิงหาคม ๒๕๕๘ ถึงวันที่ ๑๗ มกราคม ๒๕๕๙

จึงเรียนมาเพื่อโปรดพิจารณา หวังเป็นอย่างยิ่งว่าจะได้รับความอนุเคราะห์จากท่าน และขอขอบคุณมา ณ โอกาสนี้

ขอแสดงความนับถือ

(นายสืบพงษ์ ม่วงชู)
รองอธิการบดี
มหาวิทยาลัยเทคโนโลยีราชมงคลตะวันออก

งานบัณฑิตศึกษา ฝ่ายวิชาการและวิจัย
โทร. ๐ ๒๒๕๒ ๗๐๒๙ ต่อ ๓๘

EASEC-14
CONFERENCE
Structural Engineering and Construction

EASEC

Certificate of Participation

Dr. Pramin Norachan

Asian Institute of Technology

has participated as a Presenter at EASEC-14 - the Fourteenth East Asia Pacific Conference on Structural Engineering and Construction held in Ho Chi Minh City, Vietnam, on January 6-8, 2016.

ĐẠI HỌC QUỐC GIA THÀNH PHỐ HỒ CHÍ MINH
TRƯỜNG ĐẠI HỌC BÁCH KHOA

Associate Prof. HOANG NAM
HCMC University of Technology, Chairman of EASEC-14

BK TP.HCM

Seminar on "Precast Concrete Structural Systems: The Future and Applications in Building Industry in Myanmar"

4th December 2018, Wyndham Grand Hotel, Yangon

Time	Topics	Speakers
9:00 – 9:30	Opening session remarks	A.G.T.I Society
9:30 – 10:30	Delving into the Application of Precast Prestressed Concrete buildings in High Seismic Regions	Dr. Naveed Anwar
10:30 – 10:40	Open forum	
10:40 – 11:00	Coffee / Tea break	
11:00 – 11:50	Presentation from UNHABITAT	UNHABITAT Staff
11:50 – 12:00	Open forum	
12:00 – 13:00	Lunch break	
13:00 – 14:00	Precast Concrete Connections in Structural Frames	Dr. Punchet Thammarak
14:00 – 14:10	Open forum	
14:10 – 14:30	Coffee / Tea break	
14:30 – 16:00	Performance-based seismic evaluation of hybrid structural systems	Dr. Pramin Norachan
16:00 – 16:10	Open forum	
16:10	Closing Remarks	A.G.T.I Society

โครงการสัมมนาเพื่อพัฒนาความรู้ด้านการวิเคราะห์ ออกแบบ และก่อสร้างโครงสร้างพื้นฐาน ภายใต้หัวข้อ

พัฒนาการล่าสุดของเทคโนโลยี ด้านการวิเคราะห์ออกแบบและก่อสร้าง สำหรับอาคารสูง

สัมมนา Online "ไม่มีค่าใช้จ่าย"

26 ม.ค. 65

สิริวัฒน์ จุ้ยสุวรรณทัต
Meinhardt (Thailand) Company Limited

หัวข้อบรรยาย :
Design of Transfer Structures for Supporting the Discontinuous Column

9 ก.พ. 65

ทวีศักดิ์ อัศวชัยวรรณ
Siam City Concrete Company Limited

หัวข้อบรรยาย :
Experience in Concrete Innovation for Skyscraper Substructure

23 ก.พ. 65

ดร.ประมินทร์ นรชาญ
AIT Solutions

หัวข้อบรรยาย :
Overview of Finite Element Modeling and Analysis of Tall Buildings

2 มี.ค. 65

ผศ.ดร.ณัฐพงศ์ มกระธัช
มหาวิทยาลัยเทคโนโลยีพระจอมเกล้าพระนครเหนือ

หัวข้อบรรยาย :
Design View in Concrete Material & Requirements for Tall Building

9 มี.ค. 65

ผศ.ดร.ภาณุวัฒน์ จ้อยกลัด
ภาควิชาวิศวกรรมโยธาและสิ่งแวดล้อม
คณะวิศวกรรมศาสตร์ มหาวิทยาลัยศรีนครินทรวิโรฒ

หัวข้อบรรยาย :
ผลกระทบต่อแผ่นดินไหวต่ออาคารสูง และกฎหมายเกี่ยวกับแผ่นดินไหวในปัจจุบัน

16 มี.ค. 65

ณัฐพล มากเทพพงษ์
บริษัท เจ แปลน จำกัด

หัวข้อบรรยาย :
การตรวจวัดคุณสมบัติเชิงพลศาสตร์ของอาคารภายใต้การสั่นไหวแบบทั่วไป

23 มี.ค. 65

ดร.จิรวัฒน์ จันทร์เรือง
คณะวิศวกรรมศาสตร์และสถาปัตยกรรมศาสตร์
มหาวิทยาลัยเทคโนโลยีราชมงคลตะวันออก
วิทยาเขตอุเทนถวาย

หัวข้อบรรยาย :
การวิเคราะห์พลกระทบของแรงลมต่อโครงสร้างด้วยอุโมงค์ลมและพลศาสตร์ของไหลเชิงคำนวณ

20 เม.ย. 65

คุณปฏิชน มณีกาญจน์
บริษัท เอส พี ซี ดีไซน์ จำกัด

หัวข้อบรรยาย :
ประสบการณ์งานออกแบบโครงสร้างอาคาร จะเป็นวิศวกรโครงสร้างต้องทำอย่างไร?

27 เม.ย. 65

ภาคภูมิ วานิชกมลนันท์
บริษัท เอสเอ็มพี โพส เท็นชั่น จำกัด

หัวข้อบรรยาย :
Post-tensioned slab design for lateral forces

28 เม.ย. 65

อรรถสิทธิ์ คำหล้า
บริษัท อี.เอ็ม.บิวดิ้ง อินสเปคเตอร์ จำกัด

หัวข้อบรรยาย :
เทคโนโลยีแบบจำลองสารสนเทศอาคารกับกระบวนการทำงานที่เปลี่ยนไปของวิศวกรโครงสร้าง

รับผิดชอบ โดย

มหาวิทยาลัยศรีนครินทรวิโรฒ

หลักสูตรวิศวกรรมศาสตรมหาบัณฑิต (วิศวกรรมโยธา)
ภาควิชาวิศวกรรมโยธาและสิ่งแวดล้อม คณะวิศวกรรมศาสตร์
มหาวิทยาลัยศรีนครินทรวิโรฒ